IMMUNE MECHANISMS REGULATING PHARMACOKINETICS AND PHARMACODYNAMICS OF PEGYLATED LIPOSOMAL ANTICANCER AGENTS

Gina Song

A dissertation submitted to the faculty of the University of North Carolina at Chapel Hill in partial fulfillment of the requirements for the degree of Doctor of Philosophy in Pharmaceutical Sciences in the Eshelman School of Pharmacy (Division of Pharmacotherapy and Experimental Therapeutics).

Chapel Hill
2014

Approved by:

Howard L. McLeod

Teresa K. Tarrant

Christine M. Walko

Tim Wiltshire

William C. Zamboni

ABSTRACT

GINA SONG: Immune Mechanisms Regulating Pharmacokinetics and Pharmacodynamics of PEGylated Liposomal Anticancer Agents
(Under the direction of William C. Zamboni)

Nanotechnology has made significant advances in drug delivery system for the treatment of cancer. Among various nanoparticle (NP) platforms, liposomes have been most widely used as a NP drug carrier for cancer therapy. High variation in pharmacokinetics (PK) and pharmacodynamics (PD) of liposome-based therapeutics has been reported. However, the interaction of liposome-based therapeutics with the immune system, specifically the mononuclear phagocyte system (MPS), and underlying molecular mechanisms for variable responses to liposomal drugs remain poorly understood. The objective of this dissertation was to elucidate immune mechanisms for the variable responses to PEGylated liposomal doxorubicin (PLD; Doxil®), a clinically relevant NP, in animal models and in patients. *In vitro*, *in vivo* and clinical systems were investigated to evaluate the effects of chemokines (CCL2 and CCL5), heterogeneity of the tumor microenvironment, and genetic variations on PK and PD of PLD. Results showed that there was a significantly positive linear relationship between PLD exposure (AUC) and total amount of CCL2 and CCL5, most prevalent chemokines in plasma, in patients with recurrent ovarian cancer. Consistent with these findings, preclinical studies using mice bearing SKOV3 orthotopic ovarian cancer xenografts demonstrated that PLD induced the production and secretion of chemokines into plasma. In addition, *in vitro* studies using human monocytic THP-1 cells demonstrated that PLD altered monocyte migration towards CCL2 and CCL5. The PK and efficacy studies of PLD in murine models of breast cancer showed that

heterogeneous tumor microenvironment was associated with significantly different tumor delivery and efficacy of PLD, but not small molecule doxorubicin between two breast tumor models. A candidate genetic locus that was associated with clearance of PLD in 23 inbred mouse strains contains a gene that encodes for engulfment adapter PTB domain containing 1 (*Gulp1*). By using integrated approaches, we were able to identify the immunological mechanisms at the molecular, tissue, and clinical levels that may contribute to inter-individual variability in PK and PD of PLD. This dissertation research has a potential to make an impact on development of future NP-based anticancer therapeutics as well as on clinical use of PLD (Doxil®) and other PEGylated liposomal anticancer agents.

To my family, friends, and mentors who have supported me.

ACKNOWLEDGEMENTS

I feel truly blessed to have met so many generous, supportive, and inspiring people over the years spent in the University of North Carolina at Chapel Hill.

First and foremost, I would like to thank my advisor, Dr. William Zamboni. I will always be grateful for the numerous opportunities, guidance, and motivation that Dr. Zamboni provided for me to grow as a clinical scientist and succeed in my career. Next, I would like to thank Dr. Howard McLeod who served not only as the chair of my dissertation committee but also as my mentor throughout the graduate program. Thank you for your insightful advice not only for my academic development but also for lifelong career as a clinical researcher. I would like to thank Dr. Tim Wiltshire who also served as the chair of my dissertation committee. I am very grateful for your sincere dedication to graduate students, including me, and your willingness to discuss research questions whenever I asked. I would like to thank Dr. Teresa Tarrant whose expertise in immunology was integral in all steps of my dissertation research. Thank you for the great opportunities to work with your research group and to learn about chemokines. I would like to thank Dr. Chris Walko for serving as my clinical preceptor and providing invaluable opportunities for clinical rotations. Dr. Walko has enthusiasm for science and patient care and is an inspirational role model for any clinical scientist.

I would like to thank past and present members of the Zamboni ($TOND_2I$) lab, Suzan Hanna, Irene La-Beck, Mark Walsh, Whitney Kirschbrown, Suzanne Newman, Sara Metzger, Allison Schorzman, Andy Madden, Sumit Rawal, Parag Kumar, Jennifer Petschauer, and all PharmD students working in our lab for their scientific assistance and friendship. I would also

like to thank past and present members of the Wiltshire and McLeod labs for their scientific advice and support. Many thanks to Amber Frick and Cristina Benton for your support and friendship.

I am very grateful for the collaborations that made this dissertation research possible. I am very thankful to Charlene Santos and the UNC Animal Studies Core, particularly Mark Ross and Alain Valdivia, for their assistance with PK studies in animals in Chapters 2-4. I am thankful to Dr. David Barrow and his lab members for their assistance with chemokine assay in Chapters 2 and 3. I am grateful to UNC Translational Pathology Lab for their assistance with immunohistochemical staining and analyses. I am thankful to Roman Timoshchenko in Dr. Tarrant's lab for his advice and assistance with chemotaxis assay in Chapter 2. I am grateful to Dr. Chuck Perou and Dave Darr for sharing their knowledge and providing mouse models for PK and efficacy studies in Chapter 3. I would like to thank Dr. Arlin Rogers and UNC Animal Histology lab for their assistance with animal tissue processing in Chapter 3. I am thankful to Dr. Andrew Dudley for sharing his knowledge on tumor angiogenesis in Chapter 3. I am thankful to Oscar Suzuki for sharing his knowledge of and assisting with the genetic analyses in Chapter 4.

I am thankful to the Eshelman School of Pharmacy faculty for building crucial academic foundation for my education and research in pharmaceutical sciences. I would like to acknowledge my clinical rotation preceptors Drs. Carey Anders and Vicki Bae-Jump at UNC Cancer Hospitals.

I would like to thank past and present administrative staff, including Amber Allen, Chrissy Crockett, Rochelle Hurt, Arlo Brown, Michelle Gibeault, Anna Sorin, and especially, Kathy Maboll.

I am grateful to the UNC Graduate School for awarding me a prestigious Royster Society Fellowship throughout the program and North Carolina Translational and Clinical Sciences Institute for awarding me a 10K pilot grant for conducting studies in Chapter 3.

I am thankful to wonderful colleagues who have supported and positively challenged me to go for higher standards.

I would like to express my eternal appreciation and love to my family and friends, who are always there for me. I would not have been able to complete the graduate program without their support, encouragement, love and prayer.

Finally, I would like to thank our Heavenly Father for His eternal grace and blessing. My God, you are my help, my strength, and my Savior.

TABLE OF CONTENTS

LIST OF TABLES

Table

LIST OF FIGURES

LIST OF ABBREVIATIONS

ABC	Accelerated blood clearance
ANC	Absolute neutrophil count
AUC	Area-under-the concentration versus time curve
BMI	body mass index
C3-TAg	*C3(1)-T-Antigen*
CCL2	CC Chemokine ligand 2
CCL5	CC Chemokine ligand 5
CL	Clearance
CME	Clathrin-mediated endocytosis
CvME	Caveolae-mediated endocytosis
DC	Dendritic cells
DLT	Dose-limiting toxicity
EGF	Endothelial growth factor
EMMA	Efficient-mixed model association
EOC	Epithelial ovarian cancer
EPR	Enhanced permeability and retention
GEMM	Genetically engineered mouse models
GULP1	Engulfment adaptor PTB domain containing 1
GWAS	Genome wide association studies
HPLC	High-performance liquid chromatography
HVT	Healthy Volunteers
IHC	Immunohistochemistry

IV	Intravenous
KM	Kaplan-Meier
KO	Knockout
MDR	Multi-drug resistant
MPS	Mononuclear phagocyte system
MTD	Maximal tolerated dose
MO	Monocyte
MVD	Microvessel density
NL-doxo	Non-liposomal doxorubicin
NP	Nanoparticle
PBMC	Peripheral blood mononuclear cells
PD	Pharmacodynamics
PEG	Poly ethylene glycol
PK	Pharmacokinetics
PLD	PEGylated liposomal doxorubicin
PPE	Palmar plantar erythrodysesthesia
PTB	Phosphotyrosine binding
QTL	Quantitative trait loci
SD	Standard deviation
SEM	Standard error of the mean
SNP	Single nucleotide polymorphisms
TAM	Tumor-associated macrophages
T11	*T11/TP53*$^{-/-}$

TGI	Tumor growth inhibition
VEGF	Vascular endothelial growth factor

CHAPTER 1:

INTRODUCTION[1]

Overview

Nanotechnology has made significant advances in the drug delivery system for the treatment of solid tumors. Abnormal blood and lymphatic vasculature have enabled selective delivery and accumulation of nanoparticles (NPs), ranging from 1 to 1000 nm in size, in tumors through the enhanced permeability and retention (EPR) effect. NP-based therapy provides advantages over conventional medicines including increased half-life, enhanced delivery of the encapsulated drug to tumors, and improved therapeutic index. Among various NP platforms, liposomes, lipid vesicles formed by a lipid bilayer membrane surrounding an aqueous core, have been most widely used as a NP drug carrier. However, individual patient responses to liposomal drugs widely vary. Immunological properties of NP may be attributed to the high variation of the pharmacokinetics and pharmacodynamics of liposome-based therapeutics. The aim of this dissertation research was to elucidate underlying immune mechanisms for variable patient responses to liposomal anticancer agents.

[1]Parts of this chapter previously appeared as an article in the *Journal of Liposomal Research*. The original citation as follows: Song G, Wu H, Yoshino K, Zamboni WC. Factors affecting the pharmacokinetics and pharmacodynamics of liposomal drugs. *J Liposome Res* 2012;22(3):177-192.

1.1. Liposome-Based Anticancer Therapeutics

Liposomes are spherical carriers, usually 0.05 to 5.0 μm in diameter, formed by one or several lipid bilayers with inner aqueous core (1, 2). Vesicle formulations are usually based on natural and synthetic phospholipids and cholesterol (1, 2). Drugs with widely varying lipophilicity can be encapsulated in liposomes, either in the entrapped aqueous volume or at the bilayer interface (1, 2). Liposomes have been widely used for selective tumor targeting of conventional chemotherapies due to unique properties and capabilities. First, they are composed of biocompatible and biodegradable lipids (1, 2). They can encapsulate both hydrophilic and hydrophobic therapeutic agents with high efficiency, protecting the cargo from undesired degradation during the circulation in the body (1-3). They can also be further engineered with ligands, such as antibodies, to promote targeting to specific cells, tissues and organs (1-3). In addition, they can be coated with inert polymers, such as poly(ethylene) glycol (PEG) to prolong the liposome circulation half-life (1-3). Lastly, like other nanocarriers, liposomes encapsulating anticancer drugs can bypass the multi-drug resistance (MDR) transporter-mediated drug efflux (i.e., P-glycoprotein) (4, 5).

There are two drug-targeting approaches that are applicable to liposomes: passive and active targeting. Liposomal drugs can be used for various indications, including inflammatory and infectious diseases, but oncology applications of liposomes are discussed in my dissertation research.

Passive Targeting. Passive targeting of liposomes can be achieved by taking advantages of unique vascular pathophysiology and immune responses in the tumor (6). Rapid and defective angiogenesis in the tumor result in increased permeability of the blood vessels compared to continuous endothelium in the normal tissues (7). In addition, the impaired lymphatic drainage

allows retention of liposomes in the tumor leading to release of drugs from the carrier into the tumor cells (6, 7). Thus, drug-loaded liposomes can preferentially extravasate from blood into the interstitial spaces and be accumulated in the tumor by the enhanced permeability and retention (EPR) effect (6, 7). It has been shown that the size of particles influences the passive tumor accumulation of liposomes. Liu *et al*. have examined the biodistribution of liposomes of different size (30-400 nm) to tumors (8). Liposomes with a diameter between 100 and 200 nm showed a 4-fold higher tumoral uptake compared to the liposomes greater than 300 nm or less than 50 nm in size (8). For very small particles (< 10 nm), they can easily permeate the tumor tissue through the gap in the endothelium, but can also be easily pushed out from the tumor into the blood (8-10). Thus, liposomes of the optimal size can exhibit increased tumor accumulation via EPR effects.

Active Targeting. The leaky tumor vasculature allows for preferential accumulation of liposomes in the tumor, but it is non-selective process because liposomes can be accumulated in the liver and spleen primarily due to uptake by tissue resident macrophages (10). In addition, the vascular permeability may be heterogeneous in a single tumor and certain tumors may not exhibit EPR effects (7). To overcome these limitations, active targeting approach has been used to enhance selective binding of liposomes to tumor cells (i.e., Zevalin® and Bexxar®) (4, 5). Targeting agents, such as ligands binding to specific receptors on the surface of tumor cells, are attached to the surface of the nanocarrier by a wide range of conjugation approaches (4, 5). After conjugation with a targeting ligand, liposomes will recognize and bind to target tumor cells through specific ligand-receptor interactions leading to increased intracellular delivery of liposomes (10, 11). To improve the targeting specificity and efficacy, a surface marker (i.e., antigen or receptor) should be uniquely overexpressed on tumor cells relative to normal cells and

binding affinity should be optimized to enable the nanocarrier to dissociate from the binding targets and penetrate the tumor tissues (4, 5). NP-based anticancer drugs that are currently on the market and under clinical development stages are summarized in **Table 1. 1** and **Table 1. 2**, respectively.

1.2. Pharmacokinetics and Biodistribution of Liposome-based Anticancer Therapeutics

Pharmacokinetic Nomenclature. Pharmacokinetics (PK) is the study of the drug disposition in various compartments, such as plasma or tissues, of the body over the time. PK includes the several processes as a drug is absorbed, distributed throughout the body, metabolized, and/or excreted, called ADME (12). When a small molecule drug is administered intravenously (i.v.), the drug is usually quickly eliminated from the blood by the renal filtration into the urine or by the hepatic metabolism and subsequent excretion into the bile or urine depending on hydrophilicity of the drug. The cutoff size for renal clearance is approximately 5.5 nm according to the study using quantum dots (13).

In contrast to small molecule agents, the disposition of liposome-based drugs is dependent upon the carrier, liposomes, encapsulating the parent drug (1-3). This remains true until the small molecule drugs get released from the carrier and follow its classical PK disposition (1-3). The drugs encapsulated in the liposomes are protected from metabolizing enzymes in the liver before the drugs are released from the liposomes as well as from renal clearance due to the relatively large size (1-3, 10). This leads to prolonged blood circulation and increased accumulation of liposomal drugs in the target tissues, such as tumor (1-3, 10). The nomenclature used to describe the PK disposition of nanocarrier-mediated drugs include: encapsulated (the drug within or bound to the carrier), released (active-drug released from the

carrier), and sum total (encapsulated drug plus released drug) (**Figure 1.1**) (14, 15). The released drug has also been called the legacy drug, regular drug, or warhead (14, 15). After the drugs get released from its carrier, it is pharmacologically active and subject to the same routes of metabolism and clearance as the non-carrier form of the drug (14, 15). Thus, the PK profiles of the parent drug and the drug encapsulated in the liposomes are different. It would be more informative to keep track both encapsulated and released drugs to better characterize the PK of drug-loaded liposomes (14, 15).

Clearance of Liposomes by the Mononuclear Phagocyte System (MPS). Upon intravenous administration of NP-based therapeutics including liposomal drugs, NPs encounter biological barriers, such as plasma proteins and mononuclear phagocytic cells, which influence their clearance from the circulation and accumulation in the target tissues (i.e., tumor) (16, 17). A number of the plasma proteins that are adsorbed to the particle surface, called opsonins, have been identified including albumin, lipoproteins, complements, and immuglobulin (Ig) (16, 17). Complement proteins and Ig are the predominant opsonins contributing to the recognition of NPs by the cells of the mononuclear phagocyte system (MPS), including monocytes and macrophages (16). Complement activation occurs through the classical, alternative and lectin pathways and it has been shown that some activated fragments of complement activation (i.e., C3a, 4a, and 5a) by NPs may also result in hypersensitivity reaction (16). In addition to complement activation, immunogenic reactions induce the secretion and deposition of Ig (IgM and IgG) on the particle surface leading to enhanced clearance of NPs by the MPS (18). The types and extent of the protein adsorption, known as opsonization, are dictated primarily by the surface characteristics of the particles (i.e., surface charge and size) (17, 18).

The MPS consists of monocytes, macrophages and dendritic cells and is mainly responsible for antigen presentation, cytokine secretion, and phagocytosis to protect the host against pathogens and foreign particles (19). NPs have been shown to be cleared and removed from the circulation primarily by monocytes and macrophages (18). Unlike small molecule drugs that can easily diffuse through the capillary wall into the tissue, NP-based drugs distribute to tissues with the discontinuous endothelium (e.g., tumor, liver, spleen, and bone-marrow) (18). Furthermore, the enhanced uptake in these organs is attributed to NP capture by resident macrophages in these tissues (18). Thus, the blood clearance of NP-based drugs is primarily dependent on the tissue uptake in contrast to extensive renal and/or hepatic elimination of small molecule drugs (e.g., glomerular filtration and hepatic metabolism) (10, 18).

Biodistribution of Liposome-based Anticancer Therapeutics. **Liver**. The liver parenchyma is comprised of lobules containing the hepatocytes and sinusoids, a permeable discontinuous capillary network (20). The size of fenestrations in the sinusoidal epithelium ranges from 100 to 150 nm leading to unrestricted passage of plasma components to hepatocytes in the perisinusoidal space (20). The Kupffer cells, major parts of the MPS, are present inside the sinusoid capillaries and play an important role in phagocytosis of liposomes through the recognition of opsonins on the surface of liposomes or through the interaction with the scavenger receptors on the Kupffer cells (18, 20). It has been demonstrated that the surface characteristics of liposomes, such as size, shape, and flexibility and deformability, influence the uptake and internalization by the Kupffer cells (2, 10). Optimal interaction and phagocytosis by the Kupffer cells occur with the diameter of NP between 1 and 3 μm (18). The increasing dose of empty nanocarriers has shown to decrease the uptake of NP by the Kupffer cells presumably due to the saturation of phagocytic capacity of the Kupffer cells and depletion of plasma opsonins (21, 22).

In addition, NP encapsulating cytotoxic drugs was reported to alter the uptake functions of the Kupffer cells due to cytotoxicity (23). The biliary elimination of NPs is relatively slow and insignificant (<5-10% of the injected dose over 8 to 48 h) (18).

Spleen. The spleen is another important MPS organ contributing to liposome uptake by macrophages. The fenestrations in the spleen typically do not exceed 200-500 nm in width and liposomes less than 200 nm in size exhibited minimal spleen uptake (18, 24). The red pulp of the spleen is comprised of a network of reticular fibers containing macrophages responsible for filtration of pathogens and old red blood cells from circulation (18). It has been shown that the splenic uptake of liposomes is inversely related to hepatic accumulation due to the differences in the blood flow (25). Thus, higher amounts of PEG-coating nanocarriers are delivered to the spleen as they evade the capture by the Kupffer cells in the liver (10, 18, 25). High rigidity, large size (> 200 nm), and irregular shape have been shown to affect liposome permeability through the sinusoidal pore and contribute to sequestration of liposomes in the spleen (18). The spleen uptake of liposomes can lead to undesirable immunogenic reactions and influence the blood clearance of liposomes (18, 26). It has been shown that the interactions between liposomes and B cells in the spleen induce antibody secretion, primarily IgMs (26). liposomes administered during 2 to 4 days after the first liposome dose are opsonized by circulating antibodies and rapidly cleared by the macrophages in the liver (26). This phenomenon, enhanced blood clearance of a second NP dose after initial sensitization (induction), is known as the accelerated blood clearance (ABC) effect (18, 26). Interestingly, PEGylated particles are more affected by the ABC effect compared to non-PEGylated counterparts (18, 27). This is probably because grafting PEG polymer coating prevents the non-specific capture by the MPS and the presence of specific antibodies interacting with PEG polymer greatly enhances their clearance (18).

Tumors. Tumor vasculatures are characterized by abnormal architecture, such as pericyte deficiency and impaired basement membrane formation, leading to an enhanced vascular permeability (7). The size of endothelial pores in the tumor ranges from 10 to 1000 nm and this allows for preferential extravasation and accumulation of NPs inside the interstitial space (7, 28). In addition, dysfunctional lymphatic vessels in the tumor contribute to impaired drainage of NPs from the tumor tissue and increased retention in the tumor (7). This EPR effect plays a key role in the selective nanosized and macromolecular drug targeting to the tumor (7, 28).

Peripheral blood mononuclear cells (PBMC). PBMCs are another compartment in which liposomes are deposited (18). Circulating monocytes and dendritic cells are professional phagocytes that recognize the opsonized liposomes through specific receptor-ligand interactions (i.e., FcR and CR) and phagocytose them (11). After internalization, phagosomes, phagocytic vesicles, fuse with lysosomes containing enzymatic proteins (i.e., esterase) and an acidic internal condition (pH 5-6.5), form phagolysosomes, and degrade the particles (11). Once the particles are degraded, the drugs can be released. If the particles cannot be digested, the PBMC sequestering liposomes may act as a drug depot (11). It has been shown that phagocytosis of cytotoxic drugs-loaded liposomes may have detrimental effects on macrophages and alter the phagocytic capacity (i.e., saturation) (22, 23).

1.3. Cellular Internalization of Liposomes

Non-phagocytic Endocytosis Pathway for Internalization. There are biological barriers at the cellular level that liposomes need to overcome. In addition to phagocytosis discussed in the previous section, liposomes can be internalized through non-phagocytic pathways by four mechanisms: clathrin-mediated endocytosis, caveolae-mediated endocytosis,

macropintocytosis and other clathrin- and caveolae-independent endocytosis (11). Unlike phagocytosis, these endocytic mechanisms can occur in all types of cells.

Clathrin-mediated endocytosis (CME). CME is the predominant mechanism of internalization for macromolecules in most cells (29, 30). Clathrin is a main cytosolic coat protein and the CME typically takes a place in a membrane region enriched in clathrin (29). CME leads to the formation of clathrin-coated endocytic vesicles. This vesicle fuses with endosomes and lysosomes, which leads to degradation of the internalized cargo (29, 30). CME can take place in either receptor-dependent or receptor-independent manner. Viruses and drug-loaded nanocarriers conjugated with targeting ligands, such as low-density lipoprotein (LDL), transferrin, and epidermal growth factor (EGF), are internalized through receptor-mediated CME (29). Compounds displaying non-specific charges and hydrophobic interactions with the cell membrane are absorbed by receptor-independent CME, which is slower process compared to receptor-mediated CME (30).

Caveolae-mediated endocytosis (CvME). CvME is a major alternative pathway for endocytosis. Caveolae are flask-shaped membrane invaginations and abundant in endothelial cells (31). CvME differentiates from CME in that the cytosolic caveolar vesicle does not contain any enzymes and are not destined for lysosomal compartment (31). Nanocarriers encapsulating drugs highly sensitive to enzymes (i.e., peptides, proteins, nucleic acids, etc.) exploit this mechanism to bypass the lysosomal degradation of cargo (18). Ligands including albumin, folic acid, and cholesterol have been shown to be internalized through CvME (31).

Macropintocytosis and other mechanisms. Macropintocytosis is another mode of clathrin-independent endocytosis pathway. It occurs in many cells via formation of actin-driven membrane protusion (32). Macropinosomes, large endocytic vesicles, are formed and in most

cases, they acidify and shrink. They may fuse eventually with lysosomal compartment or recycle their content to the surface (32). Other clathrin- and caveolae- independent endocytosis pathways have also been reported recently, but the understanding of their implications in the cellular internalization of nanocarriers remains unclear (33).

1.4. Rate of Drug Release from the Liposome and Its Effects on the Efficacy and Toxicities

The rate of drug release from the liposome is a pivotal parameter because the encapsulated drugs must be released to exert pharmacological effects in the site of action, such as tumor (10, 14). The bioavailability of the drug to the tumor is more dependent on the rate of drug release than high tumor accumulation of liposomes (10). However, it is challenging to maintain the stability of a liposome in the circulation while improving the local drug bioavailability in the target tissue. For example, PEGylated liposomal doxorubicin, the stable liposomal formulation, was shown to have only 40-50% bioavailability in the tumors (34) and release the majority of doxorubicin after accumulation in the tumor with one-half of doxorubicin released at more than 90 hour after administration (35).

Factors Affecting Drug Release Rate from the Liposome. There are several factors that can influence the stability of the liposome and the rate of release of the drug from the liposome: drug encapsulation methods, lipid composition and the physicochemical properties of the drug (2). The drug encapsulation method plays an important role in determining the pharmacokinetics and *in vivo* drug release rate. Depending on the drug potency (active vs. prodrug), drug-to-lipid ratio needs to be carefully determined as decreased drug-to-lipid ratio may result in faster clearance of the liposomal therapeutics (2). The most widely used strategy is the transmembrane gradient loading method where a trapping agent is used to efficiently load

drugs and stabilize the formulation to prevent the premature leakage in the circulation (2). For example, ammonium sulfate is used as gradient-forming salt to load doxorubicin and improve the formulation stability of liposomes (36). Lipid composition of the liposome or lipidic nanocarrier also influences the drug release rate because a liposomally entrapped drug tends to cross the liposomal membrane along their own gradients and diffuse out of the liposome (37). The charge, phase transition, hydrogen-bonding capacity, and the cholesterol content of the liposome bilayer can have impacts on drug retention (2, 15). Physicochemical characteristics of the therapeutic agent, such as lipophilicity, water solubility, and weak base or acid, need to be taken into consideration to optimize the efficiency of drug loading, the formulation stability, and the drug release rate (2, 15).

Relationship between Drug Release Rate and the Efficacy and Toxicity of Liposomal Drugs. In general, it is believed that the liposomally encapsulated drug is delivered more selectively to the target tissue, reducing the exposure of drug to the normal tissues and minimizing the toxicities. However, it has been shown that liposome-based delivery can result in changes in the pharmacokinetics and biodistribution of the entrapped drug and, eventually, the efficacy and toxicity profile (2, 10, 18, 38). *in vivo* drug release rate has been shown to affect antitumor activity of encapsulated anticancer agent. It has been demonstrated that increased stability of the formulation and slow drug release rate are associated with enhanced tumor-growth suppression using irinotecan and vinorelbine (39, 40). However, liposomal cisplatin and mitoxantrone have shown too slow drug release rate from the liposomes, which resulted in no drug bioavailable at the tumor and poor clinical response (41, 42). Thus, optimal formulation stability plays a critical role in displaying the antitumor efficacy for non-targeted liposomes and targeted liposomes (10, 18).

Moreover, the use of doxorubicin and other anthracyclines have been clinically limited due to dose-limiting cardiotoxicity. Both PEGylated and non-PEGylated formulation liposomal doxorubicin have, however, substantially reduced the cadiotoxicity and increased the cumulative dose of doxorubicin that can be administered (43). This is due in part to decreased accumulation of liposomal or bioavailable doxorubicin in the heart tissue with continuous, non-fenestrated capillaries (44). In addition, incidence of myelosuppression was also decreased by encapsulation of doxorubicin in the liposome, but the reducing effect was dependent on the drug release rate (45). While many of conventional toxicities associated with doxorubicin were reduced by encapsulation, different toxicities appeared as dose-limiting toxicities (DLT) of PEGylated liposomal doxorubicin (PLD): mucositis and palmar-plantar erythrodysesthesia (PPE or hand-foot syndrome) (38). The incidence of PPE is PLD dose- and schedule-dependent and can be decreased or managed by reducing the dose or dosing interval (2, 38). It is thought that the accumulation of PLD in the skin and slow release rate of doxorubicin may affect the occurrence of PPE with PLD in addition to cytokine-mediated inflammation (38, 46).

Triggered Drug Release. To improve bioavailability of the drug at the site of action, such as tumor, several approaches have been employed to activate the site specific release of the drug from the liposome: internal and external triggering mechanisms and conjugation of targeting ligands on the surface of the liposome.

Internal triggering mechanisms. Studies of the tumor microenvironment have shown that there are several characteristics inherently present in the tumor that can be exploited as triggering mechanisms, such as low pH, enhanced activity of a specific enzyme, or high reducing potential (7). pH-triggered release can be demonstrated by using an acid-labile PEG-conjugate lipid, such as DOPE (dioleoylphosphatidylethanolamine), as the liposome component (47). It has

been shown that pH-sensitive liposomes released almost 100% drug content when the pH was below 5, while only 10% of the drug was released from the non-pH sensitive liposomes (48). The fact that the pH of interstitial space in the tumor does not decline below pH 6.5 needs to be taken into account when considering this approach (10). Enzyme-triggered release can also be introduced by using overexpressed secretory enzymes in the tumor tissue, such as elastase, alkaline phosphatase, phospholipase (PL) A2 and C (2, 10). The drug release in the tumor microenvironment remains poorly understood, but it has been suggested that liposomal breakdown by extracellular PL, liposome uptake by macrophages, and/or gradual loss of the gradient loading agents may play a role in releasing the drug from the liposomes in the tumor (2, 38).

External triggering mechanisms. Use of external stimuli, such as light, temperature, and ultrasound, has attracted much attention for targeted drug delivery in the clinic (2, 49). Release from thermosensitive liposomes (TSL) occurs at temperatures close to the Tm (solid gel to liquid disordered phase transition temperature) of the membrane lipids because of the increased the membrane permeability at Tm (15, 49). The Tm of the TSLs can be adjusted to the clinical attainable temperatures (Tm = 40 to 42°C) by altering the lipid composition (15, 49). ThermoDox (TSL doxorubicin; Celsion Corp Yakult Honsha KK) was the first TSL formulation to enter phase III clinical trials for the treatment of patients with hepatocellular carcinoma (ClinicalTrials.gov Identifier: NCT00617981) (49). Ultrasound was also demonstrated to trigger drug release from TSL *in vivo* (50). However, their use has been limited due in part to inaccessibility to metastatic tumors (10, 51).

Targeting ligands. Lastly, conjugation of targeting ligands (i.e., transferrin and folate) on the surface of the liposomes has been used to increase intracellular delivery (2. 5, 10). It has

been shown that the intracellular delivery of drugs and antitumor efficacy have been improved by coating a targeting ligand on the liposomes (2, 10). However, several challenges, such as relatively greater blood clearance due to antibody conjugation and a loss of a great portion of drugs in the endosome/lysosome compartment during the cellular endocytosis, need to be addressed (2, 5, 10).

1. 5. Factors Affecting the PK and Biodistribution of Liposome-based Anticancer Therapeutics

It has been shown that interpatient PK variability of liposome-mediated drug is significantly higher compared with conventional small molecule drugs (52). For example, the interindividual PK variability of PEGylated liposomal CKD-602 (S-CKD602), a camptothecin analog, was approximately 100-fold at lower doses and 10- to 25-fold at higher doses (53). Thus, it is critical to understand the mechanisms for high PK variation in patients to guide the development and optimize the use of liposomal drugs. There are several factors that can influence the PK and biodistribution of liposomal drugs (15). First, liposome-associated factors, such as surface characteristics of liposomes, have been shown to play a key role in determining the disposition *in vivo*. In addition, host-associated factors have also been reported to influence the PK and biodistribution of liposomal drugs. Lastly, drug dose and schedule can also affect the disposition of liposomal drugs.

Liposome-Associated Factors. **Particle size.** When a liposomal drug is introduced into the body, the distribution primarily depends on its particle size (2, 10, 15). Unlike conventional small molecule drugs which can diffuse freely through the endothelial wall, the transportation of intact liposomes is affected by both the particle size and the anatomical structure of the tissue (8,

28). The tissues can be classified as non-endocrine organs (heart, lung, kidney, muscle and fat tissue), endocrine tissues (liver and adrenocortical), and spleen and lymphatics according to their capillaries and extracellular matrices (15). The accessibility of non-actively targeted liposomes to these tissues is normally in this order: spleen and lymphatics > endocrine tissues (liver and adrenocortical) > non-endocrine organs (heart, lung, kidney, muscle and fat tissue) (54). In addition, particle size also influences the mechanism for cellular internalization and determines the fate of the liposomal drug in the subcellular microenvironment (11, 30).

Particle size also affects the uptake of liposomal drugs by cells of the MPS. The effect of liposome size on inactivation or depletion of monocytes was investigated by Golomb group (55). In this study, larger liposomes were internalized faster by monocytes compared to smaller liposomes. Following 30-min incubation of human monocytes with empty liposomes and the alendronate-loaded liposomes with different size, human monocytes internalized 49 ± 5 %, 61 ± 4 %, 72 ± 3 % and 80 ± 5% of empty liposomes, and liposomes containing alendronate with a size of 85 ± 20 nm, 190 ± 24nm, 400 ± 64 nm and 654 ± 124 nm, respectively (55). In addition, the increased cellular uptake of larger liposomes resulted in a greater inhibitory effect on monocytes and macrophages. *in vivo* depletion of monocytes following i.v. administration of liposomal bisphosphonates was examined using rabbits. Depletion of rabbit monocytes after treatments with small liposomes with a size of 55 nm (40±5%) was significantly less than that after treatments with larger liposomes (>67%) (55).

The effect of particle size on the tumor uptake of liposomal drugs has also been investigated. Liu et al. showed that liposomes with a size between 100 nm and 200 nm had a 4-fold higher rate of uptake in the tumor compared to the liposomes with a size less than 50 nm or greater than 300 nm (8). Charrois and Allen also demonstrated that liposomes with a size ranged

between 80 and 160 nm resulted in a significantly greater accumulation in tumor compared to liposomes with a size of 241 nm (46). The lower uptake of larger liposomes in the tumor may be explained by the size limited permeability of tumor vasculature (7). The lower accumulation of very small liposomes (< 20-30 nm in diameter) may be due in part to their high permeability but low retention in tumor. They can easily pass through the leaky capillary wall in the tumor but can also be pushed back to circulating blood (10, 56). For rigid and spherical particles, it is thought that 100-200 nm in size allows for prolonged circulation because of avoiding uptake in the liver and spleen (18, 20).

Surface charge. In general, neutral liposomes were cleared from the circulation slower than either positively or negatively charged liposomes (57). The reduced clearance of uncharged liposomes is thought to be the result of reduced opsonization and decreased uptake by the cells of the MPS (57). Surface charge can also affect the biodistribution of liposomes. For example, high concentrations of anionic lipids increase MPS uptake in the liver (58-60). Cationic liposomes often exhibit a rapid blood clearance with a large dose accumulating primarily in the liver, spleen, and lung (60, 61). In addition, cationic liposomes were found to be selectively delivered to tumor vascular endothelial cell because of the natural affinity of cationic carrier molecules for the tumor microvasculature (61, 62). Although utilization of cationic liposome for gene delivery and cancer therapy gains increasing interests, the toxic effects of positively charged compounds in cationic liposomes (i.e., embolism in the lung due to aggregate formation) and potential rapid clearance by the MPS should also be taken into consideration (2, 62). Large amounts of cationic liposomes may also cause a tissue inflammatory response (63). However, cationic liposomes can be made stable and long circulating by reducing the content of cationic lipid with the inclusion of PEG-lipid stabilizers (2, 15).

Lipid composition. The surface chemistry can alter the PK of liposomal drug by influencing the opsonization process and the drug release rate (discussed in the previous section" Factors affecting drug release rate from the liposome") (16, 17). Once liposomal drugs enter the circulation, plasma proteins are adsorbed to the liposome surface to facilitate the recognition and uptake by the cells of the MPS (16-18). The most commonly used strategy to minimize the opsonization is to graft a hydrophilic poly(ethylene glycol) (PEG) polymer layer into the surface of the liposome (64). PEG is an inert hydrophilic polymer which provides good steric hindrance by forming a water shell and preventing the protein binding to the NP (64). It has been shown that PEGylation reduces the rate of MPS uptake and prolongs circulation half-life for various types of NPs (65, 66). However, Moghimi, *et al*., found that PEGylated liposomes can trigger complement activation in the absence of anti-PEG antibodies through both C1q-dependent classical and mannose-binding lectin-associated serine protease (MBL-MASP)-dependent alternative pathways using normal and C1q-depleted human serum (67, 68). This finding indicates that the presence of surface mPEG molecules did not affect the opsonin production, but may sterically prevent deposition of C3 convertases and/or complement receptor binding, which subsequently leads to slower recognition and clearance by the MPS (69).

There are two primary types of PEGylated liposome as shown in **Figure 1.2**. One has PEG tether projected on both inside and outside of liposome. This is the PEGylated liposome used for Doxil and S-CKD602. Doxil is a PEGylated liposomal formulation of doxorubicin which is approved for the treatment of refractory ovarian cancer, Kaposi sarcoma, and multiple myeloma (38). S-CKD602 is a PEGylated liposomal formulation of CKD-602, a camptothecin analogue which inhibits topoisomerase I (53) . The other type has PEG tether only localized on the outer leaflet. This PEGylated liposome has been used for IHL-305 (70). IHL-305 is a

PEGylated liposomal formulation of irinotecan (CPT-11), also a camptothecin analogue. The significance of PEGylation on outside alone versus both the inside and outside of liposome is unclear. Studies evaluating plasma, tissues, and tumor PK of both types of PEGylated liposomes encapsulating the same drug would be helpful to address this question (15).

Ongoing investigations of alternative polymers have been made to circumvent the activation of the immune system by liposomes. These polymers should be soluble, hydrophilic, have highly flexible main chain, and high biocompatibility. Synthetic polymers, such as poly (vinyl pyrrolidone) (PVP) and poly (acryl amide) (PAA), are most promising examples of other possibly protective polymers (71) in addition to PEG. More recent papers report long circulating liposomes consisting of poly[N-(2-hydroxypropyl)methacrylamide], amphiphilic poly-N-vinylpyrrolidones, L-amino-acid-based biodegradable polymer-lipid conjugates, and polyvinyl alcohol (72-74). All groups of polymer-coated liposomes described above have been reported to prolong circulation time and reduce the liver uptake. These results are comparable with those for PEG-liposomes and the steric effects naturally rely on the quantity of polymer incorporated (75). In addition, the synthetic NPs, called leukolike vectors (LLV), were produced by coating with cellular membrane purified from leukocytes and shown to evade opsonization, delay uptake by the MPS, and enhance accumulation of drugs in tumor (76). Discher, *et al*., showed that minimal "Self" peptides, designed from human CD47 and attached to virus-size particles, were able to delay the MPS-mediated clearance of NPs, prolongs the circulation times, and improve the drug delivery to tumors (77).

Host-Associated Factors. **Age.** Age was reported to be associated with PK of S-CKD602 and Doxil (53). In PK studies as part of a phase I study of S-CKD602, patients ≥ 60 years of age had a 2.7-fold higher exposure (AUC) of S-CKD602 compared with patients < 60

years of age (P = 0.02). (53). Population PK studies of Doxil were performed as part of phase I and II studies in patients with solid tumors (n = 22 and n=12, respectively) and in patients with AIDS-related Kaposi's sarcoma (KS) (n = 37) (78, 79). Doxil clearance (CL) in patients with solid tumors who were < 60 yo and ≥ 60 yo were 54.6 ±28.5 and 23.3 ± 10.8 (mean ± SD, L/h/m2), respectively (P< 0.0001) (80). Age-related factors such as impaired function of the MPS in older patients may also be associated with PK variation of liposomal drugs.

Gender. Gender was found to be a factor affecting the PK of PEGylated liposomal drugs. Gender and age effects were reported in PK studies of PEGylated liposomal drugs including Doxil (n=70), S-CKD602 (n=45), and IHL-305 (n=39) (81). Female patients had lower CL of Doxil (P <0.001), IHL-305 (P = 0.068), and S-CKD602 (P = 0.67) as compared with male patients overall as well as when stratified by age (81). The gender effect on PK of TLI (Optisomal Topotecan) and S-CKD602 in rats was also reported (82). In this study, CL of TLI and S-CKD602 was 1.2-fold (P = 0.14) and 1.4-fold (P = 0.009) lower in female rats compared with male rats, respectively (82). The mechanisms for gender-related difference in PK of liposomal drugs remains poorly understood. Sex hormones, such as estrogen and testosterone, have been suggested to influence the PK of these formulations in association with the MPS (80).

Body composition. Body composition is defined as the relative proportion of protein, fat, water, and mineral components in the body. It can vary among individual patients as results of differences in body density and degree of obesity. Body composition was shown to be associated with the PK of S-CKD602 (53). Patients with a total body weight (TBW)/ideal body weight (IBW) ratio <1.35 have a higher plasma exposure (AUC) of S-CKD602 (P = 0.02) compared with patients with TBW/IBW ratio ≥1.35 (53). PK studies of Doxil were performed as part of phase I and II studies in patients with solid tumors (n=34) and in patients with Kaposi's sarcoma

(n=36) (80). However, there was no relationship between Doxil CL and body composition as measured by TBW/IBW ratio or body mass index (BMI) probably due to skewed distribution of body disposition in the patient population (80). Body weight was found to be a significant covariate affecting the CL and volume of distribution of liposomal daunorubicin and liposomal amphotericin B in pediatric patients (71).

The mononuclear phagocyte system (MPS). The MPS consists of bone-marrow-derived cells, including monocytes, macrophages, and dendritic cells, which are professional phagocytic cells (19). Liposome-based drugs are recognized and ingested by the cells of the MPS, primarily circulating monocytes and tissue macrophages (18). Thus, the MPS plays a key role in determining the PK and distribution of liposomal drugs (10, 18). Circulating monocytes originate in the bone-marrow from a common myeloid progenitor cell and give rise to various tissue resident macrophages as well as specialized cells (i.e., dendritic cells) (83). It has been found that there is a substantial heterogeneity in the phenotypes (e.g., CD14, CD16, CD64, or CCR2) of human monocytes leading to identification of monocyte subsets with differential physiological functions (classic inflammatory vs. resident monocyte) (83). For tissue-resident macrophage population, anatomical locations and unique tissue microenvironment can result in specialization of functions and phenotypes (19, 83). Specialized tissue-resident macrophages include osteoclast (bone), microglia (CNS), Langerhans cells (skin), alveolar macrophages (lung), kupffer cells (liver), and splenic macrophages (spleen) (19, 83). It is believed that tissue macrophages are derived from peripheral blood monocytes and local proliferation self-renews the tissue-resident populations under the steady-state-condition (19, 83). However, upon exposure to various inflammatory stimuli (i.e., viral and bacterial infections), increased recruitment of circulating precursor monocytes contributes to repopulation of tissue-resident macrophages (19, 83). Once

monocytes migrate and enter the site of inflammation or infection, they differentiate into a wide spectrum of macrophages with the distinct activation state educated by microenvironmental signals (19). It is speculated that there is a great plasticity in the activation states of macrophages leading to a broad range of functional phenotypes of macrophage (19). Classically-activated macrophages (M1) and alternatively-activated macrophages (M2) are most well-characterized extremes of a continuum of functional states of macrophages (19). Inflammation-associated diseases, such as obesity, atherosclerosis, and cancer, are characterized by recruitment and accumulation of abundant macrophages with distinct phenotypes in the site of inflammation (84). Infiltrating macrophages can influence the PK and biodistribution of liposome-based therapeutics via uptake by macrophages (18). Heterogeneity of tumor microenvironment (i.e., vascular permeability, macrophage infiltration, and interstitial fluid pressure) across different tumor types has been suggested to contribute to variability in extravasation and accumulation of nanocarrier-based therapeutics in different tumors; but there are limited clinical and preclinical experimental data (7, 28, 85). The heterogeneity of macrophage phenotypes are shown to be conserved between human and mice, thus knowledge on macrophage biology can be extrapolated to humans and translated to better understanding of interaction between nanocarrier-based delivery systems and MPS (83).

The function of the cells of the MPS was correlated with the CL of PEGylated liposomal agents across species (86). PK studies of PEGylated liposomal doxorubicin (PLD), CKD-602 (S-CKD602), and cisplatin (SPI-077) were performed at the maximal tolerated dose (MTD) in mice, rats, and dogs (86). The functions of monocytes (MO) and dendritic cells (DC) were measured by phagocytosis and reactive oxygen species (ROS) production (86). It has been shown that there is a significantly positive correlation between CL of PEGylated liposomal agents and the

function of MO and DC across species (86). In addition, the positive relationship between PLD CL and the cell function was also observed in patients with refractory epithelial ovarian cancer (EOC) after PLD administration (86). The findings suggest that probes for the function of the MPS cells may help predict the CL of PEGylated liposomes across species and in patients with EOC (86). In PK studies of S-CKD602 as part of a phase I study in patients with advanced malignancies, the presence of tumor cells in the liver was also shown to affect the CL of PEGylated liposomal CKD-602 in patients with advanced solid tumors (87). The exact mechanisms for involvement of liver tumor in increased CL of S-CKD602 are unknown, but it is possible that increased vascular permeability and enhanced activity of infiltrating macrophages in the liver may influence the biodistribution and CL of S-CKD-602 in patients with liver tumors (87). These findings may have implications in optimal dosing of PEGylated liposomal agents in patients, but further investigation is needed.

Treatment-Associated Factors. **Dose and schedule.** Dose- and schedule-dependent PK of Doxil has been reported in murine models. When the dose of Doxil was escalated from 2.5 to 20 mg/kg in tumor-bearing mice, a substantial delay in Doxil CL and a disproportional increase of the amount of Doxil accumulation in tumor were observed, indicating a saturation of MPS-mediated CL (88). In addition, when radiolabeled negatively-charged liposomes were injected into mice pretreated with Doxil, liver uptake of liposomes was reduced and liposome circulation time was greatly prolonged, suggesting a blockade of the MPS (88). This saturation of liposomal drug CL was specifically observed after Doxil administration, but not after administration of the same dose of free doxorubicin or similar phospholipid dose in drug-free liposomes (88). Repeated doses of Doxil also resulted in increase in the peak plasma concentration presumably due to saturation of the MPS-mediated Doxil CL (88).

Clinical pharmacokinetic analysis of Doxil has also suggested a dose-dependent PK due to saturation of MPS-mediated CL. In patients with Kaposi's sarcoma, there was a linear correlation between dose and AUC and half-lives of Doxil was reported be in the range of 50-55 hour for dose levels of 10-20 mg/m^2 (78). However, half-lives are increased to 60-80 hour for dose levels of 30-80 mg/m^2 in patients with solid tumors (36). In addition, the half-life is approximately 36 h in pediatric patients receiving 40-70 mg/m^2, which is significantly shorter than adults (89). Gabizon and colleagues also found that Doxil PK is cycle-dependent and prior exposure to Doxil may result in inhibition of MPS-mediated liposome CL (79). When comparing the 1st cycle to the 3rd cycle of PLD, there was a significant decrease in CL values and approximately 43% increase in dose-normalized exposure (AUC) (79). The half-life and Cmax/AUC ratio, a parameter for dose proportionality, showed a significant difference for repeated treatment cycles, indicating marked inhibition of Doxil CL (79). However, a doubling of dose did not affect the PK of Doxil. This may be attributed to the fact that Doxil-induced cytotoxicity to macrophages may be delayed (35, 38). The inhibition of Doxil CL may not be observed right after initial PLD administration due to several processes involved in the cellular internalization of PLD (e.g., Doxil uptake, liposome degradation, and intracellular release of doxorubicin); however, slower CL of liposomes can be manifested by delayed damage to the MPS upon repeated treatments (35, 79). In PK studies performed as part of phase I and II studies of Doxil in patients with solid tumors or Kaposi's sarcoma, patients with a decrease in monocyte count had a larger decrease in Doxil CL as compared with patients who had no change or an increase in monocyte count upon cycles of Doxil treatments (P=0.09) (80). Prior exposure to Doxil also influenced the exposure of S-CKD602 in patients with advanced malignancies (53).

PK studies of S-CKD602 revealed that patients receiving prior Doxil had a 2.2-fold higher exposure of S-CKD602 compared with patients not receiving PLD (P = 0.045) (53).

Drug-drug interaction. Drug-drug interactions were also reported for the PK of liposomal drugs. Pazopanib is a small-molecule inhibitor of vascular endothelial growth factor (VEGF) and platelet-derived growth factor (PDGF) receptors (90). The administration of Pazopanib every day for 8 days prior to Doxil treatment resulted in a significantly reduced penetration of Doxil from microvessels into tumor in mice bearing A549 human non-small cell lung cancer xenografts (90). However, no significant difference in doxorubicin concentration normalized by tumor weight between Pazopanib treated and control tumor was observed (90). The effect of Pazopanib on distribution of Doxil may be attributable to altered vessel permeability and oncotic pressure gradients which may play an important role in the liposomal drug delivery to tumor (15, 90). In addition, PK studies of Doxil, performed as part of a phase I study of Doxil and cisplatin combination therapy in patients with advanced malignancies, revealed that combination with cisplatin accelerated Doxil CL and reduced the incidence and severity of palmar-plantar erythrodysethesia (PPE, hand-foot syndrome) (91). By contrast, in another PK study as part of phase I studies of Doxil in combination with paclitaxel or docetaxel in patients with advanced malignancies, co-administration of paclitaxel significantly retarded the Doxil CL (92). Docetaxel reduced the CL of Doxil but to a lesser extent (92). The mechanisms for PK interactions between Doxil and other chemotherapies remain poorly understood, but are likely attributed to alteration of the MPS activity with other chemotherapies (91).

1.6. Factors Affecting the PD of Liposome-based Anticancer Therapeutics

Liposome drug delivery systems have been widely used to reduce the drug toxicity while improve or maintain the drug efficacy at the same time. Like conventional drugs, efficacy and toxicity of liposomal drugs can be accounted for to a great extent by its PK disposition. The factors that affect PK of liposomal drugs may also have an effect on PD of liposomal drugs.

Efficacy. The equivalent or improved efficacy of liposome-encapsulated drugs has been reported compared with their small molecule counterparts. In general, high tumor levels of a drug are highly correlated with enhanced antitumor activity. Thus, it is believed that prolonged circulation time and preferential accumulation of liposomal drugs in the tumor are attributed to improved therapeutic index profile of liposomally delivered drugs compared to conventional small molecules (2, 3, 10). However, tumor responses to liposomal drugs appear heterogeneous clinically. Patients with recurrent ovarian cancer or Kaposi's sarcoma receiving Doxil showed equivalent or significantly higher response rates and survival benefits with less toxic effects than patients receiving combination therapy with conventional chemotherapeutic agents (93, 94). However, in phase II and III trials of Doxil in patients with metastatic breast cancer, no evidence of survival advantage for Doxil treatment was demonstrated despite significant cardiotoxicity-reducing effects compared to free doxorubicin (95). There is no evidence to suggest clinical activity of Doxil in patients with colorectal cancer and other types of cancers (38, 96). Thus, different tumor types and the microenvironment may contribute to heterogeneous interaction between tumor cells and liposomal drugs leading to different drug release rate and antitumor activity.

In preclinical studies, antitumor activity of Doxil was dose-dependent due presumably to saturation of the MPS. Doxil was administered i.v. either with four doses of 2.5 mg/kg (days 7, 8,

10, and 11), or with one large dose of 10 mg/kg (day 9) (88). The single large dose showed superior advantages in median survival and tumor size inhibition to the multiple split doses (88). The dose-dependent antitumor activity may be attributable to dose-dependent blockade of MPS (i.e., Kupffer cells) and subsequent reduced clearance of Doxil (22, 23). The role of tumor-associated macrophages (TAMs) in the antitumor activity of Doxil was investigated in comparison with long-circulating liposome-encapsulating prednisolone phosphate in mice bearing B16. F10 melanoma (97). This study has suggested that the antitumor activity of Doxil was only partially attributed to suppressive effects on pro-angiogenic activities of TAMs and the main mechanism of action of Doxil may be cytotoxic effects on tumor cells (97).

The addition of regional hyperthermia has been shown to improve local efficacy of Doxil for the treatment of locally recurrent breast cancer (98). Patients treated with Doxil and radiation therapy were concurrently given hyperthermia therapy within 1-2 hour and 72 hours after Doxil infusion every 4 weeks for 6 months (98). All patients showed objective measurable response with 20% complete response rate. The benefits from hyperthermia may be attributable to increased liposome extravasation into the local tumor and enhanced release of doxorubicin from liposomes (98).

Lastly, family history of ovarian cancer was reported to be a factor that may be assoaicted with the efficacy of Doxil. The median time to progression was 11.5 months for high-risk patients versus 6.5 months for patients with sporadic cancer (P=0.0188) and the median overall survival for high-risk patients was 48.7 months compared with 16.2 months for the patients with sporadic cancer (P=0.0032) (99). However, high response rates in patients with hereditary ovarian cancer and mutations with *BRCA1* or *BRCA2* may be associated with a better response to

chemotherapy and larger clinical trials need to be performed to confirm the response to chemotherapy in patients with ovarian cancers associated with *BRCA1/2* mutations (99).

Toxicity. In general, toxicity related to entrapped drug is reduced when using liposomal delivery system due to limited accumulations of liposome in normal tissues with continuous and tight endothelium in the capillaries. However, liposome-based therapeutics can show altered toxicity profile compared to small molecule counterparts (38, 100, 101). Amphotericin B is a polyene antibiotic used in the treatment of systemic fungal infection. The use of non-liposomal amphotericin B is associated with extensive renal toxicity due to non-specific binding to the mammalian cell cholesterol (102). By contrast, liposome formulation of amphotericin B, AmBisome, reduces the renal and general toxicity of amphotericin B by reducing or bypassing the renal filtration of the drug (18, 25).

In addition, Doxil has a drastically different toxicity profile compared to doxorubicin, while efficacy of Doxil is equivalent or improved compared with non-liposomal counterpart (103). There is strong evidence that Doxil is associated with a reduced risk for developing cardiac toxicity, which is the major DLT of doxorubicin (25, 102, 103). Histologic examination of cardiac biopsies from patients who received cumulative doses of Doxil from 440 mg/m^2 to 840 mg/m^2, and had no prior exposure to anthracyclines, revealed significantly less cardiac toxicity than in matched doxorubicin controls ($P < 0.001$) (104). These results suggest that the decreased cardiotoxicity of Doxil may be due to reduced accumulation of doxorubicin in heart. However, new adverse effects, palmar-plantar erythrodysesthesia (PPE) (hand-foot syndrome) and stomatitis, are found to be the two major DLTs with Doxil (102, 25). The exact mechanisms for these toxicities remain poorly understood, but these toxicities were shown to be Doxil schedule-and dose-dependent (38, 79). Stomatitis usually occurs after the initial course of

treatment and increases in frequency and severity with higher doses (Cmax) (38). The relationship between PK of Doxil and PPE incidence was studied by Lyass et al. It was found that PPE incidence correlated with shorter dosing interval and prolonged half-life, but not with drug dose, maximum plasma concentration (Cmax), nor area under the concentration curve (AUC) (38, 91). It was also found that successive Doxil treatment significantly reduced the CL of Doxil leading to approximately 40% increase in AUC, which may explain a delayed occurrence of PPE along with slow release rate of doxorubicin from PEG-liposomes (38, 79). In addition, retrospective cohort studies have shown that there was a possible trend for decreasing PPE with increasing body mass index (BMI) (105). Doxil is generally well tolerated with improved safety profile compared to free doxorubicin. Proper dosing and monitoring may further enhance tolerability while preserving efficacy.

Preclinical studies have shown that administration of liposomal anticancer drug may induce transient depression of MPS activity. Liposome encapsulating doxorubicin exerted toxic effects on the liver macrophage population by impairing the phagocytic function and, subsequently, reducing the ability of colloid particle CL and bacterial CL (23, 106). PEGylated liposomal doxorubicin exhibited similar toxic effects on the liver macrophages but to a lesser extent (106). The toxic effects on hepatic macrophages may be correlated to saturation of MPS-mediated CL and schedule-dependent Doxil PK (38, 79). In addition to Doxil, our group showed toxic effects of S-CKD602 on circulating monocytes. In this study, the relationship between monocyte count and absolute neutrophil count (ANC) in the blood and PK disposition of S-CKD602 and non-liposomal CKD-602 (NL-CKD602) in patients were evaluated (107). For S-CKD602 in patients <60 years, the percent decrease in ANC and monocytes were 43 ± 31 and 58 ± 26%, respectively (P = 0.001). For S-CKD602 in patients ≥ 60, the percent decrease in ANC

and monocytes were 41 ± 31 and 45 ± 36%, respectively (P = 0.50). For NL-CKD602 (n = 42), the percent decrease in ANC and monocytes were similar (P > 0.05) (107). These findings suggest that monocytes are more sensitive to S-CKD602 as compared with neutrophils and that the increased sensitivity is related to the liposomal formulation and not the encapsulated CKD-602 (107). The relationship between changes in monocytes and the PK disposition of S-CKD602 also suggests that monocytes ingest liposomal anticancer agents which cause the release of CKD-602 from the liposome and toxicity to the monocytes (107).

Combination treatment of patients with locally recurrent or metastatic breast cancer (n = 39) using 10 mg/kg i.v. bevacizumab, a recombinant humanized monoclonal antibody for vascular endothelial growth factor –A, and 20 mg/m^2 i.v. Doxil once every 2 weeks resulted in the premature termination of a single-arm phase II trial because of higher incidence of mucositis and skin toxicities than anticipated (108). The most significant toxicity was grade 3 PPE that occurred in a high proportion of patients receiving combination therapy (41%), suggesting an additive toxic effect of the combination therapy of bevacizumab and Doxil (108). The proposed mechanisms for this synergistic toxicity include pharmacological interaction between Doxil and bevacizumab, direct effects of bevacizumab on the vasculature of affected tissues and resulting enhanced accumulation of Doxil, and bevacizumab-induced impairment of wound healing of dermal and mucosal injuries (108).

1.7. Perspective

Nanotechnology has revolutionized the drug delivery system for treatment of cancer by allowing for the enhanced delivery of a drug to the tumor via EPR effects. Among various NP platforms, liposomes have been most widely used as a NP drug carrier for cancer therapy.

Although liposome-based therapy provides several advantages over conventional medicines, high variation in PK and PD of liposome-based therapeutics has been reported. The understanding of effects of liposome characteristics on PK and PD of liposome-based therapeutics has been established; however, the interaction of liposomes-based therapeutics with the immune system *in vivo* and underlying molecular mechanisms for variable responses to liposomal drugs remain poorly understood. Two objectives are critical in optimizing the use of liposome-based therapeutics for the treatment of cancer: 1) improve understanding of biological interactions of liposomes with the immune system and 2) elucidate immune mechanisms underlying the variable responses to liposomal anticancer agents in animal models and in patients. To achieve these objectives, my dissertation research takes steps: to evaluate the relationship between PLD PK and chemokine ligands CCL2 and CCL5, key mediators for monocyte recruitment, *in vitro*, in animal models, and in patients with EOC (Specific Aim 1); to evaluate effects of the tumor microenvironment heterogeneity on tumor delivery and efficacy of PLD using murine mammary carcinoma models (Specific Aim 2); and to identify the quantitative trait loci associated with the variability in PLD PK using a panel of inbred mouse strains (Specific Aim 3). This dissertation research could have profound clinical implications, as it could reveal the role of immunological molecules, such as chemokine ligands CCL2 and CCL5, in regulating PK and PD of PLD and support the future exploration of these biomarkers as a factor for optimizing liposome-based therapy and other nanocarriers for the treatment of cancer and other diseases.

Specific Aims

Aim 1. Evaluate the relationship between chemokine ligands CCL2 and CCL5 and pharmacokinetics (PK) of PEGylated liposomal doxorubicin (PLD) *in vitro* systems, in preclinical mouse models, and in patients with recurrent ovarian cancer.

Hypothesis: High levels of chemokine will result in higher clearance of PLD; however, PLD exposure will affect the chemokine system and the mononuclear phagocyte system (MPS).

Aim 1A. Characterize the relationship between CCL2 and CCL5 and PK of PLD in patients with recurrent ovarian cancer.

Aim 1B. Evaluate effects of CCL2 and CCL5 on PK of PLD using mice bearing SKOV3 orthotopic ovarian xenografts and chemokine knockout mouse models.

Aim 1C. Determine effects of PLD on the chemotaxis of monocytes to CCL2 and CCL5 using human monocytic THP-1 cells.

Aim 2. Evaluate effects of the tumor microenvironment heterogeneity on tumor delivery and efficacy of PLD using murine mammary carcinoma models.

Hypothesis: Heterogeneity of the tumor microenvironment will affect the tumor delivery and efficacy of PLD.

Aim 2A. Evaluate effects of heterogeneous tumor microenvironment on PK of PLD in genetically engineered mouse models of breast cancer.

Aim 2B. Evaluate effects of heterogeneous tumor microenvironment on efficacy of PLD in genetically engineered mouse models of breast cancer.

Aim 3. Identify the quantitative trait loci associated with the variability in PK of PLD using a panel of inbred mouse strains.

Hypothesis: Quantitative trait loci (QTL) or genomic regions underlying the high variability in PK of PLD will be identified by genome-wide association analysis in a panel of inbred mouse strains.

Aim 3A. Evaluate the plasma disposition of PLD in a panel of inbred mouse strains.

Aim 3B. Identify the QTL by performing genome-wide association analysis to evaluate the genetic basis for the PK variability of PLD.

Table 1. 1. Clinically approved nanoparticle (NP)-based anticancer therapeutics

Composition	Trade name	Indication	Administration	Company
Liposomes and Lipidic Products				
Liposomal cytarabine	Depocyt	Malignant lymphomatous meningitis	i.v.	SkyePharma
Liposomal daunorubicin	DaunoXome	HIV-related Kaposi's sarcoma	i.v.	Gilead Sciences
Liposomal doxoruicin	Myocet	metastatic breast cancer	i.v.	Cephalon
PEGylated liposomal doxorubicin	Doxil/Caelyx	HIV-related Kaposi's sarcoma, metastatic breast cancer, refractory ovarian cancer	i.v.	Johnson & Johnson/Schering-Plough
Polymer Therapeutics				
Methoxy-PEG-poly ($_{D,L}$-lactide) taxol	Genexol-PM	Metastatic breast cancer	i.v.	Samyang
PEG-asparaginase	Oncaspar	Acute-lymphocytic leukemia (ALL)	i.v./i.m.	Enzon
PEG-hrGCSF	Neulasta	Chemotherapy-induced neutropenia	s.c.	Amgen
Other platforms				

Albumin-bound paclitaxel	Abraxane	Metastatic breast cancer	i.v.	Abraxis (Celgene)
^{90}Y-ibritumomab tiuxetan	Zevalin*	Non-Hodgkin lymphoma (NHL)	i.v.	Spectrum Pharmaceuticals
^{131}I-tositumomab	Bexxar*	NHL refractory to rituximab	i.v.	GSK

*Active targeting liposomes: Mouse anti-CD20 antibody-radioactive element conjugate.

HIV= human immunodeficiency virus. PEG= poly(ethylene)glycol.

Table 1. 2. Nanoparticle (NP)-based anticancer therapeutics in clinical trials

Composition	Product name	Indication	Administration	Stage	Company	Ref
Liposomes and Lipidic Products						
Vincristine sulfate	ONCO TCS	NHL	i.v.	Phase II/III	Inex/Enzon	109
cisplatin	LipoPlatin	NSCLC and pancreatic cancer	i.v.	Phase II/III	Regulon Inc.	110
Cytarabine and daunorubicin	CPX-351	AML and first relapse AML	i.v.	Phase II	Celator Pharma	111
Irinotecan and floxuridine	CPX-1	Colorectal cancer	i.v.	Phase II	Celator Pharm	112
Doxorubicin	Sarcodoxome	Advanced soft tissue sarcoma	i.v.	Phase I/II	GP Pharm	113
Annamycin	L-Annamycin	ALL/AML	i.v.	Phase I/II	Callisto Pharma Inc.	114
Temperature sensitive liposomal doxorubicin	ThermoDox	Hepatocellular carcinoma	i.v.	Phase III	Celsion	115
Polymer Therapeutics						
PEG-arginine deaminase	ADI-PEG 20	Hepatocellular carcinoma	i.v.	Phase I/II	Phoenix Pharmalogics-	116
Polymeric Drug Conjugates						

PEG-irinotecan	NKTR-102	Malignant solid tumors	i.v.	Phase II	Nektar	117
Polyacetal-camptothecin conjugate	XMT-1001	Various cancers	i.v.	Phase I	Mersna	118
Paclitaxel block copolymer micelle	NK 105	Breast cancer	i.v.	Phase III	NanoCarrier Co.-Nippon Kayaku Co	119
Gold coated silica	Auroshell	Refractory head and neck cancer	i.v.	Phase I	Nanospectra Biosciences	120
Albumin-bound rapamycin	ABI-009	Non-muscle invasive bladder cancer	i.v.	Phase I/II	Aadi, LLC	121
Antibody-Drug Conjugates						
Human mAb to GPnMB-auristatin conjugate	Glembatumumab vedotin* (CDX-011)	Metastatic breast cancer	i.v.	Phase II	Celldex Therapeutics	122

*Active targeting liposomes. ALL= acute-lymphocytic leukemia. AML= acute myeloid leukemia. NHL= non-hodgkin lymphoma. NSCC= non-small cell lung cancer. GPnMB= glycoprotein nonmetastatic melanoma protein B. PEG: poly(ethylene)glycol.

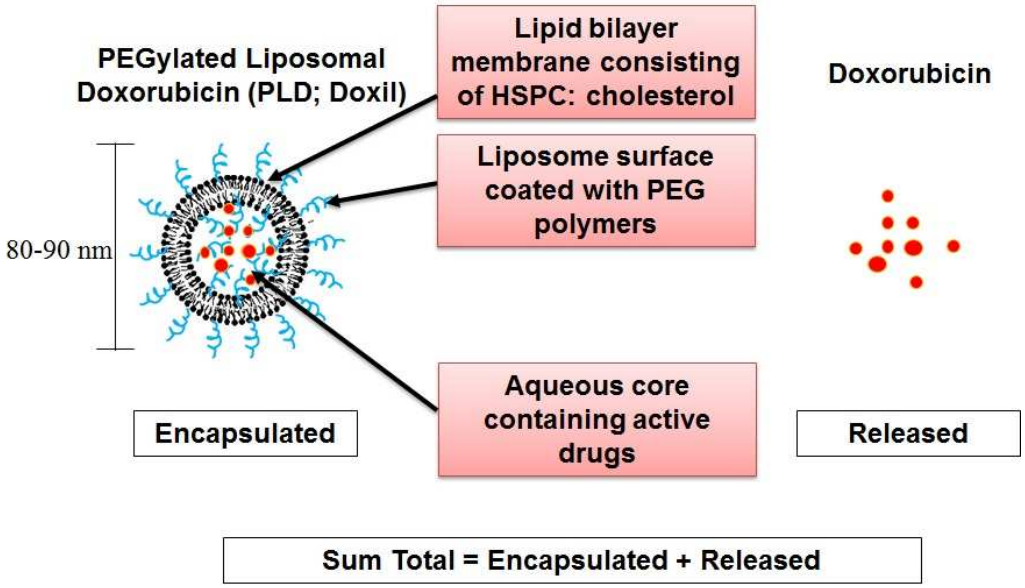

Fig. 1. 1. Schematic illustration of PEGylated liposomal doxorubicin (PLD; Doxil®) as an example of liposome-based anticancer therapeutics. A lipid bilayer membrane forms an internal aqueous compartment encapsulating doxorubicin (10,000-15,000 molecules per liposome) (36). Hydrophilic polymers, polyethylene glycol (PEG), are grafted into the liposome surface to provide resistance to protein adsorption and rapid clearance. The size of PLD is approximately 85 nm (36). Encapsulated: drugs within the liposome. Released: drugs released from the liposome. Sum total: encapsulated and released drug. HSPC= hydrogenated soy phosphatidylcholine.

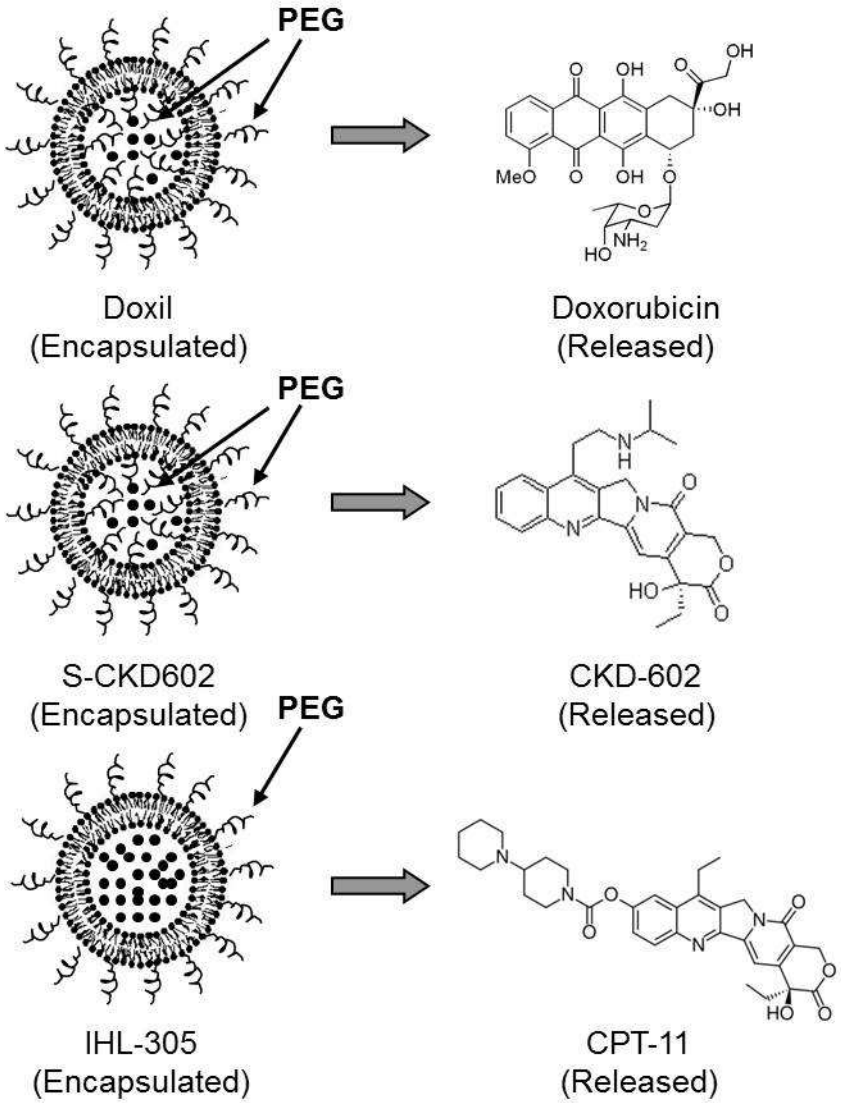

Fig. 1. 2. Structures of PEGylated Liposomes. PEG tether are projected on both the inside and outside of liposome for Doxil and S-CKD602. PEG tether are only localized on the outside of liposome for IHL-305 (15).

REFERENCES

(1) Wang J, Sui M, Fan W. Nanoparticles for tumor targeted therapies and their pharmacokinetics. Curr Drug Metab 2010;11(2):129-141.

(2) Drummond DC, Noble CO, Hayes ME, Park JW, Kirpotin DB. Pharmacokinetics and in vivo drug release rates in liposomal nanocarrier development. J Pharm Sci 2008;97(11):4696-4740.

(3) Zamboni WC. Liposomal, nanoparticle, and conjugated formulations of anticancer agents. Clinical cancer research 2005;11(23):8230-8234.

(4) Davis ME. Nanoparticle therapeutics: an emerging treatment modality for cancer. Nature Reviews Drug Discovery 2008;7(9):771-782.

(5) Peer D, Karp JM, Hong S, Farokhzad OC, Margalit R, Langer R. Nanocarriers as an emerging platform for cancer therapy. Nature nanotechnology 2007;2(12):751-760.

(6) Maeda H, Wu J, Sawa T, Matsumura Y, Hori K. Tumor vascular permeability and the EPR effect in macromolecular therapeutics: a review. J Controlled Release 2000;65(1):271-284.

(7) Fukumura D, Jain RK. Tumor microenvironment abnormalities: causes, consequences, and strategies to normalize. J Cell Biochem 2007;101(4):937-949.

(8) Liu D, Mori A, Huang L. Role of liposome size and RES blockade in controlling biodistribution and tumor uptake of GM1-containing liposomes. Biochimica et Biophysica Acta (BBA)-Biomembranes 1992;1104(1):95-101.

(9) Torchilin VP, Lukyanov AN, Gao Z, Papahadjopoulos-Sternberg B. Immunomicelles: targeted pharmaceutical carriers for poorly soluble drugs. Proc Natl Acad Sci U S A 2003 May 13;100(10):6039-6044.

(10) Li S, Huang L. Pharmacokinetics and biodistribution of nanoparticles. Molecular pharmaceutics 2008;5(4):496-504.

(11) Hillaireau H, Couvreur P. Nanocarriers' entry into the cell: relevance to drug delivery. Cellular and Molecular Life Sciences 2009;66(17):2873-2896.

(12) Ritschel WA, Kearns GL. Handbook of basic pharmacokinetics--including clinical applications. : American Pharmacists Association Washington, DC; 2004.

(13) Choi HS, Liu W, Misra P, Tanaka E, Zimmer JP, Ipe BI, et al. Renal clearance of quantum dots. Nat Biotechnol 2007;25(10):1165-1170.

(14) Zamboni WC. Concept and clinical evaluation of carrier-mediated anticancer agents. Oncologist 2008;13(3):248-260.

(15) Song G, Wu H, Yoshino K, Zamboni WC. Factors affecting the pharmacokinetics and pharmacodynamics of liposomal drugs. J Liposome Res 2012;22(3):177-192.

(16) Hashida M, Opanasopit P, Nishikawa M. Factors affecting drug and gene delivery: effects of interaction with blood components. Critical Reviews™ in Therapeutic Drug Carrier Systems 2002;19(3).

(17) Owens III DE, Peppas NA. Opsonization, biodistribution, and pharmacokinetics of polymeric nanoparticles. Int J Pharm 2006;307(1):93-102.

(18) Bertrand N, Leroux J. The journey of a drug-carrier in the body: an anatomo-physiological perspective. J Controlled Release 2012;161(2):152-163.

(19) Murray PJ, Wynn TA. Protective and pathogenic functions of macrophage subsets. Nature Reviews Immunology 2011;11(11):723-737.

(20) Wisse E, Jacobs F, Topal B, Frederik P, De Geest B. The size of endothelial fenestrae in human liver sinusoids: implications for hepatocyte-directed gene transfer. Gene Ther 2008;15(17):1193-1199.

(21) Oja CD, Semple SC, Chonn A, Cullis PR. Influence of dose on liposome clearance: critical role of blood proteins. Biochimica et Biophysica Acta (BBA)-Biomembranes 1996;1281(1):31-37.

(22) Harashima H, Sakata K, Kiwada H. Distinction between the depletion of opsonins and the saturation of uptake in the dose-dependent hepatic uptake of liposomes. Pharm Res 1993;10(4):606-610.

(23) Daemen T, Hofstede G, Ten Kate MT, Bakker-Woudenberg IA, Scherphof GL. Liposomal doxorubicin-induced toxicity: Depletion and impairment of phagocytic activity of liver macrophages. International journal of cancer 1995;61(5):716-721.

(24) Moghimi SM, Hunter AC, Murray JC. Long-circulating and target-specific nanoparticles: theory to practice. Pharmacol Rev 2001;53(2):283-318.

(25) Allen T, Hansen C. Pharmacokinetics of stealth versus conventional liposomes: effect of dose. Biochimica et Biophysica Acta (BBA)-Biomembranes 1991;1068(2):133-141.

(26) Ishihara T, Takeda M, Sakamoto H, Kimoto A, Kobayashi C, Takasaki N, et al. Accelerated blood clearance phenomenon upon repeated injection of PEG-modified PLA-nanoparticles. Pharm Res 2009;26(10):2270-2279.

(27) Ishida T, Atobe K, Wang X, Kiwada H. Accelerated blood clearance of PEGylated liposomes upon repeated injections: effect of doxorubicin-encapsulation and high-dose first injection. J Controlled Release 2006;115(3):251-258.

(28) Jain RK, Stylianopoulos T. Delivering nanomedicine to solid tumors. Nature Reviews Clinical Oncology 2010;7(11):653-664.

(29) Mukherjee S, Ghosh RN, Maxfield FR. Endocytosis. Physiol Rev 1997 Jul;77(3):759-803.

(30) Bareford LM, Swaan PW. Endocytic mechanisms for targeted drug delivery. Adv Drug Deliv Rev 2007;59(8):748-758.

(31) Conner SD, Schmid SL. Regulated portals of entry into the cell. Nature 2003;422(6927):37-44.

(32) Swanson JA, Watts C. Macropinocytosis. Trends Cell Biol 1995;5(11):424-428.

(33) Mayor S, Pagano RE. Pathways of clathrin-independent endocytosis. Nature reviews Molecular cell biology 2007;8(8):603-612.

(34) Laginha KM, Verwoert S, Charrois GJ, Allen TM. Determination of doxorubicin levels in whole tumor and tumor nuclei in murine breast cancer tumors. Clin Cancer Res 2005 Oct 1;11(19 Pt 1):6944-6949.

(35) Charrois GJ, Allen TM. Drug release rate influences the pharmacokinetics, biodistribution, therapeutic activity, and toxicity of pegylated liposomal doxorubicin formulations in murine breast cancer. Biochimica et Biophysica Acta (BBA)-Biomembranes 2004;1663(1):167-177.

(36) Gabizon A, Shmeeda H, Barenholz Y. Pharmacokinetics of pegylated liposomal doxorubicin. Clin Pharmacokinet 2003;42(5):419-436.

(37) Fahr A, Van Hoogevest P, Kuntsche J, Leigh ML. Lipophilic drug transfer between liposomal and biological membranes: what does it mean for parenteral and oral drug delivery? J Liposome Res 2006;16(3):281-301.

(38) Solomon R, Gabizon AA. Clinical pharmacology of liposomal anthracyclines: focus on pegylated liposomal Doxorubicin. Clinical Lymphoma and Myeloma 2008;8(1):21-32.

(39) Drummond DC, Noble CO, Guo Z, Hong K, Park JW, Kirpotin DB. Development of a highly active nanoliposomal irinotecan using a novel intraliposomal stabilization strategy. Cancer Res 2006 Mar 15;66(6):3271-3277.

(40) Webb MS, Harasym TO, Masin D, Bally MB, Mayer LD. Sphingomyelin-cholesterol liposomes significantly enhance the pharmacokinetic and therapeutic properties of vincristine in murine and human tumour models. Br J Cancer 1995 Oct;72(4):896-904.

(41) Zamboni WC, Gervais AC, Egorin MJ, Schellens JH, Zuhowski EG, Pluim D, et al. Systemic and tumor disposition of platinum after administration of cisplatin or STEALTH liposomal-cisplatin formulations (SPI-077 and SPI-077 B103) in a preclinical tumor model of melanoma. Cancer Chemother Pharmacol 2004;53(4):329-336.

(42) Lim HJ, Masin D, Madden TD, Bally MB. Influence of drug release characteristics on the therapeutic activity of liposomal mitoxantrone. J Pharmacol Exp Ther 1997 Apr;281(1):566-573.

(43) Theodoulou M, Hudis C. Cardiac profiles of liposomal anthracyclines. Cancer 2004;100(10):2052-2063.

(44) Gabizon A, Shiota R, Papahadjopoulos D. Pharmacokinetics and tissue distribution of doxorubicin encapsulated in stable liposomes with long circulation times. J Natl Cancer Inst 1989 Oct 4;81(19):1484-1488.

(45) Bally MB, Nayar R, Masin D, Cullis PR, Mayer LD. Studies on the myelosuppressive activity of doxorubicin entrapped in liposomes. Cancer Chemother Pharmacol 1990;27(1):13-19.

(46) Charrois GJ, Allen TM. Rate of biodistribution of STEALTH® liposomes to tumor and skin: influence of liposome diameter and implications for toxicity and therapeutic activity. Biochimica et Biophysica Acta (BBA)-Biomembranes 2003;1609(1):102-108.

(47) Shin J, Shum P, Thompson DH. Acid-triggered release via dePEGylation of DOPE liposomes containing acid-labile vinyl ether PEG–lipids. J Controlled Release 2003;91(1):187-200.

(48) Collins D, Huang L. Cytotoxicity of diphtheria toxin A fragment to toxin-resistant murine cells delivered by pH-sensitive immunoliposomes. Cancer Res 1987 Feb 1;47(3):735-739.

(49) Lindner LH, Hossann M. Factors affecting drug release from liposomes. Curr Opin Drug Discov Devel 2010 Jan;13(1):111-123.

(50) Dromi S, Frenkel V, Luk A, Traughber B, Angstadt M, Bur M, et al. Pulsed-high intensity focused ultrasound and low temperature-sensitive liposomes for enhanced targeted drug delivery and antitumor effect. Clin Cancer Res 2007 May 1;13(9):2722-2727.

(51) Andresen TL, Jensen SS, Jørgensen K. Advanced strategies in liposomal cancer therapy: problems and prospects of active and tumor specific drug release. Prog Lipid Res 2005;44(1):68-97.

(52) Schell RF, Sidone BJ, Caron WP, Walsh MD, Zamboni BA, Ramanathan RK, et al. Meta-analysis of inter-patient pharmacokinetic variability of liposomal and non-liposomal anticancer agents. Nanomedicine: Nanotechnology, Biology and Medicine 2013.

(53) Zamboni WC, Ramalingam S, Friedland DM, Edwards RP, Stoller RG, Strychor S, et al. Phase I and pharmacokinetic study of pegylated liposomal CKD-602 in patients with advanced malignancies. Clinical Cancer Research 2009;15(4):1466-1472.

(54) Igarashi E. Factors affecting toxicity and efficacy of polymeric nanomedicines. Toxicol Appl Pharmacol 2008;229(1):121-134.

(55) Epstein-Barash H, Gutman D, Markovsky E, Mishan-Eisenberg G, Koroukhov N, Szebeni J, et al. Physicochemical parameters affecting liposomal bisphosphonates bioactivity for restenosis therapy: internalization, cell inhibition, activation of cytokines and complement, and mechanism of cell death. J Controlled Release 2010;146(2):182-195.

(56) Noguchi Y, Wu J, Duncan R, Strohalm J, Ulbrich K, Akaike T, et al. Early phase tumor accumulation of macromolecules: a great difference in clearance rate between tumor and normal tissues. Cancer Science 1998;89(3):307-314.

(57) Petros RA, DeSimone JM. Strategies in the design of nanoparticles for therapeutic applications. Nature Reviews Drug Discovery 2010;9(8):615-627.

(58) Drummond DC, Meyer O, Hong K, Kirpotin DB, Papahadjopoulos D. Optimizing liposomes for delivery of chemotherapeutic agents to solid tumors. Pharmacol Rev 1999 Dec;51(4):691-743.

(59) Chonn A, Semple SC, Cullis PR. Association of blood proteins with large unilamellar liposomes in vivo. Relation to circulation lifetimes. J Biol Chem 1992 Sep 15;267(26):18759-18765.

(60) Gregoriadis G, Senior J. Control of fate and behaviour of liposomes in vivo. Prog Clin Biol Res 1982;102 pt A:263-279.

(61) Schmitt-Sody M, Strieth S, Krasnici S, Sauer B, Schulze B, Teifel M, et al. Neovascular targeting therapy: paclitaxel encapsulated in cationic liposomes improves antitumoral efficacy. Clin Cancer Res 2003 Jun;9(6):2335-2341.

(62) Campbell RB, Fukumura D, Brown EB, Mazzola LM, Izumi Y, Jain RK, et al. Cationic charge determines the distribution of liposomes between the vascular and extravascular compartments of tumors. Cancer Res 2002 Dec 1;62(23):6831-6836.

(63) Scheule RK, George JAS, Bagley RG, Marshall J, Kaplan JM, Akita GY, et al. Basis of pulmonary toxicity associated with cationic lipid-mediated gene transfer to the mammalian lung. Hum Gene Ther 1997;8(6):689-707.

(64) Torchilin VP, Shtilman MI, Trubetskoy VS, Whiteman K, Milstein AM. Amphiphilic vinyl polymers effectively prolong liposome circulation time in vivo. Biochimica et Biophysica Acta (BBA)-Biomembranes 1994;1195(1):181-184.

(65) Woodle MC, Lasic DD. Sterically stabilized liposomes. Biochimica et Biophysica Acta (BBA)-Reviews on Biomembranes 1992;1113(2):171-199.

(66) Owens III DE, Peppas NA. Opsonization, biodistribution, and pharmacokinetics of polymeric nanoparticles. Int J Pharm 2006;307(1):93-102.

(67) Hamad I, Al-Hanbali O, Hunter AC, Rutt KJ, Andresen TL, Moghimi SM. Distinct polymer architecture mediates switching of complement activation pathways at the nanosphere− serum interface: implications for stealth nanoparticle engineering. ACS nano 2010;4(11):6629-6638.

(68) Hamad I, Hunter A, Szebeni J, Moghimi SM. Poly (ethylene glycol) s generate complement activation products in human serum through increased alternative pathway turnover and a MASP-2-dependent process. Mol Immunol 2008;46(2):225-232.

(69) Moghimi S, Szebeni J. Stealth liposomes and long circulating nanoparticles: critical issues in pharmacokinetics, opsonization and protein-binding properties. Prog Lipid Res 2003;42(6):463-478.

(70) Wu H, Infante JR, Keedy VL, Jones SF, Chan E, Bendell JC, et al. Population pharmacokinetics of PEGylated liposomal CPT-11 (IHL-305) in patients with advanced solid tumors. Eur J Clin Pharmacol 2013;69(12):2073-2081.

(71) Hempel G, Reinhardt D, Creutzig U, Boos J. Population pharmacokinetics of liposomal daunorubicin in children. Br J Clin Pharmacol 2003;56(4):370-377.

(72) Torchilin V, Levchenko T, Whiteman K, Yaroslavov A, Tsatsakis A, Rizos A, et al. Amphiphilic poly-< i> N</i>-vinylpyrrolidones:: synthesis, properties and liposome surface modification. Biomaterials 2001;22(22):3035-3044.

(73) Whiteman K, Subr V, Ulbrich K, Torchilin V. Poly (HPMA)-coated liposomes demonstrate prolonged circulation in mice. J Liposome Res 2001;11(2-3):153-164.

(74) Metselaar JM, Bruin P, de Boer LW, de Vringer T, Snel C, Oussoren C, et al. A novel family of L-amino acid-based biodegradable polymer-lipid conjugates for the development of long-circulating liposomes with effective drug-targeting capacity. Bioconjug Chem 2003;14(6):1156-1164.

(75) Papahadjopoulos D, Allen TM, Gabizon A, Mayhew E, Matthay K, Huang SK, et al. Sterically stabilized liposomes: improvements in pharmacokinetics and antitumor therapeutic efficacy. Proc Natl Acad Sci U S A 1991 Dec 15;88(24):11460-11464.

(76) Parodi A, Quattrocchi N, van de Ven, Anne L, Chiappini C, Evangelopoulos M, Martinez JO, et al. Synthetic nanoparticles functionalized with biomimetic leukocyte membranes possess cell-like functions. Nature nanotechnology 2013;8(1):61-68.

(77) Rodriguez PL, Harada T, Christian DA, Pantano DA, Tsai RK, Discher DE. Minimal" Self" Peptides That Inhibit Phagocytic Clearance and Enhance Delivery of Nanoparticles. Science 2013;339(6122):971-975.

(78) Amantea MA, Forrest A, Northfelt DW, Mamelok R. Population pharmacokinetics and pharmacodynamics of pegylated-liposomal doxorubicin in patients with AIDS-related Kaposi's sarcoma. Clinical Pharmacology & Therapeutics 1997;61(3):301-311.

(79) Gabizon A, Isacson R, Rosengarten O, Tzemach D, Shmeeda H, Sapir R. An open-label study to evaluate dose and cycle dependence of the pharmacokinetics of pegylated liposomal doxorubicin. Cancer Chemother Pharmacol 2008;61(4):695-702.

(80) La-Beck NM, Zamboni BA, Gabizon A, Schmeeda H, Amantea M, Gehrig PA, et al. Factors affecting the pharmacokinetics of pegylated liposomal doxorubicin in patients. Cancer Chemother Pharmacol 2012;69(1):43-50.

(81) La-Beck NM, et al. The evaluation of gender on the pharmacokinetics (PK) of pegylated liposomal anticancer agents. American Society of Clinical Oncology Annual Meeting. J Clin Oncol; 2010.

(82) Song G, Wu H, La-Beck NM, Zamboni BA, Strychor S, Zamboni WC. Effect of gender on pharmacokinetic disposition of Pegylated liposomal CKD-602 (S-CKD602) and optisomal topotecan (TLI) in rats. AACR; 2010.

(83) Gordon S, Taylor PR. Monocyte and macrophage heterogeneity. Nature Reviews Immunology 2005;5(12):953-964.

(84) Chawla A, Nguyen KD, Goh YS. Macrophage-mediated inflammation in metabolic disease. Nature Reviews Immunology 2011;11(11):738-749.

(85) Prabhakar U, Maeda H, Jain RK, Sevick-Muraca EM, Zamboni W, Farokhzad OC, et al. Challenges and Key Considerations of the Enhanced Permeability and Retention Effect for Nanomedicine Drug Delivery in Oncology. Cancer Res 2013;73(8):2412-2417.

(86) Caron WP, Lay JC, Fong AM, La-Beck NM, Kumar P, Newman SE, et al. Translational Studies of Phenotypic Probes for the Mononuclear Phagocyte System and Liposomal Pharmacology. J Pharmacol Exp Ther 2013:jpet. 113.208801.

(87) Wu H, Ramanathan RK, Zamboni BA, Strychor S, Ramalingam S, Edwards RP, et al. Population Pharmacokinetics of Pegylated Liposomal CKD-602 (S-CKD602) in Patients With Advanced Malignancies. The Journal of Clinical Pharmacology 2012;52(2):180-194.

(88) Gabizon A, Tzemach D, Mak L, Bronstein M, Horowitz AT. Dose dependency of pharmacokinetics and therapeutic efficacy of pegylated liposomal doxorubicin (DOXIL) in murine models. J Drug Target 2002;10(7):539-548.

(89) Marina NM, Cochrane D, Harney E, Zomorodi K, Blaney S, Winick N, et al. Dose escalation and pharmacokinetics of pegylated liposomal doxorubicin (Doxil) in children with solid tumors: a pediatric oncology group study. Clin Cancer Res 2002 Feb;8(2):413-418.

(90) Tailor TD, Hanna G, Yarmolenko PS, Dreher MR, Betof AS, Nixon AB, et al. Effect of pazopanib on tumor microenvironment and liposome delivery. Mol Cancer Ther 2010 Jun;9(6):1798-1808.

(91) Lyass O, Hubert A, Gabizon AA. Phase I study of doxil-cisplatin combination chemotherapy in patients with advanced malignancies. Clin Cancer Res 2001 Oct;7(10):3040-3046.

(92) Briasoulis E, Karavasilis V, Tzamakou E, Rammou D, Soulti K, Piperidou C, et al. Interaction pharmacokinetics of pegylated liposomal doxorubicin (Caelyx) on coadministration with paclitaxel or docetaxel. Cancer Chemother Pharmacol 2004;53(5):452-457.

(93) Use of liposomal anthracyclines in Kaposi's sarcoma. Seminars in oncology: Elsevier; 2004.

(94) Gordon AN, Fleagle JT, Guthrie D, Parkin DE, Gore ME, Lacave AJ. Recurrent epithelial ovarian carcinoma: a randomized phase III study of pegylated liposomal doxorubicin versus topotecan. J Clin Oncol 2001 Jul 15;19(14):3312-3322.

(95) O'brien M, Wigler N, Inbar M, Rosso R, Grischke E, Santoro A, et al. Reduced cardiotoxicity and comparable efficacy in a phase III trial of pegylated liposomal doxorubicin HCl (CAELYX™/Doxil®) versus conventional doxorubicin for first-line treatment of metastatic breast cancer. Annals of oncology 2004;15(3):440-449.

(96) Shields AF, Lange LM, Zalupski MM. Phase II study of liposomal doxorubicin in patients with advanced colorectal cancer. American journal of clinical oncology 2001;24(1):96-98.

(97) Banciu M, Schiffelers RM, Storm G. Investigation into the role of tumor-associated macrophages in the antitumor activity of Doxil. Pharm Res 2008;25(8):1948-1955.

(98) Kouloulias VE, Dardoufas CE, Kouvaris JR, Gennatas CS, Polyzos AK, Gogas HJ, et al. Liposomal doxorubicin in conjunction with reirradiation and local hyperthermia treatment in recurrent breast cancer: a phase I/II trial. Clin Cancer Res 2002 Feb;8(2):374-382.

(99) Nicoletto MO, Bertorelle R, Borgato L, De Salvo GL, Artioli G, Lombardi G, et al. Family history of cancer rather than p53 status predicts efficacy of pegylated liposomal doxorubicin and oxaliplatin in relapsed ovarian cancer. Int J Gynecol Cancer 2009 Aug;19(6):1022-1028.

(100) Uziely B, Jeffers S, Isacson R, Kutsch K, Wei-Tsao D, Yehoshua Z, et al. Liposomal doxorubicin: antitumor activity and unique toxicities during two complementary phase I studies. J Clin Oncol 1995 Jul;13(7):1777-1785.

(101) Muggia FM, Hainsworth JD, Jeffers S, Miller P, Groshen S, Tan M, et al. Phase II study of liposomal doxorubicin in refractory ovarian cancer: antitumor activity and toxicity modification by liposomal encapsulation. J Clin Oncol 1997 Mar;15(3):987-993.

(102) Laniado-Laborín R, Cabrales-Vargas MN. Amphotericin B: side effects and toxicity. Revista iberoamericana de micología 2009;26(4):223-227.

(103) Safra T, Muggia F, Jeffers S, Tsao-Wei DD, Groshen S, Lyass O, et al. Pegylated liposomal doxorubicin (doxil): reduced clinical cardiotoxicity in patients reaching or exceeding cumulative doses of 500 mg/m2. Ann Oncol 2000 Aug;11(8):1029-1033.

(104) Berry G, Billingham M, Alderman E, Richardson P, Torti F, Lum B, et al. The use of cardiac biopsy to demonstrate reduced cardiotoxicity in AIDS Kaposi's sarcoma patients treated with pegylated liposomal doxorubicin. Ann Oncol 1998 Jul;9(7):711-716.

(105) Ko EM, Lippmann Q, Caron WP, Zamboni W, Gehrig PA. Clinical risk factors of PEGylated liposomal doxorubicin induced palmar plantar erythrodysesthesia in recurrent ovarian cancer patients. Gynecol Oncol 2013;131(3):683-688.

(106) Storm G, ten Kate MT, Working PK, Bakker-Woudenberg IA. Doxorubicin entrapped in sterically stabilized liposomes: effects on bacterial blood clearance capacity of the mononuclear phagocyte system. Clin Cancer Res 1998 Jan;4(1):111-115.

(107) Zamboni WC, Maruca LJ, Strychor S, Zamboni BA, Ramalingam S, Edwards RP, et al. Bidirectional pharmacodynamic interaction between pegylated liposomal CKD-602 (S-CKD602) and monocytes in patients with refractory solid tumors. J Liposome Res 2011;21(2):158-165.

(108) Rochlitz C, Ruhstaller T, Lerch S, Spirig C, Huober J, Suter T, et al. Combination of bevacizumab and 2-weekly pegylated liposomal doxorubicin as first-line therapy for locally recurrent or metastatic breast cancer. A multicenter, single-arm phase II trial (SAKK 24/06). Ann Oncol 2011 Jan;22(1):80-85.

(109) Sarris AH, Hagemeister F, Romaguera J, Rodriguez MA, McLaughlin P, Tsimberidou AM, et al. Liposomal vincristine in relapsed non-Hodgkin's lymphomas: early results of an ongoing phase II trial. Ann Oncol 2000 Jan;11(1):69-72.

(110) Mylonakis N, Athanasiou A, Ziras N, Angel J, Rapti A, Lampaki S, et al. Phase II study of liposomal cisplatin (Lipoplatin™) plus gemcitabine versus cisplatin plus gemcitabine as first line treatment in inoperable (stage IIIB/IV) non-small cell lung cancer. Lung Cancer 2010;68(2):240-247.

(111) Feldman EJ, Lancet JE, Kolitz JE, Ritchie EK, Roboz GJ, List AF, et al. First-in-man study of CPX-351: a liposomal carrier containing cytarabine and daunorubicin in a fixed 5:1 molar ratio for the treatment of relapsed and refractory acute myeloid leukemia. J Clin Oncol 2011 Mar 10;29(8):979-985.

(112) Batist G, Gelmon KA, Chi KN, Miller WH,Jr, Chia SK, Mayer LD, et al. Safety, pharmacokinetics, and efficacy of CPX-1 liposome injection in patients with advanced solid tumors. Clin Cancer Res 2009 Jan 15;15(2):692-700.

(113) Gentile E, Cilurzo F, Di Marzio L, Carafa M, Anna Ventura C, Wolfram J, et al. Liposomal chemotherapeutics. Future Oncology 2013;9(12):1849-1859.

(114) Booser DJ, Esteva FJ, Rivera E, Valero V, Esparza-Guerra L, Priebe W, et al. Phase II study of liposomal annamycin in the treatment of doxorubicin-resistant breast cancer. Cancer Chemother Pharmacol 2002;50(1):6-8.

(115) Tak W, Lin S, Wang Y, Zheng J, Izzo F, Park S, et al. Phase 3, randomized, double-blind, dummy-controlled, trial of radiofrequency ablation (RFA) lyso-thermosensitive liposomal doxorubicin (LTLD, Thermodox), for hepatocellular carcinoma (HCC) lesions 3-7 cm. Final program & book of abstracts 2014:16-16.

(116) Yang T, Lu S, Chao Y, Sheen I, Lin C, Wang T, et al. A randomised phase II study of pegylated arginine deiminase (ADI-PEG 20) in Asian advanced hepatocellular carcinoma patients. Br J Cancer 2010;103(7):954-960.

(117) Vergote I, Micha J, Pippitt C, Garcia A, Maslyar D. Phase II study of NKTR-102 in women with platinum-resistant/refractory ovarian cancer. J Clin Oncol 2010;28:5013

(118) Sausville E, Garbo L, Weiss G, Shkolny D, Yurkovetskiy A, Bethune C, et al. Phase I study of XMT-1001 given IV every 3 weeks to patients with advanced solid tumors. J Clin Oncol 2010;28:13121.

(119) Kato K, Chin K, Yoshikawa T, Yamaguchi K, Tsuji Y, Esaki T, et al. Phase II study of NK105, a paclitaxel-incorporating micellar nanoparticle, for previously treated advanced or recurrent gastric cancer. Invest New Drugs 2012;30(4):1621-1627.

(120) Bawa R. Nanoparticle-based therapeutics in humans: a survey. Nanotech.L.& Bus. 2008;5:135.

(121) Ledet G, Mandal TK. Nanomedicine: Emerging therapeutics for the 21st century. US pharm 2012;37(3):7-11.

(122) Yardley D, Weaver R, Melisko M, Saleh M, Arena F, Forero A, et al. A randomized phase 2 study of the antibody-drug conjugate CDX-011 in advanced GPNMB-overexpressing breast cancer: The EMERGE study. Cancer Res 2012;72(24s3):P6-10.

CHAPTER 2:

RELATIONSHIP BETWEEN CHEMOKINE LIGANDS CCL2 AND CCL5 AND THE PHARMACOKINETICS OF PEGYLATED LIPOSOMAL DOXORUBICIN[2]

Overview

Chemokines play a central role in recruitment of macrophages into tumors. Nanoparticles (NPs) are recognized and cleared by circulating monocytes and tissue macrophages. However, it remains uncertain whether chemokines influence the pharmacokinetics (PK) of NP-based therapy, such as PEGylated liposomal doxorubicin (PLD; Doxil). In patients with refractory epithelial ovarian cancer (EOC), we found that there was a significantly positive linear relationship between plasma encapsulated liposomal doxorubicin exposure and the total amount of CCL2 and CCL5, the two most abundant chemokines, secreted in plasma after PLD administration. PLD induced CCL2 secretion in tumors from mice bearing SKOV3 orthotopic ovarian cancer xenografts and altered the migration of human monocytic THP-1 cells to CCL2 and CCL5, which may in turn affect the disposition of PLD via a feedback loop. These data implicate the important role for chemokines CCL2 and CCL5 in optimizing PLD therapy for the treatment of EOC and other malignancies.

2. 1. Introduction

Nanotechnology has made significant advances in the drug delivery system for the treatment of solid tumors (1, 2). Abnormal blood and lymphatic vasculature have enabled

[2]This chapter will be submitted to the *Clinical Cancer Research* and is presented in the style of the journal.

selective delivery and accumulation of nanoparticles (NPs) in tumors through the enhanced permeability and retention (EPR) effect (3). Nanomedicines have advantages over conventional medicines including prolonged circulation time, selective delivery of entrapped drug to tumors, and improved therapeutic index (1-3). There have been great endeavors from the private-public partnerships, such as the Alliance for Nanotechnology in Cancer, in advancing nanotechnology for the diagnosis, imaging, and treatment of cancer (4). However, so far, there are limited numbers of NPs that have translated to clinical successes due to variations in the pharmacokinetics (PK) and pharmacodynamics (PD) (i.e., therapeutic outcomes) (4, 5).

PEGylated liposomal doxorubicin (PLD; Doxil®) is one of the few FDA-approved NP agents for the treatment of refractory ovarian cancer (6). However, significant variability in the PK of PLD has been reported in preclinical models and patients and its use as second-line treatment of platinum and taxane-refractory ovarian cancer has only achieved response rates of 14% to 20% as a single agent (7, 8). PLD has also been used for the treatment of metastatic breast cancer; however, in a phase III trial where cardiotoxicity and efficacy of PLD was evaluated compared with free doxorubicin for first-line treatment of metastatic breast cancer, the overall survival of PLD was not superior to that of doxorubicin despite significantly reducing effects on cardiotoxicity (9). The mechanism underlying the high PK variability and the modest impacts on overall survival of PLD remains poorly understood, but likely involves the mononuclear phagocyte system (MPS) (10-12).

NPs are removed from the circulation by the cells of the MPS, circulating monocytes and tissue macrophages (i.e., Kupffer cells and splenic macrophages) (13, 14). Once a NP enters the bloodstream, the adsorption of immunoglobulin or complement proteins to the particle surface, called opsonization, occurs (14). The modification of the surface characteristics of the particles

leads to recognition and clearance of NPs by macrophages via phagocytosis (13, 14). The liver and spleen are the major parts of the MPS and play a key role in NP removal and clearance (13-15). In addition, the tumor microenvironment is comprised of abundant infiltrating macrophages, called tumor-associated macrophages (TAMs) (16, 17). Homeostatic circulation and induced infiltration of monocytes and macrophages into these tissues are orchestrated by an intricate network of chemokines (16, 18, 19).

Chemokines are chemotactic cytokines that cause the directed migration of monocytes and stimulate the differentiation into macrophages (18, 19). Mobilization of cells that express the cognate receptor occurs along the chemokine gradient, leading to cell movement towards high local chemokine concentrations (18, 19). Of approximately 50 known chemokines, CC chemokine ligand (CCL) 2, also known as monocyte chemoattractant protein-1 (MCP-1), is overexpressed in human ovarian and breast tumors and correlates with the accumulation of TAMs (20-23). CCL2, secreted by both malignant and stromal cells, has autocrine actions on tumor cell survival and migration as well as paracrine effects on tumor development and angiogenesis via TAMs or stromal cells in the tumor microenvironment (20-23). In addition to tumor cells, studies have demonstrated that CCL2 is secreted by hepatocytes, Kupffer cells, and hepatic stellate cells and involved in inflammation in the liver (24-26). Despite well-characterized relationship between chemokines and macrophages, a potential role of chemokines in macrophages-mediated disposition of NPs has not yet been investigated. Thus, we hypothesized that chemokines drive the PK of NP-based therapy and this may be associated with the high interpatient variability in the PK of nanomedicines. To test this hypothesis, we explored the relationship between the expressions of chemokines and the PK of PLD in patients with refractory epithelial ovarian cancer (EOC) and in preclinical models for ovarian cancer. In

addition, impacts of PLD on the migration of monocytes to chemokines were investigated using human monocytic THP-1 cells. Four CC chemokine ligands, including CCL2, CCL3, CCL4, and CCL5, were evaluated based on their chemotactic effects on monocytes and macrophages (27, 28).

2.2. Materials and Methods

Chemicals

PLD (Doxil®) was purchased from Janssen (Horsham, PA). Doxorubicin was purchased from Sigma Aldrich (St. Louis, MO). Empty PEGylated liposomes with the same liposomal formulation as PLD were kindly provided by Terumo™. Human CCL2 (MCP-1) and CCL5 (RANTES) were purchased from Pepro Tech Inc. (Rocky Hill, NJ).

Human Clinical Study

Study population. The PK and PD study of PLD was performed as part of a pilot clinical study at the University of North Carolina (UNC) at Chapel Hill. Women ≥ 18 years of age that were receiving PLD as part of their standard care of treatment for recurrent EOC were eligible for enrollment in this study. Exclusion criteria consisted of women who were pregnant or breast feeding. This study was approved by the UNC Institutional Review Board and all patients provided written informed consent prior to enrollment.

For evaluation of baseline (pre-dose) chemokine concentrations, plasma samples from patients with advanced solid tumors, obtained as part of a phase I clinical study of S-CKD602, and from healthy volunteers (HVT) were evaluated (29). HVT were defined as having no history of cardiovascular disease, hypertension or diabetes, being non-smokers, having a BMI<30, and taking no chronic medications. Subjects were excluded when CRP was >3, or high cholesterol

(TC>240, LDL>160, or TG>200) was present, or a BMI was >30. All samples were collected in the morning after an overnight fast.

PLD dosage and administration. PLD (Doxil®) was administered at a dose of 40 mg/m^2 in patients receiving PLD alone or at a dose of 30 mg/m^2 in patients receiving concurrent carboplatin dosed at a target AUC 5 (Cockcroft-Gault Formula) as standard treatment for platinum refractory ovarian cancer as defined by the Gynecologic Oncology Group (GOG). PLD was administered as an IV infusion over 1 to 3 hours every 28 days, with or without carboplatin.

PK studies. Serial PK blood samples on cycle 1 were obtained prior to PLD administration, at the end of infusion, and at 2, 6, 24, 48, 72, 96, 168, and 672 hours after PLD administration. Plasma was processed immediately to measure encapsulated and released doxorubicin using solid phase separation methods as described previously (29, 30).

Multiplex chemokine assay. The plasma concentrations of CCL2, CCL3, CCL4, and CCL5 were evaluated at baseline, and at 48, 96, 168, and 672 hours after PLD administration using the Bio-Plex 200 system (BioRad, Hercules, CA) and analyzed using Bio-Plex Manager software. Plasma samples were filtered and subsequently diluted with serum to block residual non-specific antibody binding. 1000 microspheres were added per chemokine (10 µl/well) in a total volume of 60 µl, together with standard and blank samples. The suspension was incubated for 1 hour in a 96-well filter plate at room temperature (RT). Then, 10 µl of biotinylated antibody mix was added and incubated for 1 hour at RT. After washing with PBS, beads were incubated with 50 ng/well streptavidin R-phycoerythrin for 10 minutes. Finally, beads were washed again with PBS and the fluorescence intensity was measured in a final volume of 100 µl high performance ELISA buffer. The assays used FMAP reagents from R&D Systems (Minneapolis, MN). The range of the standard curve for each chemokine ligand is as follows: CCL2 (3.0 -

2,140 pg/ml), CCL3 (3.0 – 2,680 pg/ml), CCL4 (8.0 – 5,750 pg/ml), and CCL5 (25.0 – 16,450 pg/ml).

***In vitro* Chemotaxis Assay**

Human THP-1 monocytic cells were obtained from the American Type Culture Collection (ATCC) (Rockville, MD). Cells were maintained in RPMI 1640 medium with 5% FBS, 100 U/mL of penicillin and 100 mg/mL of streptomycin.

Cultured cells were resuspended in the assay medium (RPMI 1640 + 0.1% BSA) at 1 x 10^6 cells/mL, incubated for 1 hour with assay medium (control), 100 µg/mL of empty liposomes, NL-doxorubicin, or PLD for 1 hour, and then labeled with calcein AM (1:1,000) for 30 minutes at 37°C, 5% CO2. Chemotaxis of calcein-labeled THP-1 cells into assay medium, CCL2 at 50 ng/mL, or CCL5 at 100 ng/mL (200 µl/well) was measured using a BD Falcon 96-Multiwell Insert System (Becton Dickinson and Co.). Fluorescence emitted from cells that migrated through the membrane was measured at an excitation and emission wavelengths of 485 nm and 530 nm, respectively, every 2 minutes for 4 hours (Fluoroscan, Version 2.6). Each sample was assayed in triplicate and each experiment was performed three times.

***In vivo* PK Studies**

PK studies in mice bearing SKOV3 orthotopic ovarian cancer xenografts. *In vivo* experiments were performed with the approval of UNC at Chapel Hill's Institutional Animal Care and Use Committee (IACUC). Human SKOV3 ovarian cancer cell lines obtained from the ATCC were injected orthotopically under the ovarian bursa of 7- to 8-week-old female CB17 SCID mice (Taconic Farms, Albany, NY). Mice with tumors with at least 0.5 cm in any dimension were administered with PLD at 6 mg/kg IV x1 via a tail vein. Female CB17 SCID mice of the same age were also evaluated as non-tumor (NT) bearing control mice. Mice (n=3)

were euthanized prior to and at 0.083, 0.5, 1, 3, 6, 24, 48, 72, and 96 hours after administration of PLD. Each blood sample was processed to evaluate encapsulated and released doxorubicin in plasma as described previously (29, 30). The sum total (encapsulated + released) doxorubicin in liver, spleen, and tumors was measured. Doxorubicin concentration was determined using an existing high performance liquid chromatography-fluorescence (HPLC-FL) assay (29, 30).

PK studies in CCL2 and CCL5 knockout (KO) mouse models. Female wild-type (WT) C57BL/6 mice, CCL2 $^{-/-}$ mice (CCL2 KO with C57BL/6 background), and CCL5 $^{-/-}$ mice (CCL5 KO with C57BL/6 background) of 8- to 10-weeks of age were purchased from the Jackson Labs (Bar Harbor, ME). PLD was administered to mice at 6 mg/kg IV x1 via a tail vein. Mice (n=3) were euthanized prior to and at 0.083, 1, 24, 48, and 96 hours after administration of PLD. All blood and tissue samples were processed for the PK studies as described previously.

Multiplex chemokine assay. Mouse Cytokine/Chemokine Magnetic Bead Panel was purchased from Milipore (Billerica, MA). The 96-well plate kit (Miliplex®) was customized to measure CCL2 and CCL5 in plasma and tumor from SCID mice and mice bearing SKOV3 orthotopic ovarian cancer xenografts. Tumor tissues were weighed and homogenized with pH 7.4 PBS buffer spiked with a protein inhibitor cocktail (Calbiochem, MA) in 1:3 (tumor weight: PBS volume) using a Precellys (13-RD000) 24 bead mill homogenizer (Omni International, Inc.). Supernatant was extracted and used for assay. Standards and QC controls were made using Assay Buffer provided with the kit. The fluorescence intensity was measured using Luminex-100 system (Luminex, Austin, TX) and the concentrations were corrected based on dilution factors used during procedures.

PK and Statistical Analysis

PK analysis was performed by non-compartmental method using Phoenix WinNonlin® (v. 6.02, Pharsight Corp., Mountain View, CA). Statistical analyses were carried out using SAS v.9.2 (Cary, NC) and Prism5 software (GraphPad Software, Inc., La Jolla, CA). Differences in the demographics between HVT and patients with cancer were examined by the Fisher's exact test and Mann-Whitney test. Plasma concentrations of chemokines were tested for normal Gaussian distribution and the baseline chemokine data were analyzed using Mann Whitney test due to their skewed distribution profiles. Kruskal-Wallis test was performed to test overall chemokine exposure (AUC) among different chemokines. Equality of AUC of doxorubicin and chemokines between mouse models was tested using Nedelman's modification of the Bailer method for sparse samples, using a two-sample test (31). Simple linear regression was used to explore the relationship between chemokines and the PLD PK parameters. Chemokine concentrations in plasma and tumors for NT mice and mice bearing SKOV3 ovarian cancer xenograft were compared using t-test or paired t-test. *P* value of less than 0.05 was considered statistically significant. All statistical tests were two-sided.

2.3. Results

Demographics in Healthy Volunteers and Patients with Refractory Solid Tumors

Healthy volunteer subjects (HVT; n=27), patients with refractory EOC treated with PLD (n=10), and patients with refractory solid tumors enrolled in a phase I study of PEGylated liposomal CKD-602 (S-CKD602) (n=24) were evaluated for baseline (pre-dose) chemokine concentrations in plasma (29). Baseline demographics and laboratory parameters were well balanced in our patient cohorts (**Table 2. 1**).

Baseline Chemokine Concentration in Healthy Volunteers and Patients with Refractory Solid Tumors

To evaluate if baseline chemokine expressions vary between HVT and patients with refractory solid tumors, baseline plasma concentrations of CCL2, CCL3, CCL4, and CCL5 were measured using multiplex array assay (**Fig. 2. 1**). Patients with refractory EOC and other types of solid tumors had significantly higher expressions of CCL2, CCL4, and CCL5 in plasma compared to HVT ($P<0.0001$, $P=0.0006$, and $P=0.028$, respectively) (Ta**ble 2. 2**). Plasma concentrations of CCL3 in most HVT and patients with solid tumors were below the limit of quantitation (BLQ) (**Fig. 2. 1**). Among the chemokines tested, CCL5 was the most prevalent plasma chemokine followed by CCL2 in both HVT and patients with solid tumors ($P<0.0001$ for both) (**Fig. 2. 2**). There was no significant difference in the baseline plasma concentrations of all chemokines between patients with ovarian cancer and patients with other types of solid tumors (**Fig. 2. 3**).

Relationship between Chemokines and the PK of PLD in Patients with EOC

To determine whether chemokine expressions were associated with the disposition of PLD in patients with EOC, plasma concentrations of CCL2, CCL3, CCL4, and CCL5 were assessed at 48, 96, 168, and 672 hours after administration of PLD or PLD with carboplatin. Plasma concentrations of encapsulated (the drug within the liposomal carrier) and released (active-drug released from the liposomal carrier) doxorubicin were also measured in the first cycle of PLD (5). It was noted that there was a variation in the plasma concentrations of chemokines after PLD administration in patients with EOC (**Fig. 2. 4A-D**). As CCL2 and CCL5 were the most prevalent baseline chemokines in these patients, they were further explored for the relationship with the PK of PLD; however, the baseline plasma concentrations of CCL2 and

CCL5 did not correlate with the clearance (CL) of encapsulated doxorubicin in plasma, indicating that baseline expression levels of chemokine may not predict the PK of PLD (**Fig. 2. 5)**

We next assessed the total amount of plasma chemokines secreted after PLD administration. Area-under-the concentration of a chemokine versus time curve (AUC) from 0 to 96 h, a measured index of the total amount of a chemokine secreted over time, was calculated for each chemokine in individual patients (**Fig. 2. 6**). Among the four chemokines, CCL5 $AUC_{0\text{-}96h}$ was significantly higher compared to those of other chemokines, indicating that CCL5 is not only the most prevalent chemokine at baseline, but may be the major chemokine that responds to PLD in patients with EOC ($P<0.0001$) (21).

To determine whether the total amount of each chemokine secreted correlated to the plasma PLD exposure, we evaluated the relationship between plasma chemokine $AUC_{0\text{-}last}$ and plasma encapsulated doxorubicin $AUC_{0\text{-}last}$ using simple linear regression (**Fig. 2. 7A-D**). There was a significantly positive linear relationship between all chemokine $AUC_{0\text{-}last}$ and the plasma encapsulated doxorubicin $AUC_{0\text{-}last}$ in patients treated with PLD alone, indicating that PLD induced the secretion of chemokines. However, the association was not observed in patients treated with PLD plus carboplatin, indicating that co-administered carboplatin may have impacts on the interaction between PLD and chemokine systems (CCL2: $P=0.52$, CCL3: $P=0.97$, CCL4: $P=0.15$, and CCL5: $P=0.1$) (**Fig. 2. 7A-D**).

Chemokines in Non-tumor (NT) Bearing Mice and Mice Bearing SKOV3 Orthotopic Ovarian Cancer Xenografts

To further understand PLD-mediated stimulation of chemokine secretions *in vivo*, CCL2 and CCL5 were assessed in plasma from NT bearing severe combined immunodeficient (SCID) mice and in plasma and tumors from SCID mice bearing SKOV3 orthotopic ovarian cancer

xenografts. Serial blood samples were obtained including prior to and at 24, 48, and 96 hours after administration of PLD at 6 mg/kg IV x 1 via tail vein.

Baseline plasma CCL2 concentrations were higher in mice bearing SKOV3 ovarian cancer xenografts compared with NT mice (P=0.07, t-test; **Fig. 2. 8A**). In addition, baseline intratumoral CCL2 concentrations were significantly higher than in plasma in mice bearing the SKOV3 ovarian cancer xenografts (P=0.04, paired t-test; **Fig. 2. 8A**). After PLD administration, CCL2 concentrations in plasma and tumors appeared to increase in both mouse models (**Fig. 2. 8A**). However, the total amount of plasma CCL2 secreted over 96 hours after administration of PLD was significantly greater in mice bearing SKOV3 ovarian cancer xenografts compared with NT mice (AUC ± SEM: 118 ± 20 and 37 ± 7 (ng·h/ml), respectively) (P<0.05, t-test). Elevated expressions of vascular endothelial growth factors (VEGF)-A after PLD administration also confirmed PLD-mediated upregulation of pro-inflammatory cytokine production by the tumor cells (**Fig. 2. 9**). Together, these data suggest that ovarian cancer cells and the stromal cells are the primary sources of chemokine secretion at baseline and after administration of PLD (18, 21).

Although baseline intratumoral CCL5 concentrations were higher than in plasma in mice bearing SKOV3 ovarian cancer xenografts (P=0.05, paired t-test; **Fig. 2. 8B**), plasma CCL5 concentrations were similar between NT mice and mice bearing SKOV3 ovarian cancer xenografts (P=0.63, t-test; **Fig. 2. 8B**). After PLD administration, there were little changes over time in plasma CCL5 concentrations in both mouse models; but intratumoral CCL5 concentrations were decreased over 96 hours in mice bearing SKOV3 ovarian cancer xenografts (**Fig. 2. 8B**).

PLD PK in NT Mice and Mice Bearing SKOV3 Orthotopic Ovarian Cancer Xenografts

To evaluate the relationship between chemokines and the PLD PK in these mouse models, doxorubicin exposures were assessed in plasma, tumor, liver, and spleen, the major organs involved in the clearance and tissue distribution of PLD (**Fig. 2. 10A-D** and **Fig. 2. 11**). The plasma encapsulated and released doxorubicin exposure (AUC) were significantly lower in mice bearing SKOV3 ovarian cancer xenografts compared to NT mice ($P<0.05$, t-test; **Fig. 2. 10A, D**). Conversely, the PLD accumulation (AUC) in the liver was 1.6-fold greater ($P<0.05$; **Fig. 2. 10B, D**) and was 1.3-fold greater in the spleen ($P>0.05$; **Fig. 2. 10C, D**) in mice bearing SKOV3 ovarian cancer xenografts compared to NT mice. PK parameters in both mouse models are summarized in **Table 2. 3**.

PLD PK in Wild-type (WT) and Chemokine Ligand Knockout (KO) Mice

To verify the roles of CCL2 and CCL5 in the PK of PLD, we performed the PLD PK studies in WT mice (C57BL/6), $CCL2^{-/-}$ mice (CCL2 KO with C57BL/6 background), and $CCL5^{-/-}$ mice (CCL5 KO with C57BL/6 background) purchased from Jackson Laboratory. PLD was administered at 6 mg/kg IV x1 via a tail vein. The plasma encapsulated doxorubicin exposure (AUC) was significantly greater in CCL5 KO mice compared to WT mice, indicating decreased CL of PLD in CCL5 KO mice ($P<0.05$, t-test; **Fig. 2. 12A**). However, there was no difference in released free doxorubicin exposure between WT mice and KO mice (**Fig. 2. 12)**.

In addition, the PLD accumulations in the liver and the spleen were significantly decreased for CCL2 KO mice and CCL5 KO compared to WT mice ($P<0.05$) (**Fig. 2. 12B**). Other PK parameters of PLD in these mouse models are summarized in **Table 2. 4**.

Chemotaxis of Human Monocytic THP-1 Cells

PLD was also shown to affect the migratory responses of monocytes to CCL2 and/or CCL5, of which the expressions were shown to be altered by PLD in the mouse models and patients with EOC. Chemotactic responses to CCL2 and CCL5 were measured using human monocytic THP-1 cells in 96-multiwell plate (32, 33). Cultured THP-1 cells were resuspended in the assay medium and incubated with assay medium (control), 100 µg/mL of empty PEGylated liposomes, NL-doxorubicin, or PLD for 1 hour. After preincubation with empty PEGylated liposomes or NL-doxorubicin, the number of THP-1 cells migrated to CCL2 and CCL5 was similar to that of control (P>0.05, t-test; **Fig. 2. 13**). In contrast, after preincubation with PLD, the number of THP-1 cells migrated to CCL2 was decreased by approximately 53% compared to control (P=0.13, t-test), but the migration to CCL5 was increased by 130% compared to control (P=0.15, t-test) (**Fig. 2. 13)**. These results indicate that PLD suppressed the CCL2-induced chemotaxis of monocytes, but enhanced the CCL5-induced migration.

2. 4. Discussion

We demonstrated for the first time that the secretions of CCL2 and CCL5, the most prevalent circulating chemokines in patients with refractory EOC, were stimulated by PLD and was associated with the PLD PK. Baseline chemokine levels did not predict the PK of PLD in these patients, but, after PLD administration, there was a significantly positive linear relationship between total amount of plasma CCL2 and CCL5 and plasma encapsulated doxorubicin exposure. Interestingly, this association disappeared in patients for whom carboplatin was co-administered with PLD, indicating that carboplatin affects the interaction between PLD and the chemokine system. Cisplatin was shown to selectively inhibit chemotaxis of monocytes isolated from

venous blood of healthy volunteers and impaired monocyte chemotaxis was also reported in cancer patients 20 hours after receiving cisplatin (34, 35). Based on these observations, it is possible that carboplatin may impair the migratory responses of monocytes and chemokine secretion and, ultimately, affect the PK of PLD (36).

To determine the important source of CCL2 and CCL5 secretion induced by PLD, mice bearing SKOV3 orthotopic ovarian cancer xenografts and NT mice were evaluated. Plasma CCL2 concentrations in mice bearing SKOV3 ovarian cancer xenografts were notably greater than in NT mice, which was consistent with higher plasma CCL2 concentrations in patients with cancer compared to HVT. CCL5 was the most prevalent plasma chemokine in patients with EOC. Conversely, the plasma CCL5 concentrations were similar between these mouse models and were significantly lower than plasma CCL2 in mice bearing SKOV3 ovarian cancer xenografts, suggesting that plasma chemokine profile may vary across different species and/or tumor types (37). After PLD administration, in contrast to CCL5, CCL2 expression in plasma and tumors increased over 96 hours in both mouse models, indicating that CCL2 is the primary chemokine induced by PLD in mice bearing SKOV3 ovarian cancer xenografts and the secretions involve the tumor cells and the tumor microenvironments as well as other host cells (18, 20, 21).

CCL2 is a major monocyte-recruiting chemokine and CCL2 expressions correlated with TAM infiltration, elevated angiogenesis, and tumor progression (20, 23, 38, 39). It has been also shown that CCL2 plays an important role in monocyte migration to the liver, activation of stellate cells, and enhancement of liver blood vessel permeability in response to acute and chronic liver inflammation (24-26). Thus, it is possible that upregulated CCL2 expression by the tumor cells and the stromal cells as well as PLD-induced CCL2 secretion by the tumor cells and the host cells may influence macrophage infiltration to the tumors and the liver, the transvascular

transportation of PLD, and, ultimately, PLD uptake by macrophages (15, 24, 10). Significantly decreased PLD accumulations in the liver and the spleen of CCL2 KO and CCL5 KO mice compared to WT mice confirmed the role of CCL2 and CCL5 in the clearance and biodistribution of PLD (41, 42).

We also demonstrated that PLD may affect the migration of monocytes in a chemokine-dependent manner. CCL2 was shown to augment apoptotic cell removal (efferocytosis), a critical process in the regulation of inflammation, infection, and tissue repair (43). Based on data generated by others and our group, monocytes and macrophages were shown to be more sensitive to PLD-mediated toxic effects compared with other myeloid-derived cells (i.e., neutrophils) (44, 45). These data indicate that PLD-mediated suppression of the chemotaxis of monocytes to CCL2 may be due to enhanced phagocytosis of apoptotic monocytes via CCL2.

We have explored the complex interaction between PLD and chemokines and monocytes/macrophages *in vitro* and *in vivo* and its effects on the PK of PLD in patients with EOC (**Fig. 2. 14**). However, there are some limitations in our studies and further studies may be necessary to translate these findings to optimize NP-based therapy in the clinic. Given that the uptake of NPs by monocytes and macrophages may be a saturable process and multiple cycles of nanomedicines are administered in combination with other therapies, it is critical to characterize the effects on the chemokine system of multiple NP dosing as well as co-administration of medications as shown by simvastatin-mediated down-regulation of CCL2 in a time- and dose-dependent manner (34, 35, 46). In addition, different physicochemical properties of NPs such as size, shape, and charge, have been shown to determine the NP compatibility with the immune system (13, 14). The heterogeneity of the tumor microenvironment has been reported and suggested to be a contributing factor to the variable tumor delivery and responses of

nanomedicines (16, 47). Thus, comprehensive profiling of the interaction between different NP platforms and the microenvironmental components (i.e., chemokines and macrophages) in mouse cancer models and human samples will be a key part of understanding the interplay between NPs and the MPS.

Cancer-related inflammation has emerged as a critical mechanism for cancer development (48). Inflammatory CC chemokines, particularly CCL2 (MCP-1), have shown to be associated with recruitment of TAMs in tumors, promote M2 polarization and survival of TAM (49). The evidence for the involvement of CCL2 in cancer progression and metastasis provides important implications for cancer therapy and chemokine-targeting agents have emerged in clinical trials (48, 50). We demonstrated that PLD, a NP-based therapy, altered the expressions of CCL2 and CCL5 as well as the chemotaxis of monocytes, which was shown to be associated with the clearance and biodistribution of PLD in preclinical models and in patients with refractory EOC. These data implicate that chemokines are targets not only for anticancer therapy, but also for optimization of the NP-based therapy.

Table 2. 1. Baseline demographics and laboratory parameters of healthy volunteers (HVT) and patients with cancer

Demographics	**HVT (n=27)**		**Patients with cancer (n=34)**		*P*-value*
	Median	Range	Median	Range	
Age (years)	52	46 - 68	55	33 - 78	0.09
Gender (n, %)	Male (12, 44%)		Male (10, 29%)		0.29†
	Female (15, 56%)		Female (24, 71%)		
Height (cm)	169	150 - 187	167	155 - 196	0.64
Weight (kg)	72.8	46.3 – 99.4	75.7	48 – 140	0.25
BMI (kg/m^2)	25.9	18.1 – 29.7	26.7	17.4 – 42.6	0.10
Scr (mg/dL)	0.89	0.64 – 1.06	0.80	0.50 – 1.10	0.09

*, *P*-values were calculated using Mann-Whitney test; †, *P*-values were calculated using Fisher's exact test. Colorectal cancer (n=10), ovarian cancer (n=4 treated with S-CKD602; n=10 treated with PLD), sarcoma (n=3), liver cancer (n=2), lung cancer (n=1), Miscellaneous cancer (n=4): adenocarcinoma (n=1), prostate cancer (n=1), thyroid cancer (n=1), spindle cell cancer (n=1). HVT: healthy volunteers. BMI: body mass index. Scr: serum creatinine.

Table 2. 2. Baseline plasma chemokine concentrations in patients with cancer

Baseline chemokines	**HVT (n=27)**		**Patients with cancer (n=34)**		*P*-value*
	Median	Range	Median	Range	
CCL2 (pg/mL)	141.4	108.6 – 318.9	265.9	57.12 – 841.2	<0.0001
CCL3 (pg/mL)	29.31	20.90 – 37.72	37.72	20.90 – 97.3	0.41[†]
CCL4 (pg/mL)	35.59	2.99 – 58.63	64.42	2.99 – 200.3	0.0006
CCL5 (pg/mL)	18,308	3,857– 23,479	19,653	8,969– 28,237	0.028

*, *P*-values were calculated using Mann-Whitney test. [†]n=3 for HVT and n=11 for patients with cancer were included for analysis because plasma concentrations were mostly below the limit of quantitation (BLQ) of the multiplex chemokine assay. The range of the standard curve for each chemokine ligand is as follows: CCL2 (3.0 - 2,140 pg/ml), CCL3 (3.0 – 2,680 pg/ml), CCL4 (8.0 – 5,750 pg/ml), and CCL5 (25.0 – 16,450 pg/ml). HVT: healthy volunteers.

Table 2. 3. PK parameters* after administration of PLD at 6 mg/kg IV x1 in non-tumor bearing mice (NT) and mice bearing SKOV3 orthotopic ovarian cancer xenografts

Model	NT mice						Mice bearing SKOV3 orthotopic ovarian cancer xenografts				
Plasma	Encapsulated			Released			Encapsulated			Released	
	AUC (µg·h/mL)	C_{max} (µg/mL)	CL (mL/h/kg)	AUC (µg·h/mL)	C_{max} (µg/mL)		AUC (µg·h/mL)	C_{max} (µg/mL)	CL (mL/h/kg)	AUC (µg·h/mL)	C_{max} (µg/mL)
	3,967 ± 150	137	1.5	83 ± 5.9	2.6		1,676† ± 89	140	3.4	31† ± 2.1	2.7
Liver	Sum total doxorubicin						Sum total doxorubicin				
	AUC (µg·h/g)	C_{max} (µg/g)	T_{max} (h)				AUC (µg·h/g)	C_{max} (µg/g)	T_{max} (h)		
	856 ± 42	15.7	24				1,344† ± 118	21.3	48		
Spleen	Sum total doxorubicin						Sum total doxorubicin				
	AUC (µg·h/g)	C_{max} (µg/g)	T_{max} (h)				AUC (µg·h/mL)	C_{max} (µg/g)	T_{max} (h)		
	2,217 ± 314	35.4	48				1,792 ± 187	36.1	48		
Tumor							Sum total doxorubicin				
							AUC (µg·h/g)	C_{max} (µg/g)	T_{max} (h)		
							324 ± 37	8.5	24		

*, The PK of PLD was analyzed by noncompartmental analysis using Phoenix v.6.2. AUC= area-under the concentration versus time curve from 0 h to 96 h (presented as mean ± SEM); C_{max}

(μg/mL)= maximum observed concentration; CL= clearance; T_{max}= time for maximum observed concentration. †, P <0.05 (NT mice versus mice bearing SKOV3 orthotopic ovarian cancer xenografts). Equality of AUC was tested using Nedelman's modification for the Bailer method, using a two-sample test (31).

Table 2. 4. Doxorubicin exposure (AUC ± SEM)* after administration of PLD at 6 mg/kg IV x1 in wild-type (WT) and chemokine ligand knockout (KO) mice

Model	WT		CCL2 KO		CCL5 KO	
Plasma	Encapsulated	Released	Encapsulated	Released	Encapsulated	Released
	2,673 ± 234	34.9 ± 3.7	3,147 ± 380	31.2 ± 7.5	4,862† ± 450	40 ± 3.6
Liver	Sum total doxorubicin		Sum total doxorubicin		Sum total doxorubicin	
	487 ± 17		385† ± 29		449 ± 21	
Spleen	Sum total doxorubicin		Sum total doxorubicin		Sum total doxorubicin	
	1,194 ± 64		541† ± 46		944† ± 48	

*, The PK of PLD was analyzed by noncompartmental analysis using Phoenix v.6.2. AUC= area-under the concentration versus time curve from 0 to 96 h (µg/mL·h for plasma or µg/g·h for liver and spleen). AUC are presented as mean ± SEM. †, $P<0.05$ (WT versus CCL2 KO or WT versus CCL5 KO). *P*-values were calculated using Nedelman's modification of the Bailer method for sparse samples, using a two-sample test (31). WT: wild-type (C57/BL6J), KO: knockout.

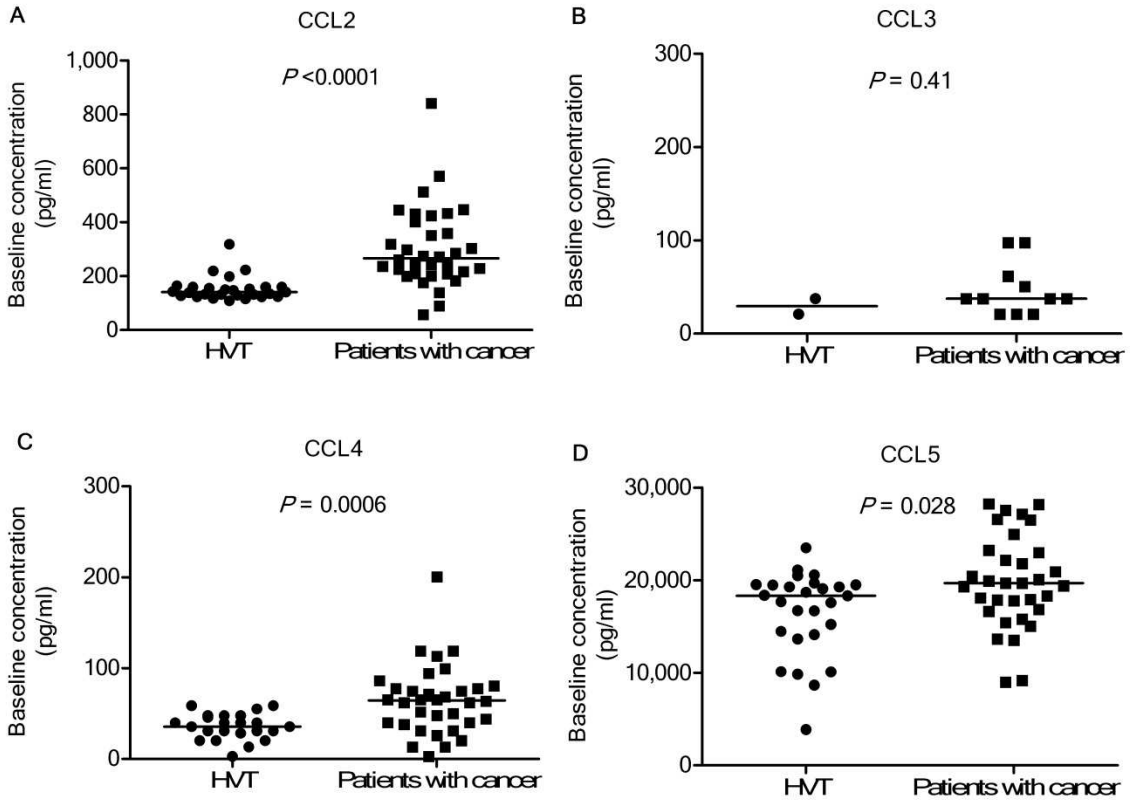

Fig. 2. 1. Baseline plasma CCL2, CCL3, CCL4, and CCL5 chemokine concentration in healthy volunteers (HVT) and patients with cancer. Plasma concentrations of (**A**) CCL2, (**B**) CCL3, (**C**) CCL4, and (**D**) CCL5. Plasma concentrations of CCL2, CCL4, and CCL5 were significantly increased in patients with cancer (n=34) compared to HVT (n=27). Plasma concentrations of CCL3 were undetectable from most samples. CCL2 and CCL5 were the most prevalent baseline chemokines in both HVT and patients with cancer. *P*-values were calculated using Mann-Whitney test (HVT versus patients with cancer). Individual and median data are presented.

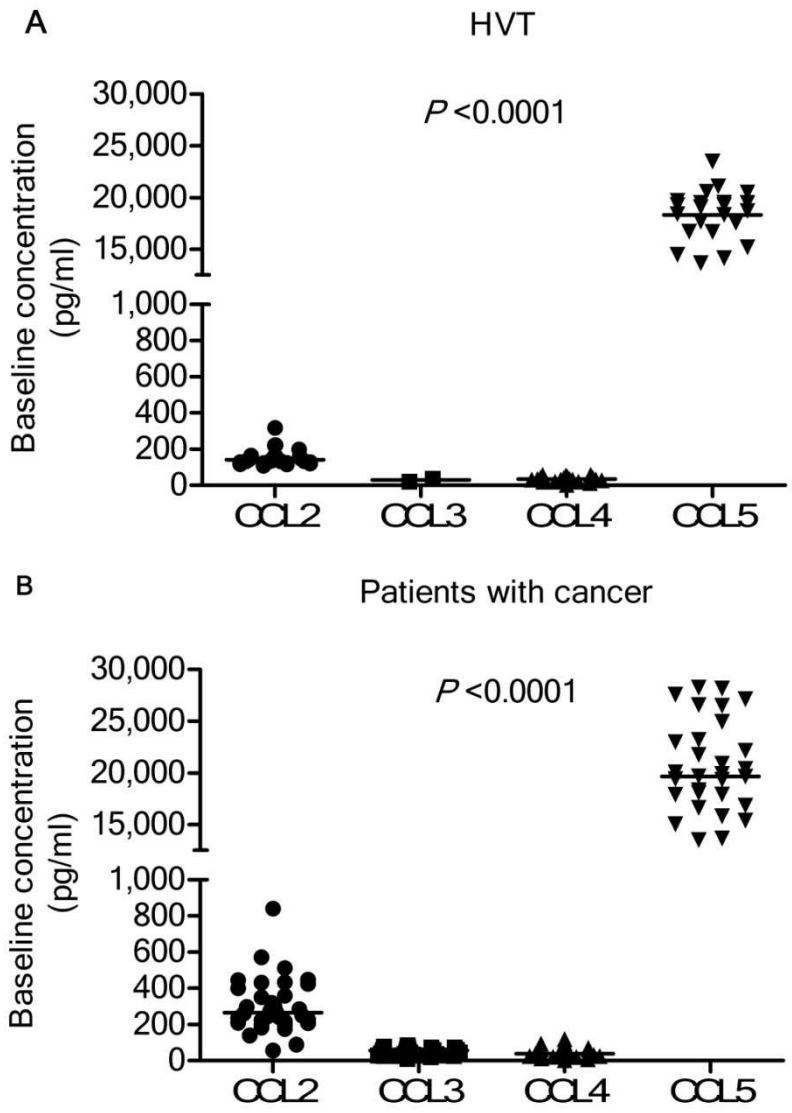

Fig. 2. 2. Baseline plasma CCL2, CCL3, CCL4, and CCL5 concentrations in healthy volunteers (HVT) and patients with cancer. CCL5 was the most prevalent plasma chemokine followed by CCL2 in (**A**) HVT and in (**B**) patients with cancer. *P*-values were calculated using Kruskal-Wallis test.

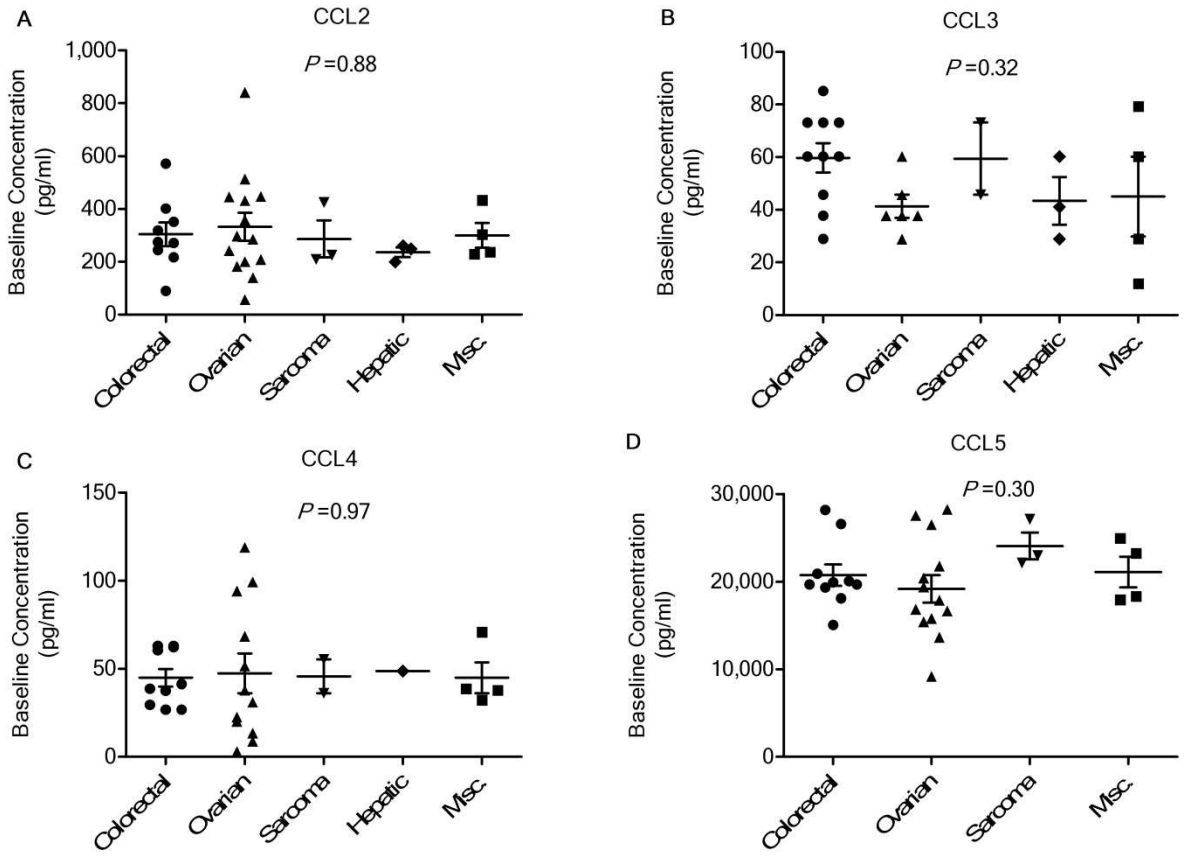

Fig. 2. 3. Baseline plasma (**A**) CCL2, (**B**) CCL3, (**C**) CCL4, and (**D**) CCL5 concentrations in patients with different types of primary cancer. There was no significant difference in plasma chemokine concentrations at baseline among different cancer types. Colorectal cancer (n=10), ovarian cancer (n=14), sarcoma (n=3), liver cancer (n=2), lung cancer (n=1), and miscellaneous cancer (n=4): adenocarcinoma (n=1), prostate cancer (n=1), thyroid cancer (n=1), spindle cell cancer (n=1). *P*-values were calculated using Kruskal-Wallis test.

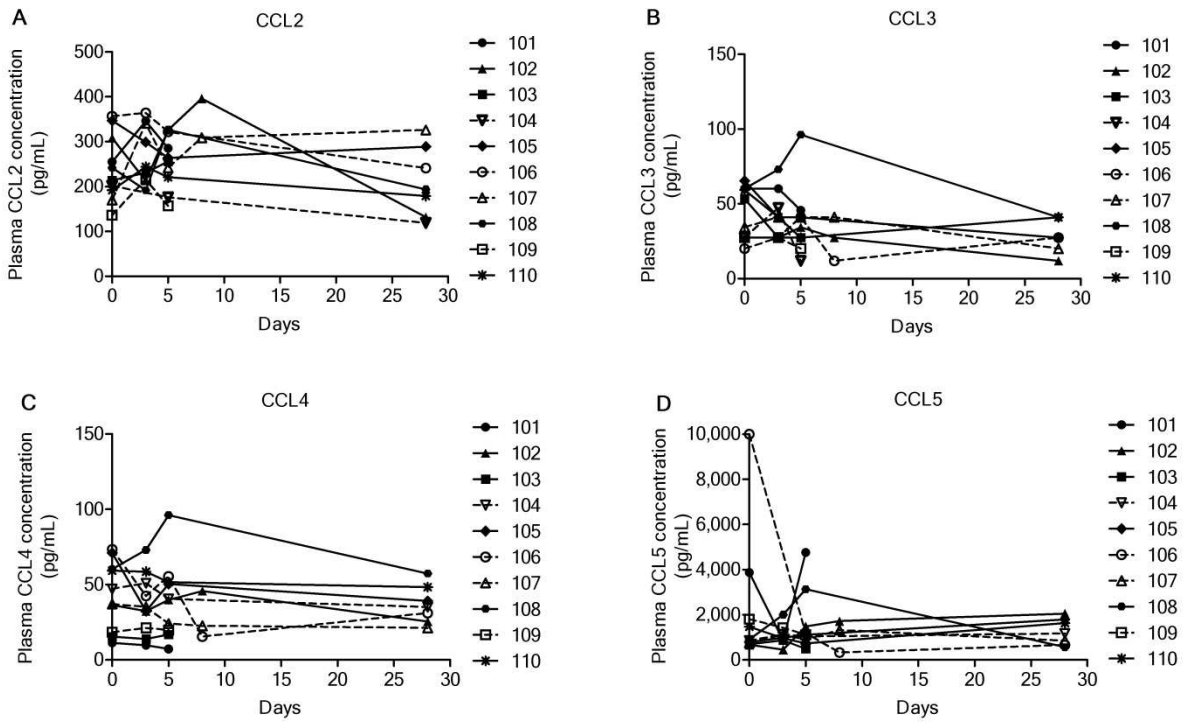

Fig. 2. 4. Plasma chemokine concentrations versus time profile after administration of PLD alone or PLD plus carboplatin in patients with refractory ovarian cancer (EOC). There was high inter-patient variability in (**A**) CCL2, (**B**) CCL3, (**C**) CCL4, and (**D**) CCL5 plasma concentrations after PLD alone or PLD with carboplatin. Solid line represents patients treated with PLD alone at 40 mg/m^2 (n=6) and dashed line represents PLD 30 mg/m^2 with carboplatin (AUC=5) (n=4)

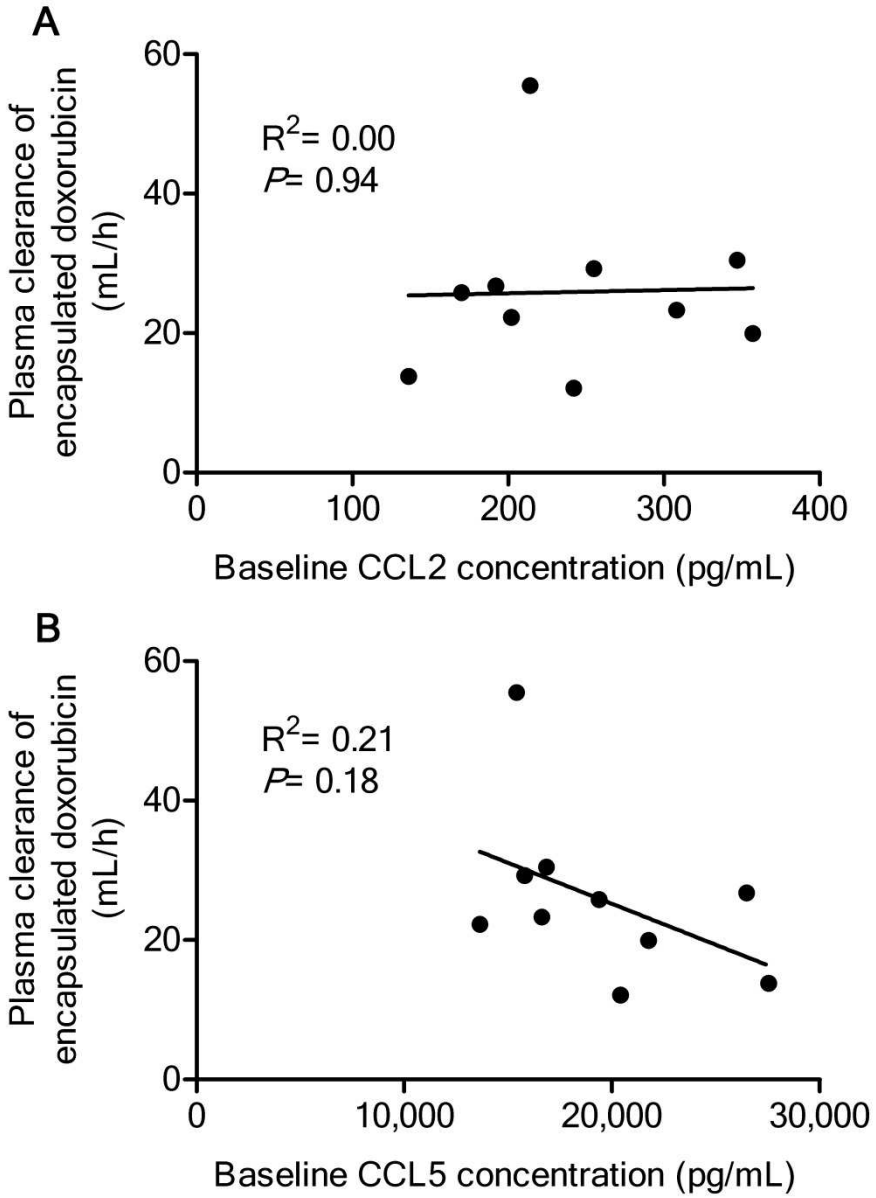

Fig. 2. 5. The relationship between baseline chemokine concentration and the PK of PLD. The most prevalent plasma chemokines, (**A**) CCL2 and (**B**) CCL5, were selected for further evaluation of association with the PLD PK. There was no association between baseline CCL2 and CCL5 concentrations and the CL of encapsulated doxorubicin after administration of PLD in patients with EOC (P>0.05, not significant). R^2 and p-values were calculated using simple linear regression.

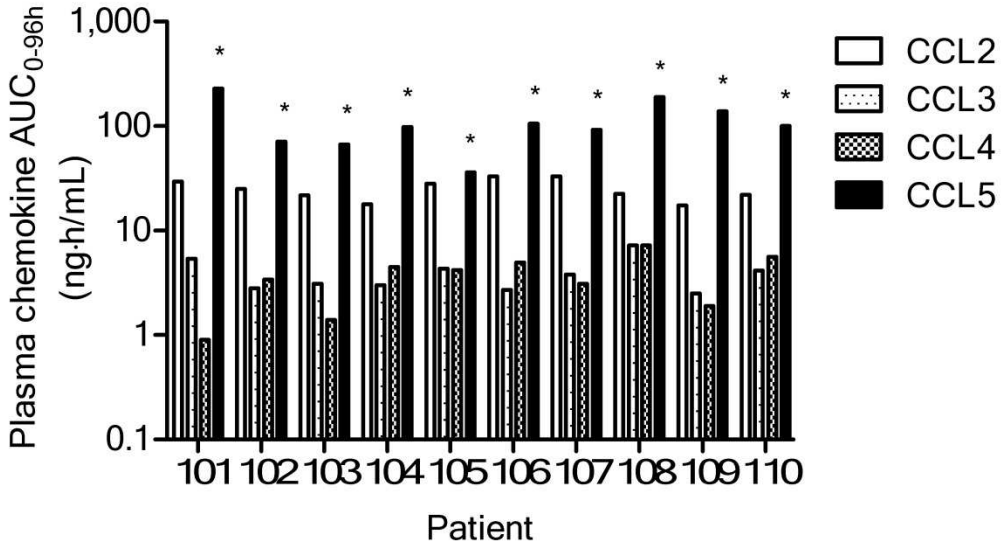

Fig. 2. 6. Total chemokine exposure ($AUC_{0\text{-}96h}$) in plasma after administration of PLD alone n=6) or in combination with carboplatin (n=4; patient 104, 106, 107, and 109) in patients with EOC. CCL5 AUC was significantly greater compared to other chemokines AUC in all patients (**P* <0.0001, Kruskal-Wallis test).

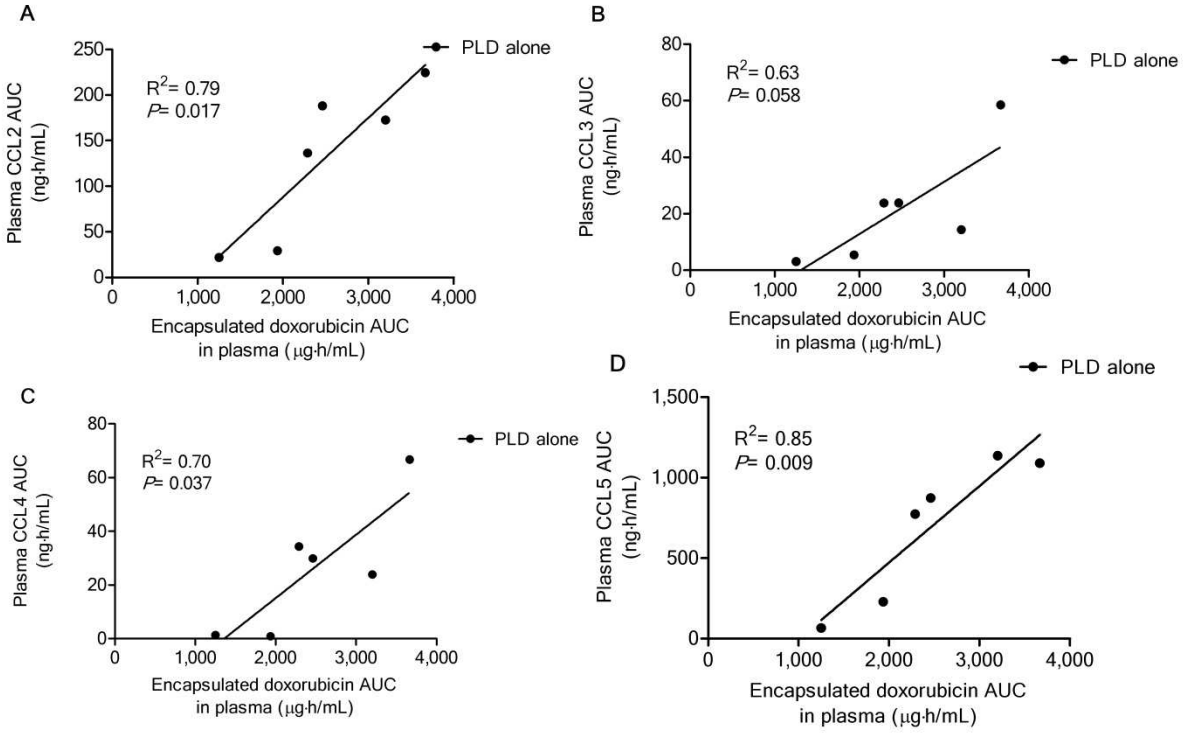

Fig. 2. 7. Relationship between total amount of chemokine (AUC) and encapsulated doxorubicin plasma exposure (AUC) in patients with EOC after administration of PLD alone. The association between (**A**) CCL2, (**B**) CCL3, (**C**) CCL4, and (**D**) CCL5 plasma AUC and encapsulated doxorubicin plasma AUC. There was a significantly positive linear relationship between all chemokine AUC values and the encapsulated doxorubicin AUC in patients treated with PLD alone; however, no association was observed in patients treated with PLD plus carboplatin (P>0.05, data are not shown). R^2 and p-values are calculated using linear regression.

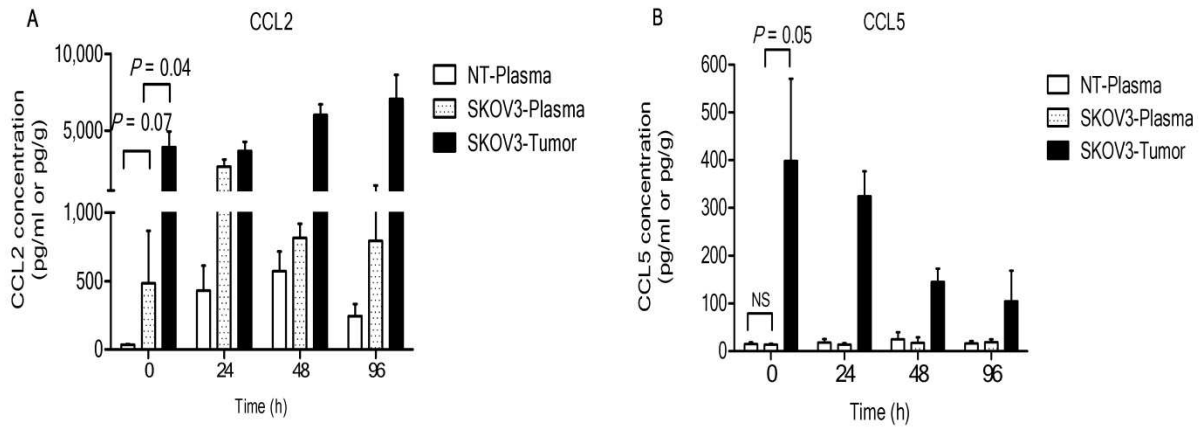

Fig. 2. 8. Plasma chemokine concentrations in non-tumor bearing (NT) mice and mice bearing SKOV3 orthotopic ovarian cancer xenografts after administration of PLD at 6 mg/kg IV x1 via tail vein. (**A**) CCL2 and (**B**) CCL5 concentration versus time profiles in plasma and tumors after administration of PLD. Baseline plasma CCL2 concentrations in mice bearing SKOV3 ovarian cancer xenografts were greater compared to NT mice (*P*=0.077, t-test); however, there was no difference in baseline plasma CCL5 concentrations between NT mice and mice bearing SKOV3 ovarian cancer xenografts. Baseline intratumoral CCL2 and CCL5 concentrations were significantly higher than in plasma in mice bearing SKOV3 xenografts (*P*=0.04 and *P*=0.05, respectively; paired t-test). CCL2 concentrations in plasma and tumors tended to increase after administration of PLD in NT mice and mice bearing SKOV3 ovarian cancer xenografts. There was little change in plasma CCL5 concentrations after administration of PLD whereas intratumoral CCL5 concentrations decreased after administration of PLD in mice bearing SKOV3 ovarian cancer xenografts. Data are presented as mean ± SEM (n=3 or 4).

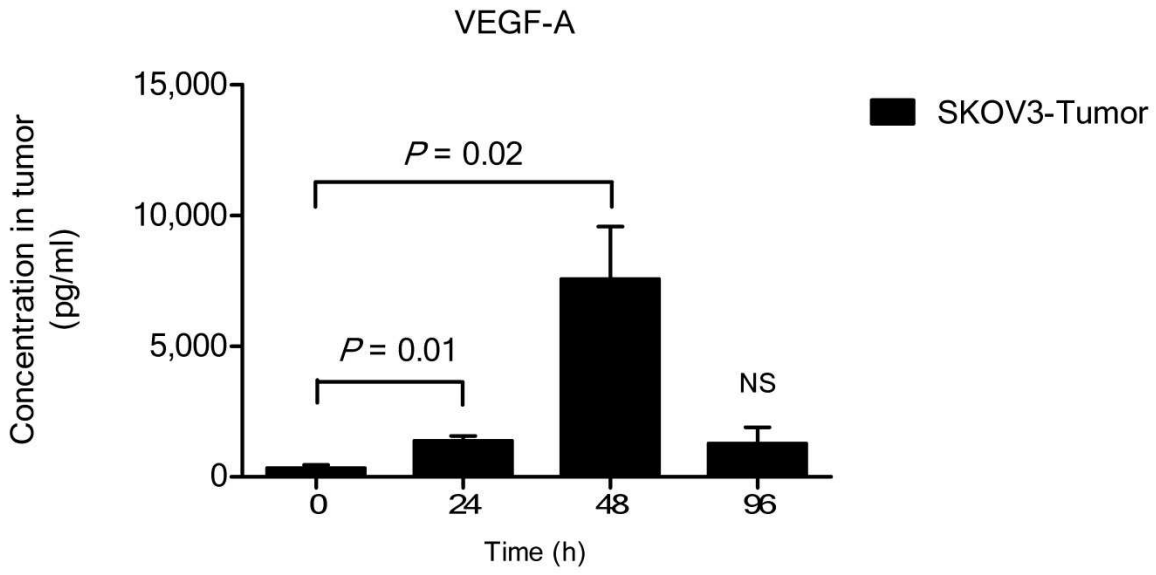

Fig. 2. 9. The intratumoral VEGF-A concentrations after administration of PLD at 6 mg/kg IV x1 via tail vein in mice bearing SKOV3 orthotopic ovarian cancer xenografts. The secretions of VEGF-A by SKOV3 tumor cells were increased over 96 hours, indicating that PLD induced the productions of proinflammatory cytokines, such as VEGF-A, by the tumor cells and the stromal cells. Data are presented as mean ± SEM (n=3).

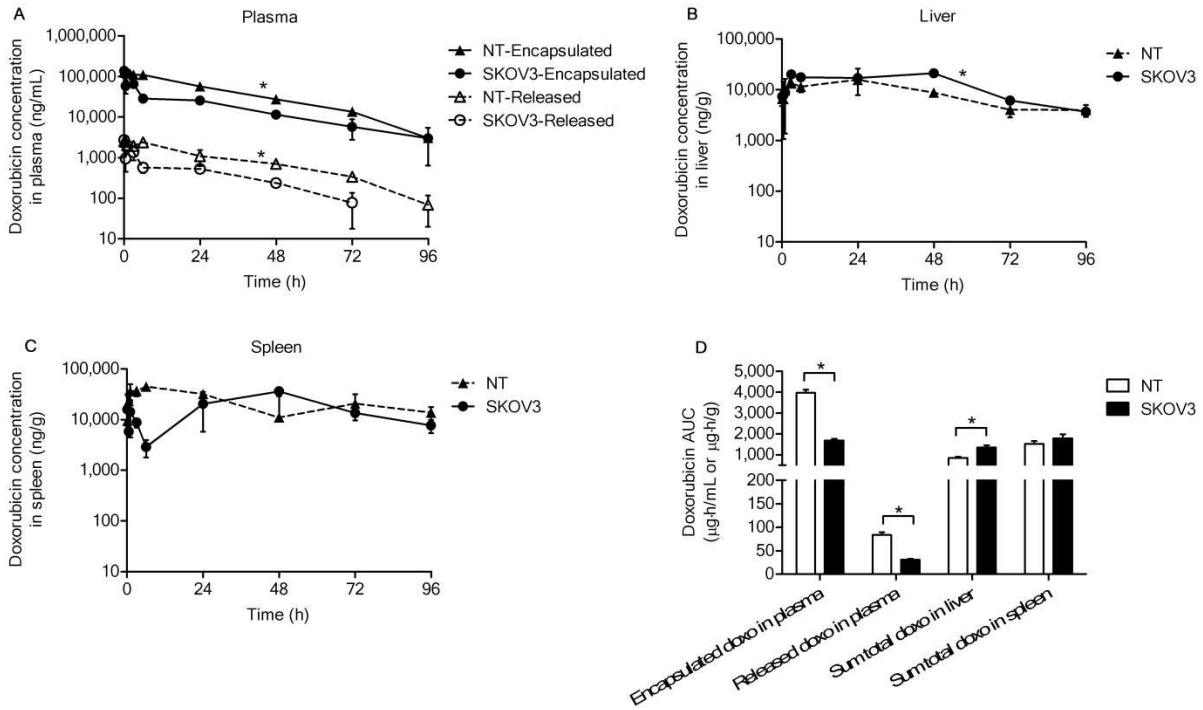

Fig. 2. 10. Concentration vs. time profiles of doxorubicin in plasma and tissues in non-tumor bearing (NT) mice and mice bearing SKOV3 orthotopic ovarian xenografts after administration of PLD at 6 mg/kg IV x1 via tail vein. Concentration versus time profiles of doxorubicin in (**A**) plasma, (**B**) liver, and (**C**) spleen in NT mice and mice bearing SKOV3 ovarian cancer xenografts. (**D**) Encapsulated and released doxorubicin exposure (AUC) in plasma, and sum total doxorubicin in the liver and spleen. Equality of AUC was tested using Nedelman's modification of the Bailer method for sparse samples, using a two-sample test (31). There was a significantly lower plasma exposure of both encapsulated and released doxorubicin in mice bearing SKOV3 ovarian cancer xenografts. The accumulation of sum total doxorubicin in the liver and spleen was lower in NT mice. Samples (n=3 mice) were obtained at each time point. Data are presented as mean ± SD (A-C) and mean ± SEM (D).

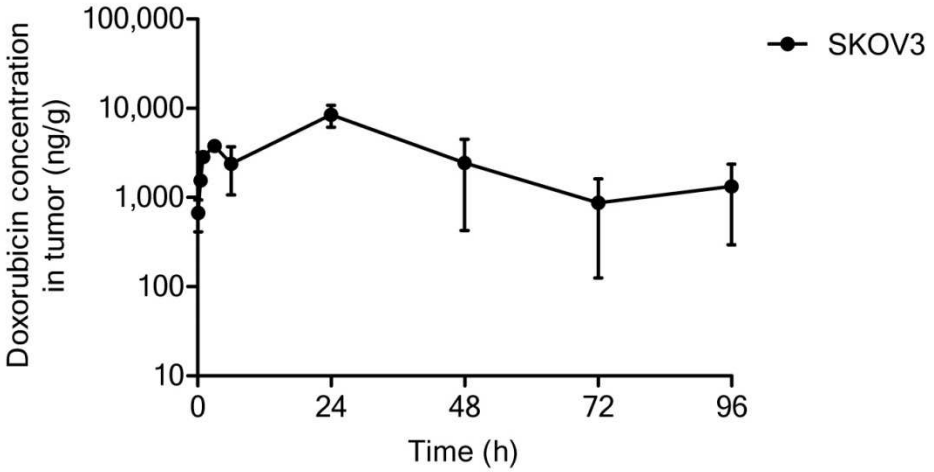

Fig. 2. 11. Sum total doxorubicin concentration versus time profile in tumors after administration of PLD at 6 mg/kg IV x1 in mice bearing SKOV3 orthotopic ovarian cancer xenografts.

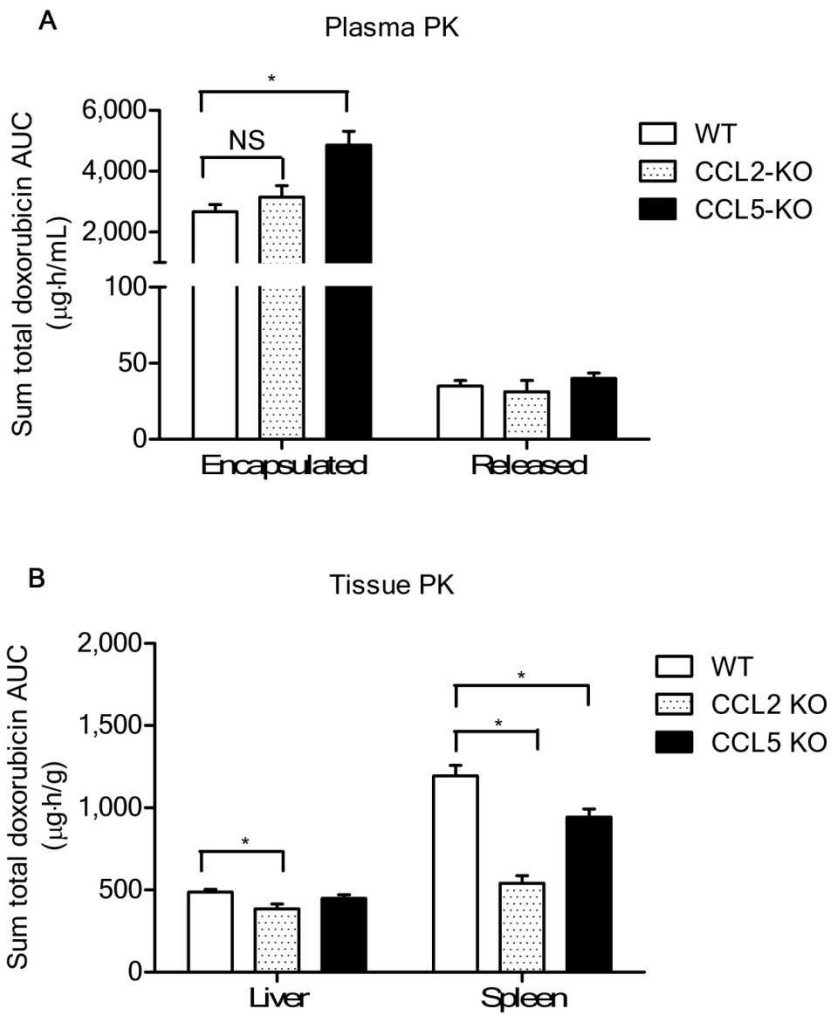

Fig. 2. 12. The PK of PLD in wild-type (WT), CCL2 knockout (KO), and CCL5 KO mice after administration of PLD at 6 mg/kg IV x1 via tail vein. (**A**) $AUC_{0\text{-}96h}$ of plasma encapsulated and released doxorubicin in WT (C57BL/6), CCL2 KO, and CCL5 KO mice. (**B**) Sum total doxorubicin $AUC_{0\text{-}96h}$ in liver and spleen in WT, CCL2 KO, and CCL5 KO mice. *P<0.05; equality of AUC was tested using Nedelman's modification for the Bailer method, using a two-sample test (31).

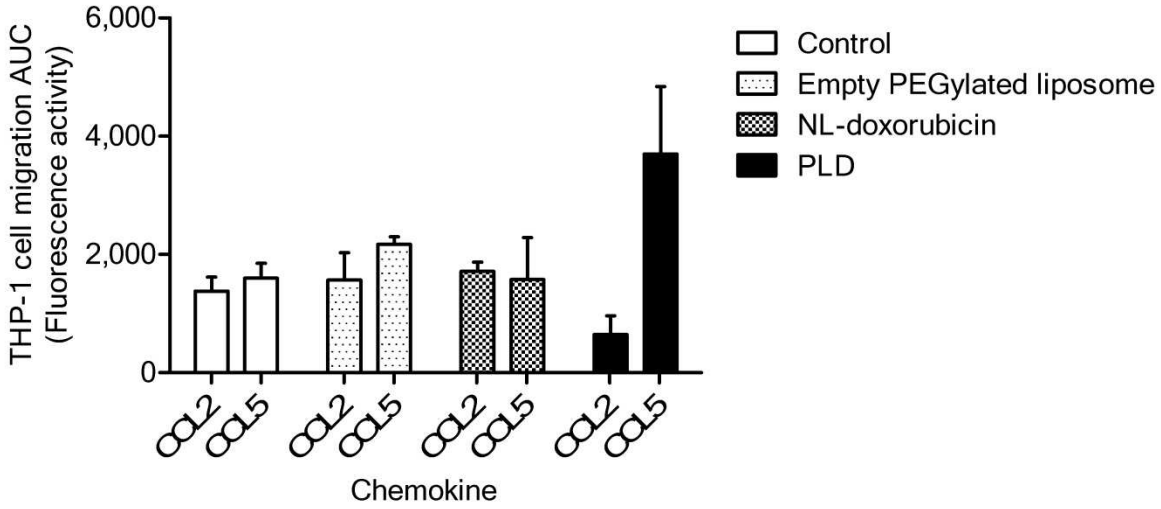

Fig. 2. 13. *In vitro* migration assay of THP-1 cells after incubating with medium (control), empty PEGylated liposomes, NL-doxorubicin or PLD. The migration of THP-1 cells preincubated with empty PEGylated liposomes and NL-doxorubicin to CCL2 and CCL5 was similar to that of control. However, PLD reduced CCL2-mediated chemotaxis of THP-1 cells by approximately 53 to 62% compared to control cells and other treatments (P>0.05, t-test). In contrast, PLD treatment has increased THP-1 cell migration to CCL5 by approximately 70 to 130% compared to control and other treatments (P>0.05, t-test) Data are presented as mean ± SEM of three individual experiments with triplicates for each treatment arm in each run. NL-doxorubicin: non-liposomal doxorubicin.

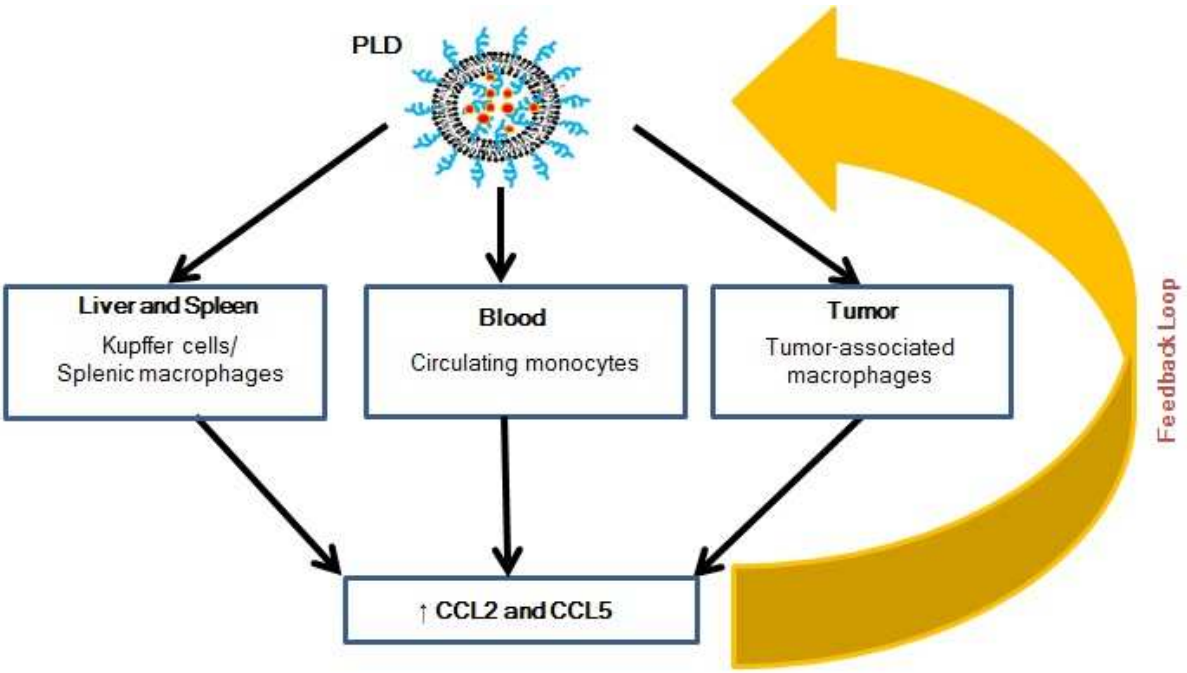

Fig. 2. 14. Feedback loop between PLD and monocytes/macrophages and chemokines. A complex interaction between PLD and monocytes and macrophages and chemokines may affect the clearance and biodistribution of PLD via a 'feedback loop'.

REFERENCES

(1) Farokhzad OC, Langer R. Impact of nanotechnology on drug delivery. ACS nano 2009;3(1):16-20.

(2) Peer D, Karp JM, Hong S, Farokhzad OC, Margalit R, Langer R. Nanocarriers as an emerging platform for cancer therapy. Nature nanotechnology 2007;2(12):751-760.

(3) Maeda H, Wu J, Sawa T, Matsumura Y, Hori K. Tumor vascular permeability and the EPR effect in macromolecular therapeutics: a review. J Controlled Release 2000;65(1):271-284.

(4) Prabhakar U, Maeda H, Jain RK, Sevick-Muraca EM, Zamboni W, Farokhzad OC, et al. Challenges and Key Considerations of the Enhanced Permeability and Retention Effect for Nanomedicine Drug Delivery in Oncology. Cancer Res 2013;73(8):2412-2417.

(5) Zamboni WC. Concept and clinical evaluation of carrier-mediated anticancer agents. Oncologist 2008;13(3):248-260.

(6) Bookman M. Standard treatment in advanced ovarian cancer in 2005: the state of the art. International Journal of Gynecological Cancer 2005;15(s3):212-220.

(7) Bookman MA. Developmental chemotherapy and management of recurrent ovarian cancer. Journal of Clinical Oncology 2003;21(10 suppl):149-167.

(8) Gordon AN, Fleagle JT, Guthrie D, Parkin DE, Gore ME, Lacave AJ. Recurrent epithelial ovarian carcinoma: a randomized phase III study of pegylated liposomal doxorubicin versus topotecan. Journal of Clinical Oncology 2001;19(14):3312-3322.

(9) O'brien M, Wigler N, Inbar M, Rosso R, Grischke E, Santoro A, et al. Reduced cardiotoxicity and comparable efficacy in a phase III trial of pegylated liposomal doxorubicin HCl (CAELYX™/Doxil®) versus conventional doxorubicin for first-line treatment of metastatic breast cancer. Annals of oncology 2004;15(3):440-449.

(10) La-Beck NM, Zamboni BA, Gabizon A, Schmeeda H, Amantea M, Gehrig PA, et al. Factors affecting the pharmacokinetics of pegylated liposomal doxorubicin in patients. Cancer Chemother Pharmacol 2012;69(1):43-50.

(11) Song G, Wu H, Yoshino K, Zamboni WC. Factors affecting the pharmacokinetics and pharmacodynamics of liposomal drugs. J Liposome Res 2012;22(3):177-192.

(12) Caron W, Song G, Kumar P, Rawal S, Zamboni W. Interpatient Pharmacokinetic and Pharmacodynamic Variability of Carrier-Mediated Anticancer Agents. Clinical Pharmacology & Therapeutics 2012;91(5):802-812.

(13) Li S, Huang L. Pharmacokinetics and biodistribution of nanoparticles. Molecular pharmaceutics 2008;5(4):496-504.

(14) Moghimi SM, Hunter AC, Murray JC. Long-circulating and target-specific nanoparticles: theory to practice. Pharmacol Rev 2001;53(2):283-318.

(15) Bertrand N, Leroux J. The journey of a drug-carrier in the body: an anatomo-physiological perspective. J Controlled Release 2012;161(2):152-163.

(16) Joyce JA. Therapeutic targeting of the tumor microenvironment. Cancer cell 2005;7(6):513.

(17) Lewis CE, Pollard JW. Distinct role of macrophages in different tumor microenvironments. Cancer Res 2006;66(2):605-612.

(18) Balkwill F. Cancer and the chemokine network. Nature Reviews Cancer 2004;4(7):540-550.

(19) Roussos ET, Condeelis JS, Patsialou A. Chemotaxis in cancer. Nature Reviews Cancer 2011;11(8):573-587.

(20) Deshmane SL, Kremlev S, Amini S, Sawaya BE. Monocyte chemoattractant protein-1 (MCP-1): an overview. Journal of Interferon & Cytokine Research 2009;29(6):313-326.

(21) Milliken D, Scotton C, Raju S, Balkwill F, Wilson J. Analysis of chemokines and chemokine receptor expression in ovarian cancer ascites. Clinical cancer research 2002;8(4):1108-1114.

(22) Soria G, Ben-Baruch A. The inflammatory chemokines CCL2 and CCL5 in breast cancer. Cancer Lett 2008;267(2):271-285.

(23) Ueno T, Toi M, Saji H, Muta M, Bando H, Kuroi K, et al. Significance of macrophage chemoattractant protein-1 in macrophage recruitment, angiogenesis, and survival in human breast cancer. Clinical Cancer Research 2000;6(8):3282-3289.

(24) Sahin H, Trautwein C, Wasmuth HE. Functional role of chemokines in liver disease models. Nature Reviews Gastroenterology and Hepatology 2010;7(12):682-690.

(25) Marra F, Romanelli RG, Giannini C, Failli P, Pastacaldi S, Arrighi MC, et al. Monocyte chemotactic protein-1 as a chemoattractant for human hepatic stellate cells. Hepatology 1999;29(1):140-148.

(26) Baeck C, Wehr A, Karlmark KR, Heymann F, Vucur M, Gassler N, et al. Pharmacological inhibition of the chemokine CCL2 (MCP-1) diminishes liver macrophage infiltration and steatohepatitis in chronic hepatic injury. Gut 2012;61(3):416-426.

(27) Mantovani A, Sica A, Sozzani S, Allavena P, Vecchi A, Locati M. The chemokine system in diverse forms of macrophage activation and polarization. Trends Immunol 2004;25(12):677-686.

(28) Viola A, Luster AD. Chemokines and their receptors: drug targets in immunity and inflammation. Annu Rev Pharmacol Toxicol 2008;48:171-197.

(29) Zamboni WC, Maruca LJ, Strychor S, Zamboni BA, Ramalingam S, Edwards RP, et al. Bidirectional pharmacodynamic interaction between pegylated liposomal CKD-602 (S-CKD602) and monocytes in patients with refractory solid tumors. J Liposome Res 2011;21(2):158-165.

(30) The development of liposomal and nanoparticle anticancer agents: methods to evaluate the encapsulated and released drug in plasma and tumor and phenotypic probes for pharmacokinetic (PK) and pharmacodynamic (PD) disposition. Proceedings of the 2007 NSTI Nanotechnology Conference; 2007.

(31) Nedelman JR, Gibiansky E, Lau DT. Applying Bailer's method for AUC confidence intervals to sparse sampling. Pharm Res 1995;12(1):124-128.

(32) Tsuchiya S, Yamabe M, Yamaguchi Y, Kobayashi Y, Konno T, Tada K. Establishment and characterization of a human acute monocytic leukemia cell line (THP-1). International journal of cancer 1980;26(2):171-176.

(33) Auwerx J. The human leukemia cell line, THP-1: a multifacetted model for the study of monocyte-macrophage differentiation. Experientia 1991;47(1):22-31.

(34) Nielsen H, Rørth M, Bennedsen J. Monocyte chemotaxis in patients with nonseminomatous testicular carcinoma. Cancer Immunology, Immunotherapy 1985;19(1):68-71.

(35) Nielsen H. Effect of cis-platinum on human blood monocyte function in vitro. Cancer Immunology, Immunotherapy 1984;18(3):223-225.

(36) Caron WP, Lay JC, Fong AM, La-Beck NM, Kumar P, Newman SE, et al. Translational Studies of Phenotypic Probes for the Mononuclear Phagocyte System and Liposomal Pharmacology. J Pharmacol Exp Ther 2013:jpet. 113.208801.

(37) Sharpless NE, DePinho RA. The mighty mouse: genetically engineered mouse models in cancer drug development. Nature Reviews Drug Discovery 2006;5(9):741-754.

(38) Salcedo R, Ponce ML, Young HA, Wasserman K, Ward JM, Kleinman HK, et al. Human endothelial cells express CCR2 and respond to MCP-1: direct role of MCP-1 in angiogenesis and tumor progression. Blood 2000;96(1):34-40.

(39) Qian B, Li J, Zhang H, Kitamura T, Zhang J, Campion LR, et al. CCL2 recruits inflammatory monocytes to facilitate breast-tumour metastasis. Nature 2011;475(7355):222-225.

(40) Alexis F, Pridgen E, Molnar LK, Farokhzad OC. Factors affecting the clearance and biodistribution of polymeric nanoparticles. Molecular pharmaceutics 2008;5(4):505-515.

(41) Anders HJ, Frink M, Linde Y, Banas B, Wornle M, Cohen CD, et al. CC chemokine ligand 5/RANTES chemokine antagonists aggravate glomerulonephritis despite reduction of glomerular leukocyte infiltration. J Immunol 2003 Jun 1;170(11):5658-5666.

(42) Villalta F, Zhang Y, Bibb KE, Kappes JC, Lima MF. The cysteine-cysteine family of chemokines RANTES, MIP-1alpha, and MIP-1beta induce trypanocidal activity in human macrophages via nitric oxide. Infect Immun 1998 Oct;66(10):4690-4695.

(43) Tanaka T, Terada M, Ariyoshi K, Morimoto K. Monocyte chemoattractant protein-1/CC chemokine ligand 2 enhances apoptotic cell removal by macrophages through Rac1 activation. Biochem Biophys Res Commun 2010;399(4):677-682.

(44) Storm G, Steerenberg P, Emmen F, van Borssum Waalkes M, Crommelin D. Release of doxorubicin from peritoneal macrophages exposed in vivo to doxorubicin-containing liposomes. Biochimica et Biophysica Acta (BBA)-General Subjects 1988;965(2):136-145.

(45) Rezaie-Majd A, Maca T, Bucek RA, Valent P, Müller MR, Husslein P, et al. Simvastatin reduces expression of cytokines interleukin-6, interleukin-8, and monocyte chemoattractant protein-1 in circulating monocytes from hypercholesterolemic patients. Arterioscler Thromb Vasc Biol 2002;22(7):1194-1199.

(46) Han KH, Ryu J, Hong KH, Ko J, Pak YK, Kim J, et al. HMG-CoA reductase inhibition reduces monocyte CC chemokine receptor 2 expression and monocyte chemoattractant protein-1–mediated monocyte recruitment in vivo. Circulation 2005;111(11):1439-1447.

(47) Jain RK, Stylianopoulos T. Delivering nanomedicine to solid tumors. Nature Reviews Clinical Oncology 2010;7(11):653-664.

(48) Balkwill F, Mantovani A. Cancer and inflammation: implications for pharmacology and therapeutics. Clinical Pharmacology & Therapeutics 2010;87(4):401-406.

(49) Murray PJ, Wynn TA. Protective and pathogenic functions of macrophage subsets. Nature Reviews Immunology 2011;11(11):723-737.

(50) Garber K. First results for agents targeting cancer-related inflammation. J Natl Cancer Inst 2009;101(16):1110-1112.

CHAPTER 3:

EFFECTS OF TUMOR MICROENVIRONMENT HETEROGENEITY ON NANOPARTICLE DISPOSITION AND EFFICACY IN BREAST CANCER TUMOR MODELS[3]

Overview

Purpose: Tumor cells are surrounded by a complex microenvironment comprised of immune cells, chemokines and cytokines, and abnormal blood and lymphatic vasculature. The purpose of our study was to evaluate the role of heterogeneity of the tumor microenvironment in the variability of nanoparticle (NP) delivery and efficacy.

Experimental designs: *C3(1)-T-Antigen* genetically engineered mouse model (C3-TAg) and *T11*/*TP53*^{Null} orthotopic syngeneic murine transplant model (T11) representing human breast tumor subtypes basal-like and claudin-low, respectively, were evaluated. For the pharmacokinetic studies, non-liposomal doxorubicin (NL-doxo) or PEGylated liposomal doxorubicin (PLD) was administered at 6 mg/kg IV x1. Area-under-the concentration versus time curve (AUC) of doxorubicin was calculated. Macrophages, collagen, and the amount of vasculature were assessed by immunohistochemistry. Chemokines and cytokines were measured by multiplex immunochemistry. NL-doxo or PLD was administered at 6 mg/kg IV weekly x6 in efficacy studies. Analyses of intermediary tumor response and overall survival were performed.

Results: Plasma AUC of NL-doxo and PLD encapsulated and released doxorubicin were similar between two models. However, tumor sum total AUC of PLD was 2-fold greater in C3-

[3]This chapter has been submitted to the *Clinical Cancer Research* and is presented in the style of the journal.

TAg compared with T11 ($P<0.05$). T11 tumors showed significantly higher expression of CCL2 and VEGF-a, greater vascular quantity, and decreased expression of VEGF-c compared to C3-TAg ($P<0.05$). PLD was more efficacious compared to NL-doxo in both models.

Conclusion: The tumor microenvironment and/or tumor cell features of breast cancer affected NP tumor delivery and efficacy, but not the small molecule drug. Our findings reveal the role of the tumor microenvironment in variability of NP delivery and therapeutic outcomes.

3. 1. Introduction

There have been major advances in nanotechnology for targeted delivery of pharmacologic agents to sites of disease, such as cancer (1, 2). In oncology, nanoparticle (NP)-based therapies exploit the enhanced permeability and retention (EPR) effect caused by the unique vascular structure of solid tumors (i.e., hypervasculature and defective lymphatic drainage) (3). The EPR effect is a key rationale that advances the use of NPs for treatment of cancer and renders the preferential delivery and accumulation of NPs to the tumor cells (3). This allows nanomedicines to have advantages over conventional medicines including prolonged circulation, selective delivery of entrapped drug to tumor, and improved therapeutic index (4). There is, however, limited data to understand the heterogeneity and factors affecting the EPR in tumors and, more importantly, correlate them to highly variable clinical responses of NP-based therapies (5).

It has been shown that NPs have immunological properties that may stimulate or suppress the immune system (6). NPs can interact with immune components in blood, which influences the uptake and clearance by the mononuclear phagocyte system (MPS), and potentially biodistribution and delivery to the targeted site such as tumors (7, 8). Previously, we have

reported that the variability in the pharmacokinetics (PK) and pharmacodynamics (PD) of nanomedicines such as Doxil® (PEGylated liposomal doxorubicin; PLD) and S-CKD602 (PEGylated liposome of CKD-602, a camptothecin analog) is associated with patient age, gender, and the function of circulating monocytes in plasma of patients with solid tumors (9-11). We also showed a bidirectional interaction between SCKD-602 and circulating monocytes in patients with solid tumors (12). However, these factors may not sufficiently explain the high variability in the PK and PD of NP-based therapies in patients with solid tumors.

Solid tumors are characterized by a complex and unique microenvironment that consists of infiltrating immune cells such as tumor-associated macrophages (TAMs), a variety of growth factors, chemokines and cytokines, dense interstitial matrix, and the abnormal blood and lymphatic vascular architecture (13, 14). These factors interplay with the tumor cells to modify the tumor microenvironment and promote tumor progression (13, 14). It has been reported that there is intra- and inter-tumor variability in the tumor cells and the microenvironment that results in the heterogeneity of molecular, pathological, and clinical features of each tumor type (15-17). Studies have revealed that abnormal vascular architecture and dense collagen matrix can act as environmental barriers hindering the delivery of NPs and result in suboptimal clinical outcomes (17). Previously, we have also reported that increased tumor delivery and release of CKD-602 from S-CKD602 in SKOV-3 ovarian xenografts compared with A375 melanoma xenografts correlated with increased expression of CD11c positive dendritic cells (DCs) in the tumors, suggesting that the variability in NP tumor disposition may be associated with the phagocytic cells (i.e., DC and TAMs) (18). Given the heterogeneity of the tumor microenvironment between and within different human cancer types and its potential impacts on the tumor delivery and therapeutic outcomes of NP-based therapy, it is imperative to evaluate the roles of the

microenvironment factors and their interaction with NPs in a systemic manner for the optimal delivery and efficacy of nanomedicines (5, 17).

Genetically engineered mouse models (GEMMs) and orthotopic syngeneic murine transplant (OST) have proven to be valuable experimental models for discovery of biomarkers and prediction of chemotherapy responses in human cancers (19, 20). RNA expression profiling of 13 distinct GEMMs of breast cancer identified mouse models that faithfully represent human intrinsic breast tumor subtypes including Basal-like (*C3(1)-T-Antigen* (C3-TAg)) (21) and Claudin-low (*T11/TP53*$^{-/-}$ (T11)) (22). No single claudin-low GEMM was found, but orthotopic syngeneic transplantable tumors from a BALB/c *TP53*^{Null} mouse was shown to faithfully recapitulate the human claudin-low expression phenotype (22). Basal-like subtype (C3-TAg) is characterized by high expression of basal gene expression features and the proliferation signature (19, 21). The majority of these tumors are clinically estrogen receptor (ER) negative, progesterone receptor (PR) negative, and HER2-negative (triple negative breast cancer), which leads to lack of validated biological targets and poor responses to current chemotherapies (19, 21). The majority of claudin-low (T11) tumors are also triple negative breast tumors with poor prognosis but were shown to have lower pathological complete response (pCR) rate to anthracycline/taxane-based chemotherapies compared to basal-like tumors (23). Claudin-low T11 tumors exhibited distinguished gene expression characteristics (i.e. more enriched in immune system responses and endothelial cell-like signature) as well as histological phenotypes (i.e. endothelial/tube-like morphology and high vascular permeability) compared to basal-like C3-TAg tumors (23, 24).

Here, we used the genomically validated basal-like C3-TAg and claudin-low T11 murine breast tumor models to test our hypothesis that the heterogeneity of the tumor cells and the tumor

microenvironment between breast tumor subtypes affect the tumor delivery and therapeutic outcomes of NP. We evaluated PEGylated liposomal doxorubicin (PLD; Doxil®) which has been used for treatment of metastatic breast cancer and non-liposomal doxorubicin (NL-doxo; Adriamycin®) as a comparator (25). Furthermore, we examined the dynamic modulation of the tumor physiology, such as TAMs, collagen, tumor vasculature, and chemokines, after treatment with both agents in these mouse models.

3. 2. Materials and Methods

Treatments. PLD was purchased from FormuMax Scientific (Palo Alto, CA) (**Table 3. 1**) and diluted with 5% dextrose to 1.2 mg/mL prior to injection. NL-doxo was purchased from Sigma Aldrich (St. Louis, MO) and diluted with 0.9% NaCl to 1.2 mg/mL prior to injection.

Animal Models. *In vivo* experiments were performed with the approval of University of North Carolina at Chapel Hill's Institutional Animal Care and Use Committee (IACUC). GEMM of strain of FVB/n carrying a transgene for *C3(1)SV40 T-antigen* (C3-TAg) were bred in-house and observed until the tumor size was met (> 0.5 cm) in any dimension (19). Tumors derived from *BALB/c TP53*$^{-/-}$ orthotopic mammary gland transplant line (T11) was transplanted into the inguinal mammary fat pad of 12 week old wild-type BALB/c mice (Jackson Labs, strain 000651) (19). Mice were housed in the UNC Lineberger Comprehensive Cancer Center's Mouse Phase I Unit (MP1U) and observed for tumors as per standard practice (22). Mice were randomized to treatment cohorts and therapy began once a tumor reached 60-100 mm^3.

PK Studies in Plasma, Tissues, and Tumor. NL-doxo and PLD were administered at 6 mg/kg IV x1 via a tail vein. Mice (n=3) were euthanized prior to and at 0.083, 0.5, 1, 3, 6, 24, 48, 72, and 96 h after administration of each drug. Each blood sample was processed to evaluate

encapsulated and released doxorubicin in plasma as described previously (18, 26). In the same mice, liver, spleen, lung, and tumors were collected, preserved by snap freezing, and stored at –80°C. To measure the sum total (encapsulated and released) doxorubicin in tumors and tissue samples, samples were thawed on ice, weighed, and homogenized with pH 7.4 PBS buffer (1g tissue: 3mL PBS) using a Precellys (13-RD000) 24 bead mill homogenizer (Omni International, Inc.). Doxorubicin concentration was determined using an existing high performance liquid chromatography-fluorescence (HPLC-FL) assay (18, 26). Noncompartmental PK analysis of NL-doxo and PLD in plasma, tumor, and tissues were performed using Phoenix v.6.2 (Pharsight Corp., CA). The area under the concentration versus time curve from 0 to t (AUC_{0-t}) was calculated using the linear up and log down rule.

Immunohistochemistry (IHC) and Digital Imaging. Tumor samples were collected at necropsy, fixed overnight in 10% neutral-buffered formalin, processed routinely, and stained with hematoxylin and eosin (H&E). IHC for F4/80 (TAM), collagen IV, and CD31 (endothelial cells) were performed as well (27). Rat monoclonal antibody against F4/80 and rabbit polyclonal antibodies against CD31 and collagen IV (Col IV) were from eBioscience (San Diego, CA), Abcam (Cambridge, MA), and EMD Millipore (Billerica, MA), respectively. IHC for F4/80 (murine macrophage marker), collagen IV, and CD31 (endothelial cells) was performed on an automated Bond II immunostainer (Leica Microsystems, Norwell, MA).[78-84] Tumor slides were dewaxed in Bond Dewax solution (AR9222) and hydrated in Bond Wash solution (AR9590). Antigen retrieval for F4/80 was done for 20 min and for 30 min for CD31 and Col IV in Bond-Epitope Retrieval solution1 pH-6.0 (AR9961). Slides were incubated for 45 min with F4/80 (1:100), for 1h with CD31 (1:200), and for 30min with Col IV (1:200). Stained slides were dehydrated and coverslipped. Detection of the antibodies was performed using the Bond Polymer

Refine Detection System without post primary step (DS9800). Positive and negative controls (no primary antibody) were included for each antibody. Stained slides were digitally imaged at 20X apparent magnification using the Aperio ScanScope XT (Aperio Technologies, Vista, CA). The Aperio ImageScope positive pen tool was used to create the different annotation layers (capsule, viable tumor, and necrotic) for each tumor section under the guidance of board-certified veterinary pathologist (A.B.R.) in a blinded manner. Medium to high magnification fields (10X - 20X) were marked for subsequent image analysis.

Morphometric Quantitation of Macrophages, Collagen, and Microvessel Density (MVD). Whole tumor images were captured using an Aperio slide scanner at the UNC Translational Pathology Laboratory. F4/80+ macrophages were classified into three groups: (a) peritumoral/peripheral - capsule; (b) intratumoral - viable; and (c) intratumoral – necrotic (28, 29). Morphology and identification of subregions were determined in consultation with a board-certified veterinary pathologist (A.B.R.). For semi-quantification of F4/80 immunoreactivity, H-scores were generated by The Aperio Membrane v9 algorithm. Staining intensity was graded as undetectable (1), weak (2), medium (3), or strong (4), and the percentage of positive cells per each intensity level was evaluated. The intensity score and the percentage of positive cells were then multiplied to give an H-score (possible range, 0-400) within each annotation layer (27, 28).

For scoring collagen IV semi-quantitatively, H-scores were generated by the Aperio color deconvolution methods. Staining intensity was graded as weak (1), moderate (2), and strong (3), and % of positive pixel per each intensity level was evaluated to calculate H-score (0-300) (27).

MVD was calculated by number of vessels divided by stained areas (mm2) using the Definien Tissue Studio software (Munich, Germany) (30). The physiologic state of the

vasculature including the size and open lumen status was assessed in representative vascularized areas within tumor (30). Collagen and MVD were assessed in capsule and viable tumor only.

Multiplex-bead Array Assay. Mouse Cytokine/Chemokine Magnetic Bead Panel was purchased from Milipore (Billerica, MA). The 96-well plate kit was customized to measure CC chemokine ligand (CCL) 2, also known as monocyte chemoattractant protein-1 (MCP-1), and CC chemokine ligand (CCL) 5, also known as regulated on activation, normally T-cell expressed and secreted (RANTES), in plasma and tumor and vascular endothelial growth factor-a (VEGF-a) and VEGF-c in tumor (14, 30). Tumor tissues were weighed and homogenized with pH 7.4 PBS buffer spiked with a protein inhibitor cocktail (Calbiochem, MA) in 1:3 (tumor weight: PBS volume) using a Precellys (13-RD000) 24 bead mill homogenizer (Omni International, Inc.). Supernatant was extracted and used for assay. Standards were made using Assay Buffer provided with the kit. Standards and QC controls were placed to appropriate wells and samples diluted with Assay Buffer were placed to designated sample wells. The resulting raw data were collected using Luminex-100 system (Luminex, Austin, TX) and the concentration was corrected based on dilution factor used during procedures.

Efficacy Studies. Once tumor mass reached 60-100 mm^3, mice were randomized into treatment groups. NL-doxo and PLD were administered at 6 mg/kg x1 weekly for 6 weeks. Tumors were measured using calipers daily and tumor volume was calculated as ($Volume = [(width)^2 \times length]/2$). Treatment outcome was assessed as intermediary tumor volume and tumor growth inhibition (TGI %) (31). TGI was calculated from the following formula: TGI (%) = (1-T/C) x 100, where T indicates the mean final tumor volume (mm3) of the treatment group and C indicates the mean final tumor volume (mm3) of the control group (31). Survival was monitored

individually and mice were euthanized for tumor ulceration, tumor size of 2 cm in any dimension with single tumor, or 1.3 cm in any dimension with multiple tumors.

Statistical Analysis. Statistical analyses were carried out using SAS v.9.2 (Cary, NC) and Prism5 software (GraphPad Software, Inc.). Equality of AUC between C3-TAg model and T11 model was tested Nedelman's modification of the Bailer method for sparse samples, using a two-sample t-test (32). Analysis of covariance (ANCOVA) with baseline tumor volume as covariate was performed followed by adjustment for multiple comparison using Holm test to test intermediary tumor volume among treatment groups (33). Kaplan-Meier (KM) survival curves were plotted, and the difference in overall survival between the groups was analyzed by the log-rank test. *P* value of less than 0.05 was considered statistically significant. All statistical tests were two-sided.

3. 3. Results

Plasma, Tissue, and Tumor Disposition of NL-doxo and PLD. To predict plasma, tissue, and tumor disposition of NL-doxo and PLD in human basal-like and claudin-low breast tumor subtypes, we performed the PK studies of NL-doxo and PLD in their murine counterparts, C3-TAg model and T11 model, respectively. Plasma, tissues, and tumor doxorubicin concentration versus time profiles after administration of NL-doxo or PLD at 6 mg/kg IV x 1 are presented in Fig. 1. AUC from 0 to 96 h, a measured index of the total doxorubicin exposure over time, was calculated by noncompartmental PK analysis. PK parameters for both treatments are presented in **Table 3. 2**.

The doxorubicin $AUC_{0\text{-}96h}$ in plasma, tissues, and tumors after NL-doxo administration were similar between two models ($P>0.05$) (**Fig. 3. 1A, 1C, 1D, 1E,** and **1F**). In PLD treated

mice, both plasma encapsulated (the drug within the liposomal carrier) and released (active-drug released from the liposomal carrier) doxorubicin $AUC_{0\text{-}96h}$ were similar in the two models (**Fig. 3. 1B**). However, after PLD administration, the sum total (encapsulated + released) doxorubicin $AUC_{0\text{-}96h}$ in tumors was 2-fold greater in C3-TAg compared to T11 (480 ± 71 versus 210 ± 30 µg·h/g, respectively; $P<0.05$) (**Fig. 3. 1C**). The doxorubicin accumulation in the liver was 1.5-fold higher in T11 compared to C3-TAg after PLD administration (687 ± 61 versus 438 ± 18 µg·h/g, respectively; $P<0.05$) (**Fig. 3. 1D**). The doxorubicin accumulation in the spleen and the lung was similar between C3-TAg and T11 after NL-doxo and PLD administration (**Fig. 3. 1E** and **F**). These data suggest that heterogeneity of the tumor microenvironment and/or tumor cell features between C3-TAg and T11 models affected PLD tumor delivery and distribution to the liver, but not NL-doxo.

Tumor-Associated Macrophages (TAMs). To evaluate the effects of TAMs on the delivery of NL-doxo and PLD and characterize the interaction with these drugs, C3-TAg tumors and T11 tumors from the PK studies were stained for F4/80 (**Fig. 3. 2**). At baseline, most TAMs were located in the hypoxic necrotic area and the periphery (capsule) with lower numbers present in viable tumor in both models (**Table 3. 3**). There was no significant difference in the baseline level of TAMs in all sub-regions between two models.

However, the time profile of TAMs over 96 h was distinguished between after NL-doxo or PLD administration (**Fig. 3. 3**). The changes in the TAM infiltration after NL-doxo administration were inconsistent between C3-TAg and T11 models (**Fig. 3. 3A** and **3C**). In contrast, after PLD, a nadir occurred at 24 h followed by TAM infiltration in both models (**Fig. 3. 3B** and **3D**). The % decrease at nadir (24 h) in TAMs localized in the vial tumors was greater in T11 compared to C3-TAg (37.2% vs. 6.6%) (**Fig. 3. 3B** and **3D**). The $AUC_{0\text{-}96h}$ of F4/80 H-

score, an indicator of total influx of TAMs, was similar between C3-TAg model and T11 model after administration of NL-doxo and PLD (**Table 3. 2**).

CCL2 and CCL5 in Tumors and Plasma. CCL2 and CCL5 are overexpressed in human and murine breast tumors and play a central role in mobilization of monocytes into tumors and differentiation into TAMs (14, 34). To evaluate whether these chemokines are associated with tumor delivery of PLD or NL-doxo *in vivo*, we measured intratumoral concentrations of CCL2 and CCL5 at 0, 24, 48, and 96 h after PLD or NL-doxo administration using multiplex chemokine assay.

Baseline CCL2 concentration was 5-fold higher in T11 tumors than C3-TAg tumors (18 ± 1.5 versus 3.8 ± 0.5 ng/g: mean ± SEM, respectively) ($P<0.0001$) (**Fig. 3. 4A**). CCL2 concentration in tumors increased over 96 h to a greater extent after PLD compared to NL-doxo in both models (**Fig. 3. 4A**). Interestingly, it was noted that the time profile of CCL2 in tumors resembled the time course of TAMs after NL-doxo and PLD in T11 (**Fig. 3. 3C, D,** and **4A**). In plasma, baseline CCL2 concentrations were 2-fold higher in T11 compared to C3-TAg (148 ± 49 versus 74 ± 8 ng/mL, respectively) ($P=0.19$) (**Fig. 3. 4B**). Plasma CCL2 concentration was significantly increased at 96 h after PLD in C3-TAg model ($P=0.023$), but little was changed in T11 model (**Fig. 3. 4B**).

In contrast to CCL2, there was no difference in baseline CCL5 tumor concentrations between two models (0.5 ± 0.1 versus 0.4 ± 0.1 ng/g: mean ± SEM) (**Fig. 3. 4C**). After PLD administration, there was a noticeable increase in CCL5 tumor concentrations at 96 h in T11 model ($P=0.002$), but a high variability was observed at 96 h in C3-TAg model ($P=0.24$) (**Fig. 3. 4C**). In plasma, baseline CCL5 concentrations were similar between two models. Little change

was observed in plasma CCL5 concentration after PLD or NL-doxo administration in both models (**Fig. 3. 4D**).

Next, we assessed the total amount of chemokine produced in tumors after PLD or NL-doxo administration by calculating the AUC from 0 to 96 h, a measured index of the total amount of a chemokine produced over time. CCL2 $AUC_{0\text{-}96h}$ was significantly greater in T11 model compared with C3-TAg model after PLD administration (707 ± 119 versus 2,332 ± 235 ng·h/g: mean ± SEM; $P<0.05$) and NL-doxo (406 ± 76 versus 1,505 ± 218 ng·h/g; $P<0.05$). However, there was no difference in plasma CCL2 $AUC_{0\text{-}96h}$, plasma CCL5 $AUC_{0\text{-}96h}$, and tumor CCL5 $AUC_{0\text{-}96h}$ between two models. Together, these data indicate that there was an inverse relationship between the levels of intratumoral CCL2 expression and tumor delivery of PLD. Moreover, PLD showed to induce CCL2 expression in tumors to a greater extent than NL-doxo and the increase was more pronounced in T11 model compared to C3-TAg model.

Collagen and the Vasculature in Tumors. To assess the effects of tumor physiology on the tumor delivery of NL-doxo and PLD, tumors at baseline were stained for extracellular collagen matrix (collagen IV) and the quantity and physiologic state of the vasculature (CD31) (**Fig. 3. 2**) (17). We also evaluated the changes from baseline at 96 h after NL-doxo or PLD administration to characterize the interaction between the drugs and these factors.

H-score of collagen at baseline was 1.5-fold greater in C3-TAg than T11 (82 ± 13 versus 53 ± 24, respectively; $P>0.05$). Collagen expression tended to modestly increase after administration of NL-doxo and PLD in both models except in T11 tumors treated with NL-doxo ($P>0.05$) (**Fig. 3. 5**).

The baseline vascular quantity measured by MVD score was significantly greater in T11 tumors compared to C3-TAg tumors (933 ± 65 versus 691 ± 67 mean MVD ± SEM,

respectively) (*P*=0.04) (**Fig. 3. 6A**). Most of the blood vessels identified were small (~87%), followed by medium (12%) and large (1%) in both models (**Fig. 3. 7**). In addition, a significantly greater number of blood vessels in T11 tumors were shown to have open lumen compared to C3-TAg tumors (*P*=0.01), indicating hyperperfusion and hyperpermeability of the vasculature in T11 tumors (**Fig. 3. 6B**). After administration of NL-doxo or PLD, the vascular quantity in C3-TAg tumors did not change over time (**Fig. 3. 6C**); however, there was a 31 % decrease in MVD score from baseline to 96 h after PLD in T11 tumors (933 ± 65 at 0 h versus 555 ± 69 at 96 h: mean MVD ± SEM; *P*>0.05) (**Fig. 3. 6D**).

Vascular Endothelial Growth Factors (VEGF) in Tumors. VEGF-a and VEGF-c are known for their central role in angiogenesis and lymphangiogenesis in the tumor microenvironment, respectively (30). As these growth factors play a crucial role in determining vascular permeability, lymphatic drainage of fluid from tumors, and EPR effects, intratumoral VEGF-a and VEGF-c were measured to examine the impacts on transvascular transport of NL-doxo and PLD. At baseline, VEGF-a was approximately 7-fold higher in T11 tumors than C3-TAg tumors (11 ± 1.6 versus 1.5 ± 1.2 ng/g: mean ± SEM; *P*=0.003) (**Fig. 3. 8A**). VEGF-c was 2-fold higher in C3-TAg tumors compared to T11 tumors at baseline (2.3 ± 0.4 versus 1.1 ± 0.1 ng/g) (*P*=0.03) (**Fig. 3. 8B**).

To explore the effects of PLD and NL-doxo on angiogenesis in different breast tumor subtypes, we evaluated the modulation of these pro-angiogenic factors over time after each drug treatment. Surprisingly, the effects of PLD and NL-doxo on expression of VEGF-a and VEGF-c appeared to vary with breast tumor subtypes. After PLD administration, VEGF-a in T11 tumors was steadily decreased in T11 but increased in C3-TAg tumors (*P*=0.02) (**Fig. 3. 8A**). This finding was consistent with the changes seen in the MVD score after PLD administration (**Fig. 3.**

4E and **F**). PLD significantly reduced VEGF-c in C3-TAg tumors (*P*=0.02), but elevated it in T11 tumors (*P*=0.05) (**Fig. 3. 8B**). NL-doxo also altered the expression of VEGF-a and VEGF-c in both models, but to a lesser extent compared to PLD (**Fig. 3. 8A** and **B**). These results suggest that T11 tumors exhibit hypervascularization and impaired lymphatic functions compared to C3-TAg tumors as demonstrated by higher VEGF-a and lower VEGF-c, which may hamper the tumor delivery of PLD (13, 17). In addition, PLD demonstrated anti-angiogenic effects and pro-lymphangiogenic effects on T11 tumors, which may return the vasculature to more normal phenotype over 96 hour, but not on C3-TAg tumors (17, 35).

Efficacy. In order to evaluate the effectiveness of PLD or NL-doxo in C3-TAg and T11 breast tumors, we performed the efficacy studies using no treatment (NT), NL-doxo, and PLD. With a null hypothesis of equal tumor growth with a chemotherapeutic agent in two groups of murine tumor models of breast cancer, 15 mice per group give 80% power to detect a difference of 1.06 SD at two-sided α level of 0.05 based on error estimates from previous study results (20). We tested 20 mice per treatment group for each mouse model to have an appropriate power to detect a difference in responses.

Intermediary tumor volume at 21 days for C3-TAg model and at 14 days for T11 model was used to quantify the therapeutic responses. The 21 day and 14 day response for each model was chosen as the primary response endpoint based on the fact that 50% of the untreated animals did not survive past 21 days for C3-TAg model and 14 days for T11 model. The median and range of survival days of untreated C3-TAg and T11 mice were 20 (12-47) and 15 (14-20), respectively (20).

Mean tumor growth is presented in **Fig. 3. 9A** and **B**. Mean tumor volume comparison indicated that PLD was more efficacious at inhibiting the growth of both breast tumors compared

to no treatment or NL-doxo (P=0.013 and P<0.0003, respectively). TGI% of NL-doxo and PLD was 34.6 and 56.8 in C3-TAg model, and 29.6 and 76.3 in T11 model, respectively, which indicates that T11 tumors may be slightly more responsive to PLD compared to C3-TAg tumors (**Fig. 3. 9C** and **D**). KM plots are presented in Fig. 6E and 6F. PLD significantly prolonged the survival of C3-TAg models (P<0.0001), but modestly in T11 models (P=0.083) compared with no treatment and NL-doxo. However, it should be noted that T11 tumors treated with PLD became ulcerative in 18 days post treatment and were terminated in accordance to IACUC guidelines as a humane endpoint for the study. Ulceration is a lesion typified by a necrosis of tissues, which may reflect responses of T11 tumors to PLD (36). Thus, the results of overall survival for T11 mice treated with PLD may not reflect the accurate survival outcomes.

3. 4. Discussion

Heterogeneity in tumor cells and/or the tumor microenvironment observed within and between tumor types is suggested to be a contributing factor to inefficient transport of nanomedicines to tumors, but there are limited preclinical and clinical data to understand the mechanisms and correlate the varying clinical responses to nanomedicines (5, 9, 11).

We used genomically validated murine breast tumor models and demonstrated that tumor delivery of PLD was significantly greater in the basal-like C3-TAg model compared to the claudin-low T11 model (P<0.05), whereas the difference in tumor delivery was not seen with NL-doxo. In addition, claudin-low T11 tumors were more responsive to PLD compared to basal-like C3-TAg tumors. To evaluate which tumor-associated factors may contribute to the variable tumor delivery and efficacy of PLD in breast tumor subtypes, we assessed the physiological factors that have shown to be associated with NP transportation into and within tumors,

including TAMs, collagen, and blood and lymphatic vasculature as well as chemokines (13, 14, 17)

TAMs are major leukocytes recruited into murine and human tumors by chemoattractants and educated by the tumor microenvironment to promote tumor progression (13, 29). Macrophages have been shown to be involved in phagocytosis and clearance of NPs (7, 8, 10, 11) and to promote delivery of NPs into tumors serving as a “Trojan Horse” (37). Based on the evidence, we evaluated TAMs in association with tumor delivery and efficacy of PLD compared to NL-doxo in two breast tumor subtypes. The baseline level of TAMs were similar between two models, which indicates that the level of TAMs may not account for the variable tumor delivery of PLD in these breast tumor subtypes (38, 39). However, the different changes of TAMs over time after NL-doxo or PLD in two models implicate the drug- and tumor-dependent interaction between TAMs and drugs. Consistent with data generated in studies by our group and others, our finding indicates that uptake of PLD by TAMs may lead to cytotoxicity and cause a temporal decrease in the number of TAMs (12, 40).

Recruitment of TAMs to solid tumors is regulated by chemokines, in particular CCL2, secreted by both malignant and stromal cells (14, 41). Hence, the system of CCL2 and its major receptor CCR2 has been shown to promote tumor cell survival and motility (42), metastasis (43), and angiogenesis (41). In addition, induction of CCL2 expression and CCL2-mediated monocyte/myeloid cell recruitment have shown to mediate therapeutic anticancer immune response elicited by immunogenic chemotherapy (i.e. doxorubicin) (44) and counteract the antitumor effects of vascular-targeted therapies (i.e. VEGF inhibitor) as a compensatory mechanism (45, 46). In consistent with these observations, the expression of CCL2 in both C3-TAg tumors and T11 tumors was increased after NL-doxo and, to a greater extent, after PLD,

suggesting that PLD is more immunogenic compared to NL-doxo (6, 7). In addition, in T11 tumors where PLD exhibited anti-angiogenic effects, PLD-mediated induction of CCL2 expression was significantly greater compared to C3-TAg tumors (45, 46).

In addition to cancer, CCL2 is also well studied for its chemotactic effects, activation of stellate cells, and angiogenesis in acute and chronic liver inflammation (47). Given that cancer can be considered as a chronic inflammatory disease, it is possible that elevated plasma CCL2 may serve as an inflammatory stimulus to monocytes and influence the migration and infiltration of macrophages to liver, spleen, and other organs (48). NP transport may be enhanced via increased angiogenesis, which influences the uptake by macrophages in the affected organs (8, 39, 47, 48). This may explain the greater accumulation of PLD in the liver and spleen from the T11 model compared to the C3-TAg model. However, to confirm this possibility, further experiments to assess hepatic blood vessels and the function of macrophages in these organs before and after PLD administration are needed.

The tumor interstitial spaces comprise a densely interconnected network of collagen fibers that interact with proteoglycans and glycosaminoglycans (17). The interstitial transport of liposomes via diffusion is determined by collagen content and substantially blocked due to interactions with collagen matrix (17). In our studies, the baseline level of collagen was similar between two breast tumor subtypes and the changes in collagen after NL-doxo and PLD were not noticeable, indicating that collagen matrix does not interact with PLD or NL-doxo in these breast tumor models.

The ratio of tumor to plasma $AUC_{0\text{-}96h}$ of PLD in C3-TAg model and T11 model was 0.30 and 0.15, respectively, which suggests that the efficiency of transvascular transportation of PLD into tumor is 2-fold higher in C3-TAg model. These findings led us to measure the amount and

physiologic state of the vasculature and pro-angiogenic factors for blood microvascular endothelial cells (VEGF-a) and lymphatic endothelial cells (VEGF-c) in these models. Interestingly, Claudin-low T11 tumors exhibit features of hypervascularization and inefficient lymphatic networks, which may increase interstitial fluid pressure (IFP) (17) and hamper the transvascular transport of PLD (17, 49). Consistent with our findings, RNA expression profiling of more than 3,000 human breast tumors showed that claudin-low tumors had the highest vasculature signature expression compared to any of the other breast tumor subtypes (24). In addition, claudin-low tumor cell lines exhibited endothelial cell-like tube morphology with high vascular permeability compared to other breast tumor subtypes (24).

The interactions between PLD and the tumor vasculature are different between two breast tumor subtypes. PLD exhibited normalizing effects on the blood and lymphatic vessels over 96 h and decreased the vascular density (MVD score) by 30% in claudin-low T11 tumors; however, no such changes were observed in basal-like C3-TAg tumors. Consistent with our finding, it has been reported that Doxil treatment exerted strong tumor growth inhibitory effects in B16.F10 melanoma-bearing mice as well as strongly reduced the intratumoral level of VEGF-a, which is produced in high amounts by melanoma cells (38). After clodronate-containing long circulating liposome (LCL), known for its TAM-suppressive effects, a significantly strong additional antitumor effect was observed with additional Doxil administration compared to that induced by clodronate-LCL alone; however, there was no additional reduction in VEGF-a expression after administration of combination of Doxil and clodronate-LCL compared to that after administration of clodronate-LCL alone (38). This indicated that Doxil mainly acts via direct cytotoxic effects on tumor cells with slightly suppressing effects on TAM-mediated angiogenesis (38). Based on this observation, T11 tumor-specific VEGF-a suppressing effect of PLD may be

associated with greater responsiveness of T11 tumors to PLD. *In vitro* studies assessing IC50 of PLD in human basal-like cells and claudin-low cells would further confirm the different sensitivity to PLD between two breast tumor types.

The fact that T11 is an OST model compared to C3-TAg GEMM may play a role as confounding factor in our study despite the conserved gene expression features between murine T11 OST tumors and human claudin-low tumors (19, 23, 24). However, the clinical relevance of our results from T11 OST models can be justified on the basis of the evidence showing that gene expression signatures derived from chemotherapy-treated T11 models successfully predicted the pathological complete response to anthracycline/taxane therapy in human patients with breast cancer (20, 23). Our findings may not be applicable to other NP platforms with different targeting strategies and/or surface characteristics (i.e., passive targeting vs. active targeting, lipid versus polymeric) (1, 2, 4, 17). Jain *et al* reported that vessel normalization with anti-angiogenic therapies improved the delivery and effectiveness of small NP (diameter, 12 nm) but not large NP (125 nm), emphasizing the importance of optimization of both NP and the tumor microenvironment (50). Thus, it is critical to profile the tumor microenvironment within and between tumor types and select patients with tumors that are likely to respond to NP-based therapies (5, 17).

Studies have reported that breast tumor classification based on gene expression profiling adds significant prognostic and predictive information to standard parameters (i.e. hormone receptor status, tumor size and grade, and node status etc.) for patients with breast cancer (16, 19-24). Intrinsic human and murine breast tumor subtypes have shown different sensitivities to chemotherapies including neoadjuvant anthracycline/taxane-based treatment (19, 20, 23). In line with that, we demonstrated that the biologic heterogeneity of breast tumors may affect the

delivery and efficacy of NP-based therapies in murine models and not all breast tumors may be uniformly conducive to NP therapies. Our findings suggest that PLD and other NP-based therapies for breast cancer need to be evaluated with respect to the heterogeneity of breast tumors in the retrospective and prospective studies.

Table 3. 1. Product information on Doxoves™-Liposomal Doxorubicin from FormuMax Scientific, Inc.

Description	Doxoves™-Liposomal Doxorubicin HCl
Catalogue #	F30204B-D
Lipid composition	HSPC/CHOL/Mpeg2000-dspe (56.3:38.4:5.3 mol%)
Active	Doxorubicin HCl
Analytical data	
Lipid concentration	40.5 ± 0.5 Mm (29.7 ± 0.4 mg/ml) (Stewart assay)
Drug concentration	4.00 ± 0.07 mg/ml (UV)
Free drug concentration	0.02 mg/ml (filtration/UV)
Drug encapsulation efficiency	> 99.0% (calculated from free drug and total drug concentration)
Hydration solution (battery)	250 mM ammonium sulfate
External buffer solution	10 wt% sucrose, 10 mM histidine pH6.5
Particle size (ZetaPALS)	Mean diameter: 79.1 ± 0.5 nm; Half-width:20.5 ± 1.0 nm, Polydispersity: 0.07 ± 0.01
Zeta potential (ZetaPALS)	-36.1 ± 1.0 mV(measured in 1 mM NaCl)
Form/color	Translucent, red and free flow liposomal dispersion, no visible particles/aggregates
Stability	Product is sterile filtered and filled in autoclaved vials

a: HSPC: fully hydrogenated phosphatidylcholine

b: CHOL: cholesterol,

c: mPEG2000-DSPE: 1,2-distearoyl-sn-glycero-3-phophoethanolamine-N-methoxy(polyethylene glycol)-2000]

Table 3. 2. Doxorubicin $AUC_{0\text{-}96h}$ in plasma, tissues, and tumor in the C3-TAg model and the T11 model after PLD or NL-doxo administration at 6 mg/kg I.V. x 1 via tail vein

Model	C3-TAg				T11		
Drug	PLD		NL-doxo		PLD		NL-doxo
Plasma	Encapsulated	Released	0.56 ± 0.03		Encapsulated	Released	0.87 ± 0.06
	1,610 ± 111	31 ± 3			1,449 ± 57	27 ± 1.6	
Tumor	Sum total doxorubicin		Doxorubicin		Sum total doxorubicin		Doxorubicin
	480 ± 71*		57 ± 10		210 ± 30*		61 ± 12
Liver	Sum total doxorubicin		Doxorubicin		Sum total doxorubicin		Doxorubicin
	438 ± 18*		199 ± 17		687 ± 61*		247 ± 15
Spleen	Sum total doxorubicin		Doxorubicin		Sum total doxorubicin		Doxorubicin
	153 ± 35		145 ± 32		306 ± 86		111 ± 17
Lung	Sum total doxorubicin		Doxorubicin		Sum total doxorubicin		Doxorubicin
	255 ± 16		133 ± 7		248 ± 19		208 ± 21

NOTE: $AUC_{0\text{-}t}$ of NL-doxo and PLD was calculated by noncompartmental analysis using Phoenix v.6.2. Data are presented as mean ± standard error of the mean (SEM).

[a]:*, P <0.05 (C3-TAg vs. T11). P-values were calculated using Nedelman's modification of the Bailer method for sparse samples, using a two-sample test (32).

[b]: NL-doxo: NL-doxorubicin.

[c]: $AUC_{0\text{-}96h}$ (µg·h/mL and µg·h/g for plasma and tissues, respectively) = area-under the concentration versus time curve from 0 h to 96 h.

Table 3. 3. Baseline and total influx of F4/80+ TAMs in the C3-TAg model and the T11 model after PLD or NL-doxo administration at 6 mg/kg I.V. x 1 via tail vein

Model	C3-TAg			T11		
Regions Of Interest (ROI)	Baseline	$AUC_{0\text{-}96h}$ post PLD	$AUC_{0\text{-}96h}$ post NL-doxo	Baseline	$AUC_{0\text{-}96h}$ post PLD	$AUC_{0\text{-}96h}$ post NL-doxo
Capsule	191 ± 4.3	16,356 ± 703	16,473 ± 604	166 ± 95.6	17,304 ± 274	15,855 ± 1,099
Viable	61 ± 9.2	9,855 ± 1182	8,605 ± 951	90 ± 21.9	12,821 ± 428	10,185 ± 1,679
Necrotic	199 ± 3.3	18,764 ± 645	18,946 ± 562	189 ± 8.1	17,656 ± 1,098	15,664 ± 1,518

NOTE: TAMs were measured by F4/80 in tumor from individual mouse via IHC. The expression of F4/80 at baseline and $AUC_{0\text{-}96h}$ of F4/80, an indicator of total influx of macrophages, after PLD or NL-doxo administration was represented as mean ± SEM of three to four mice. $AUC_{0\text{-}96h}$ was calculated by non-compartmental analysis using Phoenix v.6.2.

[a]: $AUC_{0\text{-}96h}$ = area-under the H-score of F4/80 versus time curve from 0 h to 96 h.

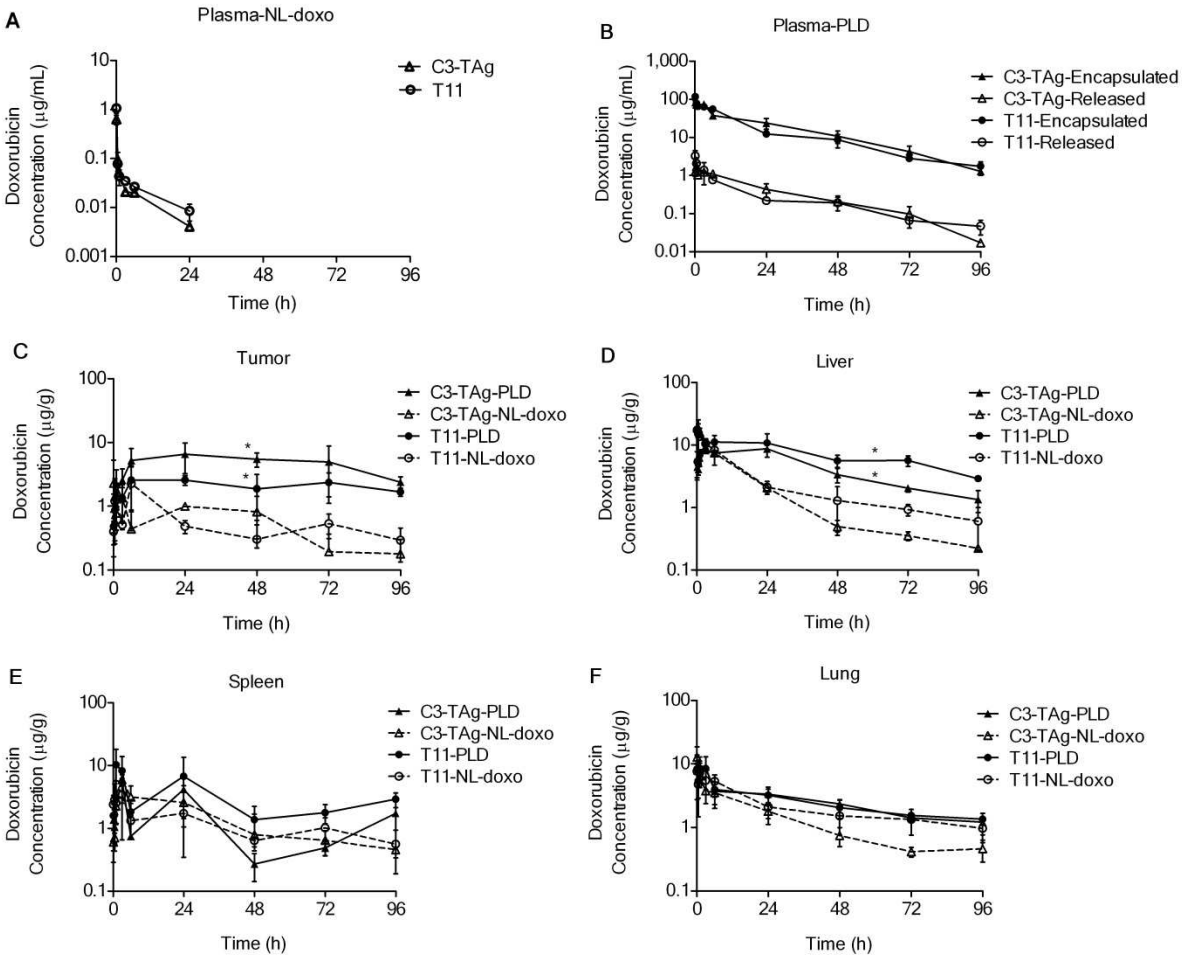

Fig. 3. 1. Concentration versus time profiles of doxorubicin after administration of PLD or NL-doxo at 6 mg/kg I.V. x 1 via tail vein in (**A** and **B**) plasma, (**C**) tumor, (**D**) liver, (**E**) spleen, and (**F**) lung in basal-like C3-TAg and claudin-low T11 breast tumor models. Samples (n=3 mice at each time point) were obtained at 0.083, 0.5, 1, 3, 6, 24, 48, 72, and 96 hours following PLD or NL-doxo administration. Encapsulated and released doxorubicin after administration of PLD in plasma (**B**) and sum total (encapsulated and released) doxorubicin in tumor and tissues (**C-F**) are presented. Each time point is represented as the mean ± standard deviation (SD). *P<0.05 ($AUC_{0\text{-}96h}$ in the C3-TAg model versus $AUC_{0\text{-}96h}$ in the T11 model). Equality of AUC was tested using Nedelman's modification of the Bailer method for sparse samples, using a two-sample test

(32). LLOQ for encapsulated doxorubicin: 300 ng/mL, released doxorubicin: 10 ng/mL, and sum total doxorubicin in tissue: 10 ng/g. NL-doxo= NL-doxorubicin. LLOQ= lower limit of quantification.

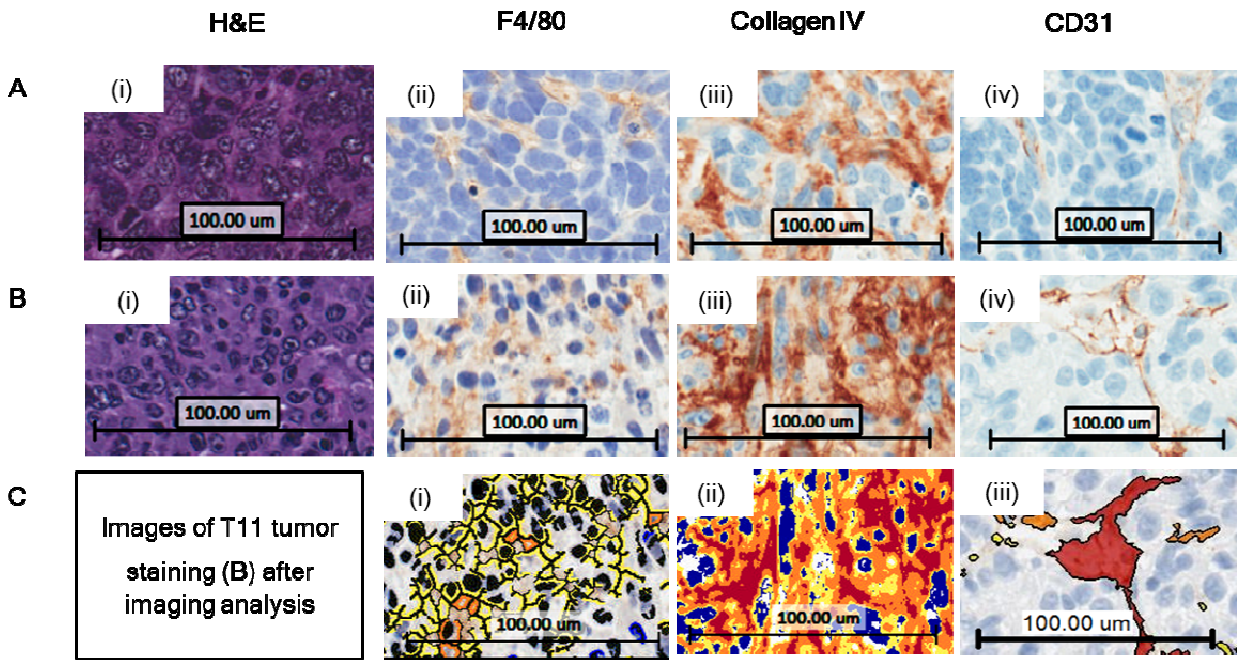

Fig. 3. 2. Hematoxylin & Eosin (H&E), and immunostaining of F4/80, Collagen IV, and CD31 in tumor from basal-like C3-TAg and claudin-low T11 breast tumor models. Representative staining of tumors (brown staining in positive cells) at baseline in the C3-TAg and the T11 models are shown at 20X apparent magnification. (**A**) Representative C3-TAg tumor sections stained for (i) H&E, (ii) F4/80, (iii) Collagen IV and (iv) CD31. (**B**) Representative T11 tumor sections stained for (i) H&E, (ii) F4/80, (iii) Collagen IV and (iv) CD31. (**C**) Digital images of (i) F4/80-, (ii) Collagen IV-, and (iii) CD31-stained T11 tumor sections after analysis through the Aperio Membrane v9 algorithm and color deconvolution methods for F4/80 and Collagen IV, respectively, and the Definiens Tissue Studio software for CD31. Digital image of each stained slide was scanned using the Aperio ScanScope XT at 20X magnification.

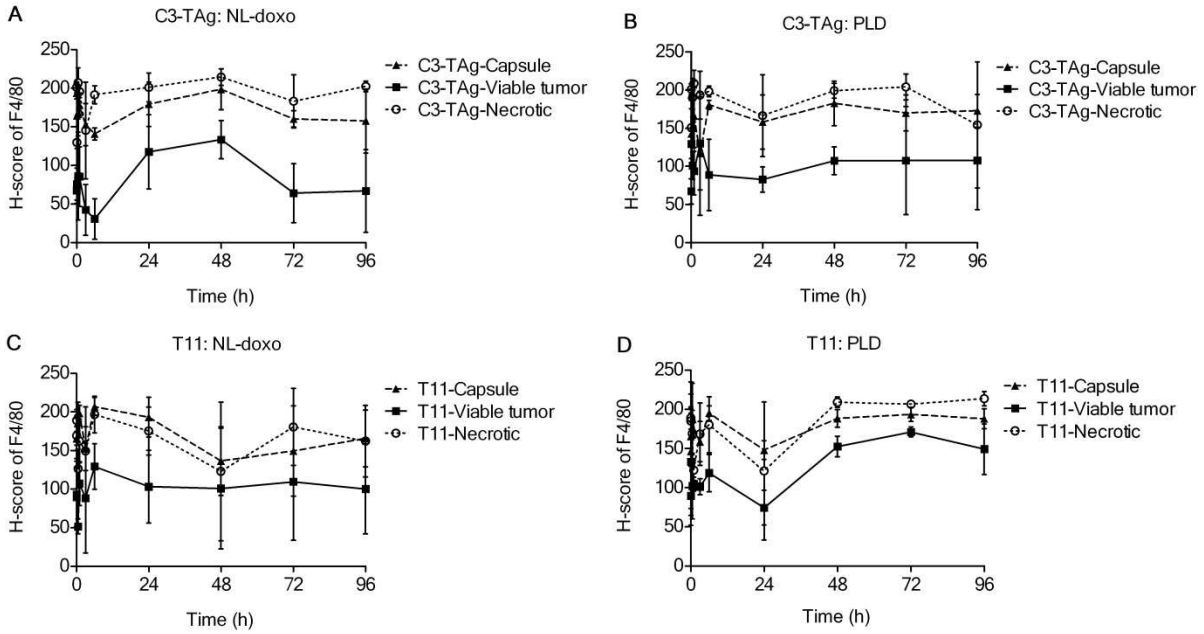

Fig. 3. 3. F4/80 H-score in tumor versus time profiles in basal-like C3-TAg and claudin-low T11 breast tumor models after administration of PLD or NL-doxo at 6 mg/kg I.V. x 1 via tail vein. F4/80 H-score over time in the C3-TAg tumors following (**A**) NL-doxo and (**B**) PLD administration. F4/80 H-score over time in the T11 tumors following (**C**) NL-doxo and (**D**) PLD administration. NL-doxo and PLD affected the infiltration of TAMs over time in a drug- and tumor type-dependent manner. Each time point is represented as mean ± SD (n=3). Capsule: Peritumoral/Peripheral tumor; Viable tumor: Intratumoral viable tumor; Necrotic: Intratumoral necrotic tumor. NL-doxo= NL-doxorubicin. TAMs= tumor-associated macrophages.

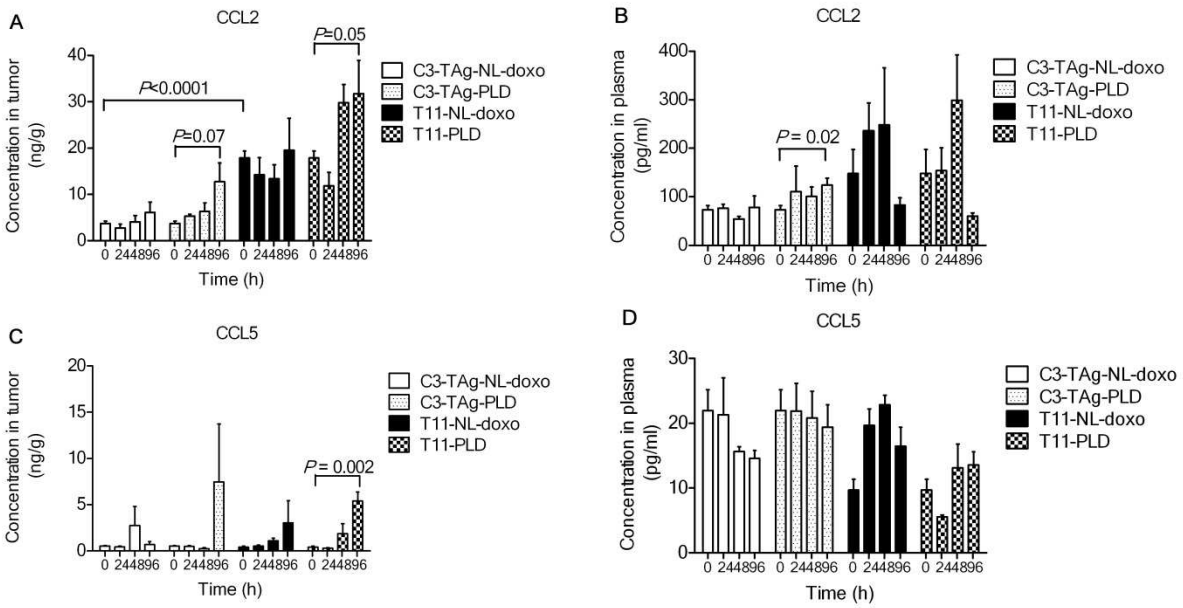

Fig. 3. 4. Profiling of chemokine ligands CCL2 and CCL5 in basal-like C3-TAg and claudin-low T11 breast tumor models after administration of PLD or NL-doxo at 6 mg/kg I.V. x 1 via tail vein. (**A**) Intratumoral CCL2 concentrations versus time profiles and (**B**) plasma CCL2 concentration versus time profiles after PLD or NL-doxo administration in the C3-TAg and the T11 models. The baseline intratumoral expressions of CCL2 were significantly higher in the T11 compared to the C3-TAg ($P<0.0001$). PLD strongly induced the secretion of CCL2 over 96 h in the C3-TAg ($P=0.07$) and the T11 tumors ($P=0.05$) when compared to the slightly increased CCL2 secretion after NL-doxo administration in both models. In plasma, baseline CCL2 concentrations were 2-fold higher in the T11 model compared to the C3-TAg model ($P=0.19$). Plasma CCL2 concentration was significantly increased at 96 h after PLD in the C3-TAg model ($P=0.02$), but little was changed in the T11 model. (**C**) Intratumoral CCL5 concentrations versus time profiles and (**D**) plasma CCL5 concentrations versus time after PLD or NL-doxo administration in the C3-TAg and the T11 models. There was no difference in the baseline intratumoral CCL5 concentrations between the two models. After PLD administration, T11

tumors showed significantly increased CCL5 concentrations at 96 hour (*P*=0.002), but a high variability was observed at 96 hour in the C3-TAg model (*P*=0.24). In plasma, the baseline CCL5 concentrations were similar between the two models and little change was observed after PLD or NL-doxo administration in both models. Data are presented as mean ± SEM (n=3 per each time point). *P*-values were calculated using *t*-test for the baseline comparison and for the change from baseline to 96 h after PLD or NL-doxo administration.

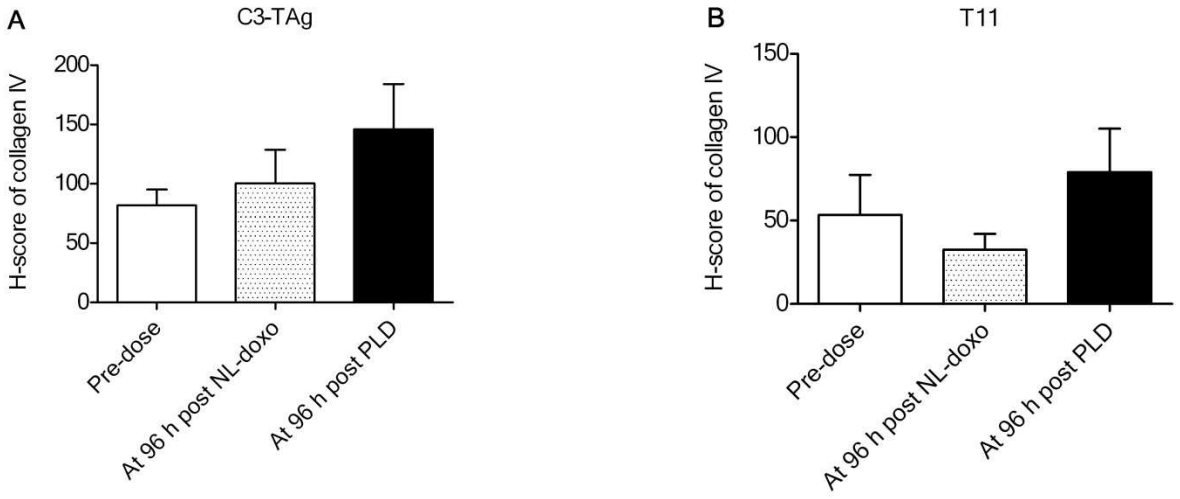

Fig. 3 5. Profiling of collagen in basal-like C3-TAg model and claudin-low T11 model at baseline and at 96 h after administration of PLD or NL-doxo at 6 mg/kg I.V. x 1 via tail vein. Data are presented as mean ± SEM of collagen H-score (n=3 or 4) in (**A**) the C3-TAg and (**B**) the T11 tumors. The baseline collagen content was similar between the two models. There was no significant change at 96 h after NL-doxo or PLD administration in both models. Collagen in the tumor capsule and the viable tumor were assessed for analysis.

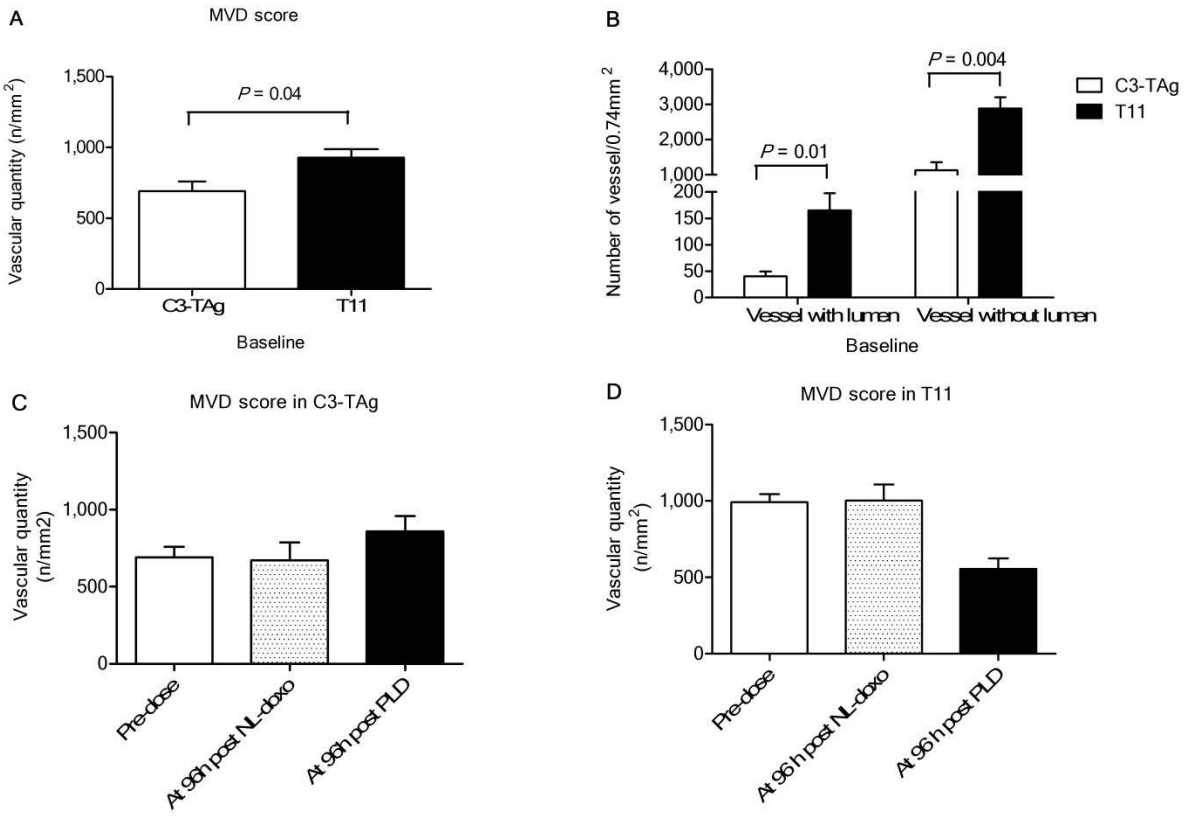

Fig. 3. 6. The amount of vasculature and the levels of VEGF-a and VEGF-c in basal-like C3-TAg and claudin-low T11 breast tumor models at baseline and at 96 h after administration of PLD or NL-doxo at 6 mg/kg I.V. x 1 via tail vein. (**A**) MVD score (number of CD31-positive objects per unit area) at baseline in the C3-TAg and the T11 tumors. The T11 tumors had a significantly greater amount of the blood vessel endothelial cells (BECs) compared to the C3-TAg tumors (*P*=0.04). BECs in the tumor capsule and the viable tumor were assessed for analysis. (**B**) Open lumen analysis of baseline tumor blood vessels in the C3-TAg and the T11 tumors showed a significantly higher number of blood vessels with lumen in the T11 tumors compared to the C3-TAg tumors (*P*=0.01). MVD score at baseline and at 96 h after NL-doxo or PLD in (**C**) the C3-TAg and (**D**) the T11 tumors. Note that there was little change in the amount of the vasculature in the C3-TAg tumors after NL-doxo or PLD, but a 30% decrease in the MVD score was observed in the T11 tumors after PLD administration. Five most vascularized areas

within the tumors (‘hotspot’/0.74 mm^2) were chosen for evaluation of the presence of lumen in the blood vasculature. Each of these five areas was analyzed and the mean was calculated per slide.

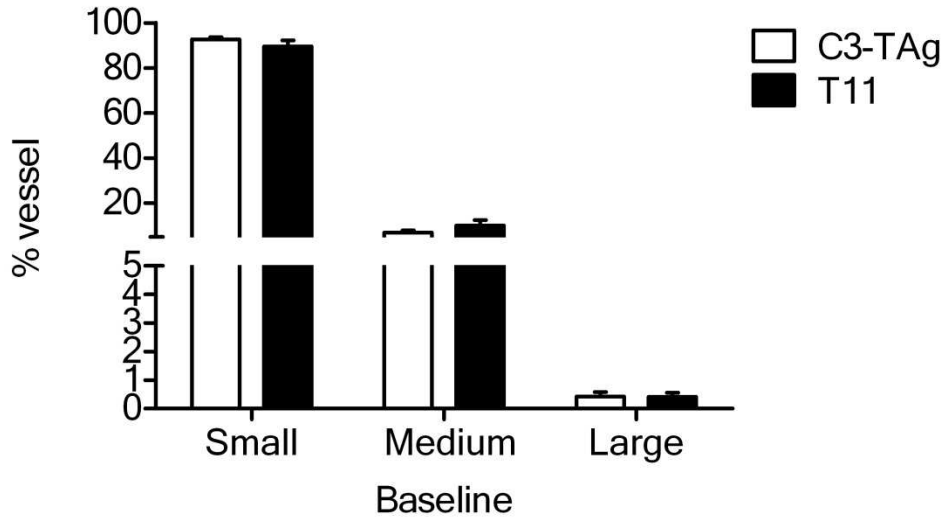

Fig. 3. 7. Size distribution of baseline blood vessels in the C3-TAg tumors and the T11 tumors. Most of the vessels identified were small (~87%), followed by medium (12%) and large (1%) in the both tumors. The vascular size was defined as small < 40 μm^2, medium >40 μm^2 and < 400 μm^2, and large > 400 µm2. Five most vascularized areas within the tumors ('hotspot'/0.74 mm2) were chosen for evaluation of the size distribution. Each of these five areas was analyzed and the mean was calculated per slide. Data are presented as mean ± SEM (n= 3 or 4).

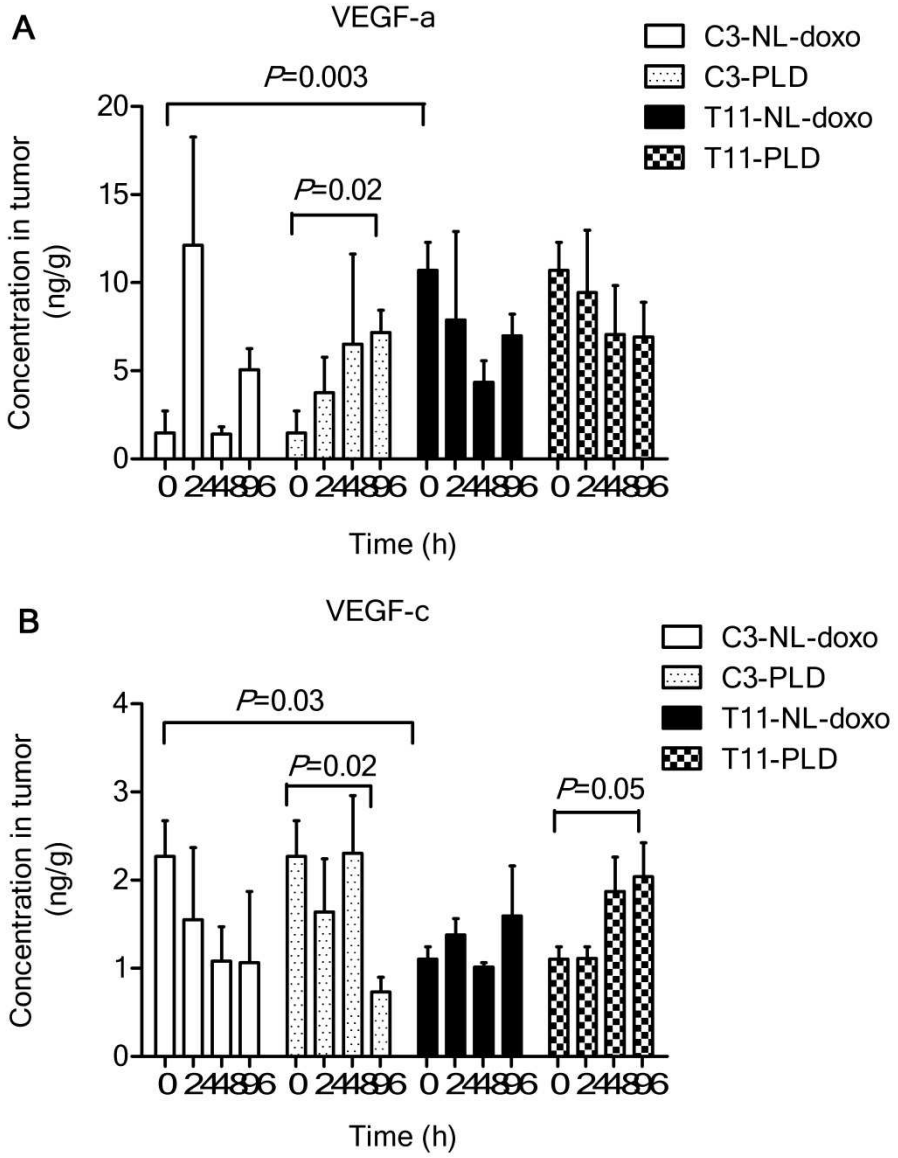

Fig. 3. 8. Intratumoral levels of VEGF-a and VEGF-c in basal-like C3-TAg and claudin-low T11 breast tumor models at baseline and at 96 h after administration of PLD or NL-doxo at 6 mg/kg I.V. x 1 via tail vein. (**A**) VEGF-a and (**B**) VEGF-c versus time profiles after administration of PLD or NL-doxo in the C3-TAg and T11 tumors. T11 tumors had significantly higher levels of VEGF-a (*P*=0.003) and decreased levels of VEGF-c (*P*=0.03) compared to C3-TAg tumors. PLD had greater impacts on the levels of VEGF-a (*P*=0.02) and VEGF-c (*P*=0.02 and *P*=0.05)

compared to NL-doxo and the effects appeared to vary with breast tumor subtypes. Data are presented as mean ± SEM (n=3 or 4). *P*-values were calculated using unpaired t-test. VEGF= vascular endothelial growth factor.

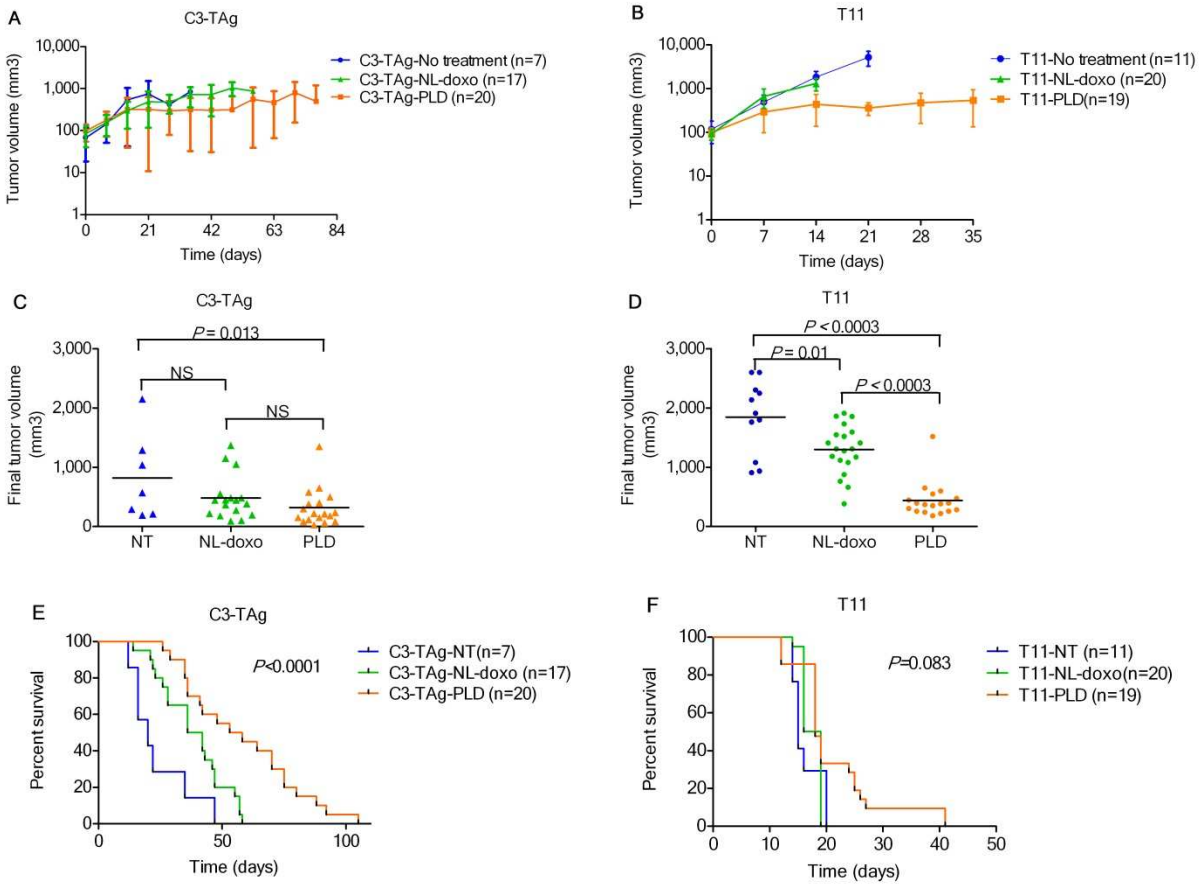

Fig. 3. 9. Efficacy studies of no treatment, NL-doxo, and PLD in basal-like C3-TAg and claudin-low T11 breast tumor models after administration of PLD or NL-doxo at 6 mg/kg I.V. every week for 6 weeks. Mean tumor growth curves in (**A**) the C3-TAg and (**B**) the T11 models. Data are presented as the mean ± SD. Intermediary tumor volumes at (**C**) 21 days post treatment for the C3-TAg model and at (**D**) 14 days post treatment for the T11 model. Mean tumor volume comparison indicated that PLD was more efficacious at suppressing tumor growth in the C3-TAg compared to no treatment (P=0.013) and in the T11 compared to no treatment or NL-doxo (P<0.0003 for both). P-values were calculated based on adjusted tumor volume, using analysis of covariance (ANCOVA) followed by adjustment for multiple comparison using Holm test. Baseline tumor volume was considered as covariate. Kaplan-Meier (KM) analysis of survival

after no treatment, NL-doxo, or PLD administration in (**E**) the C3-TAg and (**F**) the T11 models. *P*-values were calculated using two-sided log-rank test. Survival was measured from the first day of drug treatment. 7/7 (no treatment), 17/20 (NL-doxo), and 20/20 (PLD) of the C3-TAg mice were analyzed for the efficacy studies. 11/11 (no treatment), 20/20 (NL-doxo), and 19/20 (PLD) of T11 mice were analyzed for the efficacy studies.

RFERENCES

(1) Farokhzad OC, Langer R. Impact of nanotechnology on drug delivery. ACS nano 2009;3(1):16-20.

(2) Peer D, Karp JM, Hong S, Farokhzad OC, Margalit R, Langer R. Nanocarriers as an emerging platform for cancer therapy. Nature nanotechnology 2007;2(12):751-760.

(3) Maeda H, Greish K, Fang J. The EPR effect and polymeric drugs: a paradigm shift for cancer chemotherapy in the 21st century. Polymer Therapeutics II: Springer; 2006. p. 103-121.

(4) Zamboni WC. Concept and clinical evaluation of carrier-mediated anticancer agents. Oncologist 2008;13(3):248-260.

(5) Prabhakar U, Maeda H, Jain RK, Sevick-Muraca EM, Zamboni W, Farokhzad OC, et al. Challenges and Key Considerations of the Enhanced Permeability and Retention Effect for Nanomedicine Drug Delivery in Oncology. Cancer Res 2013;73(8):2412-2417.

(6) Dobrovolskaia MA, McNeil SE. Immunological properties of engineered nanomaterials. Nature Nanotechnology 2007;2(8):469-478.

(7) Zolnik BS, González-Fernández Á, Sadrieh N, Dobrovolskaia MA. Minireview: nanoparticles and the immune system. Endocrinology 2010;151(2):458-465.

(8) Li S, Huang L. Pharmacokinetics and biodistribution of nanoparticles. Molecular pharmaceutics 2008;5(4):496-504.

(9) La-Beck NM, Zamboni BA, Gabizon A, Schmeeda H, Amantea M, Gehrig PA, et al. Factors affecting the pharmacokinetics of pegylated liposomal doxorubicin in patients. Cancer Chemother Pharmacol 2012;69(1):43-50.

(10) Song G, Wu H, Yoshino K, Zamboni WC. Factors affecting the pharmacokinetics and pharmacodynamics of liposomal drugs. J Liposome Res 2012;22(3):177-192.

(11) Caron W, Song G, Kumar P, Rawal S, Zamboni W. Interpatient Pharmacokinetic and Pharmacodynamic Variability of Carrier-Mediated Anticancer Agents. Clinical Pharmacology & Therapeutics 2012;91(5):802-812.

(12) Zamboni WC, Maruca LJ, Strychor S, Zamboni BA, Ramalingam S, Edwards RP, et al. Bidirectional pharmacodynamic interaction between pegylated liposomal CKD-602 (S-CKD602) and monocytes in patients with refractory solid tumors. J Liposome Res 2011;21(2):158-165.

(13) Joyce JA. Therapeutic targeting of the tumor microenvironment. Cancer cell 2005;7(6):513.

(14)Ben-Baruch A. Host microenvironment in breast cancer development: Inflammatory cells, cytokines and chemokines in breast cancer progression-reciprocal tumor–microenvironment interactions. Breast cancer research 2002;5(1):31.

(15)Fidler IJ. Tumor heterogeneity and the biology of cancer invasion and metastasis. Cancer Res 1978;38(9):2651-2660.

(16)Perou CM, Sørlie T, Eisen MB, van de Rijn M, Jeffrey SS, Rees CA, et al. Molecular portraits of human breast tumours. Nature 2000;406(6797):747-752.

(17)Jain RK, Stylianopoulos T. Delivering nanomedicine to solid tumors. Nature Reviews Clinical Oncology 2010;7(11):653-664.

(18)Zamboni WC, Strychor S, Joseph E, Walsh DR, Zamboni BA, Parise RA, et al. Plasma, tumor, and tissue disposition of STEALTH liposomal CKD-602 (S-CKD602) and nonliposomal CKD-602 in mice bearing A375 human melanoma xenografts. Clinical Cancer Research 2007;13(23):7217-7223.

(19)Herschkowitz JI, Simin K, Weigman VJ, Mikaelian I, Usary J, Hu Z, et al. Identification of conserved gene expression features between murine mammary carcinoma models and human breast tumors. Genome Biol 2007;8(5):R76.

(20)Usary J, Zhao W, Darr D, Roberts PJ, Liu M, Balletta L, et al. Predicting drug responsiveness in human cancers using genetically engineered mice. Clin Cancer Res 2013 Sep 1;19(17):4889-4899.

(21)Maroulakou IG, Anver M, Garrett L, Green JE. Prostate and mammary adenocarcinoma in transgenic mice carrying a rat C3 (1) simian virus 40 large tumor antigen fusion gene. Proceedings of the National Academy of Sciences 1994;91(23):11236-11240.

(22)Herschkowitz JI, Zhao W, Zhang M, Usary J, Murrow G, Edwards D, et al. Comparative oncogenomics identifies breast tumors enriched in functional tumor-initiating cells. Proceedings of the National Academy of Sciences 2012;109(8):2778-2783.

(23)Prat A, Parker JS, Karginova O, Fan C, Livasy C, Herschkowitz JI, et al. Phenotypic and molecular characterization of the claudin-low intrinsic subtype of breast cancer. Breast Cancer Res 2010;12(5):R68.

(24)Harrell JC, Pfefferle AD, Zalles N, Prat A, Fan C, Khramtsov A, et al. Endothelial-like properties of claudin-low breast cancer cells promote tumor vascular permeability and metastasis. Clin Exp Metastasis 2014;31(1):33-45.

(25)O'brien M, Wigler N, Inbar M, Rosso R, Grischke E, Santoro A, et al. Reduced cardiotoxicity and comparable efficacy in a phase III trial of pegylated liposomal doxorubicin HCl (CAELYX™/Doxil®) versus conventional doxorubicin for first-line treatment of metastatic breast cancer. Annals of oncology 2004;15(3):440-449.

(26)Zamboni W, Edwards R, Mountz J, Eiseman J, Basse P, Zamboni B, et al. The development of liposomal and nanoparticle anticancer agents: Methods to evaluate the encapsulated and released drug in plasma and tumor and phenotypic probes for pharmacokinetic (PK) and pharmacodynamic (PD) disposition. Proceedings of the 2007 NSTI nanotechnology conference; 2007

(27)Takahashi O, Komaki R, Smith PD, Jürgensmeier JM, Ryan A, Bekele BN, et al. Combined MEK and VEGFR inhibition in orthotopic human lung cancer models results in enhanced inhibition of tumor angiogenesis, growth, and metastasis. Clinical Cancer Research 2012;18(6):1641-1654.

(28)OHNO S, OHNO Y, SUZUKI N, KAMEI T, KOIKE K, INAGAWA H, et al. Correlation of histological localization of tumor-associated macrophages with clinicopathological features in endometrial cancer. Anticancer Res 2004;24(5C):3335-3342.

(29)Lewis CE, Pollard JW. Distinct role of macrophages in different tumor microenvironments. Cancer Res 2006;66(2):605-612.

(30)Choi WW, Lewis MM, Lawson D, Yin-Goen Q, Birdsong GG, Cotsonis GA, et al. Angiogenic and lymphangiogenic microvessel density in breast carcinoma: correlation with clinicopathologic parameters and VEGF-family gene expression. Modern pathology 2004;18(1):143-152.

(31)Pollack VA, Savage DM, Baker DA, Tsaparikos KE, Sloan DE, Moyer JD, et al. Inhibition of epidermal growth factor receptor-associated tyrosine phosphorylation in human carcinomas with CP-358,774: dynamics of receptor inhibition in situ and antitumor effects in athymic mice. J Pharmacol Exp Ther 1999;291(2):739-748.

(32)Nedelman JR, Gibiansky E, Lau DT. Applying Bailer's method for AUC confidence intervals to sparse sampling. Pharm Res 1995;12(1):124-128.

(33)Vickers AJ. The use of percentage change from baseline as an outcome in a controlled trial is statistically inefficient: a simulation study. BMC Medical Research Methodology 2001;1(1):6.

(34)Soria G, Ben-Baruch A. The inflammatory chemokines CCL2 and CCL5 in breast cancer. Cancer Lett 2008;267(2):271-285.

(35)Willett CG, Boucher Y, di Tomaso E, Duda DG, Munn LL, Tong RT, et al. Direct evidence that the VEGF-specific antibody bevacizumab has antivascular effects in human rectal cancer. Nat Med 2004;10(2):145-147.

(36)Workman P, Aboagye E, Balkwill F, Balmain A, Bruder G, Chaplin D, et al. Guidelines for the welfare and use of animals in cancer research. Br J Cancer 2010;102(11):1555-1577.

(37)Choi M, Stanton-Maxey KJ, Stanley JK, Levin CS, Bardhan R, Akin D, et al. A cellular Trojan Horse for delivery of therapeutic nanoparticles into tumors. Nano letters 2007;7(12):3759-3765.

(38)Banciu M, Schiffelers RM, Storm G. Investigation into the role of tumor-associated macrophages in the antitumor activity of Doxil. Pharm Res 2008;25(8):1948-1955.

(39)Zhao G, Rodriguez BL. Molecular targeting of liposomal nanoparticles to tumor microenvironment. International journal of nanomedicine 2013;8:61.

(40)Storm G, Steerenberg P, Emmen F, van Borssum Waalkes M, Crommelin D. Release of doxorubicin from peritoneal macrophages exposed in vivo to doxorubicin-containing liposomes. Biochimica et Biophysica Acta (BBA)-General Subjects 1988;965(2):136-145.

(41)Saji H, Koike M, Yamori T, Saji S, Seiki M, Matsushima K, et al. Significant correlation of monocyte chemoattractant protein-1 expression with neovascularization and progression of breast carcinoma. Cancer 2001;92(5):1085-1091.

(42)Fang WB, Jokar I, Zou A, Lambert D, Dendukuri P, Cheng N. CCL2/CCR2 chemokine signaling coordinates survival and motility of breast cancer cells through Smad3 protein- and p42/44 mitogen-activated protein kinase (MAPK)-dependent mechanisms. J Biol Chem 2012;287(43):36593-36608.

(43)Qian B, Li J, Zhang H, Kitamura T, Zhang J, Campion LR, et al. CCL2 recruits inflammatory monocytes to facilitate breast-tumour metastasis. Nature 2011;475(7355):222-225.

(44)Ma Y, Mattarollo SR, Adjemian S, Yang H, Aymeric L, Hannani D, et al. CCL2/CCR2-Dependent Recruitment of Functional Antigen-Presenting Cells into Tumors upon Chemotherapy. Cancer Res 2014 Jan 15;74(2):436-445.

(45)Bergers G, Hanahan D. Modes of resistance to anti-angiogenic therapy. Nature Reviews Cancer 2008;8(8):592-603.

(46)Ferrara N. Role of myeloid cells in vascular endothelial growth factor-independent tumor angiogenesis. Curr Opin Hematol 2010;17(3):219-224.

(47)Sahin H, Trautwein C, Wasmuth HE. Functional role of chemokines in liver disease models. Nature Reviews Gastroenterology and Hepatology 2010;7(12):682-690.

(48)Mantovani A. Cancer: inflammation by remote control. Nature 2005;435(7043):752-753.

(49)Heldin C, Rubin K, Pietras K, Östman A. High interstitial fluid pressure—an obstacle in cancer therapy. Nature Reviews Cancer 2004;4(10):806-813.

(50)Chauhan VP, Stylianopoulos T, Martin JD, Popović Z, Chen O, Kamoun WS, et al. Normalization of tumour blood vessels improves the delivery of nanomedicines in a size-dependent manner. Nature nanotechnology 2012;7(6):383-388.

CHAPTER 4:

QUANTITATIVE TRAIT LOCUS CONTAINING *GULP1* GENE IS ASSOCIATED WITH ENHANCED CLEARANCE OF PEGYLATED LIPOSOMAL DOXORUBICIN (PLD) IN INBRED MOUSE STRAINS[4]

Overview

Purpose: High variability in the pharmacokinetics (PK) of PEGylated liposomal doxorubicin (PLD) has been reported. We hypothesized that genetic variations may be associated with the variable disposition of PLD. **Methods**: We characterized the plasma disposition of encapsulated and released doxorubicin after administration of PLD 6 mg/kg IV x1 via tail vein in 23 different male inbred mouse strains. Non-compartmental PK analysis was performed to find the best PK parameter to discriminate the mouse strains. We carried out genome wide analyses to identify the quantitative trait loci linked to the phenotype using haplotype associated mapping (SNPster) and the efficient mixed-model association (EMMA) algorithm. **Results**: An approximately 13-fold difference in the plasma clearance (CL) of PLD was observed across strains. A locus containing engulfment adapter PTB domain containing 1 (*Gulp1*) on chromosome 1 was identified by both SNPster and EMMA linking the PLD CL to the genetic variations in 23 inbred strains. The gene expression analysis demonstrated that *Gulp1* expression was differentially regulated in various tissues with the highest expression in adipose tissue. In addition, there was a significantly positive relationship between *Gulp1* expression in adipose tissue and the CL of PLD among these inbred strains. **Conclusions**: Our finding suggests that genetic variations implicated in the

[4]This chapter will be submitted to the *Journal of Pharmacology and Experimental Therapeutics* and is presented in the style of the journal.

phagocytosis, specifically *Gulp1* in adipose tissue, may contribute to the variability in the PK of PLD.

4. 1. Introduction

Nanocarrier-based drug delivery systems have advanced diagnosis, imaging, and treatment of diseases, such as inflammation and cancer (1). The use of nanoparticles (NPs), particles ranging from 1 to 1000 nm in size, has enabled conventional small molecule agents to overcome the limiting factors, such as poor solubility, limited bioavailability, and unwanted toxicity (2). A number of NP-based diagnostic and therapeutic agents have been investigated under various stages of preclinical and clinical development (3, 4). For diagnostic and imaging applications, studies have shown that NP-based imaging contrasts allow for the molecular imaging of the target site (i.e., tumors) as well as improve sensitivity and specificity of the imaging due to favorable physicochemical and pharmacokinetic properties of NPs (4). Moreover, more than 20 NP-based therapeutic agents have been approved by the U.S. Food and Drug Administration (FDA) and successfully translated into the clinic (3, 5). Among various NP platforms, liposomal drugs are one of the most commonly used NPs for therapeutics purposes (3, 5).

The mononuclear phagocyte system (MPS) consists of monocytes, macrophages and dendritic cells and is mainly responsible for antigen presentation, cytokine secretion, and phagocytosis that protects the host against pathogens and foreign particles (6). NPs have been shown to be cleared and removed from the circulation by the MPS, primarily the monocytes and macrophages (7). The pharmacokinetics (PK) of NPs is dependent on the carrier until the drug gets released from the carrier (2, 8). After the drug is released from the carrier, the PK of the drug will be the same as that of the small molecule drug (2, 9). We have previously shown that

the variability in the PK and pharmacodynamics (PD) of nanomedicines such as Doxil® (PEGylated liposomal doxorubicin; PLD) and S-CKD602 (PEGylated liposome of CKD-602, a camptothecin analog) is associated with patient's age, gender, and the function of circulating monocytes in plasma of patients with solid tumors (10-12). However, the molecular mechanisms underlying this relationship have not yet been investigated and remain poorly understood.

Genome-wide association studies (GWAS) have advanced the field of human genetics and play a key role in embracing personalized medicine in the clinic by enhancing molecular understanding of human diseases and prediction of patients' response to therapies (13). The identification of the quantitative trait loci (QTLs) and/or genetic variants, such as single nucleotide polymorphisms (SNPs) for various phenotypes and diseases in human has positively influenced the health care in many ways, such as disease susceptibility (i.e., *BRCA1* and *BRCA2* for breast and ovarian cancer) (14) and pharmacogenomics (i.e., CYP2C9 and VKORC1 for warfarin treatment) (15). However, only a limited number of clinically useful biomarkers have been identified by human GWAS and implemented into the clinic due to challenges including small size population with genetic variant(s) of interest, inaccessibility to relevant tissues, and uncontrolled environmental factors (13).

As alternative strategies to overcome these barriers present in human GWAS, increasing efforts have been made to advance the genetic mapping studies using model organisms, such as mice (16). Advances in microarray and sequencing technology have made it possible to yield an almost complete map of genetic variation in numerous laboratory mouse strains (17). Studies have shown that candidate gene(s) for quantitative phenotypic traits identified by GWAS in commonly used laboratory strains successfully translated to identification of the genetic basis of disease and traits in humans (16, 18-20). Thus, these mice can serve as valuable experimental

tools to model the phenotypic variation within the human population and potentially identify the genes implicated in the phenotype in humans (16).

PLD has been approved for the treatment of Kaposi's sarcoma, multiple myeloma, and refractory ovarian cancer (5). However, it is noted that significant variability in the pharmacokinetics (PK) of PLD has been reported in preclinical models and patients (21). Thus, it is imperative to elucidate the mechanisms underlying the high interpatient variability in the PK and, ultimately, modest efficacy of PLD (22). In this study, we aimed to investigate the molecular basis of variable disposition of PLD using a panel of inbred mouse strains through GWAS.

4. 2. Materials and Methods

Mice. All animal experiments were performed with the approval of University of North Carolina (UNC) at Chapel Hill's Institutional Animal Care and Use Committee (IACUC). The 23 inbred strains used were purchased from the Jackson Laboratories (Bar Harbor, ME): 129S1/SvlmJ, A/J, BALB/cByJ, C57BLKS/J, C58/J, CBA/J, CE/J, KK/HIJ, LG/J, LP/J, MA/MyJ, NOD/ShiLtJ, NON/ShiLtJ, NZO/HILtJ, NZW/LacJ, PL/J, RIIIS/J, SJL/J, SM/J, SWR/J and three wild-derived inbred strains: PERA/EiJ, PWD/PhJ, WSB/EiJ. Ten to twelve week old mice were used in the study. Mice were housed in a pathogen free facility at the Genetic Medicine Building of the UNC at Chapel Hill. Animals were fed an irradiated NIH-31 modified 6% mouse/rat Sterilizable Diet (Teklad/Harlan Laboratories, Inc.) consisting of 18.0% crude protein, 6.0% crude fat, and 5.0% crude fiber and had access to water ad libitum (reverse osmosis, 1 ppm Cl). Mice were housed on irradiated Enrich-o'cobs laboratory enrichment bedding (bed-o'cobs/The Andersons, Inc.) in static microisolators on an alternating 12-hour

light/dark cycle at 21ºC to 22ºC and 40% to 60% humidity. All experiments were approved by the IACUC and conducted in agreement with the NIH policy.

PK Studies. PLD (Doxil®) used for PK studies in mice was purchased from Janssen (Horsham, PA). PLD was administered at 6 mg/kg IV x1 via a tail vein. Mice (n=4 per inbred strain) were euthanized at 0.083, 3, 24, and 48 hours after administration of PLD. Blood was collected via terminal cardiac puncture using lithium heparin as an anticoagulant under ketamine/DexDomitor anesthesia and processed for plasma by centrifugation (1,500 g for 5 minutes). Plasma was processed immediately to measure encapsulated and released doxorubicin using solid phase separation methods as described previously (23). Doxorubicin concentration was determined using an existing high performance liquid chromatography-fluorescence (HPLC-FL) assay (23). PK analysis of encapsulated and released doxorubicin was performed by non-compartmental method using Phoenix WinNonlin® (v. 6.02, Pharsight Corp. - Mountain View, CA). Area-under- the concentration versus time curve (AUC) from 0 to the last measurable sample ($AUC_{0\text{-last}}$), clearance (CL), Cmax, and Tmax were calculated. The area under the concentration versus time curve (AUC) was calculated using the linear up and log down rule.

Quantitative Trait Loci (QTL) Mapping. We performed a genome-wide association mapping study using two different algorithms: EMMA (Efficient Mixed-Model Association; 24) and SNPster (25). We used the Mouse Diversity Array (MDA) SNPs which contains approximatley 356,596 SNPs expected to cover most of genetic variation in the 23 inbred strains (genotypes available from http://cgd.jax.org/cgdsnpdb/) (26).

The EMMA algorithm is based on the mixed-model in which the population structure and genetic relatedness in strains are corrected and an *F*-test is performed at each SNP to test association with the phenotype (24). The SNPster software performs ANOVA tests using

haplotypes inferred from 3 consecutive SNPs based on SNP data available from the MDA (26). Each inferred haplotype is tested for the association with input traits by calculating an F statistics with ANOVA. A weighted bootstrap method is used to detect association peaks based on the population structure in the mouse diversity panel (25). For the phenotype, we used the log-transformed values of the plasma clearance (CL) of encapsulated doxorubicin.

PK and Statistical Analysis. PK analysis was performed by non-compartmental method using Phoenix WinNonlin® v. 6.02 (Pharsight Corp., Mountain View, CA). Statistical analyses were carried out using Prism5 software (GraphPad Software, Inc.). Simple linear regressions were used to explore the linear relationship between *Gulp1* gene expression and the CL of PLD and between the CL of the plasma encapsulated doxorubicin and the number of monocytes in blood. Genome wide significance threshold ($-Log_{10}P$ score) with a conservative Bonferroni correction was 6.7 and 6.0 for the EMMA and the SNPster, respectively, in the genome wide association mapping with the CL phenotype (24, 25). The false discovery rate (FDR) for the EMMA was 19% for the SNPs with $- Log_{10}P$ score >4.3. *P* value of less than 0.05 was considered statistically significant. All statistical tests were two-sided.

4. 3. Results

Characterization of the PK of PLD in 23 different mouse strains

To identify the genetic basis for the variability in the PK of PLD, a panel of 23 inbred mouse strains was used to model genetic diversity. As a phenotypic measure, we evaluated the plasma PK of PLD in male mice from each of 23 inbred mouse strains.

The PK Analysis of PLD in 23 Inbred Mouse Strains. To determine whether genetic factors influence the PK of PLD, 23 inbred mouse strains representing broad genetic variation across the mouse genome were evaluated for the PK of PLD. Plasma encapsulated (the drug

within the liposomal carrier) and released (active-drug released from the liposomal carrier) doxorubicin concentration versus time profiles after administration of PLD at 6 mg/kg IV x 1 are presented in **Fig. 4. 1**. A distinct interstrain variation in the plasma disposition of PLD components was observed. SJL/J mice displayed the highest plasma clearance (CL) of PLD, whereas 129S1/SvlmJ mice had the lowest plasma CL PLD (**Fig. 4. 1**). Consistent with high variation seen in the encapsulated doxorubicin, there was a notable difference in release of doxorubicin from liposome carriers among inbred mouse strains (**Fig. 4. 1**).

To characterize the dispositions of plasma encapsulated and released components of PLD in 23 inbred mouse strains, non-compartmental PK analysis was performed. As the PK of NPs are dependent on the carrier and prolongation of NP circulation in blood stream is critical for distribution to target tissues (i.e., sites of inflammation and tumor cells), plasma clearance (CL) of encapsulated doxorubicin was assessed. The CL of encapsulated doxorubicin showed robust discrimination between the different strains (**Fig. 4. 2A**). There was an approximately 13-fold difference between strains with the highest and lowest CL of PLD. We also evaluated the exposure (AUC) of free doxorubicin in plasma to assess the variability in the rate of release of doxorubicin from the liposome carriers. There was approximately 5-fold difference between strains with the highest and lowest exposure of free doxorubicin in plasma after administration of PLD (**Fig. 4. 2B**). The PK parameters of plasma encapsulated and released doxorubicin following administration of PLD in 23 inbred mouse strains are summarized in **Table 4. 1**.

Confirmatory PK Studies in Inbred Mouse Strains with low, intermediate, and high CL. To confirm this strain-specific plasma PK profile of encapsulated and released components of PLD, three inbred mouse strains displaying low, intermediate, and high CL of PLD were selected for a second set of independent confirmatory PK studies. The concentrations versus time

profiles of plasma encapsulated and released doxorubicin after administration of PLD were reproducibly observed with low intrastrain variability (n=3 per time point) in this confirmatory PK studies (**Fig. 4. 3, Table 4. 2**).

The Relationship between the CL of PLD and the Number of Monocytes in Blood. NPs are removed from the circulation by the cells of the MPS, such as circulating monocytes. However, it is not known whether variability in the monocyte levels in blood contributes to differential PK between individuals. Thus, we used the monocyte cell count in the blood as a phenotype for the number of MPS cells. These data were obtained from the Jackson Laboratory Mouse Phenome Database web site (phenotypes are available from http://phenome.jax.org; 27). All 23 strains had phenotype values available for the circulating monocyte cell count (n/µL x 10^3). The monocyte cell counts were measured across on average 13 different individual mice per strain. The distribution of the plasma CL of encapsulated doxorubicin with respect to the monocyte cell counts in blood showed that there is no correlation between the PLD CL and the monocyte counts across different inbred strains (**Fig. 4. 4A** and **B**). In addition, there was no relationship between monocyte counts in blood and the exposure (i.e., AUC) of released doxorubicin in plasma (**Fig. 4. 4C** and **D**).

Identification of Candidate Genes for the Variability in the CL of PLD

Quantitative Trait Loci (QTL) Mapping. To uncover the QTL associated with the variability of the PK of PLD, we performed genome wide association mapping studies using two SNPster and EMMA. For phenotypes, we used the CL of encapsulated doxorubicin after administration of PLD as trait based on the robust discrimination between the different strains (**Fig. 4. 2A**). The haplotype association mapping algorithm using SNPster software infers

haplotypes from three adjacent SNPs across the genome and calculates the strength of genetic associations between genotype and phenotype pairings (25). At each genetic locus, the association score is represented as the negative Log10 transformed P value (-Log_{10}P score). SNPster analysis was performed for the encapsulated doxorubicin CL phenotype across 23 strains using 356,596 informative SNPs. We found the QTL with the highest -Log_{10}P score of 3.60 on chromosome 1 (44261431-44834919bp) (**Fig. 4. 5A, 5C** and **6**). Due to the conservative algorithm and limited power of the study, the strongest signals were not genome wide significant.

To address the conservative algorithm and limited power of the study, a second analysis using EMMA was performed. The locus identified with the SNPster analysis was confirmed by EMMA mapping algorithm (24). The QTL identified through EMMA was at position between 44273428 and 45015110bp and the highest -Log_{10}P score of SNP was 5.40 (**Fig. 4. 5B, 5C,** and **7**). Although the SNP at the position 44296740bp (rs33510908) has -Log_{10}P score of 5.40, which is slightly below the genome wide significance threshold with a conservative Bonferroni correction, it was overlapped with the locus identified by the SNPster algorithm (**Fig. 4. 5**).

Gene Expression Analysis of *Gulp1*. The QTL for the CL of PLD identified by two separate genome wide association mapping methods was found to be approximately 200 kb away from the *Gulp1* gene (44608516-44845719bp, GeneID: 51454, MGI: 1920407). *Gulp1* gene encodes phosphotyrosine-binding (PTB) domain containing engulfment adapter protein 1 (GULP1), which is mammalian homologue of *Caenorhabditis elegans* CED-6 (28). Studies have shown that GULP1/CED-6 plays a critical role as an adapter protein in phagocytosis of apoptotic cells and this function has been conserved in *C. elegans*, rodents, and human GULP1/CED-6 proteins (28, 29). Based on the mechanistic link between phagocytes-mediated PLD CL and the function of *Gulp1* gene, we assessed the relationship between the available expression data of

Gulp1 and the plasma CL of encapsulated doxorubicin after administration of PLD. The *Gulp1* RNA expression data from the liver, lung, spleen (the general primary MPS organs), and in adipose tissues in untreated inbred mouse strains were evaluated from the BioGPS portal (30, 31). The expression of *Gulp1* was significantly higher in adipose tissue of mouse strains compared to other tissues (**Fig. 4. 8A**). In addition, there was a significant positive relationship between *Gulp1* gene expression levels and plasma CL of PLD (R^2=0.40, *P*=0.027). However, the association was not observed in other tissues (**Fig. 4. 8B, C,** and **D)**.

4. 4. Discussion

The application of nanotechnology to medicine, known as nanomedicine, offers the potential to revolutionize various fields of medicines including diagnosis and treatment due to enhanced delivery of drug to the target site (4). Advances in understanding of NP pharmacology, however, have revealed that there are several biological barriers to overcome and the underlying mechanisms for the molecular interaction of NP with cells and tissues remain poorly understood (8). Here, we are the first to use a GWAS approach using a panel of inbred mouse strains to uncover the genetic variant(s) linked to the PK of PLD and identified that a locus containing *Gulp1* is associated with the enhanced plasma CL of PLD.

Inbred mouse strains have several advantages for use in the genetic association studies compared with the human population. Due to unique breeding strategies designed to carry out GWAS, these recombinant inbred strains are homozygous at each locus, thereby increasing the power of the association approaches (26, 32). In addition, classical inbred strains can model a larger amount of genetic diversity with most strains genotyped or sequenced completely (17, 26, 32). Finally, they are completely reproducible due to identical genetic structure within individuals of the same strain (16, 26). Consistent with these known benefits, 23 male inbred

mouse strains consisting of 21 classical inbred strains and 2 wild-derived inbred strains successfully demonstrated a differential plasma CL of PLD across different strains. In addition, the CL of encapsulated doxorubicin after administration of PLD was reproducible in an independent confirmatory PK studies with low variability within a strain.

NPs are removed from the circulation by the cells of the MPS, primarily monocytes and macrophages (7, 9). Once a NP enters the bloodstream, the adsorption of immunoglobulin or complement proteins to the particle surface, called opsonization, occurs (33). The opsonized particles are rapidly recognized and ingested by monocytes and macrophages via phagocytosis (34). Thus, the capture of NPs by the phagocytes plays a pivotal role in determining the disposition and therapeutic effects of nanomedicines. SJL/J strain displayed the most rapid plasma clearance (CL) of encapsulated doxorubicin after administration of PLD. In addition, the difference in the CL of PLD was approximately 13-fold compared to that of 129S1/SvlmJ with the lowest CL. This indicates that there is a substantial variability in NP uptake by the phagocytes across inbred mouse strains.

The rate of *in vivo* drug release is also an important parameter as it dictates the pharmacological activity of the drug at the target site and toxicities (35). We also measured the exposure (AUC) of released doxorubicin in plasma after administration of PLD and assessed the variability in the drug release from the liposome carrier in these mouse strains. Moderate variation (~5-fold difference) between strains was observed with this phenotype and there was no correlation between the CL of encapsulated doxorubicin and the exposure of released doxorubicin in plasma. This may be due in part to the complex intracellular interaction of phagolysosome containing NPs with environmental factors, such as pH and enzymes for degradation of carriers (34, 35). In addition, the metabolism of released doxorubicin may be

different across the mouse strains (16). It has also been reported that the majority of doxorubicin release after administration of PLD does not occur until after accumulation in the tissues (i.e., tumors) (36).

We also investigated the effects of monocyte cell counts on the PK of PLD, including the PLD CL and the exposure (AUC) of released doxorubicin. There was, however, no observed correlation between the number of circulating monocytes and the PK of PLD, indicating that the disposition of PLD is not likely affected by the number of monocytes in the blood, but rather by the function of the cells (11). This is consistent with the findings in our prior studies in patients with recurrent ovarian cancer. The phagocytosis of monocytes (MO) and dendritic cells (DC) and the production of reactive oxygen species (ROS) were evaluated in patients with recurrent epithelial ovarian cancer (EOC) administered PLD (11). There were significant associations between PLD CL and phagocytosis and ROS production in blood MO/DC in these patients, suggesting that probes of MPS function may help predict PLD CL in patients with EOC.

We mapped the association of CL of PLD to a locus containing *Gulp1* on chromosome 1 using two genomewide analyses, SNPster and EMMA. *Gulp1* encodes an engulfment adapter protein with an N-terminal phosphotyrosine-binding (PTB) domain and C-terminal proline-rich region (29). Adapter protein GULP1 has been shown to physically interact with CED-1/CD91 and transduce the recognition signal inside the phagocyte to trigger the cytoskeletal rearrangements required for phagocytosis (37). GULP proteins have shown to be involved in phagocytosis of apoptotic cells through Classical B scavenger receptor type I (SR-BI) *in vitro* and *ex vivo* (28, 38). Given a key role of phagocytes in the CL of NP, our finding of a candidate locus containing *Gulp1* from GWAS of the PLD CL strengthens the mechanistic link between the dispositions (PK) of NPs and the phagocytes, such as monocytes and macrophages.

We assessed the association of *Gulp1* gene expression in different tissues with the PLD PK in these mouse strains. Interestingly, *Gulp1* expression was differentially regulated in various tissues with the highest expression in adipose tissue. In addition, there was a significantly positive relationship between *Gulp1* expression in adipose tissue and the CL of PLD among these inbred strains. Adipose tissue is involved in not only metabolism, but also inflammation and immune system, especially the MPS (39). It has been shown that adipose tissue in obese patients is infiltrated by immune cells, predominantly macrophages, and these adipose tissue macrophages (ATMs) mediate chronic inflammation responsible for obesity-induced insulin resistance and pathogenesis of type-2 diabetes (40). Interestingly, ATMs in obese animals exhibit distinct cellular localization and inflammatory phenotypes (41). It has been shown that obesity stimulates the recruitment of monocytes and triggers ATMs from resident into classically-activated macrophages, which display a pro-inflammatory M1 phenotype and are primarily found around dying adipocytes (40, 41). Upon exposure to various inflammatory stimuli (i.e., viral and bacterial infections), increased recruitment of circulating precursor monocytes contributes to repopulation of tissue-resident macrophages (39). Thus, different activation states and consequential functions of macrophages in adipose tissue may result in distinct *Gulp1* expression and positive correlation with the CL of PLD compared to other tissues (i.e., liver, lungs, and spleen). In addition, human adipocytes have shown to significantly upregulate the mRNA expression of *Gulp1* upon the treatment of superparamagnetic iron oxide nanoparticles (SPIONs), supporting our observation of the positive correlation between *Gulp1* expression in adipose tissues and the CL of PLD after PLD administration in 23 inbred strains (42).

Because the probability scores ($-Log_{10}P$ values) in the haplotype mapping analysis (SNPster) and EMMA are based in part on the number of strains sharing the phenotype, adding

more strains may increase the genetic diversity and the power to detect the peak(s) with genome wide significance (24, 25). In addition, some of the smaller peaks on other chromosomes may prove to be important and biologically related to the phenotype (i.e., obesity). QTL analyses of crosses between other mouse strains with high and low CL of PLD may provide additional information on importance of multiple genes and gene-gene interaction in the PLD PK (Flint and Eskin, 2012). In addition, further functional characterizations of *Gulp1* (i.e., knockout mice) would validate the relationship between *Gulp1* and the PLD PK observed in our pioneering works (43). However, *Gulp1* knockout mice are not currently available.

In summary, we performed the first GWAS using a panel of inbred mouse strains to uncover the genetic variant(s) linked to the PK of PLD and identified a locus containing *Gulp1* that is associated with the plasma CL of PLD. Our data implicate that the genetic variations may play a role in the variability in the PLD PK. Further studies are needed to validate the relationship between *Gulp1* and the PK of PLD and translate these findings to obese and non-obese humans for personalized PLD therapy and other nanomedicines.

Table 4. 1. PEGylated liposomal doxorubicin plasma PK parameters in a panel of inbred mouse strains. The mouse strains were grouped according to their ancestry (44).

Strain	Encapsulated						Released		
	Cmax (µg/ml)	tmax (h)	V_d (ml/kg)	$t_{1/2}$ (h)	AUC (µg /ml·h)	CL (ml/kg/h)	Cmax (µg/ml)	tmax (h)	AUC (µg·h/ml)
Group 1: Bagg albino derivatives									
A/J	140.92	0.083	46.54	26	3,481	1.23	0.85	3	31.17
BALB/cByJ	127.29	0.083	64.18	84	3,612	0.53	2.96	3	41.94
CBA/J	192.64	0.083	52.61	47	3,940	0.77	1.60	3	42.40
CE/J	197.77	0.083	32.10	34	5,715	0.66	1.29	3	37.04
LG/J	212.41	0.083	26.63	24	6,047	0.78	1.88	0.083	42.44
PL/J	278.14	3	17.10	17	7,543	0.69	1.77	0.083	43.38
Group 2: Swiss mice									
NOD/ShiLtJ	204.39	0.083	37.72	14	2,958	0.31	1.27	3	19.35
MA/MyJ	226.85	0.083	28.40	36	6,841	0.54	1.64	0.083	49.03
RIIIS/J	180.14	0.083	38.35	30	4,558	0.89	2.53	0.083	85.12
SJL/J	176.55	0.083	37.81	14	2,958	1.82	1.27	3	19.35
SWR/J	143.94	0.083	46.3	19	2,951	1.70	0.85	0.083	24.16
Group 3: Japanese and New Zealand inbred strains									
KK/HIJ	155.95	0.083	35.93	33	5,242	0.75	2.30	3	92.98
NON/ShiLtJ	173.58	0.083	48.59	41	4,257	0.79	2.64	0.083	73.45
NZO/HILtJ	192.79	3	27.98	27	5,971	0.72	2.76	3	83.69
NZW/LacJ	221.77	0.083	27.20	21	5,269	0.90	1.65	0.083	34.11

Group 4: C57/C58 strains									
C57BLKS/J	171.35	0.083	45.08	31	3,509	1.0	3.90	3	46.58
C58/J	170.04	3	30.52	24	5,160	0.89	1.50	0.083	33.87
Group 5: Castle's mice									
129S1/SvlmJ	188.53	0.083	33.00	164	8,165	0.14	1.41	0.083	46.13
LP/J	239.69	0.083	28.22	26	6,090	0.74	2.32	0.083	46.52
Group 6: C.C. Little's DBA & related strains									
SM/J	146.53	0.083	56.63	39	3,225	0.98	2.75	0.083	59.57
Group 7: Wild-derived strains									
PERA/EiJ	144.64	0.083	48.07	145	5,113	0.23	1.46	3	57.14
WSB/EiJ	113.90	0.083	50.61	52	4,379	0.68	1.61	24	63.10
PWD/PhJ	165.34	0.083	38.08	16	3,342	1.59	1.59	0.083	35.23

Table 4. 2. Concentrations versus time values of encapsulated and released doxorubicin in plasma after administration of PEGylated liposomal doxorubicin (PLD) in inbred mouse strains (n=3 mice per time point per each strain) with low (129S1/SvlmJ), intermediate (SWR/J), and high (SJL/J) clearance of PLD.

Strain	Doxorubicin	Concentration in plasma Mean ± SD, µg/ml (CV %)			
		0.083 (h)	3 (h)	24 (h)	48 (h)
129S1/SvlmJ	Encapsulated	199 ± 8.1 (4)	182 ± 5.8 (3)	156 ± 9.5 (6)	136 ± 12 (9)
	Released	1.0 ± 0.1 (14)	1.1 ± 0.08 (7)	0.7 ± 0.2 (34)	0.6 ± 0.1 (16)
SWR/J	Encapsulated	150 ± 8.1 (5)	99 ± 5.4 (5)	64 ± 2.8 (4)	25 ± 4.8 (19)
	Released	0.9 ± 0.1 (12)	0.9 ± 0.2 (23)	0.6 ± 0.1 (16)	0.2 ± 0.1 (43)
SJL/J	Encapsulated	133 ± 26 (19)	89 ± 22 (25)	46 ± 3.5 (8)	15 ± 7.5 (65)
	Released	0.9 ± 0.08 (8)	0.8 ± 0.04 (4)	0.4 ± 0.1 (20)	0.2 ± 0.1 (50)

CV: Coefficient of variance

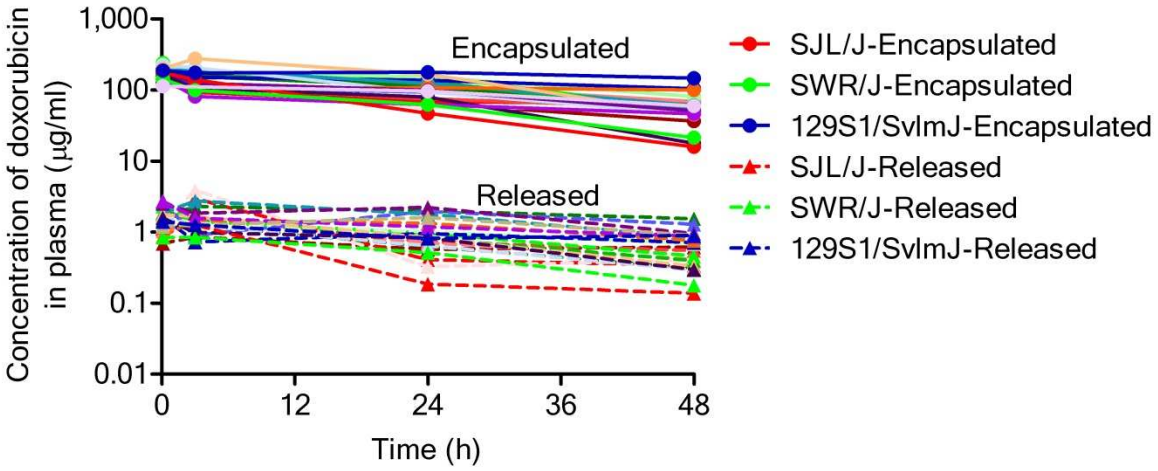

Fig. 4. 1. Plasma concentration versus time profile of encapsulated and released doxorubicin after administration of PLD 6 mg/kg IV x1 in 23 inbred mouse strain males. In the PK studies, individual samples (n=1 per time point) were obtained at 0.083, 3, 24, and 48 hours after administration of PLD. The inbred mouse strains had distinct concentration vs. time profiles of encapsulated and released doxorubicin in plasma.

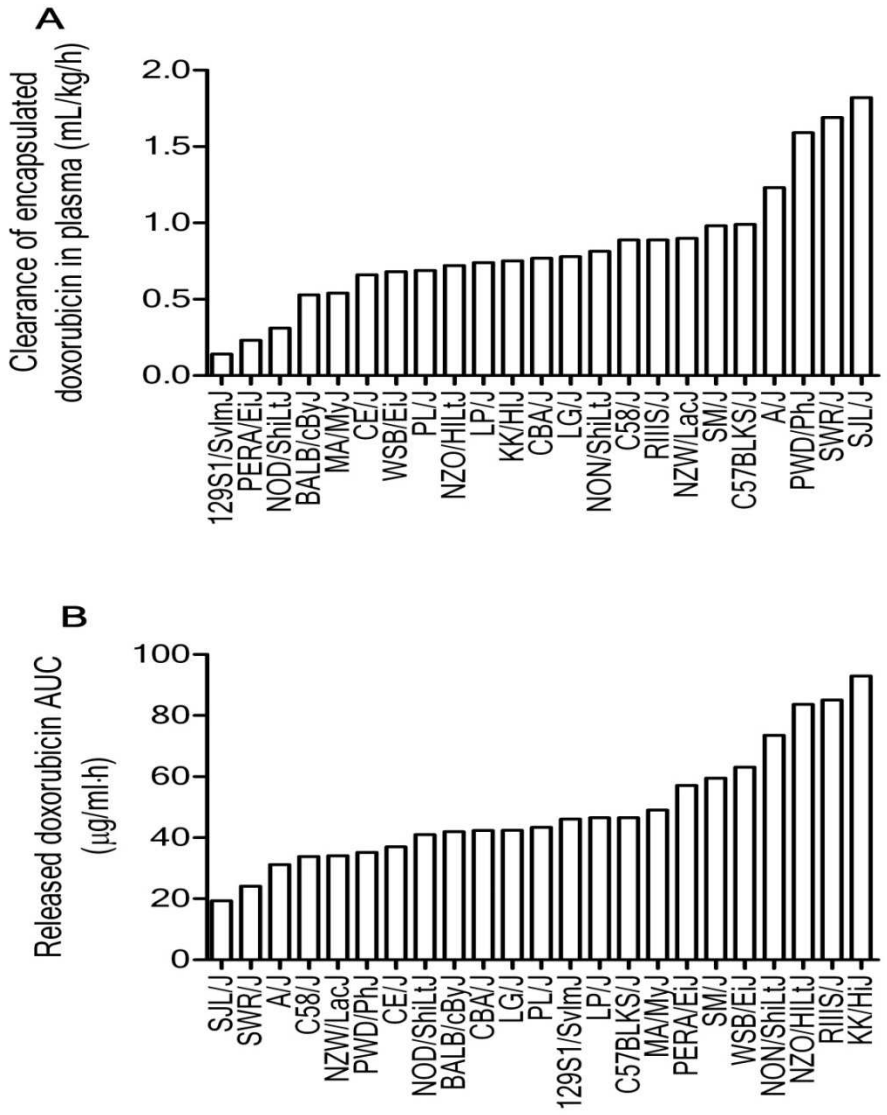

Fig. 4. 2. Summary of phenotypes measured by the PLD PK. (**A**) Clearance (CL) of encapsulated doxorubicin and (**B**) released doxorubicin exposure (AUC) in plasma after administration of PLD 6 mg/kg IV x1 in 23 inbred mouse strain males. The CL of plasma encapsulated doxorubicin showed 13-fold difference between mouse strain with the lowest CL of PLD (129S1/SvlmJ) and the highest CL of PLD (SJL/J).

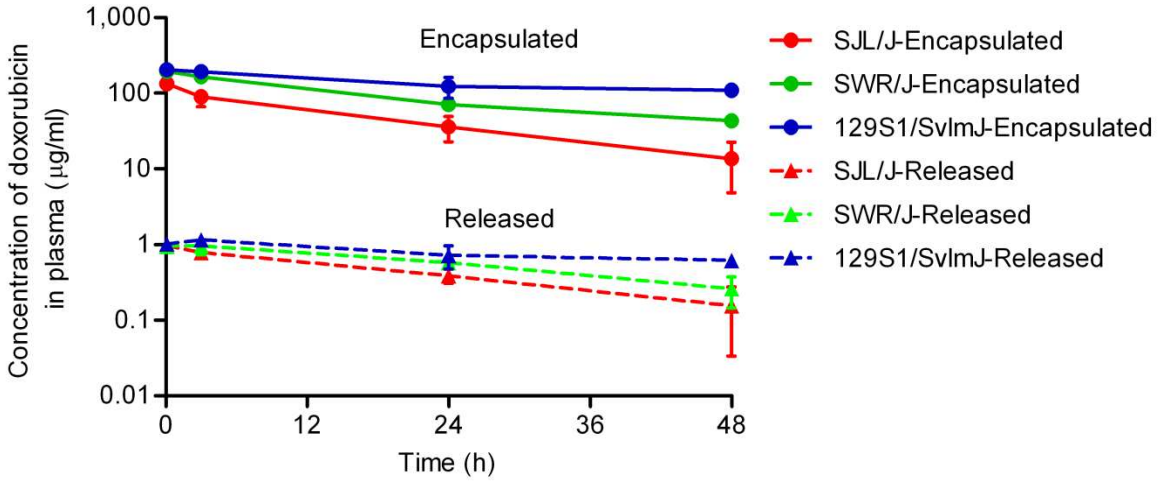

Fig. 4. 3. Plasma concentration vs. time profiles of encapsulated and released doxorubicin after PLD administration at 6 mg/kg IV x1 in an independent confirmatory PK studies. In the confirmatory PK studies in mouse strains with low (129S1/SvlmJ), intermediate (SWR/J), and high (SJL/J) CL of PLD, mice (n=3) were evaluated at each time point. The strain-specific plasma profiles of encapsulated and released components of PLD were reproducibly observed in independently performed confirmatory PK studies with low variability within a strain. Data are presented as mean ± SD.

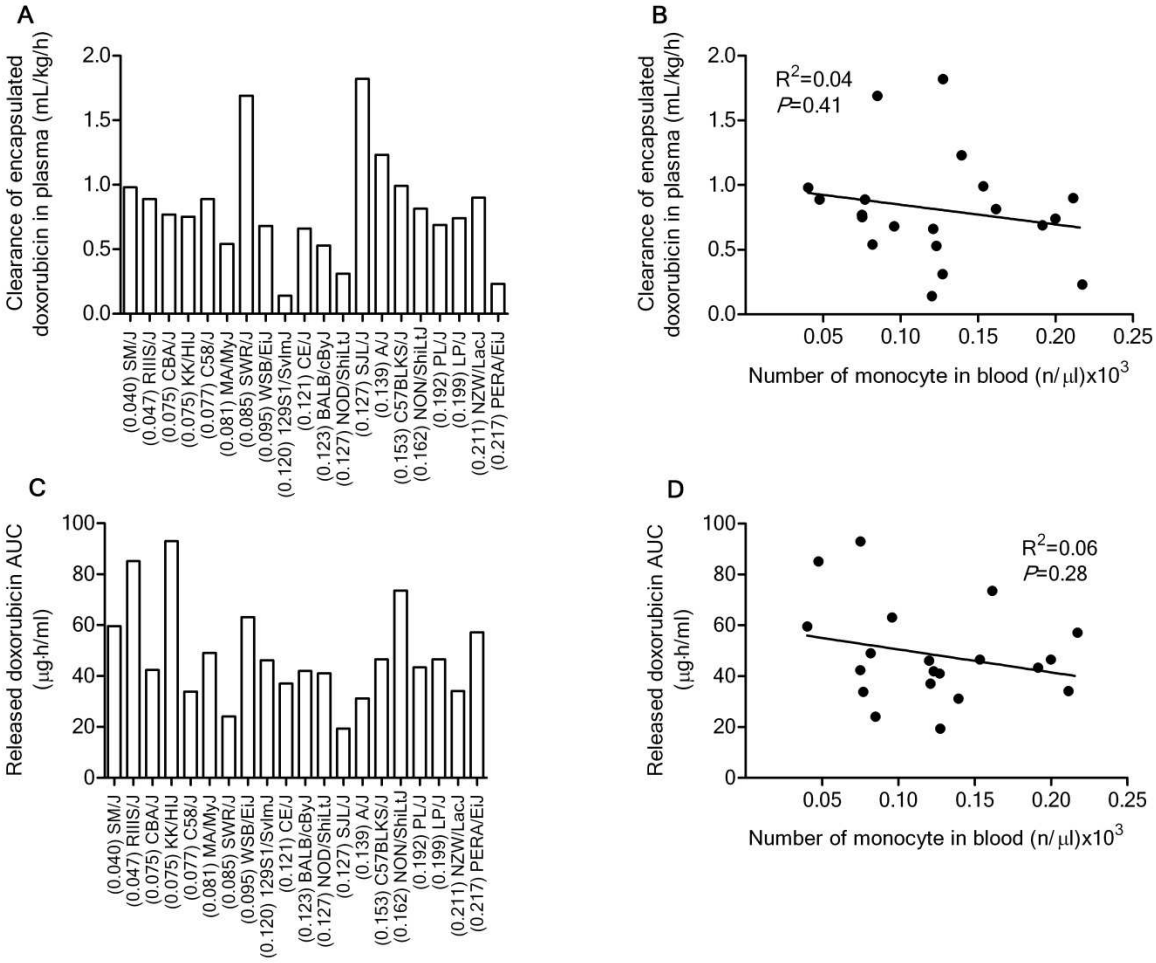

Fig. 4. 4. The relationship between the PK of PLD and the monocyte cell counts in blood in inbred mouse strains. R^2 and *p*-values are calculated using linear regression. (**A and B**) The correlation between the CL of encapsulated doxorubicin and the number of monocytes in blood was assessed in inbred mouse strains. There was no association between the CL of encapsulated doxorubicin and the number of monocytes in blood. (**C** and **D**) There was no association between the exposure (AUC) of released doxorubicin and the number of monocytes in blood in inbred mouse strains. AUC: area under the concentration versus time profile.

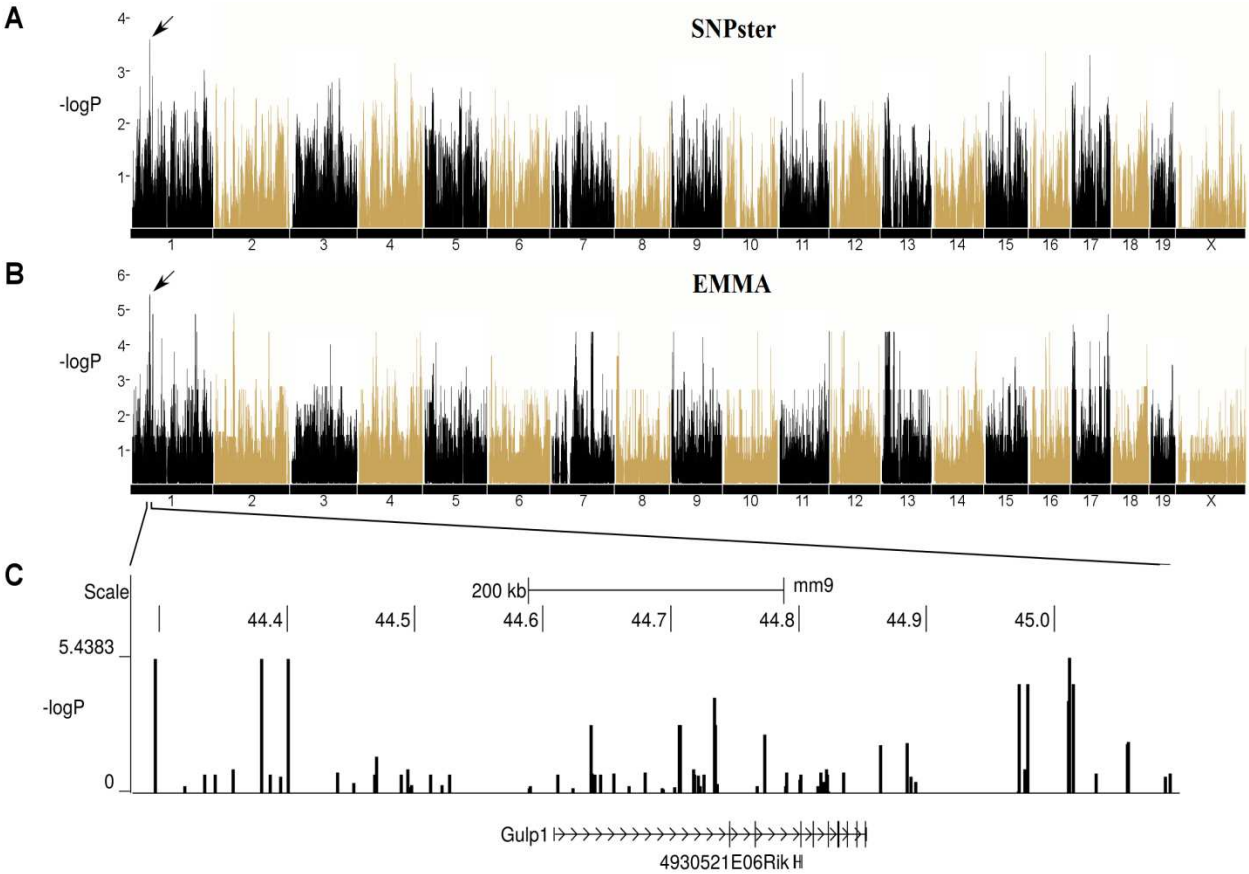

Fig. 4. 5. Genome wide analyses of the plasma CL of encapsulated doxorubicin from 23 mouse strains. The chromosomes numbers are indicated on the x-axis and $-Log_{10}P$ scores on the y-axis. (**A**) A genome wide scan with the haplotype associated mapping (SNPster) algorithm using the CL of encapsulated doxorubicin as a phenotype. A locus with the highest peak of $-Log_{10}P$ score of 3.60 was found on chromosome 1 (arrow). (**B**) EMMA using the CL of encapsulated doxorubicin as a phenotype identified and confirmed a locus with $-Log_{10}P$ score of 5.40 on chromosome 1 (arrow). (**C**) Magnification of the locus on the chromosome 1 identified by SNPster and EMMA analyses shows the underlying gene, *Gulp1*, and their chromosome positions. The threshold for genome wide significance is $-Log_{10}P$ score of 6.7 with a false discovery rate of 19%. CL: clearance.

Chromosome 1 position (mm9)	SNP ID	129S1/SvImJ (0.14)	PERA/EiJ (0.23)	NOD/ShiLtJ (0.31)	BALB/cByJ (0.53)	MA/MyJ (0.54)	CEJ (0.66)	WSB/EiJ (0.68)	PLJ (0.69)	NZO/HILtJ (0.72)	LPJ (0.74)	KK/HIJ (0.752)	CBA/J (0.77)	LG/J (0.78)	NON/LtJ (0.815)	C58/J (0.89)	RIIIS/J (0.89)	NZW/LacJ (0.9)	SM/J (0.98)	C57BLKS/J (0.99)	A/J (1.23)	PWD/PhJ (1.59)	SWR/J (1.69)	SJL/J (1.82)	SNPster -logP
44261431	rs33503276	2	2	2	1	2	2	0	2	1	1	2	2	2	2	1	1	1	2	1	2	0	2	2	0.18
44261688	rs33504853	3	3	3	2	3	1	2	1	2	2	1	1	1	1	2	2	2	1	2	1	0	1	1	3.56
44262520	rs33508090	3	3	3	2	3	1	2	1	2	2	1	1	1	1	2	2	2	1	2	1	0	1	1	3.60
44263683	rs30790932	3	3	3	2	3	1	0	1	2	2	1	1	1	1	2	2	2	1	2	1	0	1	1	3.48
44270739	rs4222320	2	2	2	2	0	1	0	1	2	2	1	1	1	1	2	2	2	1	2	1	0	1	1	1.60
44272711	rs33507378	3	3	3	2	0	1	0	1	2	2	1	1	1	1	2	2	2	1	2	1	0	1	1	3.33
44273428	rs33510689	3	3	3	2	0	1	1	1	2	2	1	1	1	1	2	2	2	1	2	1	0	1	1	3.31
44296740	rs33510908	3	3	3	2	3	1	1	1	2	2	1	1	1	1	2	2	2	1	2	1	0	1	1	3.52
44319825	rs31917300	2	2	2	1	2	2	2	2	1	1	2	2	2	2	1	1	1	2	1	0	0	2	2	0.30
44335443	rs33511296	0	0	0	0	0	0	0	0	0	0	0	0	0	0	0	0	0	0	0	0	0	0	0	0.00
44343651	rs33515664	0	0	0	0	0	0	0	0	0	0	0	0	0	0	0	0	0	0	0	0	0	0	0	0.00
44358165	rs33515943	0	0	0	0	0	0	0	0	0	0	0	0	0	0	0	0	0	0	0	0	0	0	0	0.00
44358304	rs33516792	0	0	0	0	0	0	0	0	0	0	0	0	0	0	0	0	0	0	0	0	0	0	0	0.00
44379870	rs32751808	0	0	0	0	0	0	0	0	0	0	0	0	0	0	0	0	0	0	0	0	0	0	0	0.00
44386954	rs33516737	0	0	0	0	0	0	0	0	0	0	0	0	0	0	0	0	0	0	0	0	0	0	0	0.00
44395115	rs33512451	3	3	3	2	3	1	0	1	2	2	1	1	1	1	2	2	2	1	2	1	0	2	1	3.35
44400800	rs3687130	3	3	3	2	3	1	0	1	2	2	1	1	1	1	2	2	2	1	2	1	0	2	1	3.29
44439262	rs30805456	2	2	2	2	2	1	0	1	2	2	1	1	1	1	2	2	2	1	2	1	0	2	1	1.11
44452506	rs33515296	1	1	2	2	2	1	0	1	2	2	1	1	1	1	2	2	2	1	2	1	0	1	1	0.07
44468341	rs33515321	0	0	2	2	2	1	0	1	2	2	1	1	1	1	2	2	2	1	2	1	0	1	1	1.00
44468879	rs32784514	0	0	2	2	2	1	0	1	2	2	1	1	1	1	2	2	2	1	2	1	0	1	1	1.04
44469886	rs31726152	0	0	2	2	2	1	2	1	2	2	1	1	1	1	2	2	2	1	2	1	0	1	1	1.24
44489371	rs48152894	2	2	0	1	0	2	1	2	1	1	2	2	2	2	1	1	1	2	1	2	0	2	2	0.03
44494304	rs31964448	2	2	0	1	0	2	1	2	1	1	2	2	2	2	1	1	1	2	1	2	2	2	2	0.00
44494787	rs33521240	2	2	0	1	0	2	1	2	1	1	2	2	2	2	1	1	1	2	1	2	0	0	2	0.22
44496476	rs33522256	2	2	1	1	1	2	1	2	1	1	2	2	2	2	1	1	1	2	1	2	0	0	2	0.03
44497825	rs31087442	2	2	1	1	1	2	1	2	1	1	2	2	2	2	1	1	1	2	1	2	0	1	2	0.10
44512516	rs46406392	0	0	2	2	0	1	2	1	2	2	1	1	1	1	2	2	2	1	2	1	0	2	1	0.24
44521240	rs32016076	0	0	0	2	0	1	2	1	2	2	1	1	1	1	2	2	2	1	2	1	2	0	1	0.12
44527012	rs32433552	3	3	0	2	0	1	3	1	2	2	1	1	1	1	2	2	2	1	2	1	3	0	1	0.93
44589292	rs48294411	2	2	3	1	3	2	2	2	1	1	2	2	2	2	1	1	1	2	1	2	0	3	2	0.10
44590446	rs32228948	0	2	2	1	2	2	2	2	1	1	2	2	2	2	1	1	1	2	1	2	0	0	2	0.20
44612072	rs47585920	0	2	2	1	2	2	2	2	1	1	2	2	2	2	1	1	1	2	1	2	0	1	2	0.35
44623581	rs32773207	0	3	3	1	3	2	2	0	1	1	2	2	2	2	1	1	1	2	1	2	1	1	2	2.56
44637816	rs46051391	0	2	2	2	2	1	1	0	2	2	1	1	1	1	2	2	2	1	2	1	0	2	1	0.45
44638145	rs32498583	3	3	3	2	3	1	1	0	2	2	1	1	1	1	2	0	2	1	2	1	0	3	1	1.11
44640468	rs47481269	2	2	2	1	2	2	2	2	1	1	2	2	2	2	1	0	1	2	1	2	0	2	2	0.10
44640763	rs31957585	2	2	3	1	3	2	2	2	1	1	2	2	2	2	1	0	1	2	1	2	0	3	2	0.07
44645039	rs36998612	0	0	2	2	2	1	1	1	2	2	1	1	1	1	2	2	2	1	2	1	0	2	1	0.35
44655496	rs31984083	0	0	2	3	2	1	1	1	3	3	1	1	1	1	3	3	3	1	3	1	2	2	1	0.03
44655539	rs32621825	3	3	3	2	3	1	0	1	2	2	1	1	1	1	2	2	2	1	2	1	3	3	1	0.68
44667513	rs36749752	0	0	2	3	0	1	2	1	3	3	1	1	1	1	3	3	3	1	3	1	2	2	1	0.00
44680282	rs32196409	0	0	2	2	0	1	2	1	2	2	1	1	1	1	2	2	2	1	2	1	0	2	1	0.32
44693612	rs38243424	2	0	1	1	0	2	1	2	1	1	2	2	2	2	1	1	1	2	1	2	0	1	2	0.03
44693680	rs37241356	0	0	3	2	3	1	3	1	2	2	1	1	1	1	2	2	2	1	2	1	0	2	1	1.33
44694512	rs36740612	0	0	3	2	3	1	3	1	2	2	1	1	1	1	2	2	2	1	2	1	0	2	1	1.47
44703296	rs39534166	2	2	1	2	1	1	0	1	2	2	1	1	1	1	2	2	2	1	2	1	0	2	1	0.26
44706621	rs36612732	0	0	0	0	0	0	0	0	0	0	0	0	0	0	0	0	0	0	0	0	0	0	0	0.00
44706819	rs39400030	0	0	0	0	0	0	0	0	0	0	0	0	0	0	0	0	0	0	0	0	0	0	0	0.00
44707135	rs36357352	0	0	0	0	0	0	0	0	0	0	0	0	0	0	0	0	0	0	0	0	0	0	0	0.00
44717985	rs37819132	0	0	0	0	0	0	0	0	0	0	0	0	0	0	0	0	0	0	0	0	0	0	0	0.00
44718684	rs36607170	2	1	2	2	2	1	2	0	2	2	1	1	1	1	2	2	2	1	2	1	0	2	1	0.30
44721405	rs36387119	2	1	2	2	2	1	2	0	2	2	1	1	1	1	2	2	2	1	2	1	0	2	1	0.32
44723400	rs37992203	3	2	3	1	3	2	1	2	1	1	2	2	2	2	1	1	1	2	1	2	0	1	2	1.88
44726221	rs36652103	0	0	0	0	0	0	0	0	0	0	0	0	0	0	0	0	0	0	0	0	0	0	0	0.00
44734395	rs37914196	0	2	0	1	0	2	2	2	1	1	2	2	2	2	1	1	1	2	1	2	0	1	2	0.10
44734841	rs37112673	0	1	2	2	2	1	0	1	2	2	1	1	1	1	2	2	2	1	2	1	0	2	1	0.00
44736109	rs31423925	0	2	3	1	3	2	0	2	1	1	2	2	2	2	1	1	1	2	1	2	3	1	2	0.15
44767929	rs32257821	3	2	3	1	3	2	3	2	1	1	2	2	2	2	1	1	1	2	1	2	0	1	2	1.33
44773410	rs36280438	3	1	3	2	3	1	3	1	2	2	1	1	1	1	2	2	2	1	2	1	0	1	1	1.54
44773444	rs36844891	2	2	2	1	2	2	2	2	1	1	2	2	2	2	1	1	1	2	1	2	0	0	2	0.38
44789823	rs32736035	3	3	3	2	3	1	3	1	2	2	1	1	1	1	2	2	2	1	2	1	3	0	1	1.27
44790344	rs30857694	3	3	3	2	3	1	3	1	2	2	1	1	1	1	2	2	2	1	2	1	0	0	1	3.10
44790378	rs32052591	3	3	3	2	3	1	3	1	2	2	1	1	1	1	2	2	2	1	2	1	0	3	1	1.31
44801381	rs32780749	2	2	2	1	2	2	2	2	1	1	2	2	2	2	1	1	1	2	1	2	0	2	2	0.28
44801411	rs37108418	3	3	3	2	3	1	3	1	2	2	1	1	1	1	2	2	2	1	2	1	0	3	1	1.56
44815322	rs31012866	3	3	3	2	3	1	3	1	2	2	1	1	1	1	2	2	2	1	2	1	0	3	1	1.54
44817278	rs31971049	3	3	3	2	3	1	3	1	2	2	1	1	1	1	2	2	2	1	2	1	0	3	1	1.61
44817303	rs37161271	2	2	0	1	0	2	0	0	1	1	2	2	2	2	1	1	1	2	1	2	0	2	2	0.10
44818944	rs30551340	2	2	3	1	3	2	0	0	1	1	2	2	2	2	1	1	1	2	1	2	3	2	2	0.07
44819211	rs36613494	0	0	0	0	0	0	0	0	0	0	0	0	0	0	0	0	0	0	0	0	0	0	0	0.00
44819572	rs37846853	0	0	0	0	0	0	0	0	0	0	0	0	0	0	0	0	0	0	0	0	0	0	0	0.00
44821632	rs37957094	0	0	0	0	0	0	0	0	0	0	0	0	0	0	0	0	0	0	0	0	0	0	0	0.00
44821857	rs37463747	0	0	0	0	0	0	0	0	0	0	0	0	0	0	0	0	0	0	0	0	0	0	0	0.00
44822222	rs37725007	2	2	2	2	2	1	0	1	2	2	1	1	1	1	2	2	2	1	2	1	0	2	1	1.10
44823062	rs36283977	3	3	3	2	3	1	0	1	2	2	1	1	1	1	2	2	2	1	2	1	3	3	1	0.71
44834919	rs31521814	3	3	3	2	3	1	0	1	2	2	1	1	1	1	2	2	2	1	2	1	3	3	1	0.82
44864213	rs32652311	0	0	0	0	0	0	0	0	0	0	0	0	0	0	0	0	0	0	0	0	0	0	0	0.00
44885231	rs30811714	0	0	0	0	0	0	0	0	0	0	0	0	0	0	0	0	0	0	0	0	0	0	0	0.00
44887911	rs37623729	0	0	0	0	0	0	0	0	0	0	0	0	0	0	0	0	0	0	0	0	0	0	0	0.00
44888136	rs36936796	0	0	0	0	0	0	0	0	0	0	0	0	0	0	0	0	0	0	0	0	0	0	0	0.00
44891255	rs36659237	0	0	0	0	0	0	0	0	0	0	0	0	0	0	0	0	0	0	0	0	0	0	0	0.00
44972044	rs36889491	0	0	0	0	0	0	0	0	0	0	0	0	0	0	0	0	0	0	0	0	0	0	0	0.00
44972094	rs38671078	0	0	0	0	0	0	0	0	0	0	0	0	0	0	0	0	0	0	0	0	0	0	0	0.00
44972107	rs37602546	0	0	0	0	0	0	0	0	0	0	0	0	0	0	0	0	0	0	0	0	0	0	0	0.00
44976717	rs37491684	0	0	0	0	0	0	0	0	0	0	0	0	0	0	0	0	0	0	0	0	0	0	0	0.00
44979143	rs37187498	0	0	0	0	0	0	0	0	0	0	0	0	0	0	0	0	0	0	0	0	0	0	0	0.00

Fig. 4. 6. Haplotype distribution on the locus on chromosome 1 identified by the haplotype association mapping algorithm (SNPster). The CLs of encapsulated doxorubicin from 23 mouse strains were used as phenotypes, and genotypes were downloaded from the Mouse Diversity Array (Yang et al., 2011). Strain names are positioned above the alleles, which are listed and arranged according to the CL of encapsulated doxorubicin. Each haplotype is indicated by a number and corresponding color. The positions (mm^9) of the SNPs on chromosome 1 are listed on the left, and $-Log_{10}P$ scores for the haplotype are given on the right. The position of the identified quantitative trait locus (QTL), *Gulp1*, is highlighted.


Chromosome 1 position (mm9)
SNP ID
129S1/SvImJ (0.14)
PERA/EiJ (0.23)
NOD/ShiLtJ (0.31)
BALB/cByJ (0.53)
MAMyJ (0.54)
CEJ (0.66)
WSB/EiJ (0.68)
PLJ (0.69)
NZO/HILtJ (0.72)
LP/J (0.74)
KK/HIJ (0.752)
CBA/J (0.77)
LG/J (0.78)
NON/LtJ (0.815)
C58/J (0.89)
RIIIS/J (0.89)
NZW/LacJ (0.9)
SMJ (0.98)
C57BLKS/J (0.99)
A/J (1.23)
PWD/PhJ (1.59)
SWR/J (1.69)
SJL/J (1.82)
EMMA -logP
44273428 rs33510689 0.64
44296740 rs33510908 5.40
44319825 rs31917300 0.23
44335443 rs33511296 0.68
44343651 rs33515664 0.68
44358165 rs33515943 0.91
44358304 rs33516792 0.62
44379870 rs32751808 5.40
44386954 rs33516737 0.68
44395115 rs33512451 0.62
44400800 rs3687130 5.40
44439262 rs30805456 0.78
44452506 rs33515296 0.36
44468341 rs33515321 0.68
44468879 rs32784514 0.15
44469886 rs31726152 1.43
44489371 rs48152894 0.68
44494304 rs31964448 0.17
44494787 rs33521240 0.92
44496476 rs33522256 0.17
44497825 rs31087442 0.29
44512516 rs46406392 0.68
44521240 rs32016076 0.29
44527012 rs32433552 0.70
44589292 rs48294411 0.14
44590446 rs32228948 0.23
44612072 rs47585920 0.68
44623581 rs32773207 0.15
44637816 rs46051391 2.70
44638145 rs32498583 0.76
44640468 rs47481269 0.68
44640763 rs31957585 0.18
44645039 rs36998612 0.68
44655496 rs31984083 0.32
44655539 rs32621825 0.74
44667513 rs36749752 0.23
44680282 rs32196409 0.78
44693612 rs38243424 0.15
44693680 rs37241356 0.10
44694512 rs36740612 0.09
44703296 rs39534166 0.17
44706621 rs36612732 0.68
44706819 rs39400030 0.03
44707135 rs36357352 2.70
44717985 rs37819132 0.92
44718684 rs36607170 0.68
44721405 rs36387119 0.67
44723400 rs37992203 0.22
44726221 rs36652103 0.68
44734395 rs37914196 3.82
44734841 rs37112673 2.71
44736109 rs31423925 0.32
44767929 rs32257821 0.22
44773410 rs36280438 2.30
44773444 rs36844891 0.68
44789823 rs32736035 0.23
44790344 rs30857694 0.63
44790378 rs32052591 0.78
44801381 rs32780749 0.48
44801411 rs37108418 0.68
44815322 rs31012866 0.23
44817278 rs31971049 0.78
44817303 rs37161271 0.68
44818944 rs30551340 0.23
44819211 rs36613494 0.42
44819572 rs37846853 0.41
44821632 rs37957094 0.68
44821857 rs37463747 0.92
44822222 rs37725007 0.68
44823062 rs36283977 0.03
44834919 rs31521814 0.78
44864213 rs32652311 1.88
44885231 rs30811714 1.96
44887911 rs37623729 0.41
44888136 rs36936796 0.60
44891255 rs36659237 0.41
44972044 rs36889491 0.03
44972094 rs38671078 0.68
44972107 rs37602546 4.37
44976717 rs37491684 0.92
44979143 rs37187498 4.37
45010795 rs6223934 1.88
45011361 rs52052882 3.67
45012103 rs31793326 5.44
45014439 rs48358822 0.92
45015087 rs46460131 3.67
45015110 rs32670612 4.37

Fig. 4. 7. Genotype distribution on the locus on chromosome 1 identified by the efficient mixed-model for association (EMMA). The CLs of encapsulated doxorubicin from 23 mouse strains were used as phenotypes, and genotypes were downloaded from the Mouse Diversity Array (Yang et al., 2011). Strain names are positioned above the alleles, which are listed and arranged according to the CL of encapsulated doxorubicin. The positions (mm^9) of the SNPs on chromosome 1 are listed on the left, and $-Log_{10}P$ scores for each position are given on the right. The position of the identified quantitative trait locus (QTL), *Gulp1*, is highlighted. Gray and black block represent A allele and C allele, respectively. White block represents missing allele. CL: clearance.

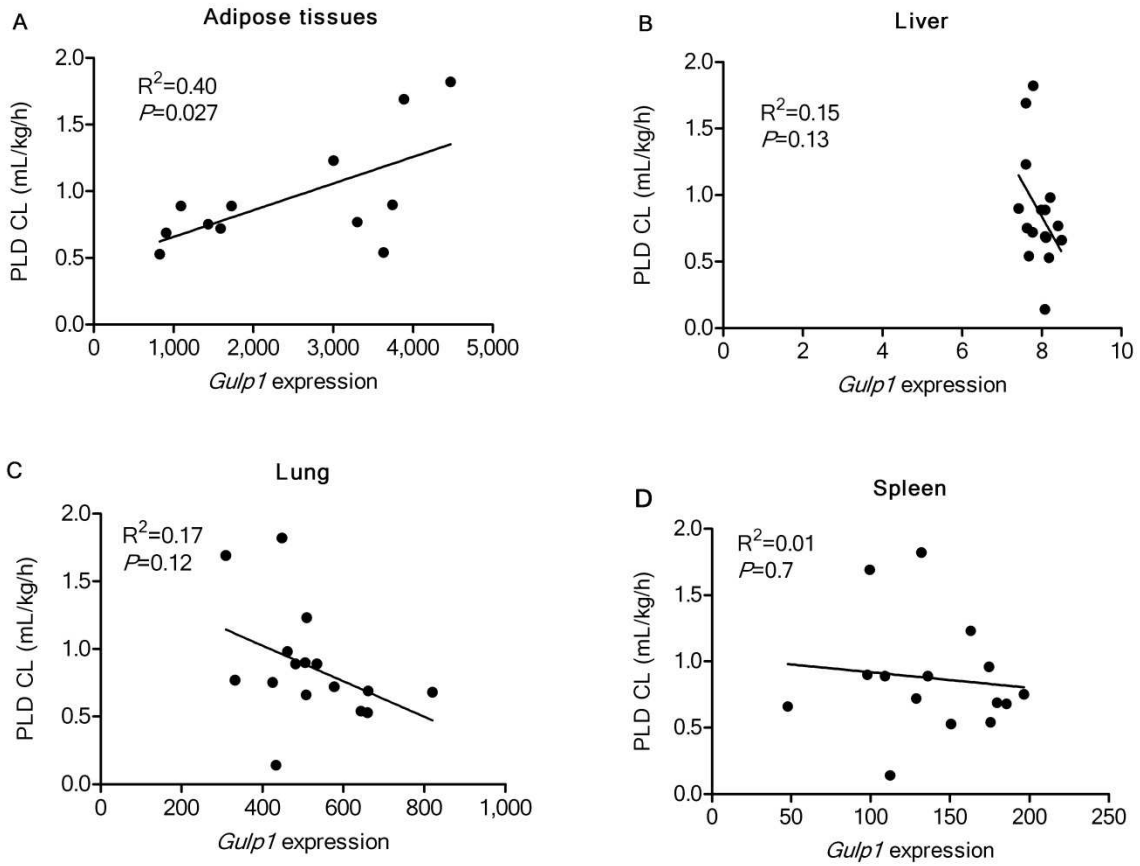

Fig. 4. 8. Evaluation of association between G*ulp1* gene expression in tissues and the CL of encapsulated doxorubicin after administration of PLD in 23 male inbred mouse strains. R^2 and *p*-values are calculated using linear regression. *Gulp1* was significantly more highly expressed in (**A**) adipose tissues compared to other tissues associated with the mononuclear phagocyte system (MPS), such as (**B**) liver, (**C**) spleen, and (**D**) lung. In addition, there was a significantly positive relationship between *Gulp1* gene expression in adipose tissues and PLD CL. CL: clearance.

REFERENCES

(1) Farokhzad OC, Langer R. Impact of nanotechnology on drug delivery. ACS nano 2009;3(1):16-20.

(2) Zamboni WC. Concept and clinical evaluation of carrier-mediated anticancer agents. Oncologist 2008;13(3):248-260.

(3) Danhier F, Feron O, Préat V. To exploit the tumor microenvironment: Passive and active tumor targeting of nanocarriers for anti-cancer drug delivery. J Controlled Release 2010;148(2):135-146.

(4) Duncan R, Gaspar R. Nanomedicine (s) under the microscope. Molecular pharmaceutics 2011;8(6):2101-2141.

(5) Zhang L, Gu F, Chan J, Wang A, Langer R, Farokhzad O. Nanoparticles in medicine: therapeutic applications and developments. Clinical Pharmacology & Therapeutics 2007;83(5):761-769.

(6) Murray PJ, Wynn TA. Protective and pathogenic functions of macrophage subsets. Nature Reviews Immunology 2011;11(11):723-737.

(7) Bertrand N, Leroux J. The journey of a drug-carrier in the body: an anatomo-physiological perspective. J Controlled Release 2012;161(2):152-163.

(8) Future directions of liposome-and immunoliposome-based cancer therapeutics. Seminars in oncology: Elsevier; 2004.

(9) Li S, Huang L. Pharmacokinetics and biodistribution of nanoparticles. Molecular pharmaceutics 2008;5(4):496-504.

(10) La-Beck NM, Zamboni BA, Gabizon A, Schmeeda H, Amantea M, Gehrig PA, et al. Factors affecting the pharmacokinetics of pegylated liposomal doxorubicin in patients. Cancer Chemother Pharmacol 2012;69(1):43-50.

(11) Caron WP, Lay JC, Fong AM, La-Beck NM, Kumar P, Newman SE, et al. Translational Studies of Phenotypic Probes for the Mononuclear Phagocyte System and Liposomal Pharmacology. J Pharmacol Exp Ther 2013:jpet. 113.208801.

(12) Song G, Wu H, Yoshino K, Zamboni WC. Factors affecting the pharmacokinetics and pharmacodynamics of liposomal drugs. J Liposome Res 2012;22(3):177-192.

(13) Altshuler D, Daly MJ, Lander ES. Genetic mapping in human disease. Science 2008 Nov 7;322(5903):881-888.

(14) Schwartz GF, Hughes KS, Lynch HT, Fabian CJ, Fentiman IS, Robson ME, et al. Proceedings of the international consensus conference on breast cancer risk, genetics, & risk management, April, 2007. Breast J 2009;15(1):4-16.

(15) Ginsburg GS, Willard HF. Genomic and personalized medicine: foundations and applications. Translational Research 2009;154(6):277-287.

(16) Flint J, Eskin E. Genome-wide association studies in mice. Nature Reviews Genetics 2012;13(11):807-817.

(17) Yang H, Ding Y, Hutchins LN, Szatkiewicz J, Bell TA, Paigen BJ, et al. A customized and versatile high-density genotyping array for the mouse. Nature methods 2009;6(9):663-666.

(18) Hillebrandt S, Wasmuth HE, Weiskirchen R, Hellerbrand C, Keppeler H, Werth A, et al. Complement factor 5 is a quantitative trait gene that modifies liver fibrogenesis in mice and humans. Nat Genet 2005;37(8):835-843.

(19) Harrill AH, Watkins PB, Su S, Ross PK, Harbourt DE, Stylianou IM, et al. Mouse population-guided resequencing reveals that variants in CD44 contribute to acetaminophen-induced liver injury in humans. Genome Res 2009 Sep;19(9):1507-1515.

(20) Bopp SE, Ramachandran V, Henson K, Luzader A, Lindstrom M, Spooner M, et al. Genome wide analysis of inbred mouse lines identifies a locus containing ppar-γ as contributing to enhanced malaria survival. PLoS One 2010;5(5):e10903.

(21) Caron W, Song G, Kumar P, Rawal S, Zamboni W. Interpatient Pharmacokinetic and Pharmacodynamic Variability of Carrier-Mediated Anticancer Agents. Clinical Pharmacology & Therapeutics 2012;91(5):802-812.

(22) Bookman M. Standard treatment in advanced ovarian cancer in 2005: the state of the art. International Journal of Gynecological Cancer 2005;15(s3):212-220.

(23) Zamboni WC, Strychor S, Joseph E, Walsh DR, Zamboni BA, Parise RA, et al. Plasma, tumor, and tissue disposition of STEALTH liposomal CKD-602 (S-CKD602) and nonliposomal CKD-602 in mice bearing A375 human melanoma xenografts. Clinical Cancer Research 2007;13(23):7217-7223.

(24) Kang HM, Zaitlen NA, Wade CM, Kirby A, Heckerman D, Daly MJ, et al. Efficient control of population structure in model organism association mapping. Genetics 2008 Mar;178(3):1709-1723.

(25) McClurg P, Janes J, Wu C, Delano DL, Walker JR, Batalov S, et al. Genomewide association analysis in diverse inbred mice: power and population structure. Genetics 2007 May;176(1):675-683.

(26) Yang H, Wang JR, Didion JP, Buus RJ, Bell TA, Welsh CE, et al. Subspecific origin and haplotype diversity in the laboratory mouse. Nat Genet 2011;43(7):648-655.

(27) Peters LL, Barker JE. Hematology and clotting time survey in 43 inbred strains of mice. MPD:6201. Mouse Phenome Database web site, The Jackson Laboratory, Bar Harbor, Maine USA. http://phenome.jax.org, Mar, 2014.

(28) Smits E, Criekinge WV, Plaetinck G, Bogaert T. The human homologue of Caenorhabditis elegans CED-6 specifically promotes phagocytosis of apoptotic cells. Current biology 1999;9(22):1351-1354.

(29) Su HP, Brugnera E, Van Criekinge W, Smits E, Hengartner M, Bogaert T, et al. Identification and characterization of a dimerization domain in CED-6, an adapter protein involved in engulfment of apoptotic cells. J Biol Chem 2000 Mar 31;275(13):9542-9549.

(30) Lattin JE, Schroder K, Su AI, Walker JR, Zhang J, Wiltshire T, et al. Expression analysis of G Protein-Coupled Receptors in mouse macrophages. Immunome Res 2008 Apr 29;4:5-7580-4-5.

(31) Wu C, Orozco C, Boyer J, Leglise M, Goodale J, Batalov S, Hodge CL, Haase J, Janes J, Huss JW. (2009) BioGPS: An extensible and customizable portal for querying and organizing gene annotation resources. *Genome Biol* **10**:R130.

(32) Frazer KA, Eskin E, Kang HM, Bogue MA, Hinds DA, Beilharz EJ, et al. A sequence-based variation map of 8.27 million SNPs in inbred mouse strains. Nature 2007;448(7157):1050-1053.

(33) Moghimi SM, Hunter AC, Murray JC. Long-circulating and target-specific nanoparticles: theory to practice. Pharmacol Rev 2001;53(2):283-318.

(34) Hillaireau H, Couvreur P. Nanocarriers' entry into the cell: relevance to drug delivery. Cellular and Molecular Life Sciences 2009;66(17):2873-2896.

(35) Drummond DC, Noble CO, Hayes ME, Park JW, Kirpotin DB. Pharmacokinetics and in vivo drug release rates in liposomal nanocarrier development. J Pharm Sci 2008;97(11):4696-4740.

(36) Charrois GJ, Allen TM. Drug release rate influences the pharmacokinetics, biodistribution, therapeutic activity, and toxicity of pegylated liposomal doxorubicin formulations in murine breast cancer. Biochimica et Biophysica Acta (BBA)-Biomembranes 2004;1663(1):167-177.

(37) Lauber K, Blumenthal SG, Waibel M, Wesselborg S. Clearance of apoptotic cells: getting rid of the corpses. Mol Cell 2004;14(3):277-287.

(38) Osada Y, Sunatani T, Kim IS, Nakanishi Y, Shiratsuchi A. Signalling pathway involving GULP, MAPK and Rac1 for SR-BI-induced phagocytosis of apoptotic cells. J Biochem 2009 Mar;145(3):387-394.

(39) Chawla A, Nguyen KD, Goh YS. Macrophage-mediated inflammation in metabolic disease. Nature Reviews Immunology 2011;11(11):738-749.

(40) Weisberg SP, McCann D, Desai M, Rosenbaum M, Leibel RL, Ferrante AW,Jr. Obesity is associated with macrophage accumulation in adipose tissue. J Clin Invest 2003 Dec;112(12):1796-1808.

(41) Lumeng CN, DelProposto JB, Westcott DJ, Saltiel AR. Phenotypic switching of adipose tissue macrophages with obesity is generated by spatiotemporal differences in macrophage subtypes. Diabetes 2008 Dec;57(12):3239-3246.

(42) Sharifi S, Daghighi S, Motazacker M, Badlou B, Sanjabi B, Akbarkhanzadeh A, et al. Superparamagnetic iron oxide nanoparticles alter expression of obesity and T2D-associated risk genes in human adipocytes. Scientific reports 2013;3.

(43) Lammers T, Rizzo LY, Storm G, Kiessling F. Personalized nanomedicine. Clin Cancer Res 2012 Sep 15;18(18):4889-4894.

(44) Petkov PM, Ding Y, Cassell MA, Zhang W, Wagner G, Sargent EE, et al. An efficient SNP system for mouse genome scanning and elucidating strain relationships. Genome Res 2004 Sep;14(9):1806-1811.

CHAPTER 5:

CONCLUSION

Overview

The application of nanotechnology to drug delivery system has made remarkable impacts on pharmaceutical and biotechnology industries as well as treatment of human diseases. The development of nanotechnology products offers a wide range of advantages over conventional small molecule drugs including: (1) protection of drugs from a premature degradation due to interaction with biological barriers; (2) enhanced cell- or tissue-specific targeted delivery of drugs; (3) delivery of macromolecule drugs to intracellular sites of action; (4) delivery of poorly water-soluble drugs; (5) improved pharmacokinetics and tissue distribution of drug; (6) improved therapeutic index (1, 2). Indeed, nanoparticles, particles ranging from 1 to 1000 nm in size, are emerging as a class of therapeutics for solid tumors (1). The development of nanotechnology platforms hold promise for cancer therapy in that the nanotechnology-based therapeutics can enable pharmaceutically suboptimal drugs with biological activity to be revived and commercialized (1-3). Moreover, nanotechnology has been useful for increasing intracellular delivery of drugs with low membrane permeability, such as DNA or siRNA, which are emerging as new classes of bioactive macromolecules (4, 5). Although nanotechnology has the potential to revolutionize drug delivery and advance the treatment of cancer, to date, only a few nanoparticle (NP)-based therapeutics are clinically approved and this technology has not made a significant clinical impact on cancer therapy (1, 2). Moreover, when compared to conventional small molecule drugs, significantly high and clinically relevant inter-individual variation in the

pharmacokinetics (PK) and pharmacodynamics (PD) of NP-based anticancer drugs has been reported (6, 7).

There has been increasing effort to characterize and optimize physicochemical characteristics of the NPs, such as surface size, charge, and hydrophilicity, which can influence the biocompatibility, circulating half-life and biodistribution to tissues (3, 5, 8, 9). In parallel, the understanding of pathophysiology of cancer, in particular solid tumors, has advanced. Consequently, currently approved NP-based therapeutic products for cancer therapy exploit the enhanced permeability and retention (EPR) effect caused by abnormal tumor blood and lymphatic vasculature for simple passive extravasation of NPs (10). However, it still remains poorly understood how involvement of the mononuclear phagocyte system (MPS), including monocytes and macrophages, in PK and biodistribution of NPs influence the therapeutic responses of NP-based therapeutics (6). Like conventional drugs, "one-size-fits-all approach" may not be appropriate for the application of nanotechnology for cancer therapy, as complex and heterogeneous tumor biology as well as the immune system may contribute to variable interaction with NPs and, eventually, heterogeneous clinical responses to NP-based therapeutics.

The overall goal of this dissertation research was to elucidate underlying immune mechanisms for variable patient responses to liposomal anticancer agents, the most common class of NPs that have been approved for clinical use. To achieve these goals, three hypothesis-driven aims were developed and investigated in the context of use of PEGylated liposomal doxorubicin (PLD; Doxil®), a clinically relevant NP. PLD, is the first liposome-based therapeutic approved by the U.S. Food and Drug Administration (FDA) in 1995 for the treatment of HIV-related Kaposi's sarcoma (11). It was subsequently approved for the treatment of recurrent ovarian cancer and multiple myeloma based on enhanced efficacy and reduced cardiotoxicity

compared to free doxorubicin (11). Although PLD has been used in clinic for more than 20 years, the mechanisms for variable responses and modest efficacy in patients remain unknown. *In vitro, in vivo* and clinical systems were investigated to elucidate the immunological mechanisms underlying inter-individual variation in PK and PD of PLD. Major findings, novelties, potential clinical impacts of these findings, limitations, and areas of future investigations in each aim are discussed.

5. 1. Discussion

Aim 1. Evaluate the relationship between chemokine ligands CCL2 and CCL5 and pharmacokinetics (PK) of PEGylated liposomal doxorubicin (PLD) in vitro systems, in preclinical mouse models, and in patients with recurrent ovarian cancer.

Liposomes are removed from the circulation by the cells of the MPS, peripheral blood monocytes and tissue resident macrophages. Liver and spleen are the major parts of the MPS (i.e., Kupffer cells and splenic macrophages and play a key role in the recognition and clearance of opsonized liposomes (5, 12, 13). In addition, the tumor microenvironment is comprised of abundant infiltrating macrophages, called tumor-associated macrophages (TAMs) (14, 15). Homeostatic circulation and recruitment of peripheral circulating monocytes into these tissues are orchestrated by an intricate network of chemokines (14, 16, 17). Chemokines are chemotactic cytokines that cause the directed migration of monocytes along the chemokine gradient and stimulate the differentiation into macrophages (16, 17). CC chemokine ligand (CCL) 2, also known as monocyte chemoattractant protein-1 (MCP-1), is overexpressed in human ovarian and breast tumors and correlates with the amount of infiltrating TAMs (18-20). CCL2 is also

involved in inflammation in the liver via secretion from hepatocytes, Kupffer cells, and hepatic stellate cells (21, 22).

Despite well-characterized relationship between chemokines and macrophages, a potential role of chemokines in macrophages-mediated clearance of liposomal drugs has not been investigated yet. Thus, we hypothesized that chemokines drive the pharmacokinetics (PK) of nanoparticles (NP) and this may be associated with high interpatient variability in the PK of NP-based therapy. To test this hypothesis, we investigated the relationship between the expressions of chemokine ligands and the PK of PLD in patients with refractory epithelial ovarian cancer (EOC), in preclinical models for ovarian cancer, and in human monocytic THP-1 cells *in vitro* in Chapter 2.

Plasma concentrations of CCL2, CCL3, CCL4, and CCL5 were assessed from serial blood samples at prior to and post PLD administration alone and in combination with carboplatin. CCL2 and CCL5 were the most prevalent baseline chemokines in these patients, and the baseline plasma concentrations of CCL2 and CCL5 did not correlate with the clearance (CL) of encapsulated doxorubicin in plasma, indicating that baseline levels of chemokine may not predict the PK of PLD. We then assessed the total amount (AUC) of plasma chemokines secreted after PLD administration. There was a significantly positive linear relationship between all chemokine $AUC_{0\text{-last}}$ and PLD $AUC_{0\text{-last}}$ in plasma in patients treated with PLD alone, indicating that PLD induced the production and secretion of chemokines into plasma. However, there was not an association in patients treated with PLD plus carboplatin, indicating that co-administration of carboplatin may influence the interaction between PLD and the chemokine systems (23, 24). In preclinical studies using mice bearing SKOV3 orthotopic ovarian cancer xenografts, ovarian cancer cells were found to be the primary source for PLD-mediated stimulation of secretions of

CCL2 and CCL5. *In vivo* studies using CCL2 KO and CCL5 KO mice verified that these chemokines have a significant impact on plasma clearance and biodistribution of PLD. In addition, *in vitro* studies using human monocytic THP-1 cells demonstrated that PLD impaired monocyte migration towards CCL2, but enhanced CCL5-induced migration.

Collectively, we demonstrated for the first time that PLD, a NP-based therapy, altered the expressions of CCL2 and CCL5 as well as monocyte chemotaxis, which was shown to be associated with the clearance and biodistribution of PLD in preclinical models and in patients with refractory EOC. These data implicate that chemokines can be targets not only for development of new anticancer therapy, but also for optimization of NP-based therapy.

Based on the implications of these studies, the following future directions are suggested as follows:

[**1**] It has been reported that the MPS-mediated clearance of NPs is a saturable process and the PK of PLD is dose- and schedule-dependent (25, 26). NP-based anticancer drugs are administered via multiple cycles and often in combination with other chemotherapies. Thus, it is critical to characterize the effects of multiple doses of NP-based therapy as well as potential interaction between NP-based therapy and other co-medications via the chemokine system. It has been shown that simvastatin down-regulated the expression of CCL2 in a time- and dose-dependent manner in patients (27, 28).

[**2**] It is known that physicochemical properties of NPs play a significant role in determining the PK and biodistribution of NPs (3, 5, 8, 9). In addition, heterogeneity of the tumor microenvironment across different tumor types has been reported and suggested to be a contributing factor to inter-individual variability in the tumor delivery and clinical responses of NP-based therapy (14, 29). Thus, comprehensive profiling of the interaction between different

NP platforms and the microenvironment factors (i.e., chemokines and TAMs) in mouse cancer models and human samples will be a key part to advancing our understanding of the interplay between NPs and the tumor microenvironment and subsequent effects on the PK and PD (efficacy and toxicity) of NP-based therapy.

Aim 2. Evaluate effects of the tumor microenvironment heterogeneity on tumor delivery and efficacy of PLD using murine mammary carcinoma models.

Solid tumors are characterized by unique tumor microenvironment that consists of infiltrating immune cells, such as TAMs, a variety of growth factors, chemokines and cytokines, dense interstitial matrix, and the abnormal blood and lymphatic vasculature (14, 30). Microenvironmental factors interplay with the tumor cells to modify the tumor microenvironment and promote tumor progression (14, 30). It has been reported that there is intra- and inter-tumor variability in the tumor cells and the microenvironment that results in the heterogeneity of molecular, pathological, and clinical features of each tumor type (31, 32). In addition, we also found that tumor cells and/or stromal cells are the primary source for PLD-induced secretion of CCL2 and CCL5 in Chapter 2. Thus, we hypothesized that the heterogeneity of the tumor cells and the tumor microenvironment between breast tumor subtypes affect the tumor delivery and therapeutic outcomes of PLD in Chapter 3. To test our hypothesis, we used the genomically validated *C3(1)-T-Antigen* (C3-TAg) and *T11/TP53*$^{-/-}$ (T11) murine breast tumor models that faithfully represent human intrinsic breast tumor subtypes, basal-like and claudin-low, respectively (33-35). We evaluated PLD, which has been used for treatment of metastatic breast cancer, and non-liposomal doxorubicin (NL-doxo; Adriamycin®) as a comparator (36).

The PK studies showed that the ratio of tumor to plasma $AUC_{0\text{-}96h}$ of PLD in C3-TAg model and T11 model was 0.30 and 0.15, respectively, suggesting that the efficiency of transvascular transportation of PLD into the tumor is 2-fold higher in C3-TAg model compared to T11 model. However, the difference in tumor delivery between two models was not seen with NL-doxo. These findings led us to measure tumor-associated factors and found that claudin-low T11 tumors exhibited features of hypervascularization and inefficient lymphatic networks, which may increase interstitial fluid pressure (IFP) and hamper the transvascular transport of PLD (29). In addition, the interactions between PLD and the tumor microenvironment factors (e.g., the vascular density, VEGF-A, VEGF-C, and CCL2) were different between two breast tumor subtypes. PLD significantly prolonged the survival of C3-TAg models ($P<0.0001$), but modestly in T11 models ($P=0.083$) compared with no treatment and NL-doxo. However, it was noted that T11 tumors treated with PLD became ulcerative in 18 days post treatment, which may reflect responses of T11 tumors to PLD, but were terminated in accordance to IACUC guidelines (37). Thus, the results of overall survival for T11 mice treated with PLD may not represent the accurate survival outcomes.

Collectively, this is the first report that heterogeneous tumor microenvironment and/or tumor cell features between two intrinsic breast tumor subtypes correlated with significantly different tumor delivery and efficacy of PLD, but not small molecule doxorubicin, using validated murine models. Our findings implicate that profiling of the tumor and the microenvironment and selection of patients with tumors conducive to the NPs are required for the optimal delivery and therapeutic outcomes of NP-based therapy.

Limitations in our studies and future investigations as a follow-up to our experiments are as follows:

[**1**] First, the fact that T11 is a transplant model compared to C3-TAg genetically engineered mouse models (GEMM) may play a role as confounding factor in our study despite the conserved gene expression features between murine T11 OST tumors and human claudin-low tumors (33-35). Although the clinical relevance of our study results can be justified on the basis of the evidence showing that gene expression signatures derived from chemotherapy-treated T11 models successfully predicted the pathological complete response to anthracycline/taxane therapy in human patients with breast cancer, additional studies using the same mouse model (i.e., T11 OST or C3-TAg OST) would be helpful to rule out any effects of model-derived physiology on the tumor delivery and efficacy of PLD (33).

[**2**] It has been reported that the primary mode of antitumor efficacy of PLD is via direct cytotoxic effects on tumor cells with slight suppressing effects on TAM-mediated angiogenesis (38). In this study, administration of PLD in addition to clodronate-containing long circulating liposome (LCL) exhibited a significantly additional antitumor inhibition compared to that induced by clodronate-LCL, an agent with strong TAM-suppressing effects (38). However, there was no additional reduction in VEGF-a expression after administration of combination of PLD and clodronate-CLC compared to that after administration of clodronate-LCL alone. These data indicate that PLD mainly acts via direct cytotoxic effects on tumor cells with slight suppressing effects on TAM-mediated angiogenesis (38). Consistent with these findings, we also demonstrated that T11 tumor-specific VEGF-a suppressing effect of PLD may be associated with greater responsiveness of T11 tumors to PLD. However, i*n vitro* studies assessing IC50 of PLD in human basal-like cells and claudin-low cells would further confirm the different sensitivity to PLD between two breast tumor types.

[**3**] The vessel normalization strategies using anti-angiogenic therapies showed improvement of the tumor delivery and effectiveness of NP in a size-dependent manner, emphasizing the importance of optimization of both surface properties of NPs and the tumor microenvironment (39). Thus, it is critical to profile the interaction of other NP platforms (i.e., polymers) with the tumor microenvironment within and between tumor types.

Aim 3. Identify the quantitative trait loci associated with the variability in PK of PLD using a panel of inbred mouse strains.

NPs are cleared by the mononuclear phagocytes, primarily monocytes and macrophages (13). Thus, PK and biodistribution of NPs are dependent on the clearance (CL) of the carrier until the drug gets released from the carrier (5, 40). We have previously shown that the variability in the PK and PD of nanomedicines such as Doxil® (PEGylated liposomal doxorubicin; PLD) and S-CKD602 (PEGylated liposome of CKD-602, a camptothecin analog) is associated with patient age, gender, and the function of circulating monocytes in plasma of patients with solid tumors (41-43). However, molecular mechanisms underlying this relationship have not yet been investigated and remain poorly understood. In Chapter 4, we aimed to investigate the molecular basis of high inter-patient variability in the PK of PLD using a panel of inbred mouse strains. Previous studies have shown that candidate gene(s) for the quantitative phenotypic trait identified by GWAS in commonly used laboratory strains successfully translated to identification of the genetic basis of disease and traits in humans (44-46). Thus, these mice can serve as valuable experimental tools to model the phenotypic variation within the human population and identify the genes implicated in the human phenotypes (44).

We used 23 inbred mouse strains representing the genetic variation present within the human population were evaluated for the PK of PLD. A distinct inter-strain variation in the plasma disposition of encapsulated and released doxorubicin was observed and reproduced with low intra-strain variability (n=3 per time point) in a second set of inbred mouse strains that were independently administered the same dose of PLD. The PK analysis revealed that the plasma CL of PLD showed the robust discrimination between the different strains and there was no correlation between the PLD CL and the circulating monocyte counts across different inbred strains.

Genome wide association mapping studies (GWAS) were performed to uncover the quantitative trait loci (QTL) associated with the variability of PLD CL using two different analysis methods, haplotype association mapping algorithm (SNPster) and the efficient mixed-model for association (EMMA) mapping algorithm (47, 48). Interestingly, both SNPster and EMMA analysis identified and confirmed a QTL on chromosome 1 (44273428-45015110bp) with the highest $-Log_{10}P$ score of 3.60 and 5.40, respectively. In addition, this plausible association explained 59% of the phenotypic variance for the CL of PLD in males of 23 inbred mouse strains. The QTL for the CL of PLD identified by two GWAS mapping methods above was found to be approximately 200 kb away from the *Gulp1* gene (44608516-44845719bp, GeneID: 51454, MGI: 1920407). *Gulp1* gene encodes phosphotyrosine-binding (PTB) domain containing engulfment adapter protein 1 (GULP1), which is mammalian homologue of *Caenorhabditis elegans* CED-6 (49). GULP1/CED-6 plays a critical role as an adapter protein in phagocytosis of apoptotic cells and this function has been conserved in *C. elegans*, rodents, and human GULP1/CED-6 proteins (49, 50). Based on the mechanistic link between phagocyte-mediated CL of PLD and the function of *Gulp1* gene, we assessed the relationship between the

available *Gulp1* expression data and the plasma CL of PLD. *Gulp1* was found to be highly expressed in adipose tissue of mouse strains compared to other tissues. In addition, *Gulp1* gene expression levels were significantly correlated with plasma CL of PLD (R^2=0.40, *P*=0.027); however, the correlation was not observed in other tissues.

This was the first study using a GWAS approach to uncover the genetic variant(s) linked to the PK of PLD. We identified a candidate locus containing *Gulp1* associated with the plasma CL of PLD using a panel of inbred mouse strain, indicating that the genetic variations may play a role in the variability in the PLD PK. Based on the implications and limitations of these studies, further studies are recommended as follows:

[**1**] Because the power of GWAS to detect the QTL is primarily dependent on the number of mouse strains sharing the phenotype, adding more strains may increase the genetic diversity and the power to detect the QTL with genome wide significance (47, 48). Thus, it would be critical to validate the study finding in an independent set of inbred mouse strains with appropriate power.

[**2**] In addition, some of the smaller peaks on other chromosomes identified by GWAS analyses may prove to be important and biologically related to the phenotype (i.e., obesity). Thus, QTL analyses of crosses between mouse strains with high and low CL of PLD may provide additional information on importance of multiple genes and gene-gene interaction in the PLD PK (44).

[**3**] Finally, functional characterizations of *Gulp1* (i.e., knockout mice) are required to validate the relationship between *Gulp1* and the PLD PK observed in our pioneering works (51). However, *Gulp1* knockout mice are not currently available, but need to be developed to address these issues.

5. 2. Perspective

This dissertation research has the potential to make an impact on development of future NP-based anticancer therapeutics as well as on clinical use of PLD (Doxil®) and other PEGylated liposomal agents. Dynamic bi-direnctional interaction between PLD and the mononuclear phagocyte system (MPS) and chemokines and subsequent effects on the PK and PD of PLD in recurrent ovarian cancer and breast cancer are major findings in this dissertation research. The feedback loop associated with chemokines, such as CCL2 and CCL5, can be a target for optimizing NP-based therapy and provide guidance on careful selection of appropriate tumor models (xenografts versus GEMM) and human cancer types (i.e., ovarian cancer versus prostate cancer) at various preclinical and clinical stages for development of NP-based therapeutics. This research can also make an impact on clinical use of PLD. Given the heterogeneity of tumor cells and tumor microenvironment within breast cancer, optimal selection of patients with a breast tumor subtype responsive to PLD (i.e., claudin-low subtype) could maximize patients' benefits from PLD or other PEGylated liposomal drugs. Inbred mouse strain-dependent CL of PLD also highlights the challenges in translating the basic research on NP-based medicines to the clinic. The interaction of NPs with the immune system, in particular the MPS, can make a profound effect on the circulating time, tumor accumulation, and therapeutic outcomes of NP-based anticancer drugs. There is limited understanding of which preclinical models can recapitulate tumors in patients which represent a complex interaction between the immune system and a particular NP-based drug. Therefore, further research is required to improve our understanding of NP behavior in humans and determine optimal tumor models for translating to patients.

Based on recent scientific advances in nanotechnology, NP-based drug delivery is expected to have a continued substantial impact on tumor targeting therapy. Despite the promise, this technology has not made a significant clinical impact on cancer therapy. Collaborative efforts from experts in immunology, oncology, biotechnology, pharmacology, and medicine will enhance our knowledge of NP behavior in humans, optimize the use of NP-based therapeutics, and maximize patients' benefit.

REFERENCES

(1) Davis ME. Nanoparticle therapeutics: an emerging treatment modality for cancer. Nature Reviews Drug Discovery 2008;7(9):771-782.

(2) Peer D, Karp JM, Hong S, Farokhzad OC, Margalit R, Langer R. Nanocarriers as an emerging platform for cancer therapy. Nature nanotechnology 2007;2(12):751-760.

(3) Petros RA, DeSimone JM. Strategies in the design of nanoparticles for therapeutic applications. Nature Reviews Drug Discovery 2010;9(8):615-627.

(4) Farokhzad OC, Langer R. Impact of nanotechnology on drug delivery. ACS nano 2009;3(1):16-20.

(5) Li S, Huang L. Pharmacokinetics and biodistribution of nanoparticles. Molecular pharmaceutics 2008;5(4):496-504.

(6) Caron W, Song G, Kumar P, Rawal S, Zamboni W. Interpatient Pharmacokinetic and Pharmacodynamic Variability of Carrier-Mediated Anticancer Agents. Clinical Pharmacology & Therapeutics 2012;91(5):802-812.

(7) Schell RF, Sidone BJ, Caron WP, Walsh MD, Zamboni BA, Ramanathan RK, et al. Meta-analysis of inter-patient pharmacokinetic variability of liposomal and non-liposomal anticancer agents. Nanomedicine: Nanotechnology, Biology and Medicine 2013.

(8) Drummond DC, Noble CO, Hayes ME, Park JW, Kirpotin DB. Pharmacokinetics and in vivo drug release rates in liposomal nanocarrier development. J Pharm Sci 2008;97(11):4696-4740.

(9) Song G, Wu H, Yoshino K, Zamboni WC. Factors affecting the pharmacokinetics and pharmacodynamics of liposomal drugs. J Liposome Res 2012;22(3):177-192.

(10) Maeda H, Wu J, Sawa T, Matsumura Y, Hori K. Tumor vascular permeability and the EPR effect in macromolecular therapeutics: a review. J Controlled Release 2000;65(1):271-284.

(11) Gabizon A, Shmeeda H, Barenholz Y. Pharmacokinetics of pegylated liposomal doxorubicin. Clin Pharmacokinet 2003;42(5):419-436.

(12) Moghimi SM, Hunter AC, Murray JC. Long-circulating and target-specific nanoparticles: theory to practice. Pharmacol Rev 2001;53(2):283-318.

(13) Bertrand N, Leroux J. The journey of a drug-carrier in the body: an anatomo-physiological perspective. J Controlled Release 2012;161(2):152-163.

(14) Joyce JA. Therapeutic targeting of the tumor microenvironment. Cancer cell 2005;7(6):513.

(15) Lewis CE, Pollard JW. Distinct role of macrophages in different tumor microenvironments. Cancer Res 2006;66(2):605-612.

(16) Balkwill F. Cancer and the chemokine network. Nature Reviews Cancer 2004;4(7):540-550.

(17) Roussos ET, Condeelis JS, Patsialou A. Chemotaxis in cancer. Nature Reviews Cancer 2011;11(8):573-587.

(18) Deshmane SL, Kremlev S, Amini S, Sawaya BE. Monocyte chemoattractant protein-1 (MCP-1): an overview. Journal of Interferon & Cytokine Research 2009;29(6):313-326.

(19) Milliken D, Scotton C, Raju S, Balkwill F, Wilson J. Analysis of chemokines and chemokine receptor expression in ovarian cancer ascites. Clinical cancer research 2002;8(4):1108-1114.

(20) Soria G, Ben-Baruch A. The inflammatory chemokines CCL2 and CCL5 in breast cancer. Cancer Lett 2008;267(2):271-285.

(21) Sahin H, Trautwein C, Wasmuth HE. Functional role of chemokines in liver disease models. Nature Reviews Gastroenterology and Hepatology 2010;7(12):682-690.

(22) Marra F, Romanelli RG, Giannini C, Failli P, Pastacaldi S, Arrighi MC, et al. Monocyte chemotactic protein-1 as a chemoattractant for human hepatic stellate cells. Hepatology 1999;29(1):140-148.

(23) Nielsen H, Rørth M, Bennedsen J. Monocyte chemotaxis in patients with nonseminomatous testicular carcinoma. Cancer Immunology, Immunotherapy 1985;19(1):68-71.

(24) Lyass O, Hubert A, Gabizon AA. Phase I study of doxil-cisplatin combination chemotherapy in patients with advanced malignancies. Clin Cancer Res 2001 Oct;7(10):3040-3046.

(25) Gabizon A, Isacson R, Rosengarten O, Tzemach D, Shmeeda H, Sapir R. An open-label study to evaluate dose and cycle dependence of the pharmacokinetics of pegylated liposomal doxorubicin. Cancer Chemother Pharmacol 2008;61(4):695-702.

(26) Gabizon A, Tzemach D, Mak L, Bronstein M, Horowitz AT. Dose dependency of pharmacokinetics and therapeutic efficacy of pegylated liposomal doxorubicin (DOXIL) in murine models. J Drug Target 2002;10(7):539-548.

(27) Rezaie-Majd A, Maca T, Bucek RA, Valent P, Müller MR, Husslein P, et al. Simvastatin reduces expression of cytokines interleukin-6, interleukin-8, and monocyte chemoattractant protein-1 in circulating monocytes from hypercholesterolemic patients. Arterioscler Thromb Vasc Biol 2002;22(7):1194-1199.

(28) Han KH, Ryu J, Hong KH, Ko J, Pak YK, Kim J, et al. HMG-CoA reductase inhibition reduces monocyte CC chemokine receptor 2 expression and monocyte chemoattractant protein-1–mediated monocyte recruitment in vivo. Circulation 2005;111(11):1439-1447.

(29) Jain RK, Stylianopoulos T. Delivering nanomedicine to solid tumors. Nature Reviews Clinical Oncology 2010;7(11):653-664.

(30) Ben-Baruch A. Host microenvironment in breast cancer development: Inflammatory cells, cytokines and chemokines in breast cancer progression-reciprocal tumor–microenvironment interactions. Breast cancer research. 2002;5(1):31.

(31) Fukumura D, Jain RK. Tumor microenvironment abnormalities: causes, consequences, and strategies to normalize. J Cell Biochem 2007;101(4):937-949.

(32) Fidler IJ. Tumor heterogeneity and the biology of cancer invasion and metastasis. Cancer Res. 1978;38(9):2651-60.

(33) Usary J, Zhao W, Darr D, Roberts PJ, Liu M, Balletta L, et al. Predicting drug responsiveness in human cancers using genetically engineered mice. Clin Cancer Res 2013 Sep 1;19(17):4889-4899.

(34) Maroulakou IG, Anver M, Garrett L, Green JE. Prostate and mammary adenocarcinoma in transgenic mice carrying a rat C3 (1) simian virus 40 large tumor antigen fusion gene. Proceedings of the National Academy of Sciences 1994;91(23):11236-11240.

(35) Herschkowitz JI, Zhao W, Zhang M, Usary J, Murrow G, Edwards D, et al. Comparative oncogenomics identifies breast tumors enriched in functional tumor-initiating cells. Proceedings of the National Academy of Sciences 2012;109(8):2778-2783.

(36) O'brien M, Wigler N, Inbar M, Rosso R, Grischke E, Santoro A, et al. Reduced cardiotoxicity and comparable efficacy in a phase III trial of pegylated liposomal doxorubicin HCl (CAELYX™/Doxil®) versus conventional doxorubicin for first-line treatment of metastatic breast cancer. Annals of oncology 2004;15(3):440-449.

(37) Workman P, Aboagye E, Balkwill F, Balmain A, Bruder G, Chaplin D, et al. Guidelines for the welfare and use of animals in cancer research. Br J Cancer 2010;102(11):1555-1577.

(38) Banciu M, Schiffelers RM, Storm G. Investigation into the role of tumor-associated macrophages in the antitumor activity of Doxil. Pharm Res 2008;25(8):1948-1955.

(39) Chauhan VP, Stylianopoulos T, Martin JD, Popović Z, Chen O, Kamoun WS, et al. Normalization of tumour blood vessels improves the delivery of nanomedicines in a size-dependent manner. Nature nanotechnology 2012;7(6):383-388.

(40) Zamboni WC. Concept and clinical evaluation of carrier-mediated anticancer agents. Oncologist 2008;13(3):248-260.

(41) La-Beck NM, Zamboni BA, Gabizon A, Schmeeda H, Amantea M, Gehrig PA, et al. Factors affecting the pharmacokinetics of pegylated liposomal doxorubicin in patients. Cancer Chemother Pharmacol 2012;69(1):43-50.

(42) Song G, Wu H, La-Beck NM, Zamboni BA, Strychor S, Zamboni WC. Effect of gender on pharmacokinetic disposition of Pegylated liposomal CKD-602 (S-CKD602) and optisomal topotecan (TLI) in rats. AACR; 2010.

(43) Caron WP, Lay JC, Fong AM, La-Beck NM, Kumar P, Newman SE, et al. Translational Studies of Phenotypic Probes for the Mononuclear Phagocyte System and Liposomal Pharmacology. J Pharmacol Exp Ther 2013:jpet. 113.208801.

(44) Flint J, Eskin E. Genome-wide association studies in mice. Nature Reviews Genetics 2012;13(11):807-817.

(45) Hillebrandt S, Wasmuth HE, Weiskirchen R, Hellerbrand C, Keppeler H, Werth A, et al. Complement factor 5 is a quantitative trait gene that modifies liver fibrogenesis in mice and humans. Nat Genet 2005;37(8):835-843.

(46) Harrill AH, Watkins PB, Su S, Ross PK, Harbourt DE, Stylianou IM, et al. Mouse population-guided resequencing reveals that variants in CD44 contribute to acetaminophen-induced liver injury in humans. Genome Res 2009 Sep;19(9):1507-1515.

(47) McClurg P, Janes J, Wu C, Delano DL, Walker JR, Batalov S, et al. Genomewide association analysis in diverse inbred mice: power and population structure. Genetics 2007 May;176(1):675-683.

(48) Kang HM, Zaitlen NA, Wade CM, Kirby A, Heckerman D, Daly MJ, et al. Efficient control of population structure in model organism association mapping. Genetics 2008 Mar;178(3):1709-1723.

(49) Smits E, Criekinge WV, Plaetinck G, Bogaert T. The human homologue of< i> Caenorhabditis elegans</i> CED-6 specifically promotes phagocytosis of apoptotic cells. Current biology 1999;9(22):1351-1354.

(50) Su HP, Brugnera E, Van Criekinge W, Smits E, Hengartner M, Bogaert T, et al. Identification and characterization of a dimerization domain in CED-6, an adapter protein involved in engulfment of apoptotic cells. J Biol Chem 2000 Mar 31;275(13):9542-9549.

(51) Lammers T, Rizzo LY, Storm G, Kiessling F. Personalized nanomedicine. Clin Cancer Res 2012 Sep 15;18(18):4889-4894.

APPENDIX A: EFFECT OF GENDER ON PHARMACOKINETIC DISPOSITION OF PEGYLATED LIPOSOMAL CKD-602 (S-CKD602) AND OPTISOMAL TOPOTECAN (TLI) IN RATS[5]

INTRODUCTION

S-CKD602 is a PEGylated liposomal formulation of CKD-602, a camptothecin analogue (1). Optisomal Topotecan (TLI) is a sphingomyelin-stabilized liposomal formulation of topotecan (2). The cytotoxicity of CKD-602, topotecan, and other camptothecin analogues is related to the duration of exposure. PEGylated and sphingomyelin liposomal formulations have been designed to prolong drug circulation time, increase tumor delivery, and improve the therapeutic index (3). The pharmacokinetics (PK) of liposomal agents is highly variable in patients (4). Moreover, the factors associated with this variability are unknown. Thus, we evaluated the plasma PK disposition of TLI and S-CKD602 in male and female rats.

METHODS

PK studies in plasma. TLI was administered at 0.93mg/kg IV x1 and S-CKD602 at 0.6 mg/kg IV x1 to male and female Sprague-Dawley rats via a bilateral jugular vein cannula. Plasma samples for TLI were obtained in 6 cohorts (n= 3 rats per cohort, total = 18 rats per gender): 1) pre, 1, and 3 min; 2) 5, 10, and 20 min; 3) 0.5, 1, and 2 hr; 4) 4, 8, and 12 hr; 5) 24, 36, and 48 hr; 6) 60 and 72 h post dose. Plasma samples (n= 3 rats per time point per gender) for S-CKD602 were obtained prior to the end of the infusion, and at 4, 8, 24, 48, and 72 hr after

[5] Parts of this appendix 1 previously appeared in the *Proceeding of 2010 AACR Annual Meeting*. The original citation is as follows: Song G, Wu H, La-Beck NM, Zamboni BA, Strychor S, Zamboni WC. Effect of gender on pharmacokinetic disposition of Pegylated liposomal CKD-602 (S-CKD602) and optisomal topotecan (TLI) in rats. : AACR; 2010.

administration. Total (lactone and hydroxyl acid) form of sum total (encapsulated and released) CKD-602 and topotecan were measured via LC/MS.

Pharmacokinetic analysis. The pharmacokinetics of TLI and S-CKD602 were evaluated by non-compartmental methods using WinNonlin® (v5.2.1, Pharsight Corp., Mountain View, CA). The maximum concentration (Cmax) and time to reach Cmax (tmax) were obtained directly from the concentration-time profile. The terminal elimination rate constant (λz) was estimated by log-linear regression of at least three data points in the terminal phase. The terminal half-life (t½) was calculated as 0.693/λz. The AUC from time 0 to infinity (AUC_{inf}) was determined by adding AUC_{last} and Clast/λz.. Below limit of quantification (BLQ) concentrations were excluded from the data analysis.

Statistical analysis. Statistical analyses were carried out using SAS v.9.2 (Cary, NC). Two-way analysis of variance (ANOVA) was performed to test the effects of gender on the clearance of TLI and S-CKD602. *P* value of less than 0.05 was considered statistically significant. All statistical tests were two-sided.

RESULTS

Plasma concentration versus time profiles of sum total after administration of S-CKD602 at 0.6 mg/kg or TLI at 0.93 mg/kg IV x 1 are presented in **Fig. A. 1**. Clearances (CLs) of TLI were 0.026 ± 0.0038 and 0.021 ± 0.0015 L/h/kg in male and female rats, respectively. The CLs of S-CKD602 were 0.0037 ± 0.0004 and 0.0027 ± 0.0001 L/h/kg in male and female rats, respectively. The CL was 1.2-fold (p=0.14) and 1.4-fold (p=0.009) lower in female rats compared with male rats for TLI and S-CKD602, respectively. PK parameters of S-CKD602 and TLI in male and female rats were summarized in **Table A. 1**.

CONCLUSION

The CL of TLI and S-CKD602 was lower in female rats as compared with male rats. These studies suggest that gender may affect the disposition of liposomal formulations of drugs and may play a role in the high PK variability reported in patients treated with liposomal formulations of anticancer agents. Further studies evaluating the physiological difference between male and female which may affect the liposomal disposition are warranted.

Table A.1. PK parameters after administration of TLI at 0.93 mg/kg or S-CKD602 at 0.6 mg/kg IV x1 to male and female Sprague-Dawley rats via a bilateral jugular vein cannula

	Cmax (µg/mL)	$T_{1/2}$ (h)	AUC_{inf}/Dose (µg·h/mL/mg/kg)	CL (mL/h/kg)	Vd_{ss} (mL/kg)
TLI (Male)	16.81 ± 2.45	1.25 ± 0.14	39.88 ± 4.93	26 ± 3.8	67 ± 1.1
TLI (Female)	13.09 ± 2.36	1.20 ±0.09	48.68 ± 6.69	21 ± 1.5	63 ± 8
S-CKD602 (Male)	15.07 ± 2.97	15.10 ± 1.18	271.39 ± 27.01	3.7 ± 0.4	68 ± 7
S-CKD602 (Female)	12.67 ± 0.60	15.32 ± 2.11	371.21 ± 7.67	2.7 ± 0.1	56 ± 5

Cmax; maximum concentration; t½, terminal half-life; AUCinf/Dose, area the curve from time zero to infinity normalized by dose; CL: clearance; Vd_{ss}: volume of distribution at steady-state

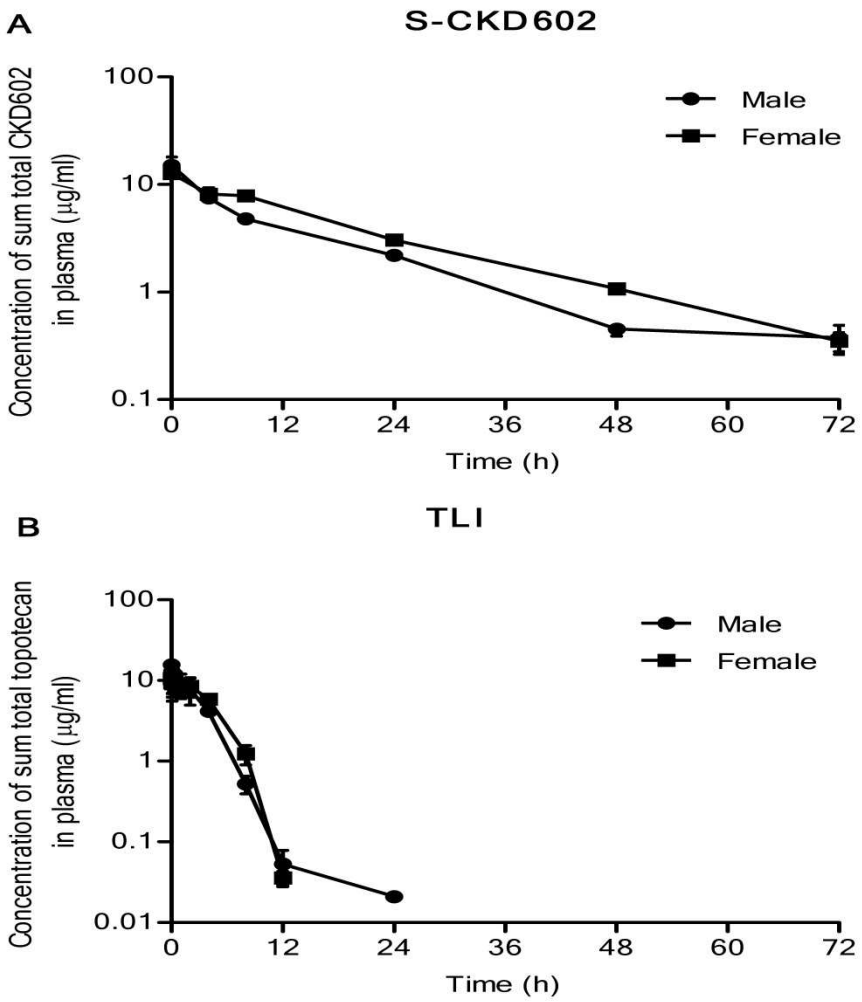

Fig. A. 1. Plasma concentration versus time profiles of (A) sum total CKD602 after administration of S-CKD602 at 0.6 mg/kg and (B) sum total topotecan after administration of TLI at 0.93 mg/kg I.V. x 1 via a bilateral jugular vein. Plasma samples for TLI were obtained in 6 cohorts (n= 3 rats per cohort, total = 18 rats per gender). Plasma samples for S-CKD602 were obtained in n= 3 rats per time point per gender. Each time point is represented as the mean ± standard deviation (SD). Concentrations of sum total topotecan at 36, 48, 60, and 72 hr after TLI administration were BLQ. BLQ: below limit of quantitateon.

REFERENCES

(1) Zamboni WC, Strychor S, Joseph E, Walsh DR, Zamboni BA, Parise RA, et al. Plasma, tumor, and tissue disposition of STEALTH liposomal CKD-602 (S-CKD602) and nonliposomal CKD-602 in mice bearing A375 human melanoma xenografts. Clinical Cancer Research 2007;13(23):7217-7223.

(2) Pharmacokinetic study of optisomal topotecan (topotecan liposomal injection, TLI, OPTISOME) and non-liposomal topotecan in male sprague-dawley rats. Proceedings of AACR-NCI-EORTC; 2007.

(3) Peer D, Karp JM, Hong S, Farokhzad OC, Margalit R, Langer R. Nanocarriers as an emerging platform for cancer therapy. Nature nanotechnology 2007;2(12):751-760.

(4) Zamboni WC. Concept and clinical evaluation of carrier-mediated anticancer agents. Oncologist 2008;13(3):248-260.

APPENDIX B: COMPARTMENTAL PHARMACOKINETIC MODEL FOR NON-LIPOSOMAL CKD-602 AND PEGYLATED LIPOSOMAL CKD-602 (S-CKD602) IN MICE BEARING A375 HUMAN MELANOMA XENOGRAFTS

Overview

Purpose: To develop a pharmacokinetic (PK) model for non-liposomal CKD-602 and pegylated liposomal CKD-602 (S-CKD602) in mice bearing A375 human melanoma xenografts that can be used in prediction of biodistribution of pegylated liposomal anticancer agents in mice.

Methods: Non-liposomal CKD-602 PK data after single I.V. administration of CKD-602 at 30 mg/kg and encapsulated, released, and sum total (encapsulated and released) CKD-602 pharmacokinetic data following single I.V. administration of S-CKD602 at 1 mg/kg to mice bearing A375 human melanoma xenografts were used from the previous PK study. Initial PK analysis of CKD-602 and S-CKD602 was performed by non-compartmental analysis using WinNonlin® 5.2.1. Plasma and tumor data from the previous PK study was simultaneously fit using stepwise strategy. Various compartmental models with linear or nonlinear elimination were evaluated for encapsulated CKD-602 after S-CKD602 administration. The PK parameters associated with released CKD-602 were determined from the PK model of CKD-602 after administration of non-liposomal CKD-602 and fixed in the final PK model for S-CKD602. Sensitivity analysis was performed for various PK parameters to determine the effect of each parameter on the S-CKD602 model solution.

Results: The PK of non-liposomal CKD-602 in plasma and tumor after administration of CKD-602 was better described by a three-compartment model with linear clearance compared with other compartmental models. The PK of encapsulated CKD-602 in plasma after administration of S-CKD602 was better described by one-compartmental model with linear clearance compared with other models. However, the prediction of released CKD-602

concentration in tumor from the final PK model for S-CKD602 was not accurate. The final PK model for S-CKD-602 was shown to be most sensitive to $CL_{encapsulated}$ and $CL_{released}$ for encapsulated CKD-602 AUC in plasma and released CKD-602 AUC in tumor, respectively.

Conclusion: Compartmental modeling approach can be used to describe the pharmacokinetics of encapsulated drugs, but caution should be used to predict released drugs in tissues after administration of liposomal formulations drugs. Development of more sophisticated PK models is warranted to accurately predict the disposition of both encapsulate and released drugs in plasma, tissues, and tumor after administration of pegylated liposomal formulation of anticancer agents.

Key words: CKD-602, S-CKD602, modeling, pharmacokinetics, tumor

INTRODUCTION

S-CKD602 is a pegylated liposomal formulation (STEALTH®) of CKD-602, a camptothecin analog that inhibits topoisomerase I (1). Non-liposomal CKD-602 administered i.v. at 0.5mg/m2/day for 5 consecutive days repeated 21 days is approved in Korea for the treatment of newly diagnosed SCLC and for relapsed ovarian cancer (1). The pegylated liposome formulation is characterized by better PK profiles including prolonged plasma exposure and superior tumor delivery of encapsulated active drug compared with conventional liposome. The disposition of encapsulated drug is governed by characteristics of the liposome and it results in the alteration of pharmacokinetic profile and biodistribution of the drug (2). Once the drug is released from the liposome, the pharmacokinetics of the drug will be the same as after administration of the nonliposomal dug (2). In animal models, a 3- to 10-fold increase in therapeutic index was observed with S-CKD602 compared with nonliposomal CKD-602 (3). The cytotoxicity of camptothecin analaogues has been reported to be related to the duration of time the concentration is above a critical threshold (3).

Zamboni et al. evaluated the plasma, tissues, and tumor disposition of S-CKD602 and non-liposomal CKD-602 in female SCID mice bearing A375 human melanoma xenografts (4). The encapsulated and released CKD-602 in plasma after administration of S-CKD602 was measured with the new sample processing methods. The determination of the tumor ECF disposition of released CKD-602 was also evaluated by microdialysis methods (4). The results suggested that S-CKD602 provides pharmacokinetic advantages in plasma and tumors when compared with the non-liposomal formulation of CKD-602 at 1/30th the dose. The sum total (encapsulated and released) CKD-602 plasma exposure following S-CKD602 administration was found to be 25-fold greater than CKD-602 plasma exposure after non-liposomal CKD-602

administration (4). After administration of S-CKD602, 82% of CKD-602 was found to remain encapsulated in plasma over 72 hour. The overall tumor delivery, as measured by the exposure of sum total CKD-602 was similar after administration of non-liposomal CKD-602 and S-CKD602. However, the duration of exposure was 3-fold longer for S-CKD602 compared with non-liposomal CKD-602 (4).

The purpose of this study is to develop a compartmental pharmacokinetic model for non-liposomal CKD-602 following CKD-602 administration and encapsulated and released CKD-602 after administration of S-CKD602 in order to evaluate the disposition of pegylated liposomal formulation of anticancer agents in plasma and tumor.

METHODS

Pharmacokinetic data following I.V. administration of 30 mg of non-liposomal CKD-602 and 10 mg of S-CKD602 into mice bearing A375 human melanoma xenografts were obtained from Zamboni et al (4).

Noncompartmental analysis. Initial pharmacokinetic analysis of non-liposomal CKD-602 and encapsulated and released CKD-602 was performed by non-compartmental analysis (NCA) using WinNonlin® 5.2.1. Initial PK parameters were obtained from NCA.

Compartmental analysis. CKD-602 data in plasma and tumor after administration of non-liposomal CKD-602 was fit using model A-D (4) with stepwise nonlinear least-square regression approach. To predict the concentration in tumor ECF, sub-compartment in tumor was evaluated with plasma and tumor ECF data fitting to the final model E (**Fig. B. 1**).

Sum total (encapsulated and released) CKD-602 data in plasma and tumor following S-CKD602 administration was fit using model F-I (**Fig. B.2**). To predict the concentration in tumor ECF,

sub-compartment in tumor was evaluated with sum total CKD-602 plasma and tumor ECF CKD-602 data fitting to the final model J after administration of S-CKD602 (**Fig. B. 2)**.

Encapsulated CKD-602 in plasma after administration of S-CKD602 was fit using model K-L (**Fig. B. 3**). Then, based on the best models for non-liposomal CKD-602, both encapsulated CKD-602 in plasma and released CKD-602 in tumor were simultaneously fit using model M and fixing parameters associated with released CKD-602.

All computer model fittings were conducted using WinNonlin 5.2.1. (Pharsight®) with Gauss-Newton (Levenberg and Hartley) method selected for minimization algorithm. The initial estimates for compartmental modeling were derived from those obtained from the noncompartmental analysis. Criteria for goodness-of-fit of modeling included visual inspections, model convergence, parameter variances (%CV), correlation between parameters, and Akaike's information criterion (AIC).

Sensitivity analysis. To determine the effect of the various parameters on model solution, sensitivity analysis was performed for parameters based on the final PK model of S-CKD602. The value of each parameter was 50% decreased and 100% increased, and the model simulations were repeated using WinNonlin® 5.2.1. The new AUC of encapsulated CKD-602 in plasma and the new AUC of released CKD-602 in tumor were evaluated from noncompartmental analyses of each simulation. The relative sensitivity coefficients for significant parameters were calculated using the following equation and plotted.

$$\text{Relative sensitivity coefficient} = \frac{dAUC/dP}{AUC/P}$$

i.e., the percentage change in the AUC divided by the percentage change in the parameter value (P).

RESULTS

Non-compartmental pharmacokinetic analysis. Concentrations of CKD-602 in plasma, tumor and tumor ECF as a function of time following I.V. administration of non-liposomal CKD-602 and S-CKD602 were obtained from a previous study (4). Descriptive pharmacokinetic parameters for non-liposomal CKD-602 and for S-CKD602 are presented in **Table B. 1**. After administration of non-liposomal CKD-602, the plasma concentration-time profile of CKD-602 peaked at 0.083 (h) after administration, had a multi-phasic decline, and no longer detectable after 16 h. After administration of S-CKD602, the plasma concentration-time profile of CKD-602 peaked at 0.083 (h) after administration and had a single-phase elimination profile and was detectable at 72 h after administration. The concentration of CKD-602 in tumor ECF after non-liposomal CKD-602 administration was consistent with the profile of sum total CKD-602 in tumor homogenates. The concentration of CKD-602 in tumor ECF after administration of S-CKD602 was consistent with the profile of sum total CKD-602 in tumor homogenates.

Compartmental modeling approach. Pharmacokinetic models A-D (**Fig. B. 1**) were used to fit CKD-602 plasma concentration-versus time data obtained from the previous PK study in mice. Linear elimination was assumed in all these models. Three compartment models with linear elimination (Model C and D) fit the data better than one- or two-compartment models of CKD-602. With the exception of clearance from the central compartment, all parameters associated with CKD-602 disposition obtained during the fitting of the CKD-602 concentration-time data were held constant. A three-compartment model for CKD-602 provided a good description of concentration-time profile in plasma and tumor (**Fig. B. 4A** and **B**). For anticancer agents encapsulated in liposome to exert their anti-tumor activity in the system, the active form of the anticancer agent must be released from the liposome into tumor ECF and then penetrate

into the cell (2). However, when incorporating the sub-compartment in the tumor to describe tumor ECF concentration into three-compartment model of CKD-602 (Model E), prediction was not accurate (**Fig. B. 4E** and **F**).

The same approach was used to fit sum total CKD-602 plasma concentration-versus time data after administration of S-CKD602 using Model F-I (**Fig. B. 2**). Linear elimination was assumed in all these models due to predictive results of Model J. Two compartment models with linear elimination using Model G and H (**Fig. B. 2**) fit the data better than one- or three-compartment models of sum total CKD-602. With the exception of clearance from the central compartment, all parameters associated with sum total CKD-602 disposition obtained during the fitting of the sum total CKD-602 concentration-time data were held constant. A two-compartment model with tissue clearance for sum total CKD-602 provided a good description of concentration-time profile in plasma and tumor after administration of S-CKD602. Incorporating the sub-compartment in the tumor to describe tumor ECF concentration into two-compartment model of CKD-602 (Model I) was not fit to observed tumor ECF concentration (**Fig. B. 4E and F**).

Pharmacokinetic models K-L (**Fig. B. 3**) were used to fit encapsulated CKD-602 in plasma concentration-versus time data after administration of S-CKD602. One compartment model with linear elimination (Model K) fit the data better than Model L with non-linear elimination (**Fig. B. 4C** and **D**). Based on the best model (Model K) for encapsulated CKD-602, both encapsulated CKD-602 plasma concentration-versus time data and sum total tumor CKD-602 concentration-versus time data were simultaneously fit using Model M and fixing parameters associated with released CKD-602. The predicted released CKD-602 concentration in tumor from Model M was not fit to sum total CKD-602 concentration in tumor after S-CKD602

administration (**Fig. B. 4C** and **D**). Comparison of model performance was presented in **Table B. 2** and final PK parameter estimates from the final Model M was presented in **Table B. 3**.

Sensitivity analysis. The results showed that CLencapsulated and CLreelased are most sensitive for encapsulated CKD-602 plasma exposure and CKD-602 tumor exposure in the final PK model for S-CKD602 (**Fig. B. 5A** and **B**).

DISCUSSION

In this study, compartmental pharmacokinetic models were developed and evaluated to describe the distribution of non-liposomal CKD-602 and S-CKD602 in plasma and tumor of mice bearing A375 human melanoma xenografts. The disposition of CKD-602 after administration of non-liposomal CKD-602 in plasma and tumor was better described by a three-compartment model (Model D) with linear clearance, which was consistent with the previous study (1, 3). For anticancer agents encapsulated in liposome to exert their anti-tumor activity in the system, the active form of the anticancer agent must be released from the liposome into tumor ECF and then penetrate into the cell (2). Facilitated liposome extravasations through leaky capillary membrane of tumor microvasculature has been proposed and investigated to elucidate the mechanism of more selective tumor delivery compared with the active drugs and higher interstitial accumulation of liposomal formulations (5, 6). Thus, subcompartment in tumor tissues was incorporated into the model to evaluate any limiting effect of tumor microvasculature permeability on disposition of encapsulated and released active drug. However, when incorporating the subcompartment in the tumor to describe tumor ECF concentration to three-compartment model of CKD-602 (Model E), prediction was not accurate (**Fig. B. 4E** and **F)**,

which indicates diffusion into the capillary membrane is not limiting factor for disposition of CKD-602 in tumor ECF.

For sum total (encapsulated and released) CKD-602, a two compartment model with tissue clearance better described the disposition of the plasma sum total CKD-602. Incorporating the sub-compartment into tumor was able to describe the general characteristics of disposition of CKD-602 in tumor ECF. However, it failed to describe the peak concentration at early time points and careful caution should be used due to high variability in concentration in tumor ECF at individual time point in extrapolating this result.

For encapsulated CKD-602 after administration of S-CKD602, one compartment model with linear clearance better described the disposition of encapsulated CKD-602 in plasma compared with the same model with non-linear elimination. However, in the phase I study which evaluated the dispositions of encapsulated, released, and sum total CKD-602 using compartmental analysis, non-linear pharmacokinetics was demonstrated among patients treated with high dose (7). In the PK study using mice bearing A375 human melanoma xenografts (4), the dose for S-CKD602 was maximum tolerable dose for mice (1 mg/kg), but the sampling time points (t_{last}= 72h) were relatively short compared to those in phase I study (t_{last}= 336h) (7).

When one compartment model for encapsulated CKD-602 was combined with the best model for CKD-602 (Model D) using stepwise approach, the disposition of predicted released CKD-602 following S-CKD602 administration was not fit to the sum total CKD-602 concentration-versus time profile available from the mouse PK study (**Fig. B. 4C** and **D**). This is in part due to the incorrect model assumption (Model M) that encapsulated CKD-602 would be either cleared by the major RES organs such liver and spleen (CLencapsulated) or all degraded to release the active drug, CKD-602 into tissues over the sampling duration (t_{last}= 72h). However,

82% of CKD-602 following S-CKD602 administration was found to remain encapsulated in plasma over 72 hour. Therefore, the difference between predicted released CKD-602 and observed sum total CKD-602 in tumor may be attributable to encapsulated CKD-602 which extravasate tumor microvasculature and accumulate in the interstitial fluid.

The clearance of pegylated liposomes has been suggested by many studies to take place via the mononuclear phagocyte system (MPS). The MPS cells such macrophage and dendritic cells are highly distributed in liver, spleen and bone marrow (8). Based on this hypothesis, the sensitivity analyses was performed to evaluate in which elimination step (CL) has effects on the disposition of active, released CKD-602 in plasma and tumor. The result showed that CLencapsulated and CLreleased are most sensitive parameters for encapsulated CKD-602 exposure in plasma and released CKD-602 exposure in tumor following S-CKD602 administration, respectively. However, given the fact that the compartmental models developed were not validated due to lack of data, caution should be used to extrapolate the results.

Considering complex and unknown mechanism for disposition of liposomal formulations, development of more sophisticated pharmacokinetic models such as PBPK models are warranted to predict the disposition of non-pegylated and pegylated liposomal anticancer agents and improve the therapeutic index.

Table B. 1. Pharmacokinetic parameters from noncompartmental analysis for non-liposomal CKD-602 and S-CKD602 after administration of non-liposomal CKD-602 and S-CKD 602 at a single I.V. dose of 30mg/kg and 10 mg/kg, respectively

Parameters	CKD-602	Sum total CKD-602
Tmax (h)	0.08	0.08
Cmax (ng/mL)	7344.2	18246.75
T ½ (h)	0.8	8.88
AUC inf (ng/mL*h)	9717.85	203502.84
CL (mL/h/kg)	3087.10	4.91
V (mL/kg)	3918.03	62.94

Table B. 2. Comparison of model performance

Models	Major Characteristics	AIC
CKD-602		
Model A	1 compartment, linear	82.00
Model B	2 compartment, linear	107.40
Model C	3 compartment, linear	107.97
Model D	3 compartment, with tissue clearance	250.95
Model E	3 compartment with sub-compartment in tumor	64.10
Sum total CKD-602		
Model F	1 compartment, linear	149.92
Model G	2 compartment, linear	149.44
Model H	2 compartment, with tissue clearance	123.18
Model I	3 compartment	297.65
Model J	2 compartment with sub-compartment in tumor	102.32
Encapsulated and released CKD-602		
Model K	1 compartment, linear	152.81
Model L	1 compartment, non-linear	160.61

Model M	Encapsulated and released CKD-602	125.75

Table B. 3. Final PK parameter estimates and CV% from the final PK Model M for encapsulated and released CKD-602 with linear clearance of encapsulated CKD-602

Parameters	Parameter Estimates	
	Mean	% CV
Vreleased1 (mL/kg)	3677.64	7.81
Vreleased2 (mL/kg)	4128.86	10.66
Vreleased3(mL/kg)	2913	106.31
Vencapsulated (mL/kg)	74.17	4.79
CLencapsulated(mL/h/kg)	6.154	8.4
CLencap-released (mL/h/kg)	2.15	24.67
CL released (mL/h/kg)	3125.4	8.8
CLd (mL/h/kg)	14408.74	22.72
CLd2(mL/h/kg)	514.03	109.82

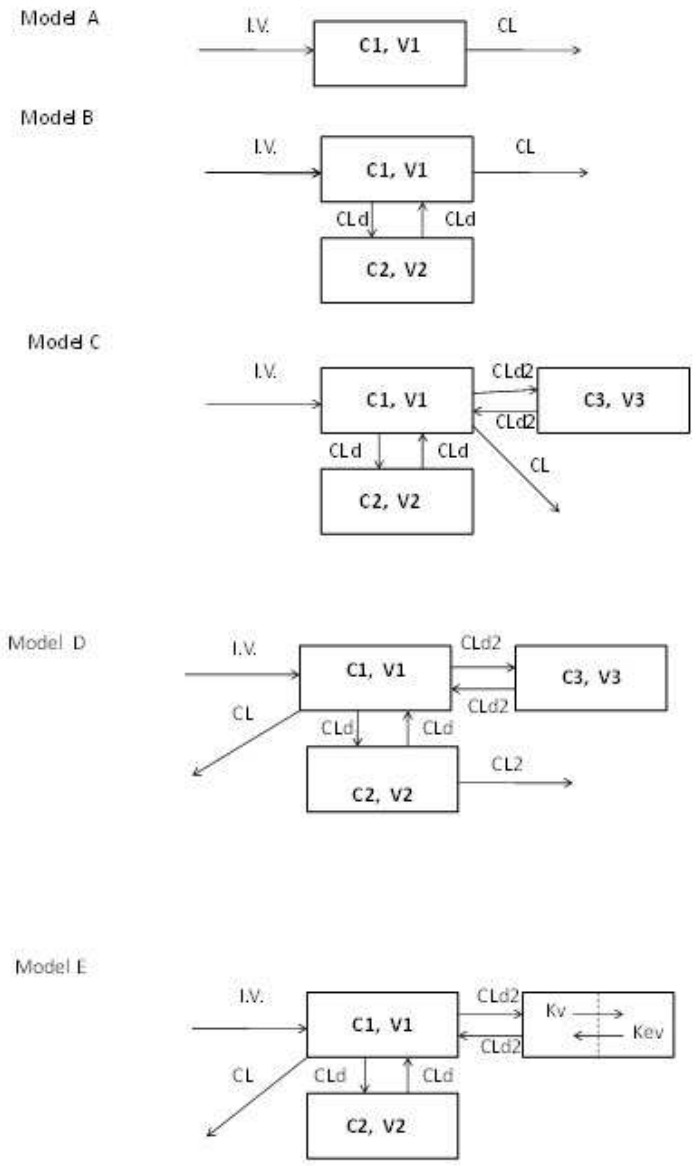

Fig. B. 1. Pharmacokinetic models of non-liposomal CKD-602

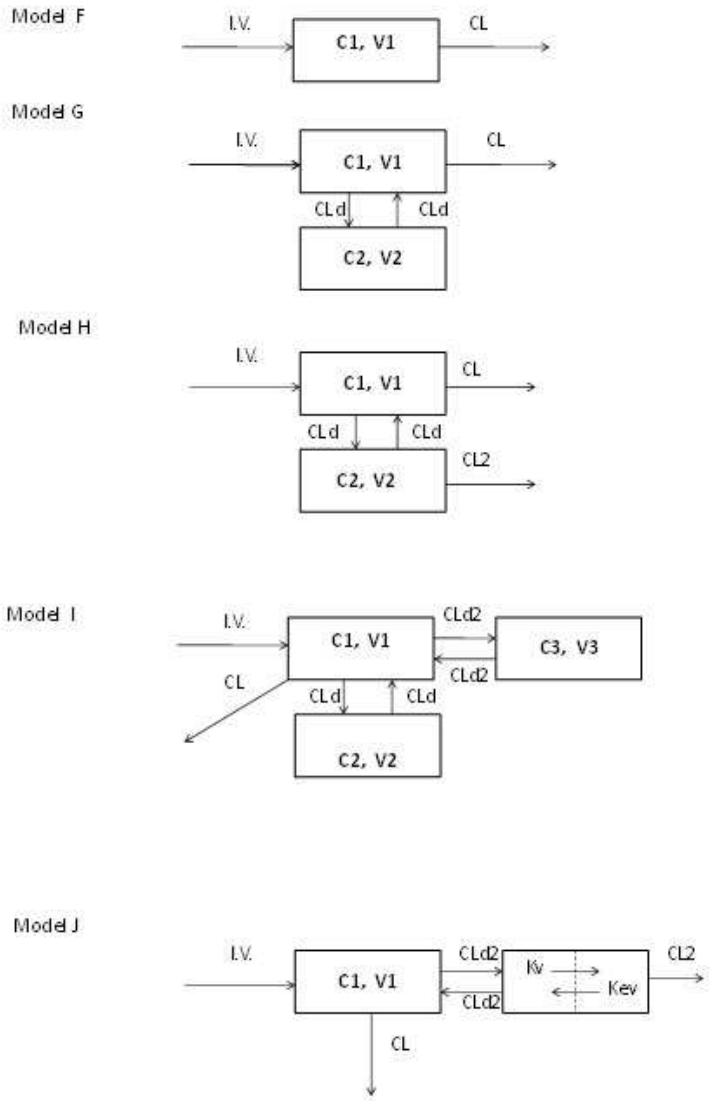

Fig. B. 2. Pharmacokinetic models of sum total CKD-602 after administration of S-CKD602

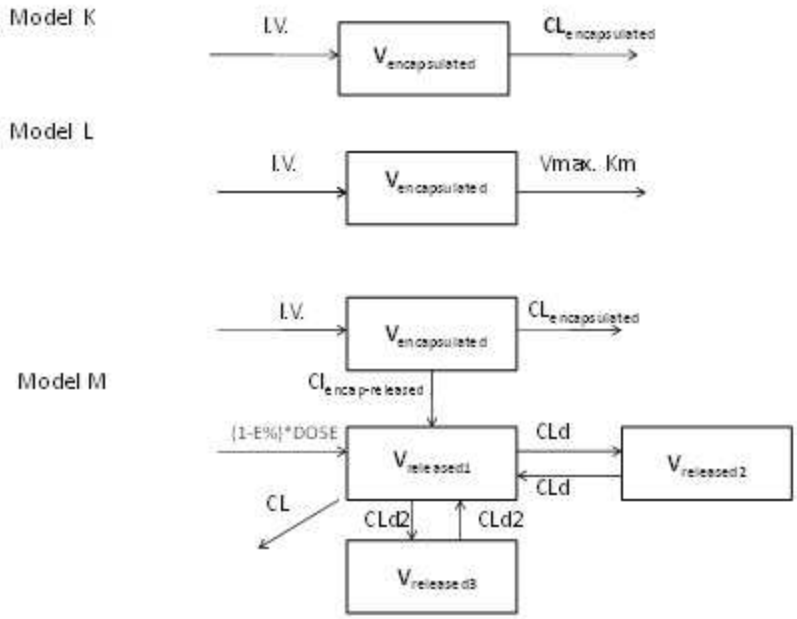

Fig. B. 3. Pharmacokinetic models of encapsulated CKD-602 and released CKD-602 after administration of S-CKD602

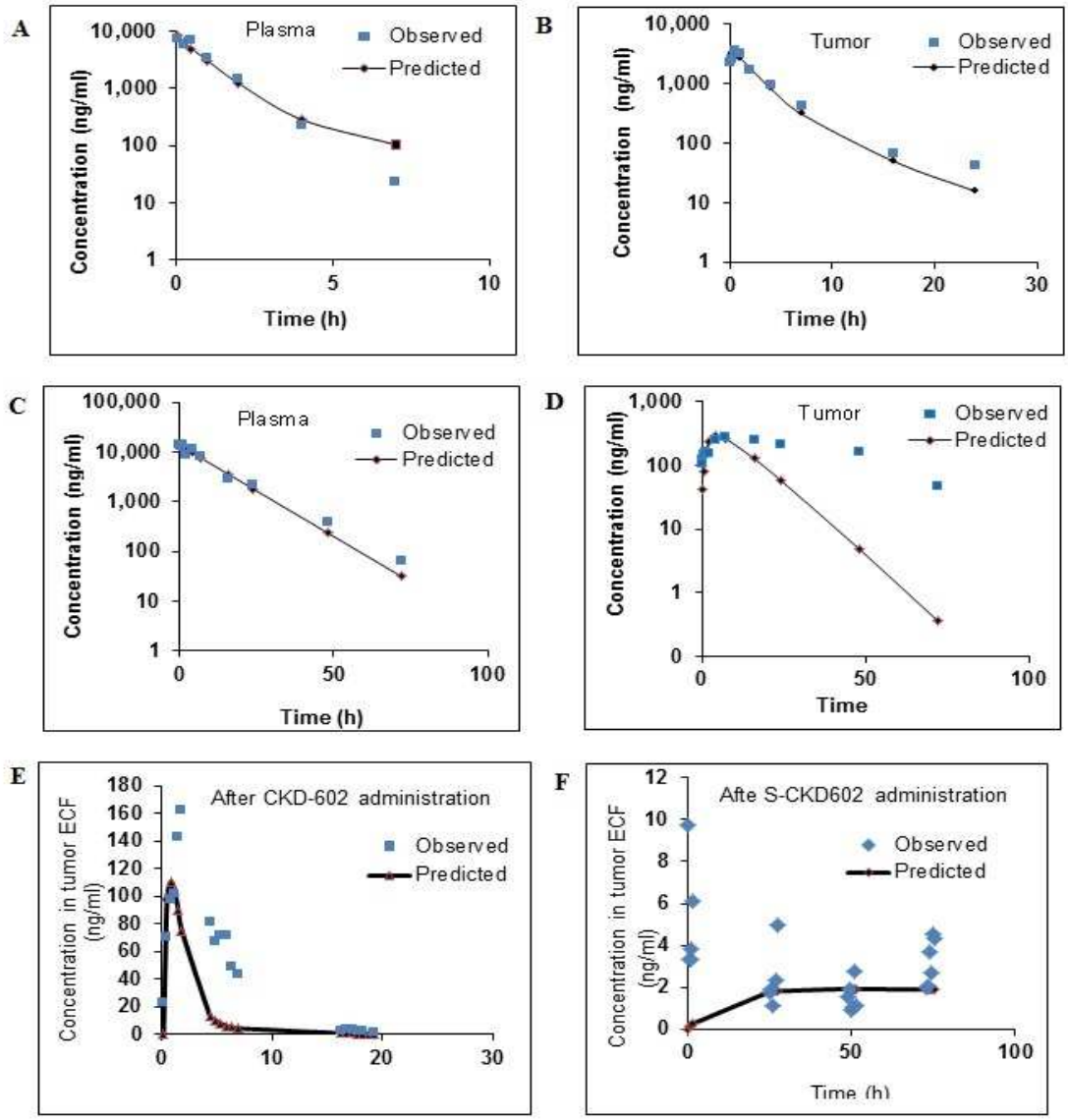

Fig. B. 4. Concentration versus time profile of (A) CKD-602 concentration in plasma and (B) tumor after non-liposomal CKD-602 administration IV x 1, (C) encapsulated CKD-602 concentration in plasma and (D) released CKD-602 in tumor after S-CKD602 administration, IV x1, (E) CKD-602 concentration in tumor ECF after non-liposomal CKD-602 or (F) S-CKD602 administration IV x1.

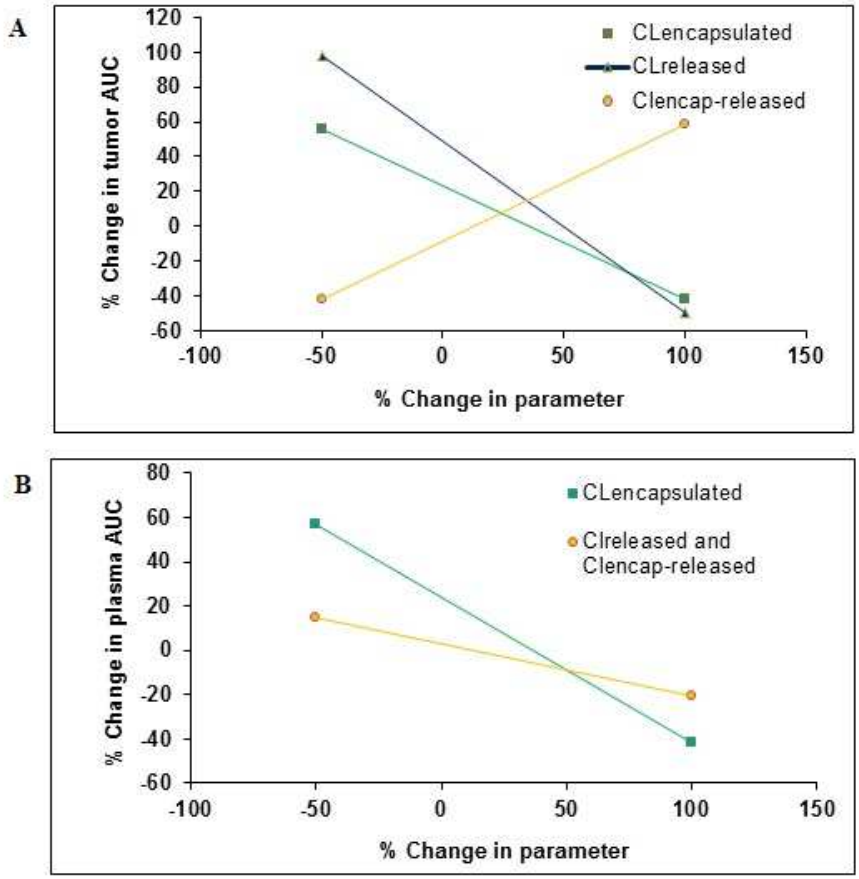

Fig. B. 5. Sensitivity analysis for released CKD-602 exposure in tumor from the final PK model of S-CKD602 and for encapsulated CKD-602 exposure in plasma from the final PK model of S-CKD602

NOTE

The following differential equations, based on the scheme displayed in Figure 5 (Model M), were fit to encapsulated and released CKD-602 concentration-time data after S-CKD602 I.V. administration.

DZ(1) = ((-CLen/V1)*Z(1))-((CLen2/V1)*Z(1))
DZ(2) = (CLen2/V1)*Z(1)-(CLrel/V2)*Z(2)-(CLD/V2)*Z(2)-
(CLD2/V2)*Z(2)+(CLD/V3)*Z(3)+(CLD2/V4)*Z(4)
DZ(3) = (CLD/V2)*Z(2)-(CLD/V3)*Z(3)
DZ(4) = (CLD2/V2)*Z(2)-(CLD2/V4)*Z(4),

Where V1 is the volume of the central compartment for encapsulated CKD-602, V2, V3, and V4 are peripheral compartments for released CKD-602. CLen is eliminating clearance for encapsulated CKD-602. CLen2 is formation clearance for released CKD-602 from encapsulated CKD-602. CLd and CLd2 are the distributional clearances.

REFERENCES

(1) Crul M. CKD-602. Chong Kun Dang. Curr Opin Investig Drugs 2003 Dec;4(12):1455-1459.

(2) Zamboni WC. Liposomal, nanoparticle, and conjugated formulations of anticancer agents. Clinical cancer research 2005;11(23):8230-8234.

(3) Yu NY, Conway CA, Pena RL. Improvement in therapeutic index by STEALTH (R) CKD-602 vs free CKD-602 and topotecan in human tumor xenografts. Proceedings of the American Association for Cancer Research 2005;2005(1):562.

(4) Zamboni WC, Strychor S, Joseph E, Walsh DR, Zamboni BA, Parise RA, et al. Plasma, tumor, and tissue disposition of STEALTH liposomal CKD-602 (S-CKD602) and nonliposomal CKD-602 in mice bearing A375 human melanoma xenografts. Clinical Cancer Research 2007;13(23):7217-7223.

(5) Wu NZ, Da D, Rudoll TL, Needham D, Whorton AR, Dewhirst MW. Increased microvascular permeability contributes to preferential accumulation of Stealth liposomes in tumor tissue. Cancer Res 1993 Aug 15;53(16):3765-3770.

(6) Maeda H, Wu J, Sawa T, Matsumura Y, Hori K. Tumor vascular permeability and the EPR effect in macromolecular therapeutics: a review. J Controlled Release 2000;65(1):271-284.

(7) Relationship between the plasma and tumor disposition of STEALTH liposomal CKD-602 and macrophages/dendritic cells (MDC) in mice bearing human tumor xenografts. Proc Annu Meet Am Assoc Cancer Res; 2006.

(8) Zamboni W, Strychor S, Maruca L, Ramalingam S, Zamboni B, Wu H, et al. Pharmacokinetic study of pegylated liposomal CKD-602 (S-CKD602) in patients with advanced malignancies. Clinical Pharmacology & Therapeutics 2009;86(5):519-526.

APPENDIX C: PHARMACOKINETIC STUDIES OF PEGYLATED LIPOSOMAL DOXORUBICIN (PLD) IN CC CHEMOKINE LIGAN RECEPTOR CCR2 KNOCKOUT (KO) AND CCR5 KO MICE

METHODS

PK studies in CCR2 and CCR5 knockout (KO) mouse models. Female wild-type (WT) C57BL/6 mice, CCR2 $^{-/-}$ mice (CCR2 KO with C57BL/6 background), and CCR5 $^{-/-}$ (CCR5 KO with C57BL/6 background) mice of 8- to 10-weeks of age were purchased from the Jackson Labs (Bar Harbor, ME). PLD was administered to mice at 6 mg/kg IV x1 via a tail vein. Mice (n=3) were euthanized prior to and at 0.083, 1, 24, 48, and 96 hour after administration of PLD.

Sample processing. Blood and tissue samples were processed as described in Chapter 2.

Pharmacokinetic analysis. The pharmacokinetics of encapsulated and released doxorubicin were evaluated by non-compartmental methods using WinNonlin® (v5.2.1, Pharsight Corp., Mountain View, CA). The maximum concentration (Cmax) and time to reach Cmax (tmax) were obtained directly from the concentration-time profile. The terminal elimination rate constant (λz) was estimated by log-linear regression of at least three data points in the terminal phase. The terminal half-life ($t½$) was calculated as $0.693/\lambda z$. The AUC from time 0 to last ($AUC_{0\text{-last}}$) was determined using the trapezoidal rule with linear interpolation.

Statistical analysis. Statistical analyses were carried out using SAS v.9.2 (Cary, NC) and Prism5 software (GraphPad Software, Inc.). Equality of AUC of doxorubicin between mouse models was tested using Nedelman's modification of the Bailer method for sparse samples, using a two-sample test (1). *P* value of less than 0.05 was considered statistically significant. All statistical tests were two-sided.

RESULTS

To verify the roles of CCR2 and CCR5 in the PK of PLD, we performed the PLD PK studies in WT mice, CCR2 KO mice, and CCL5 KO mice. PLD was administered at 6 mg/kg IV x1 via a tail vein. The plasma encapsulated doxorubicin exposure was significantly greater in CCR5 KO mice compared to WT mice, indicating decreased CL of PLD in CCR5 KO mice ($P<0.05$, t-test; **Fig. C. 1A and D**). However, there was no difference in released free doxorubicin exposure (AUC) between WT mice and KO mice (**Fig. C. 1A and D)**. The PLD accumulations in the liver were significantly decreased for both CCR2 KO mice and CCR5 KO compared to WT mice ($P<0.05$) (**Fig. C. 1B and E**). Knockout of *CCR2* and *CCR5*, however, did not influence the accumulation of PLD in the spleen compared to WT mice (**Fig. C. 1C and E**). PK parameters of PLD in these mouse models are summarized in **Table C**. **1**.

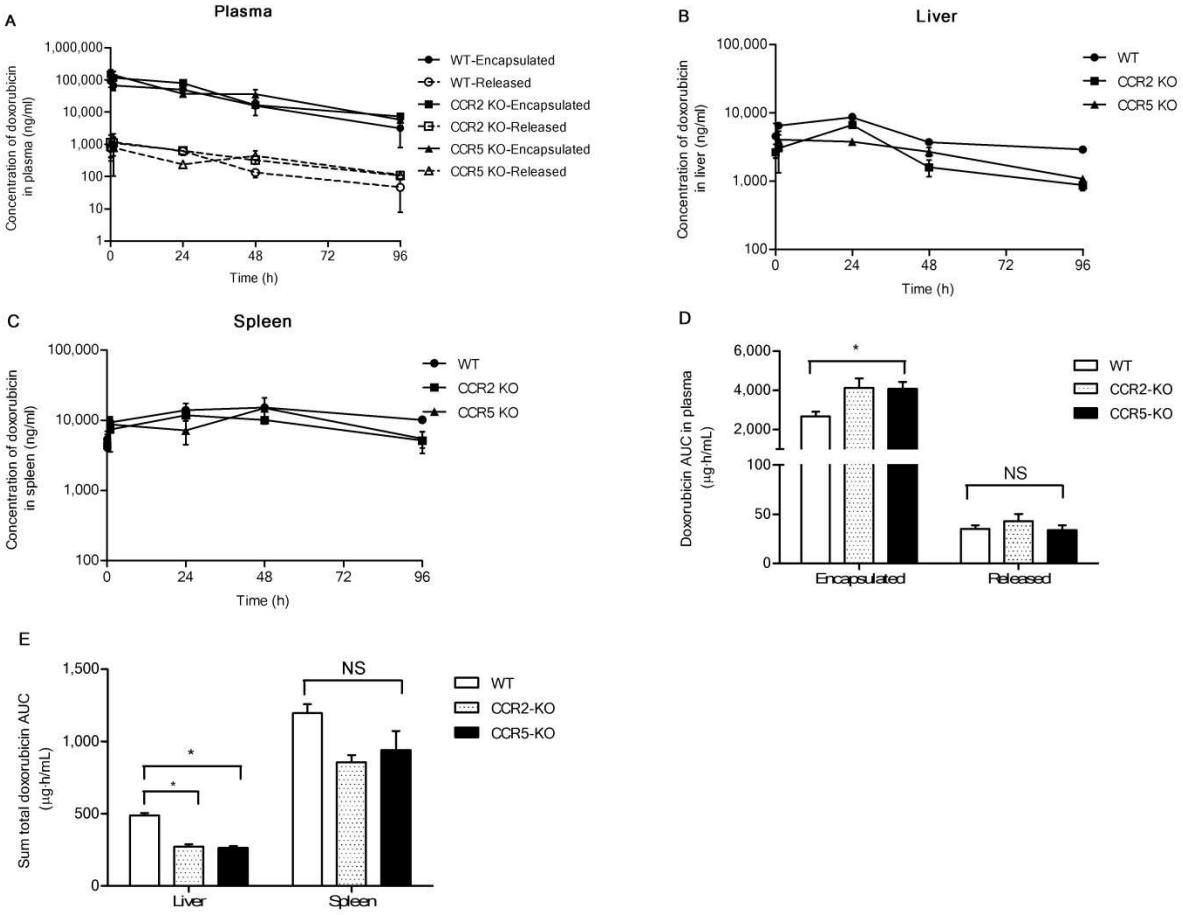

Fig. C. 1. The PK of PLD in wild-type (WT), CCR2 knockout (KO), and CCR5 KO mice after administration of PLD at 6 mg/kg IV x1 via tail vein. Concentration versus time profiles of doxorubicin in (**A**) plasma, (**B**) liver, and (**C**) spleen in WT mice, CCR2 KO and CCR5 KO mice. (**D**) Encapsulated and released doxorubicin exposure (AUC) in plasma, and (**E**) sum total doxorubicin in the liver and spleen. Equality of AUC was tested using Nedelman's modification of the Bailer method for sparse samples, using a two-sample test (1). Samples (n=3 mice) were obtained at each time point. Data are presented as mean ± SD (**A**, **B**, and **C**) and mean ± SEM (**D** and **E**).

Table C. 1. PK parameters after administration of PLD at 6 mg/kg IV x1 in WT, CCR2 KO, and CCR5 KO mice

	Plasma							
	Encapsulated doxorubicin				Released doxorubicin			
	Cmax (µg/ml)	$T_{1/2}$ (h)	CL (mL/h/kg)	$AUC_{0\text{-last}}$ (µg·h/ml)	Cmax (µg/ml)	Tmax (h)	$T_{1/2}$ (h)	$AUC_{0\text{-last}}$ (µg·h/ml)
WT	90.8	18.5	2.2	2,673 ± 233	1.2	1	20.5	35 ± 3.7
CCR2 KO	152.9	21.6	1.4	4,125 ± 467	1.1	0.083	28.1	43 ± 7.4
CCR5 KO	155.4	21.2	1.4	4,065 ± 353	0.8	0.083	39.8	34 ± 4.8
	Liver				**Spleen**			
	Sum total doxorubicin							
	Cmax (µg/ml)	Tmax (h)	$T_{1/2}$ (h)	$AUC_{0\text{-last}}$ (µg·h/ml)	Cmax (µg/ml)	Tmax (h)	$T_{1/2}$ (h)	$AUC_{0\text{-last}}$ (µg·h/ml)
WT	8.6	24	N/A	487 ± 17	16.1	6	108	1,194 ± 63
CCR2 KO	6.6	24	N/A	272 ± 17	11.8	24	N/A	857 ± 47
CCR5 KO	4.0	1	39.4	262 ± 14	14.9	48	N/A	941 ± 131

Note: Cmax; maximum concentration; Tmax: time to reach Cmax; T½, terminal half-life; $AUC_{0\text{-last}}$: area under the curve from time zero to last measurable concentration; CL: clearance; Vd_{ss}: volume of distribution at steady-state; N/A: non-available.

In the liver and spleen, as three data points in the terminal phase were not available, the terminal elimination rate (λ_z) was not estimable. $AUC_{0\text{-last}}$ of PLD was calculated by noncompartmental analysis using Phoenix v.6.2. Data are presented as mean ± standard error of the mean (SEM).

REFERENCES

(1) Nedelman JR, Gibiansky E, Lau DT. Applying Bailer's method for AUC confidence intervals to sparse sampling. Pharm Res 1995;12(1):124-128.

APPENDIX D: EVALUATION OF EFFECTS OF DOSE AND REPEATED DOSES ON CLEARANCE SATURATION OF PLD IN MURINE BREAST CANCER MODEL

METHODS

Treatments. PLD was purchased from FormuMax Scientific (Palo Alto, CA) and diluted with 5% dextrose to 1.2 mg/mL prior to injection.

Animal models. *In vivo* experiments were performed with the approval of University of North Carolina at Chapel Hill's Institutional Animal Care and Use Committee (IACUC). *T11/TP53*^{Null} orthotopic syngeneic murine transplant model (T11) representing human breast tumor claudin-low subtype was evaluated. Tumors derived from *BALB/c TP53*$^{-/-}$ orthotopic mammary gland transplant line (T11) was transplanted into the inguinal mammary fat pad of 12 week old wild-type BALB/c mice (Jackson Labs, strain 000651) (1). Mice were housed in the UNC Lineberger Comprehensive Cancer Center's Mouse Phase I Unit (MP1U) and observed for tumors as per standard practice (2). Mice were randomized to treatment cohorts and therapy began once a tumor reached 60-100 mm^3.

PK studies in the plasma and tumors. To evaluate effects of dose on the plasma clearance and tumor accumulation of PLD, PLD was administered at 1 mg/kg IV x1 via a tail vein as compared to 6 mg/kg used in the previous studies (See Chapter 3). Mice (n=3) were euthanized prior to and at 0.083, 1, 6, 24, 48, and 96 h after administration of PLD. To investigate the effect of repeated injections of PLD on the plasma and tumor levels of PLD, the dosing interval for 3 multiple injections was 5 days, or approximately 5-6 half-lives (PLD $t_{1/2}$ in mice, 15- 20 hr), which would allow for clearance of 95 % of the injected dose. The levels of sum total (encapsulated and released) doxorubicin in the plasma and tumor were measured at a fixed time (96 hr) after the last injection. Each blood sample was processed to evaluate

encapsulated and released doxorubicin in plasma as described previously (18, 26). In the same mice, tumors were collected, preserved by snap freezing, and stored at – 80°C to measure the sum total (encapsulated and released) doxorubicin in tumor. The procedures for sample processing are described in detail in Chapter 3.

PK analysis. See Chapter 3.

Statistical analysis. Statistical analyses were carried out using Prism5 software (GraphPad Software, Inc.). Analysis of variance (ANOVA) was performed to compare the levels of doxorubicin in the plasma and tumors after repeated doses of PLD. *P* value of less than 0.05 was considered statistically significant. All statistical tests were two-sided.

RESULTS

Effects of dose on plasma clearance and tumor accumulation of PLD. When the dose of PLD was escalated from 1 mg/kg to 10 mg/kg, plasma levels (Cmax) increased by, approximately, the same factor (6-fold) of the dose escalation (**Table D. 1**). Consistent with Cmax, there was a proportional increase in the plasma exposure (AUC) of PLD and the plasma clearance (CL) of PLD remained the same after administration of PLD at doses of 1 mg/kg and 6 mg/kg (**Fig. D. 1, Table D. 1**). The amount of released doxorubicin from the carrier in the plasma was also increased proportionally, indicating that he dose range from 1 mg/kg to 6 mg/kg does not result in a saturation of the MPS-mediated clearance of PLD. However, dose escalation resulted in a disproportionate increase in tumor uptake of PLD which increased by 10-fold when the dose of PLD is raised 6-fold (**Fig. D. 2, Table D. 1**).

Effects of repeated doses of PLD on plasma clearance and tumor accumulation of PLD. We also investigated the effect of repeated doses of PLD on the plasma and tumor levels

of PLD at a fixed time (96 h) after the last injection. After 3 doses of PLD at the interval of 96 h, there were no changes in the plasma levels of PLD (**Fig. D. 2A**) indicating no saturation phenomenon takes place under this particular dose-schedule (6 mg/kg doses with an interval limited to 5 days). When we compared the tumor accumulation of PLD after a single dose of 6 mg/kg to that after 3rd injection of 6 mg/kg, a 1.6-fold increment was observed, but the difference was not significant (**Fig. D. 2B**).

CONCLUSION

The saturation of the MPS-mediated clearance of PLD has been reported in murine models and patients. It has been shown that dose escalation from 2.5 mg/kg to 10 mg/kg of PLD resulted in a saturation of PLD clearance and a disproportional increase of the amount of PLD accumulating in the tumor due to a partial blockade of the MPS with relative reduction of liver uptake and greater prolongation of liposome circulation (3). In the same study, repeated doses of 4 mg/kg PLD with an interval 4 days also caused a saturation phenomenon (3). PK studies of PLD were performed in patients (n=12) receiving successive doses of 60, 30, 45 mg/m^2 (arm A) or 30, 60, 45 mg/m^2 (arm B) every 4 weeks. In contrast to animal studies, there was no significant difference in the PK parameters with doubling doses; however, there was a gradual and significant inhibition of clearance from the 1st through the 3rd cycle of PLD (4).

In our preclinical studies using dose escalation from 1 mg/kg to 6 mg/kg of PLD, there was no significant change in clearance and a linear correlation between dose and plasma exposure (AUC) was observed. When repeated doses of 6 mg/kg PLD with an interval 5 days were administered, no saturation effect was observed in the plasma levels of PLD upon multiple injections. However, a disproportional increase in tumor uptake (AUC) of PLD with dose

escalation and non-significant 58% increase in the tumor levels of PLD when going from 1st to 3rd cycles of PLD occurred. These findings suggest that dose escalation of PLD within the therapeutic dose range does not cause significant saturation of the MPS (i.e., Kupffer cells in the liver), but the tumor uptake of PLD may interact with the tumor cells and/or tumor microenvironment (i.e., VEGF-A) leading to altered extravasation of PLD from the capillaries to tumor as discussed in Chapter 3. Difference in dosing interval (4 days vs. 5 days) used in the repeated dose study, rapid replenishment of bone marrow-derived macrophage population in the liver in mice, and distinct immune competency in different mouse models (xenografts vs. GEMMs) may also account for different effects of dose and repeated doses of PLD (5).

Table D.1. PK parameters of PLD after administration of PLD at 1 mg/kg or 6 mg/kg IV x1 in claudin-low T11 breast tumor model.

	Plasma							
	Encapsulated doxorubicin				Released doxorubicin			
PLD Dose	Cmax (µg/ml)	$T_{1/2}$ (h)	$AUC_{0\text{-last}}$ (µg·h/ml)	CL (mL/h/kg)	Cmax (µg/ml)	Tmax (h)	$T_{1/2}$ (h)	$AUC_{0\text{-last}}$ (µg·h/ml)
1 mg/kg	18	9.2	246 ± 31	4.1	0.2	0.083	13.4	4 ± 0.1
6 mg/kg	117	17.0	1,449 ± 57	4.0	3.3	0.083	19.4	27 ± 1.6

	Tumor			
	Sum total (encapsulated + released) doxorubicin			
PLD Dose	Cmax (µg/ml)	Tmax (h)	$T_{1/2}$ (h)	$AUC_{0\text{-last}}$ (µg·h/ml)
1 mg/kg	0.3	24	N/A	20 ± 2
6 mg/kg	2.6	16	157	210 ± 30

Cmax; maximum concentration; Tmax: time to reach Cmax; T½, terminal half-life; $AUC_{0\text{-last}}$: area under the curve from time zero to last measurable concentration; CL: clearance; Vd_{ss}: volume of distribution at steady-state; N/A: non-available. In the tumor, the terminal elimination rate (λ_z) was not estimable due to lack of data points in the in the terminal phase.

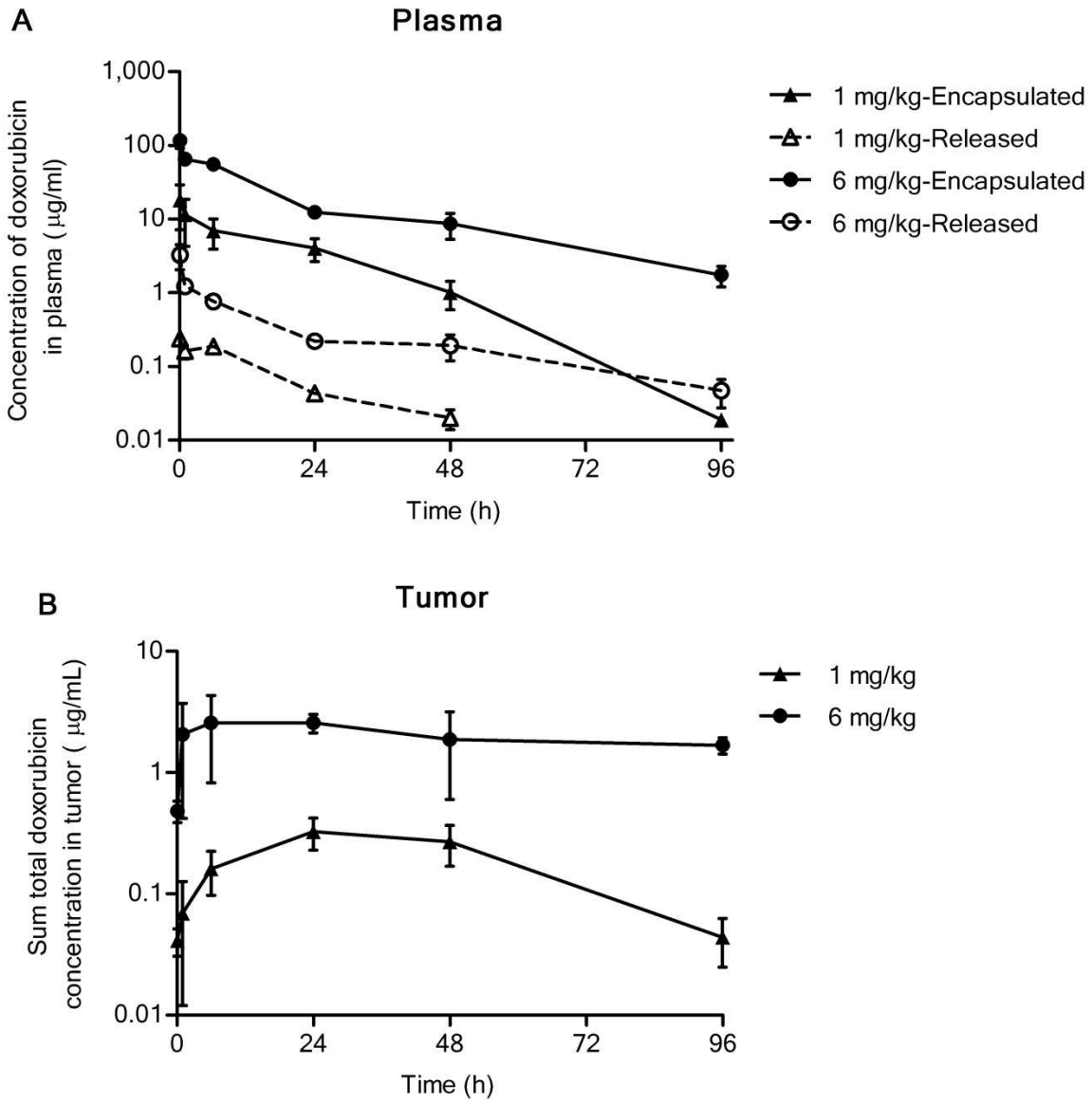

Fig. D. 1. Concentration versus time profiles of doxorubicin after administration of PLD at 1 mg/kg or 6 mg/kg I.V. x 1 via tail vein in (A) plasma and (B) tumor in claudin-low T11 breast tumor models. Samples (n=3 mice at each time point) were obtained at 0.083, 1, 6, 24, 48, and 96 hours following PLD administration. Each time point is represented as the mean ± SD. LLOQ for encapsulated doxorubicin: 300 ng/mL, released doxorubicin: 10 ng/mL, and sum total doxorubicin in tissue: 10 ng/g.

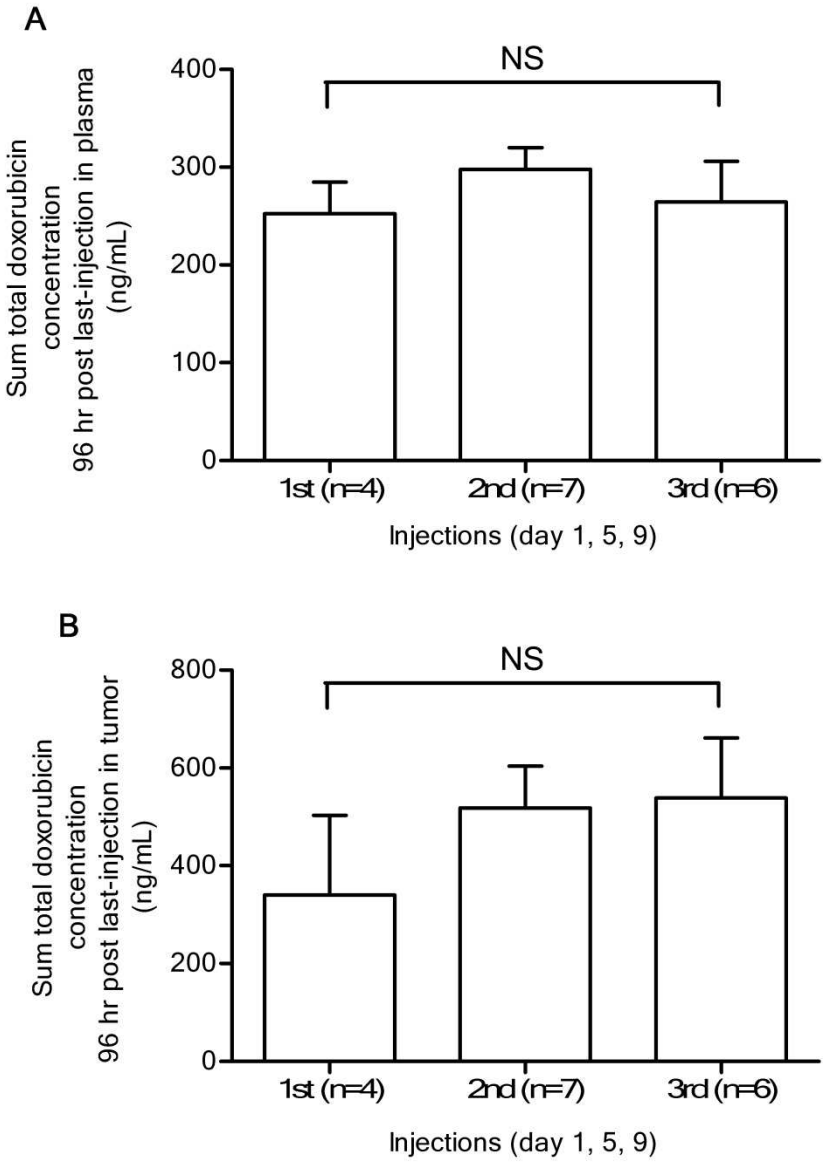

Fig. D. 2. Sum total (encapsulated and released) doxorubicin concentrations in (A) plasma and (**B**) tumor at 96 h post last-injection of PLD in claudin-low T11 breast tumor models. T11 mice were injected with PLD I.V. at dose of 6 mg/kg x 3. The dosing interval was 96 h. Plasma and tumor levels of PLD were measured 96 h after the last injection. Data are presented as mean ± SEM.

REFERENCES

(1) Herschkowitz JI, Simin K, Weigman VJ, Mikaelian I, Usary J, Hu Z, et al. Identification of conserved gene expression features between murine mammary carcinoma models and human breast tumors. Genome Biol 2007;8(5):R76.

(2) Herschkowitz JI, Zhao W, Zhang M, Usary J, Murrow G, Edwards D, et al. Comparative oncogenomics identifies breast tumors enriched in functional tumor-initiating cells. Proceedings of the National Academy of Sciences 2012;109(8):2778-2783.

(3) Gabizon A, Tzemach D, Mak L, Bronstein M, Horowitz AT. Dose dependency of pharmacokinetics and therapeutic efficacy of pegylated liposomal doxorubicin (DOXIL) in murine models. J Drug Target 2002;10(7):539-548.

(4) Gabizon A, Isacson R, Rosengarten O, Tzemach D, Shmeeda H, Sapir R. An open-label study to evaluate dose and cycle dependence of the pharmacokinetics of pegylated liposomal doxorubicin. Cancer Chemother Pharmacol 2008;61(4):695-702.

(5) Sharpless NE, DePinho RA. The mighty mouse: genetically engineered mouse models in cancer drug development. Nature Reviews Drug Discovery 2006;5(9):741-754.